



HAL
open science

Growth and activity of neuronal cultures : emergence of organized behaviors

Tanguy Fardet

► **To cite this version:**

Tanguy Fardet. Growth and activity of neuronal cultures : emergence of organized behaviors. Biological Physics [physics.bio-ph]. Université Sorbonne Paris Cité, 2018. English. NNT : 2018USPCC002 . tel-01956310

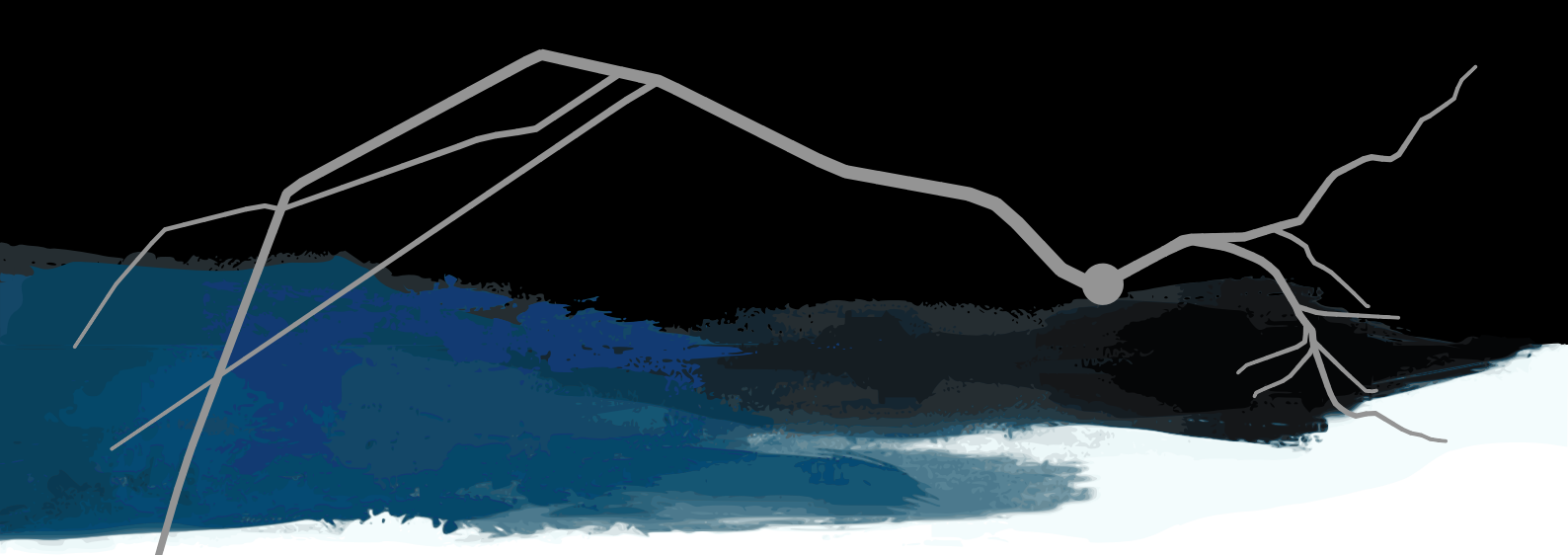
HAL Id: tel-01956310

<https://theses.hal.science/tel-01956310>

Submitted on 15 Dec 2018

HAL is a multi-disciplinary open access archive for the deposit and dissemination of scientific research documents, whether they are published or not. The documents may come from teaching and research institutions in France or abroad, or from public or private research centers.

L'archive ouverte pluridisciplinaire **HAL**, est destinée au dépôt et à la diffusion de documents scientifiques de niveau recherche, publiés ou non, émanant des établissements d'enseignement et de recherche français ou étrangers, des laboratoires publics ou privés.

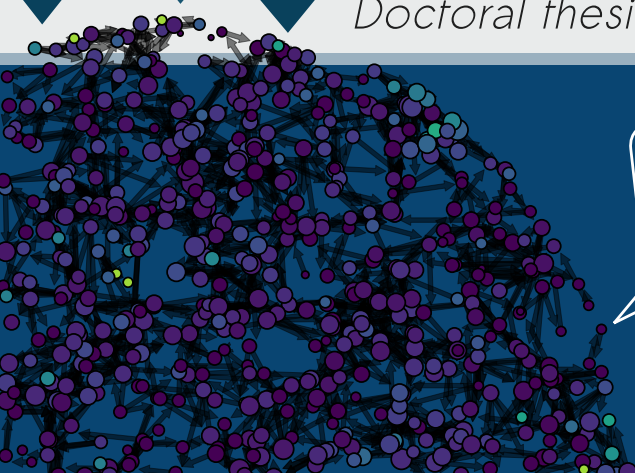


Growth and activity of neuronal cultures

Emergence of organized behaviors

Doctoral thesis

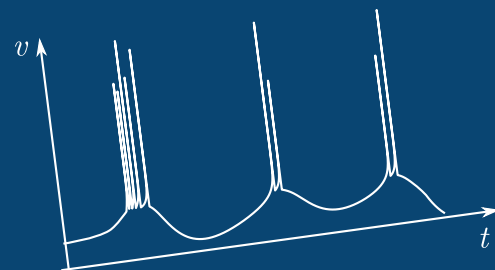
Tanguy Fardet



$$C_m \dot{V} = -g_L(V - E_L) + g_L \Delta_T \exp\left(\frac{V - V_{th}}{\Delta_T}\right) - w + I(t)$$

$$\tau_w \dot{w} = a(V - E_L) - w$$

$$Sc = \dot{v} - q$$



Thèse de doctorat
de l'Université Sorbonne Paris Cité
Préparée à l'Université Paris Diderot
Ecole doctorale **Physique en Île-de-France** (ED 564)
Laboratoire Matière & Systèmes Complexes

Thèse de doctorat de Physique

Growth and activity of neuronal cultures

Emergence of organized behaviors

Par *Tanguy Fardet*

Dirigée par Pascal Monceau,
co-encadrée par Samuel Bottani et Stéphane Métens.

Soutenue publiquement le 18 septembre 2018 devant le jury composé de

Président	Pr. Jean-Marc DIMEGLIO	Université Paris Diderot
Rapporteurs	Dr. Romain BRETTE	Inserm–Institut de la Vision
	Dr. Jordi SORIANO	Université de Barcelone
Examineurs	Dr. Alexandra BENCHOUA	Inserm–CECS/I-Stem
	Dr. Alain DESTEXHE	CNRS–UNIC
	Dr. Catherine VILLARD	CNRS–Institut Curie
Directeur de thèse	Dr. Pascal MONCEAU	Université d'Évry
Membres invités	Dr. Samuel BOTTANI	Université Paris Diderot
	Dr. Elisha MOSES	Weizmann Institute



Acknowledgments

Disclaimer — The views and opinions expressed in the following are those of the 2018.09 version of Tanguy Fardet and do not necessarily reflect those of previously encountered versions. As such, previous or future versions should not be judged for any omission or oversight which might be noticed here: these are the sole responsibility of the current version and its erratic memory.

First of all, I would like to thank my three supervisors, Pascal Monceau, Samuel Bottani, and Stephane Métens, without whom none of this would have been possible. Their support and goodwill, starting from our first encounter, made these three years a very pleasant experience, both personally and scientifically. Being able to discuss all subjects and decide where we would go together was extremely pleasant, as was the large amount of freedom they left me. I was also very pleased to share many work-unrelated moments with them, be it when we visited Washington or Israel, or simply during breaks, when we talked about Japan, books, SF...

Thank you Pascal, I really appreciated the rigor you applied when tackling the various problems we faced. Thank you also for bearing with me as I pushed a bit to move to different languages and tools (python, git...). Most of all, thanks for these nice conversations on science, teaching, and our shared interest over Japan.

Thank you Samuel for your very critical thinking on the PhD and your advice on writing which helped me a lot. I also greatly appreciated the time we spent in Rehovot and our various interesting conversations on equally various and interesting themes — it *is* enjoyable to be able to talk about a good SF book with one's supervisor. Let me not forget, of course to thank you (in the name, I think, of all the members of 911) for your percolator!

Thank you Stéphane, for the same rigor Pascal displayed, and your help hammering some solutions out of the AdEx equations. I was glad for the company of your sharp mind (and tongue! ^^), notably during our SfN trip, where I especially enjoyed the tour of the city and our visit of the incredible National Museum of the American Indian.

Thank you all three for three enjoyable years!

I am of course also very grateful to the whole jury for approving this manuscript, and special thanks go to Jordi Soriano and Romain Brette for taking the time to review the whole of it, in details. I thank of course the president of the jury, Jean-Marc DiMeglio, not only for his benevolence on D-day¹, but also for helpful discussions as he helped review the advancement of the thesis after the first and second years. I also appreciated the kindness of Alexandra Benchoua and Alain Destexhe, who also provided interesting insights from different viewpoints in neuroscience. Eventually, I would like to thank again Jordi Soriano, together with Catherine Villard and Elisha Moses, not only for participating in the jury, but also for interesting and helpful discussions during the three years of my PhD.

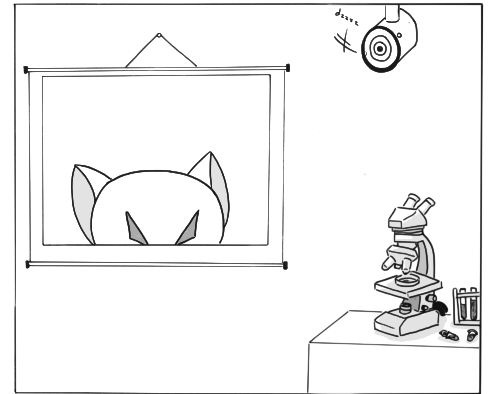
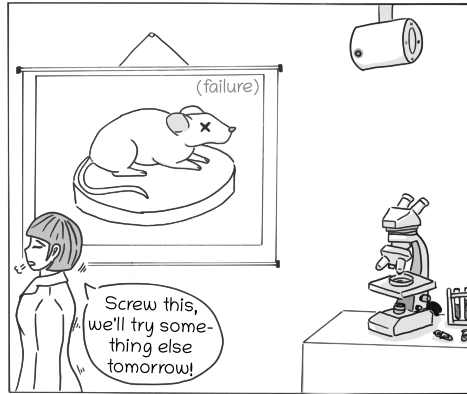
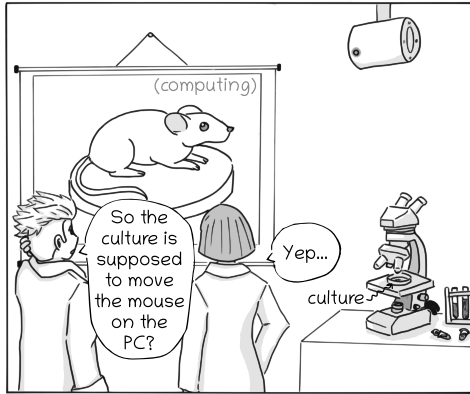
In particular, I would like to convey all my gratitude to Elisha Moses for his kindness, as he hosted me in his lab, at the Weizmann Institute, and allowed me to work with the cultures and microscopes there, to test experimentally the theoretical predictions that I made through my model. These few weeks at the Weizmann were

¹Defense-day

Using neuronal cultures to actually process incoming signals and perform computations is a daring endeavor...

Many have tried to follow this path and failed...

Or have they?



珠里 03.2018

quite intense, and it was a great satisfaction to be able to perform directly the experiments testing my predictions. I also really appreciated the time I spent with the people of this lab². I would of course like to thank Perla Zalberg for her efficiency and her surprising mastery of French, but mostly, I would like to discern the medal of honor to Nirit Tsory, who was like a second mum to me there. She walked me through all the experimental procedures, how to use the confocal... and provided me with priceless support and help to make sure we manage to make everything in time.

This PhD also gave me the opportunity to interact with many people from all around the world in the field of neuroscience. I especially appreciated meeting the people from the NEST community, with whom I had very pleasant times both at conferences or during various (mostly online) meetings.

I would like to thank all of them, of course, but above all Hans Ekkehard Plesser, with whom I spent long hours engineering a proper numerical implementation for the AdExp model, and Dennis Terhorst, for his help and many interesting conversations. Many thanks also to the people involved in the NESTML project³, to those involved in the structural plasticity⁴ and to Nilton Kamiji for some fun conversations and discussions on the impact of adaptation.

I also had the chance to participate in the 2017 JSPS Summer Program, which enabled me to spend almost 3 months in Japan, in the team of Taro Toyozumi. I am very grateful to Taro for his critical approach of the nucleation problem and very helpful discussions on the synaptic strength and plasticity, as well as general scientific or unscientific conversations during lunch time. I also really appreciated the very multicultural team there, with very interesting and pleasant people⁵, and I would like to address all my thanks to Reiko Kiyotaki for her help, good mood, and, with the assistance of Shun Ogawa, a very nice discovery of top-grade sake.

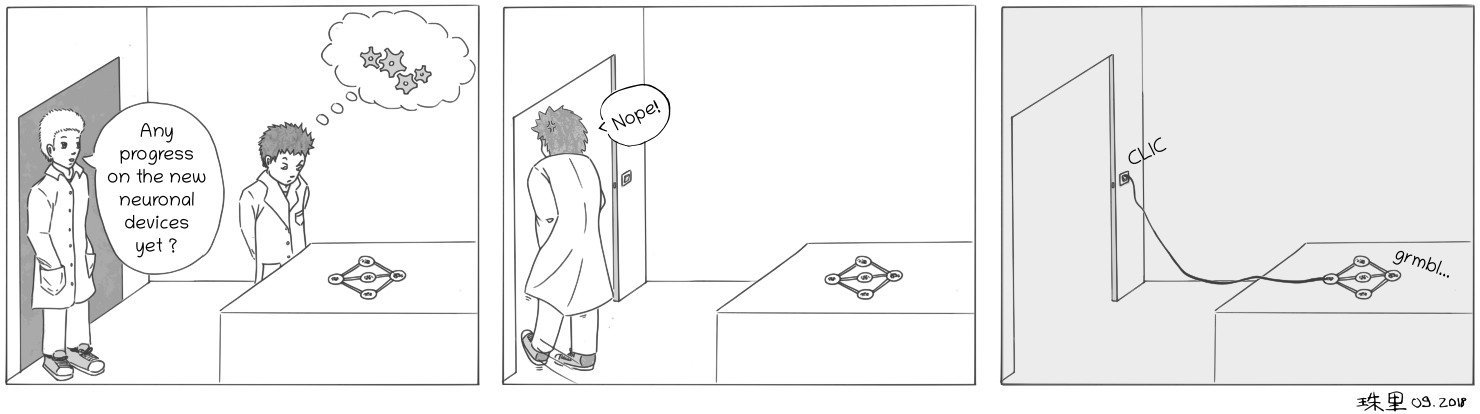
Of course you don't have to go to the other side of the world to find nice and interesting people, and I would also like to thank the researchers at the MSC lab for their interesting inputs. I am specially grateful to Atef Asnacios for his advice on mechanical models and papers related to cytoskeleton-generated forces in growth cones, as well as to Julien Tailleur for discussions on the SDEs and the Heun

²Eyal, Mica, Yuri, Nirit, and Yaron

³Jochen, Dimitri, Inga

⁴Alex and Sandra

⁵Lukasz, Roberto, Takuya, Shun, Haiping, Kazu, Mireille, and Alireza



algorithm. Many thanks also to Jean-Pierre Henri and Fabien Gerbal for their useful comments on the slides, and to Marlène Hanoomi for her good mood and help when planning the various missions and conferences.

Lastly, I would like to stress the great work done by the three interns who came to work in the lab during these three years: Mathieu Ballandras, who worked on the model to study adaptation-terminated bursts, Alessio Quaresima, who invested an incredible amount of time and effort into the difficult implementation of DeNSE and the various models included in it, and Mallory Dazza, who studied the nucleation of the bursts in cultures, and will continue as a PhD student in the NeuroPhysics team.

I guess this more or less wraps up the (mostly) science-related part of these acknowledgments, and I will now move to other persons, with whom I have mostly interacted in more casual conditions. Here, of course, the people from the 911 office (and its adopted members) come first. Faces came and left, obviously, during these three years, but the overall good mood and cheerfulness remained! Let me first thank my *sempais*, Mathieu and Olivier, who initiated the lasting traditions of cinematic and humorous quotes, as well as sudo-Japanese conversations for the former and indistinct mumbling for the latter.

The golden generation of 2015 comes next, with Solène, Antoine, and Raphael, who shared these entire 3 years with me. I will follow the new tradition by thanking Solène for sheltering my dear books in her house⁶, but also for accepting to follow me during our long debates on the Fermi paradox, the universal basic income and its countless variations, and so on and so forth. . . Thanks also to Antoine, for helping me drive the rest of the office nuts with our polyphonic songs, and cheers to Raphael for a long-running course on how to make ~~terrible~~ original skateboards!

Cheers also to the young ones: Paul, Romain, Quentin, who, despite their young age, also tried to follow our (sometimes) serious and (often) convoluted debates ;P. More seriously⁷, many thanks to all of them for long discussions, often on society, teaching, and science, but also on music or the occasional Python challenge, with Paul, on swing/rock with Romain, and on climbing with Quentin.

Besides the feisty PhD students, postdocs also shared the office and I would like to thank Caroline, Julien, Adrien, and Eduardo for their kindness and interesting discussion on what comes next.

To finish, I would like to thank my family for their love and support during all these years.

⁶hopefully they will return someday. . .

⁷who am I kidding?

A big hug to my grand-parents, uncles, and aunts, however disappointed they might be when they realize that this thesis will not bring us much closer to curing Alzheimer's or Parkinson's disease. Many thanks to my dad for his support and his presence over the years when I wanted to discuss.

Kisses to my little sister, who understood the burden of writing, since she was working on her memoir, but remained lively and energetic as ever.

A special thank to my favorite English teacher, my mum, who did so many things, and even took the time to read the whole manuscript to correct my mistakes. . . hats off!

And eventually, all my love to my sweet Julie, who did not only bear with me during these years, but also suffered through the preparation of the buffet before (and after) the defense *and* took the time to draw these amazing comic strips to lighten up the tone of these all too serious acknowledgments. . . you're the best!

Summary

In this thesis, I provide models and numerical tools to better understand and predict the behavior and development of neuronal cultures and devices. Neuronal cultures have proven invaluable in improving our understanding of how the brain processes information, by enabling researchers to investigate neuronal and network response functions to various perturbations and stimuli. Furthermore, recent progress in microfluidics have opened the gate towards more elaborated neuronal devices, bringing us one step closer to complex signal processing with living *in vitro* neurons.

My first point will be to propose a mechanism so as to explain the epileptiform bursts of activity present in cultures, mechanism which I formulate as a concise theoretical model. I subsequently test the predictions of this model on cultures and show that they are indeed compatible with the behavior observed *in vitro*. I further develop this description in the second part of the thesis, where I analyze its spatiotemporal dynamics and the fact that bursts nucleate in specific areas in the network. Since predictions and analysis of these nucleation centers strongly depends on the network structure, I develop a simulation platform to enable efficient modeling of the network development. This software takes into account the interactions between the neurons and their environment and is the first platform to provide versatile and complete models to simulate the entire growth process of

Résumé

Dans cette thèse, je propose plusieurs modèles et outils numériques afin de mieux comprendre et prédire le comportement et le développement de cultures et dispositifs neuronaux. Les cultures de neurones ont en effet été un outil précieux durant les 20 dernières années : elles ont permis de mieux comprendre la manière dont le cerveau traite les différentes informations qui lui parviennent en donnant aux scientifiques la possibilité de tester les effets de médicaments sur les neurones, ainsi que d'obtenir leurs réponses détaillées à diverses perturbations et stimuli. De plus, de récentes avancées en microfluidiques ont ouvert la voie à la conception de dispositifs neuronaux plus élaborés, rapprochant encore un peu plus la perspective du traitement de signaux complexes via des neurones *in vitro*.

Dans une première partie, je propose un mécanisme pour expliquer les bouffées d'activité épileptiformes présentes dans les cultures, mécanisme que je formule via un modèle théorique concis. J'effectue ensuite une vérification expérimentale des prédictions du modèle sur des cultures et montre que celles-ci sont effectivement compatibles avec le comportement observé *in vitro*. Dans une seconde partie, je décris plus en détail la description de la dynamique spatiotemporelle du phénomène, notamment le fait que les bursts nucléent en des zones bien précises du réseau neuronal. Comme les prédictions et analyses effectuées dépendent fortement de la structure de ce réseau, je présente ensuite la réalisation d'une plateforme de simulation afin de permettre de modéliser efficacement le développement des réseaux neuronaux. Ce logiciel prend en compte les interactions entre les neu-

neurons. I demonstrate that this simulator is able to generate valid neuronal morphologies, then use it to postulate new network topologies to describe neuronal cultures, as well as to reproduce existing neuronal devices. I then show that the activities sustained by these structures are compatible with the experimental recordings. Eventually, I discuss several future directions for which the use of neuronal devices would enable to circumvent current limitations of neuronal cultures, thus providing new information on the processes which underlie brain development and plasticity.

rones et leur environnement et constitue la première plateforme à fournir des modèles polyvalents et complets pour décrire l'intégralité du processus de croissance neuronale. Je montre ensuite que ce simulateur est capable de générer des morphologies valides et l'utilise pour proposer des nouvelles topologies de réseaux afin de décrire les cultures de neurones. Je reproduis également des dispositifs neuronaux existants et montre que les activités entretenues par ces structures sont compatibles avec les observations expérimentales. Enfin, je discute plusieurs directions de recherche possibles, pour lesquelles l'utilisation de dispositifs neuronaux spécifiques permettrait de contourner les limitations des cultures neuronales et fournirait ainsi de nouvelles informations sur les processus sous-tendant le développement et la plasticité cérébrale.

Keywords

- neurons
- networks
- cultures
- devices
- activity
- bursts
- development
- adaptation
- nucleation
- DeNSE

Mots clés

- neurones
- réseaux
- cultures
- dispositifs
- activité
- bouffées
- développement
- adaptation
- nucléation
- DeNSE

Table of contents

	Glossary	vii
1	Introduction	1
1.1	What is this all about?	2
1.1.1	The big picture	2
1.1.2	Neuronal cultures and devices	3
1.1.3	A thesis in computational neuroscience	7
1.2	Brain cells	10
1.2.1	Neurons: structure and function	10
1.2.2	Neuronal development: from seed to tree	11
1.2.3	Companions: glial cells	13
1.3	Neuronal dynamics	14
1.3.1	The biological reality	14
1.3.2	Neurons as excitable units	15
1.3.3	Simple models for spiking neurons	16
1.4	Information transfer: connections between cells	22
1.4.1	Chemical connections: synapses	22
1.4.2	Electrical connections: gap junctions	25
1.4.3	Other pathways for information transfer	26
1.5	Coupled neurons: network and dynamics	27
1.5.1	Typical activities of neuronal cultures	27
1.5.2	Emerging behaviors: synchronization and bursting	28
2	Mechanisms governing epileptiform bursts	35
2.1	Possible bursting mechanisms	36
2.1.1	Burst initiation, deterministic or stochastic?	36
2.1.2	Burst termination: adaptation or depression?	38
2.2	The influence of neuronal adaptation	41
2.2.1	A concise model for periodic bursting	41
2.2.2	Shaping bursts through adaptation channels	46
2.3	Statistical properties of bursting behaviors	54
2.3.1	The transition to synchronous bursting	54
2.3.2	Synchronous bursts as percolation events	58
2.3.3	Statistical properties of the interburst interval	59
3	Topology and spatio-temporal bursting patterns	69
3.1	Nucleation centers in experiments and simulations	70
3.1.1	Resilience of the nucleation mechanism <i>in silico</i>	70

3.1.2	Who are the first to fire?	71
3.2	Structure and initiation-termination mechanisms	72
3.2.1	The possible driving mechanisms	72
3.2.2	Influence of the termination mechanism	73
3.2.3	The complex influence of topology	73
3.3	Structural and dynamical properties	75
3.3.1	Topological properties of spatial cultures	75
3.3.2	Burst nucleation in neuronal cultures <i>in silico</i>	78
3.3.3	Limitations of the predictions	86
4	Accounting for neuronal development	91
4.1	DeNSE, a unifying platform for neuronal growth	92
4.1.1	Existing software, assessment, and objectives	92
4.1.2	Modeling and analyzing developing neurons with DeNSE	94
4.2	Growth cones, steering and interactions	96
4.2.1	Modeling an extending growth cone	96
4.2.2	Beyond the isolated growth cone: interactions	102
4.3	Branching patterns	108
4.3.1	Growth cone splitting	108
4.3.2	Lateral branching	112
4.3.3	Pruning	114
4.4	From neuronal morphologies to neuronal networks	117
4.4.1	A complete neurite tree	117
4.4.2	Coupling neurons: synapses and network	118
5	Conclusion, towards neuronal devices	131
5.1	Current limitations of neuronal cultures	132
5.1.1	The unfortunate side-effect of isolation	132
5.1.2	Preventing percolation	133
5.2	Neuronal devices as the next step	133
5.2.1	Directed information flow	134
5.2.2	Development under stimulation	134
5.2.3	Structured networks	135
5.3	Concluding remarks	139
A	Neuronal dynamics and the AdExp model	143
A.1	Pacemaker neurons	143
A.2	Firing patterns	143
B	Excitability, restlessness, and susceptibility	147
B.1	Transitions of the AdExp model	147
B.2	Susceptibility	147
B.3	Restlessness	149

C	Self-consistent equations for the bursting behavior	151
C.1	Neuronal model (AdEx) and parameters	151
C.2	Hypotheses underlying the equivalent model	151
C.3	Stability of the synchronized state	151
C.4	Linear evolution of V submitted to a constant current	153
C.5	Modeling a burst with instantaneous Dirac synapses	153
C.6	Bursting in heterogeneous networks: continuous synapses	155
C.7	Effect of the last spike	156
C.8	Resting period: interburst dynamics	156
D	Simulating networks of spiking neurons	159
D.1	Simulation choice and protocols	159
D.2	Network models and parameters	159
D.3	Properties of spatial networks	163
E	Experimental protocols	165
E.1	Culture preparation and feeding procedures	165
E.2	Calcium imaging	165
E.3	Application of the blockers	166
F	Nucleation centers	167
F.1	Preliminary burst delimitation	167
F.2	Detection via a clustering algorithm	167
F.3	Predicting nucleation centers by graph centralities	168
G	Growth models	169
G.1	Simple random walker	169
G.2	Run-and-Tumble model	169
G.3	Self-referential forces	170
G.4	Critical resource and competition	171
H	Modeling the environment	175
H.1	Principle of growth cone sensing	175
H.2	Making the forward step	175
I	Branching models	177
I.1	Growth cone split	177
I.2	Lateral branching	177
I.3	Quantifying and analyzing branching patterns	178
J	Papers	179
J.1	Review on percolation (IOP Conf. Series 2017)	179
J.2	Inhibitory and dynamical quorum percolation (Physica A 2018)	192

J.3	Bursting and adaptation (Frontiers in Neuroscience 2018)	221
	Bibliography	237
	Books	237
	Articles	238
	Others	251
	Index	253

Glossary

action potential sudden and localized increase of the membrane potential of a neuron that is actively propagated mostly from the soma and the base of the axon towards the periphery of the axonal tree; it is the base unit of significance in neuronal communications 15, 16, 23, 34, 50, *see* spike

AdExp adaptive Exponential Integrate-and-Fire 17–19, 34, 39–43, 55, 133, 178, *see* aEIF

aEIF adaptive Exponential Integrate-and-Fire *see* AdExp

AHP After HyperPolarization *See* “The biological reality” (subsection 1.3.1), 15, 17, 34, 43, 45, 51

ANN Artificial Neural Network 2, 3

API Application Programming Interface 84

centrifugal order integer describing the number of bifurcation points that separate a terminal segment of a tree (a growth cone, in the case of a neurite) from its root (the soma) 100

CNS Central Nervous System 13, 24

CV Coefficient of Variation 57, 58

DIV Day In Vitro 12, 69, 73

EDR Exponential Distance Rule 67, 69, 73, 82, 111, 114, 125, 145, 146, 154

EEG ElectroEncephaloGraphy 2, 27

fAHP fast After HyperPolarization 43–45, 152

fMRI functional Magnetic Resonance Imaging 2, 27

FP2L Front-based Power-Law Lateral 103, 104

IBI Inter-Burst Interval 42, 43, 46–48, 55–58, 65, 66, 76, 77

integrate-and-fire models are simple mathematical descriptions of neurons as excitable units; they model the neuron as an integrator (storing incoming inputs) that will emit a spike (fire) when the cumulated inputs reach a certain level. Such models contain at least one continuous variable (the membrane potential) and have a discrete output function (spiking events). Examples are: leaky integrate-and-fire (LIF), exponential integrate-and-fire (EIF) 16, 17, *see* aEIF

ISI Inter-Spike Interval 20, 56

mAHP medium After HyperPolarization 43–46, 152

MEA Micro-Electrode Array 4, 5, 62, 67

mEPSC miniature Excitatory Post Synaptic Current 33, 64, 146

mEPSP miniature Excitatory Post Synaptic Potential 33

mini Miniature excitatory post-synaptic current, post-synaptic event triggered by the spontaneous release of vesicle at an excitatory synapse. *See also* mEPSC and mEPSP 33–35, 50, 64, 66, 70, 76, 146

MT microtubule 12, 13, 88–90, 94–96, 99, 102

PSC Post Synaptic Current 24, 35

QP Quorum Percolation 54, 165, 178

sAHP slow After HyperPolarization 35, 42, 43, 45, 152

spike sudden and localized increase of the membrane potential *see* action potential

STD Short-Term Depression 32, 35, 66

Chapter 1

Introduction

As hinted in the title, the main focus of this manuscript shall be the investigation of the various mechanisms underlying the growth and epileptiform activity of neuronal cultures. The objective behind this endeavour, beyond the potential insights provided by a deeper understanding of these phenomena, is to prepare for the next step, namely the design and investigation of neuronal devices, which will be described hereafter.

Before going into the heart of the subject, I will first provide some context and necessary notions, which will be referred to regularly in the main matter.

Contents

1.1	What is this all about?	2
1.1.1	The big picture	2
1.1.2	Neuronal cultures and devices	3
1.1.3	A thesis in computational neuroscience	7
1.2	Brain cells	10
1.2.1	Neurons: structure and function	10
1.2.2	Neuronal development: from seed to tree	11
1.2.3	Companions: glial cells	13
1.3	Neuronal dynamics	14
1.3.1	The biological reality	14
1.3.2	Neurons as excitable units	15
1.3.3	Simple models for spiking neurons	16
1.4	Information transfer: connections between cells	22
1.4.1	Chemical connections: synapses	22
1.4.2	Electrical connections: gap junctions	25
1.4.3	Other pathways for information transfer	26
1.5	Coupled neurons: network and dynamics	27
1.5.1	Typical activities of neuronal cultures	27
1.5.2	Emerging behaviors: synchronization and bursting	28

1.1 What is this all about?

1.1.1 The big picture

How did we humans become sapient creatures? How do thoughts and consciousness emerge from the myriads of electro-chemical signals our brain hosts? What exactly would an answer to these questions bring us?

*consciousness
and
intelligence as
an emergent
phenomenon*

None of these daunting questions will be answered in this manuscript; however, they have doubtlessly led many researchers to the investigation of the brain. This incredible structure, which has emerged and been selected over millions of year in all animals, is itself composed of intricate networks made by up to several billion cells, resulting in trillions of connections. There are many ways to study such a system; for instance from a global, macroscopic perspective, studying the interactions of large brain areas using ElectroEncephaloGraphy (EEG) or functional Magnetic Resonance Imaging (fMRI), or taking a bottom-up approach, building on from the neuron to smaller, then larger networks, until we reach a sufficient degree of complexity, the level where a first flash of consciousness would appear.

Moreover, though there are many limitations to the human brain, and despite the fact that it might be very far from the optimal structure in term of computational power¹, its processing capabilities with respect to its actual power consumption are indeed beyond compare.

However, the brain seemed just too complex, functioning at scales that involve too many interacting units, to be studied with current mathematical and physical descriptions. So I started thinking about how I could get the chance of studying the emergence of complex signal processing, however remote it might be from actual thoughts or consciousness.

*how to
approach this
question?*

Well, single neurons already perform some signal processing through the complex interactions between the afferent signals inside the dendritic tree and the integration and comparison performed in the soma and axonal hillock — to transmit or not an action potential to the neighboring neurons. But this felt a little too limited, compared to the actual brain, especially since I discovered network theory during my Masters degree, which was quite stimulating and seemed to go beyond what I had seen before.

I was thus looking for “complex”, but not intractable networks. . .

Artificial Neural Networks

In parallel to the biological study of the brain, the field of artificial intelligence, or more accurately “machine learning”, given our current capabilities, started investigating questions such as attention (Olah et al. 2016; Xu et al. 2015), intent, and consciousness (Russell et al. 1995; Searle 1980).

*trying to build
an artificial
intelligence?*

These two fields became closer and closer as perceptrons and Artificial Neural Networks (ANNs) were discovered. With ANNs, computer scientists began to incorporate some of the biological knowledge on neurons to help machines become more “autonomous” (Marblestone et al. 2016). On the other hand, could we, by finding ways to implement cognitive mechanisms *in silico*, gain some insights into potential biological mechanisms? As technology and theory advanced, more complex networks were used, up to the current *deep learning* methods which reproduce the principle of

¹ Optimality in the brain is always considered with respect to some constraints, either wiring length, energy consumption. . . and is probably not optimal at all from an “absolute” perspective.

a modular and hierarchical brain encoding more and more abstract information and concepts in higher layers.

Other machine learning technics, such as *reservoir computing* (Lukoievius et al. 2009), were also inspired by biological neuronal systems, which decided me to start my Masters internship in the team of Peter Dominey, investigating how the structure of the reservoir and the learning rule might impact the efficiency of the algorithm.

The hope for these methods was that, by finding general principles for computation and analysis, we would obtain leads as to how our brain processes information, generalizes concepts, and makes decisions. ANNs indeed led to considerable progress in what machines could do without requiring human intervention, even enabling them to outperform humans at chess, go, managing problems... However, these feats were significantly conditioned by improvements in hardware performance, as no theoretical breakthrough was encountered so far, and the energy efficiency of current machine learning methods are still quite far from narrowing the gap with the brain². The reasons behind the emergence of computing capabilities thus stay elusive, and most machine learning techniques remain quite distant from biological mechanisms.

1.1.2 Neuronal cultures and devices

Part of the complexity of the brain comes from its intricate 3D structure, which deeply influences the connectivity of the neurons. Another problem lies in the fact that neuron or areas in the brain can seldom be studied in isolation but are generally subjected to a large number of incoming stimuli.

However, starting in 1880 with Wilhelm Roux and confirmed by Ross Harrison first culture of frog neurons (Harrison 1907), the ability to cultivate neurons changed this fact. For the past 15-20 years, protocols for long term cultures of primary mammalian neurons (Beaudoin et al. 2012; Potter et al. 2001) have enabled researchers to use neurons that are embedded in much simpler, 2-dimensional networks, as new case models. This led to tremendous simplifications in how the system can be studied, controlled, and monitored. From then on, it was at last possible to study the processes of real biological units without the topological complexity of the brain and in “isolation” from unwanted stimuli.

simplifying the system

Through this new system, it now seemed possible to bridge the gap between computer science and neuroscience, trying to harness the power-efficiency and adaptability of biological units to reproduce and adapt computational principles that had been investigated on their silicon-based counterparts.

Yet, as a former PhD student in the NeuroPhysics group once said:

“ Leaving well-behaved models and semi-conductors for the realm of biology is easier said than done. ”

Renaud Renault

² the observation of the discrepancy between brain and machine consumption is in fact a significant argument in favor of neuromorphic hardware, which might provide a way around the energy wall (Hasler et al. 2013).

*how to
compute with
simple
networks?*

Indeed, to reproduce the complexity of current artificial circuits such as perceptrons, reservoir computing, or multi-layer networks, many technical problems must first be overcome, in order to answer these fundamental questions: starting from a single neuronal cell, how can one build a structure capable of processing signals in a predefined and reliable way? What is required to compute with biological neurons?

Making, observing, stimulating

To answer these questions, one must first make the culture, then keep the neurons alive in order to record and analyze their activity.

Many protocols exist to obtain neuronal cultures; the neurons used in this study were primary cells, i.e. obtained directly from the animals (Beaudoin et al. 2012), then dissociated. However, direct brain slices can also be used (Humpel 2015; Mathis et al. 2011) and other cultures are derived from stem-cells (Darville et al. 2016) or other immortalized neuronal cell lines (Amini et al. 2013). Once the neurons are obtained, they are put in a growing and nutritive medium where they develop and form the network; details on the plating and media can be found in “Culture preparation and feeding procedures” (section E.1).

Once the neurons are in the culture, their electrical activity can be observed directly by patching them with electrodes; such technique led to significant improvements in our understanding of single neuron behavior, but becomes limited when large networks are involved. However, the planar nature of most cultures makes them easily recorded by a Micro-Electrode Array (MEA), generalizing the previous principle to many cells at a time³; the cultures can also be observed under the microscope, in order to observe the neuronal development. Optical and electrical recording thus showed that, after 5 or 7 days, the network becomes connected enough for collective activity to emerge.

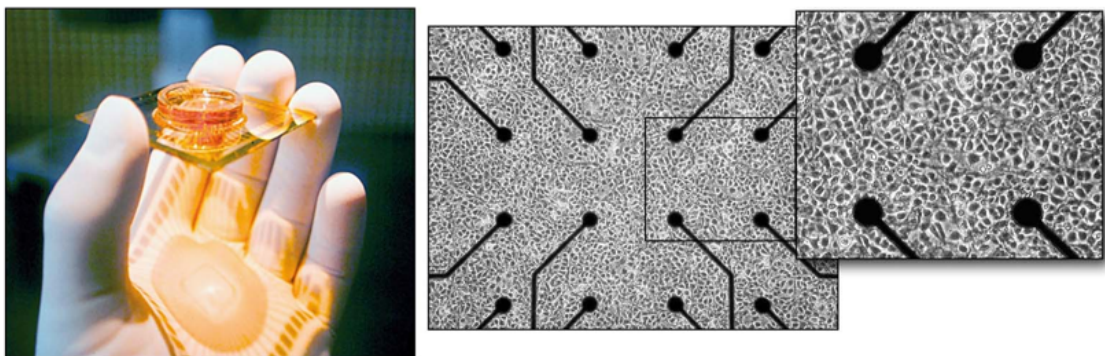


Figure 1.1.: MEA culture dish and zoom on the electrodes.

These arrays are generally composed of 10-micrometer electrodes which can stimulate the tissue-and track the response. The picture shows a 1-week old culture of ~ 50000 neurons and glial cells from embryonic rat cortex, growing on an MEA and forming a dense network 1–2 mm across. Fifty-nine $30\mu\text{m}$ electrodes spaced at $200\mu\text{m}$ intervals connect a few hundreds of the network’s neurons to the outside world, by allowing their activity to be recorded or evoked by electrical stimulations. Original figure from Bakkum et al. 2007

³at the cost of moving from intra to extracellular recording, which leads to a decrease in the precision with which the variations of the potential can be measured.

*first, build and
characterize
the system*

Apart from electrical recordings, fluorescent probes can be used to optically monitor the neuronal activity, making neurons light up when they activate. Such microscopy techniques enable one to obtain more detailed spatial information and to combine several optical probes; they can thus often give more information, compared to electrode-based recordings, but have lower temporal resolution and sensitivity, making it difficult to discern single spikes; furthermore previous calcium indicators were toxic for the cells, preventing long-term recordings of cultures. New probes have improved temporal resolution and are genetically encoded so that they do not affect the cells anymore; however, with the recent progress in CMOS-MEA technologies, the two main advantages of calcium imaging in cultures would be to couple morphological and activity-recordings, and the concurrent use of calcium reporters with other probes, e.g. to identify which neurons are inhibitory (DeRosa et al. 2015).

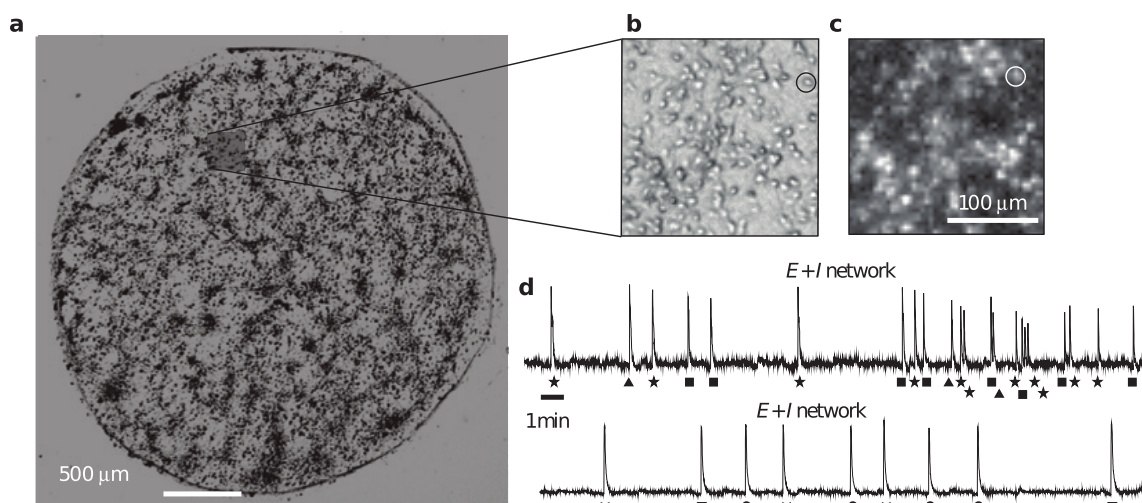


Figure 1.2.: Optical recording of a neuronal culture using Ca^{2+} .

(a) Bright-field image of a circular culture, grown on glass, containing about 3000 neurons. (b) Inset showing a subarea of the culture and the distribution of neurons inside. The circle identifies a single neuron. (c) Corresponding fluorescence image during a spontaneous activity event. Bright spots are firing neurons. The resolution of the image is the same as the actual measurements. (d) Fluorescence signal from a 30-minute recording of the spontaneous activity in the culture shown in a, averaged over the 500 brightest neurons. Figure adapted from Orlandi et al. 2013.

In both MEAs and calcium imaging, the observation setup can often simultaneously be used to stimulate the neurons locally, both in time and space, enabling the precise study of the neurons' and network's response functions.

*then interact
to probe
further*

Complex circuits and devices

In the past decade, protocols to culture neurons over long timescales have been refined, to the extent that obtaining networks and keeping them alive is no longer an issue. In parallel, researchers therefore started investigating how to interact more extensively with the neurons, developing new methods to stimulate them, but also to guide the development of the neurons, in order to obtain specific patterns of connectivity in the network.

*progressively
increase the
complexity*

Thanks to progress in microfluidics and chemical patterning, it is now possible to design complex structures which spatially segregate neurons into distinct populations while directing the connectivity in a precise and reproducible fashion. Figure 1.3 gives examples of prototypes of such devices.

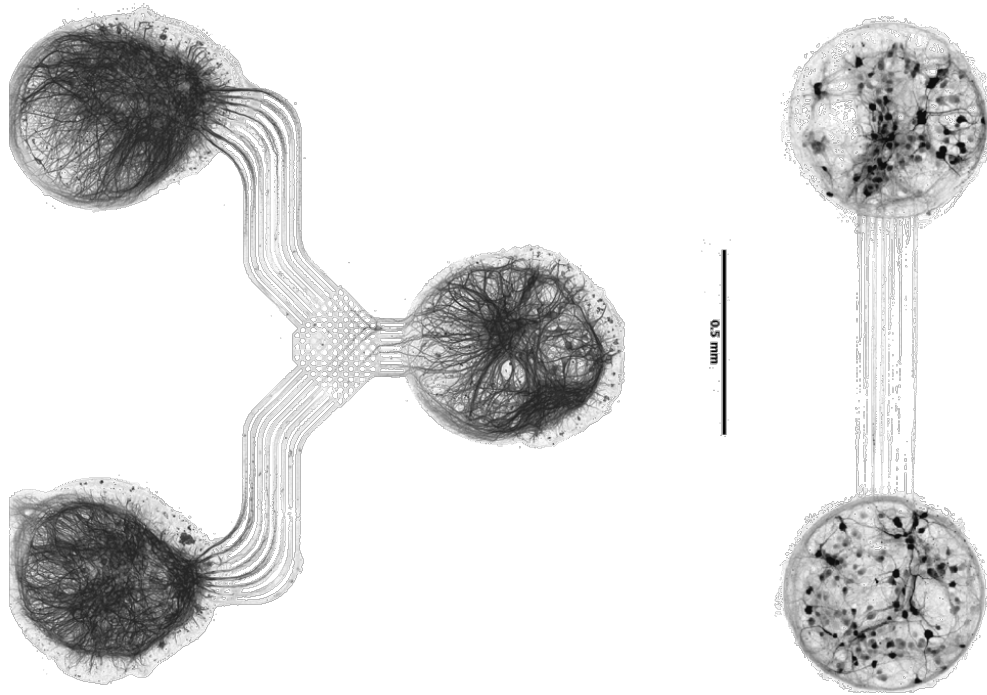


Figure 1.3.: Proof of concept for neuronal devices.

Right device represents the basis of a neuronal diode, with two chambers linked by asymmetrical funnels — wide top entrance and narrow bottom entrance — which allows neurons from the top chamber to project axons to the bottom chamber by prevents neurons from the bottom chamber to project back. Left device shows a three-chamber devices with a “multiplexer” guiding the axons towards the right chamber. Image adapted from Renault 2015.

This new ability of shaping the network connectivity at the level of populations and not individual neurons enables both a good reproducibility from a statistical standpoint, and the study of interactions at a larger scale compared to the previous neuron-neuron communications.

Fundamental and medical implications

Thanks to neuronal cultures, many medical advances were made in drug testing, modeling of viral infections or neurodegenerative diseases (Amini et al. 2013; Costa et al. 2011; Schlachetzki et al. 2013). They have also brought a significant amount of fundamental knowledge on the physiology of neurons, their development, but also on more global properties such as circuit formation or short term synaptic plasticity. Furthermore, since they typically display epileptiform activity, which will be one of the central theme of this thesis, neuronal cultures are seen as a promising way of improving our understanding of epileptic activity (Dichter 2009).

*understanding
epileptiform
activity*

Moreover, the ability to design more complex neuronal devices, with different activity patterns, or precisely tuned bursting frequency, could also provide new perspectives in the field of neuroprosthetics⁴. For instance, medical protocols such as the Vagus Nerve Stimulation (VNS) or Spinal Cord Stimulation (SCS) have been used to treat epilepsy (Ben-Menachem et al. 2015), chronic pain (Deer et al. 2014), or to recover some motor function after paralysis (Ievins et al. 2017). Though such treatment are not exempt of risks (Mekhail et al. 2011), their efficiency has been conformed by numerous studies, and if neuronal devices can enable more physiological stimulation methods, this might help reduce the severity of potential complications.

*improving
neuro-
prosthetics*

Eventually, aside from potential applications in neuroprosthetics, neuronal devices also provide case models to study the propagation of neuro-degenerative diseases (Takeda et al. 2015), axonal regeneration (Tong et al. 2015), or more generally, the propagation of signals on complex structures.

*diseases and
signal
processing*

1.1.3 A thesis in computational neuroscience

And this is how I decided to do a PhD in computational neuroscience, focusing on neuronal cultures and devices. I found a nice lab in Paris, started discussing and writing a project, and this manuscript is the result, 3 years later. So let me try to contextualize all this in a nutshell.

First of all, what is computational neuroscience? Historically, the field progressively emerged and gained importance with the development of computer science. It gradually became known as *cybernetics*, with studies on neurons and networks by researchers such as von Neuman (Neumann 1956), McCulloch and Pitts (McCulloch et al. 1943), or Arbib (Arbib 2018), and was eventually defined as *computational neuroscience* in the eighties–nineties, for instance by Eric Schwartz:

“ Computational neuroscience might be characterized as that area of overlap between neuroscience and computer science which required sufficient specialized expertise to justify a new subdiscipline. ”

(Schwartz 1993)

However, the scope of a field can obviously change in time and, as overlapping notions between neuroscience and computer science is getting wider and wider, more and more people would now provide a significantly different definition, such as

“ Computational neuroscience is the theoretical study of the brain to uncover the principles and mechanisms that guide the development, organization, information processing, and mental abilities of the nervous system. ”

(Trappenberg 2010)

Indeed, since computer science is intricately associated to many scientific fields, defining computational neuroscience through an overlap does not seem to really make sense anymore, even though it was not purely restricted to methods but also to a way of approaching “neuronal algorithmics”.

⁴ also called neural prosthetics (Shenoy et al. 2012), these prostheses are aimed at restoring motor functionality in patients suffering from neurological injuries or disorders. See also the wikipedia page on neuroprosthetics for additional examples: <https://en.wikipedia.org/wiki/Neuroprosthetics>.

computational neuroscience as the study of computation in the brain

In this manuscript, I will be referring to computational neuroscience as a *subpart of neuroscience focused on understanding and modeling how computation and signal processing is performed by single neurons or brain-cell assemblies.*

This definition aims at grouping together studies sharing a similar goal (the understanding of computation, as opposed to development, or diseases) but not necessarily with similar methodologies or technical aspects.

However, given that many of these studies belong to theoretical neuroscience, two important issues are the quality and availability of the computational material (model, software, and algorithms) and the relation between the models and the current experimental capabilities. As for the first part, many people (Manninen et al. 2018; Nordlie et al. 2009) have already stressed the importance of implementing workflows to ensure that:

providing open, reliable, and reproducible material

- a study can be replicated (results can be obtained again by rerunning the code provided by the authors),
- the models can be reproduced using different software thanks to the model and code descriptions,
- if deemed useful, the code is clear and documented enough so as to be reusable by others in a different study.

In that perspective, I must say that, apart from my theoretical work, this PhD actually included a large amount of computational and software engineering work to which this manuscript will not do justice. Indeed, they were designed only as tools to help me study more and more complex phenomena, not for themselves; the details of their internal routines and how I implemented, debugged, and tested them would be out of place in this manuscript.

However, I believe that this is a necessary dark side of computational neuroscience, and all I can hope for is that the open-source (Gleeson et al. 2017) software that I spent so many hours designing – trying to apply the good practice methods I mentioned above – will eventually prove useful to future studies and researchers.

with a few additional objectives

Regarding the second topic, one of the questions I often hear is “how can we, theorists, make things go forward”? I am rather optimistic about this issue, as there are many ways to proceed (forward is vague enough after all. . .); for instance one can

- tackle research debt⁵ by improving existing models, building simple and clear theoretical frameworks or unified descriptions for phenomena. . .
- provide new and experimentally-testable hypotheses to actually get answers (or new questions) on these phenomena;
- design new tools when needed (make them, make them good, make them free).

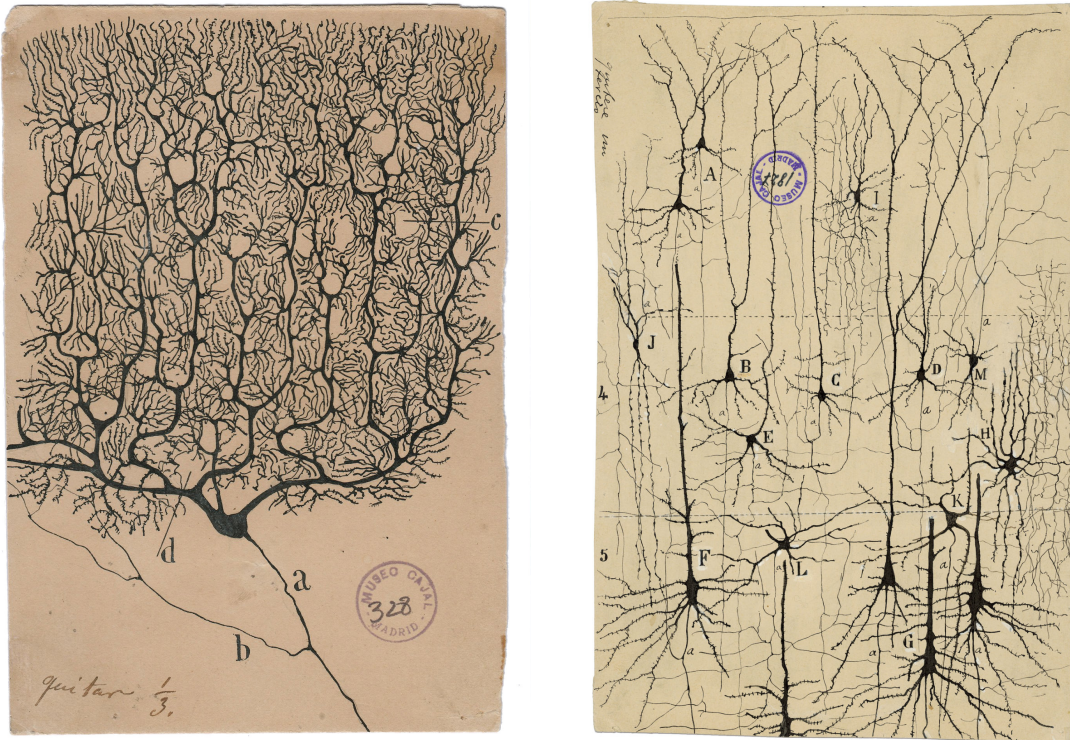
⁵<https://distill.pub/2017/research-debt/>

This was basically my endeavor these past three years: help improve a little our understanding of how computation is performed by brain cells through simple mathematical frameworks, new computational tools — that I made as documented, reusable, and reliable as I could — and experiments or experimental proposals. And this is where we begin.

1.2 Brain cells

1.2.1 Neurons: structure and function

Brain cells, and neurons in particular, display very specific morphologies compared to most cells in other body parts. These morphologies are adapted to their specific function of information collection and transmission.



(a) Drawing of a Purkinje neuron, with its exuberant dendritic arbor. (b) Cortical layers including several pyramidal cells.

Figure 1.4.: Two of the first drawings of neurons by the pioneer artist and pathologist Santiago Ramón y Cajal, safeguarded by the Cajal Institute in Madrid, and duely stamped by Pedro Manzano.

neurons are shaped to receive and transmit signals

In fact, Cajal, the first person to ever see a neuron⁶, had the brilliant insights, just from looking at the cell structure, that neurons passed electrical information in only one direction, and communicated together at small, localized places, the *synapses*.

Indeed, we now know that neurons (also called nerve cells) are excitable cells which are able to receive and transmit electro-chemical signals. As shown on Figures 1.4 and 1.5, neurons gather incoming signals from their neighbors through rootlike *dendrites*. These signals are then integrated inside the *soma* and in the region of the *axon hillock*; depending on the context and on their strength, the neuron will then choose to transmit or not a new signal via a longer terminal, the *axon*.

⁶ Santiago Ramón y Cajal, in the years 1890s, used a small microscope, working by gaslight, and observed thin slices of brain tissue, which he had previously subjected to a silver-staining solution. He discovered not the continuous network expected at the time, but a set of individual cells connected together: the neurons. Read more on the online article from Fields 2017.

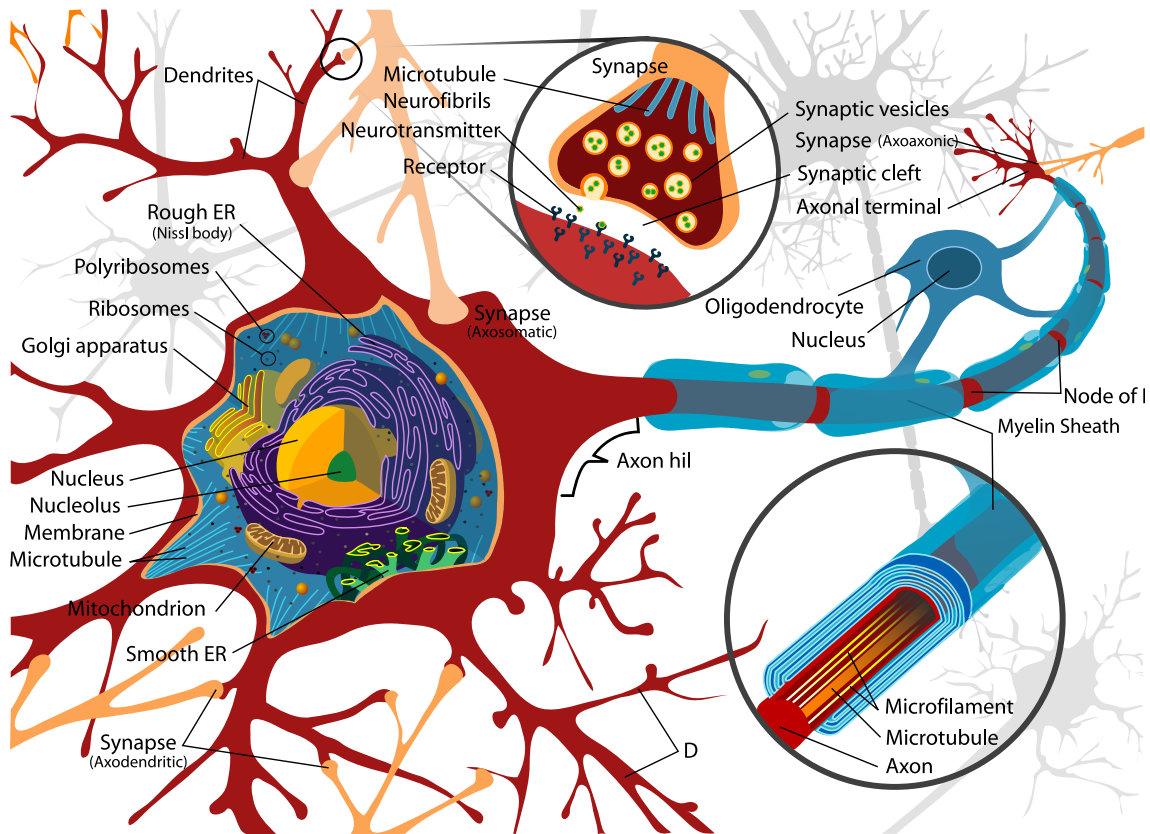


Figure 1.5.: Schematics of a neuronal cell in the central nervous system. Internal organelles (endoplasmic reticulum (ER)...) visible inside the cell body, or soma; are common to all animal cells. However, the long protrusions coming out of the cell, which differentiate into the dendrites and the axon, are specific to neuronal cells. Adapted from Wikimedia commons, public domain images by LadyofHats and Andrew c.

To improve the speed and reliability of the signal's propagation, the axon can be covered in a sheath of myelin; however, myelination is not present on all axons, nor necessary if signals are conveyed over small distances.

The signals transmitted are conveyed under the form of localized electric waves, which progress along the axons and dendrites. In the axon, they can be transmitted from one neuron to the next at *synapses*, where the information is “converted” to chemical signals which cross the inter-cellular space to reach the membrane of the target neuron, where they are converted back to electric waves.

1.2.2 Neuronal development: from seed to tree

To generate the intricate structure of a neuron, the cell undergoes a multi-stage development from an initial ovoid or slightly elongated shape to reach its final arborescent structure.

Polarization

The first stage, which is especially visible in *in vitro* culture, is the progressive apparition of protrusions, making the cell appear “spiny”, cf. Figure 1.8.



(a) Stage 1 neuron.

(b) Stage 2 neuron.

(c) Stage 3 neuron.

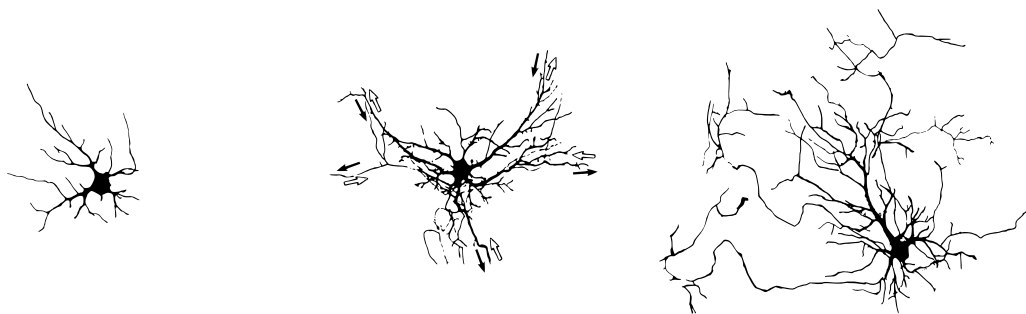
Figure 1.6.: Early development of a neuron: at stage 1 (a), the cell is only composed of a soma and small protruding filopodia; when it reaches stage 2 (b) the filopodia evolve into minor, unpolarized processes which compete with one another until one undergoes axonal specification — stage 3 (c) after 1.5 to 3 DIVs. At that point, the axon elongates more significantly while the outgrowth of the other neurites (the dendrites) is less pronounced. Neuron morphologies are taken from (Baj et al. 2014).

These immature neurites first compete with one another until one prevails and differentiates into the axon. This special neurite elongates faster and often longer than the others.

The formation of the neuronal processes — dendrites and axon — is made possible by the action of intracellular filaments which compose the cytoskeleton and maintain the underlying structure of the axon and dendrites.

*biopolymers
support these
elongated
processes*

Among the filaments involved in the neuronal morphogenesis, the main actors are two polymers: *actin* and *microtubules (MTs)* (Coles et al. 2015; Conde et al. 2009). The former forms rather flexible filaments, which are mostly responsible for the initial protrusion of filopodia and lamellipodia during stage 1. The latter is more rigid and bundles into shafts which support the elongated tubular structure of the neurite, especially in axons where they form homogeneous bundles with a single polarization, leading to even more rigid and resilient structures (Sakakibara et al. 2013).



(a) Neuronal outgrowth.

(b) Dynamic period.

(c) Mature neuron.

Figure 1.7.: Later development of a neuron: after 4 DIVs, steady elongation and branching of the neurites occurs (a); once the arborescence of the structure is established, neurons often undergo a dynamic phase (b) of successive elongation and retraction of the branches (black and white arrows), where some are selected and others will be pruned. Eventually, the established branches are stabilized (c) and resume their elongation until the final shape is obtained. Neuron morphologies are taken from (Baj et al. 2014).

Neurite outgrowth

Once the neurites are differentiated into axon and dendrites, both start elongating and branching to form the arborescent structure which characterizes neurons. This phenomenon, however, is not continuous but interspersed with numerous periods of retraction or pausing which are tightly linked with the cytoskeletal, and especially the MTs dynamics (Coles et al. 2015).

Though the principles of this development may first appear rather straightforward, subtle variations in the proportion of the mechanisms involved will lead to vastly different structures, as one can see on Figure 1.4. One of the central goal of this thesis will thus be to provide simple models which should allow to study these phenomena through a generic and efficient simulation tool, as will be developed in “Accounting for neuronal development” (chapter 4).

1.2.3 Companions: glial cells

Despite our focus on neurons, they are not the only cells in the Central Nervous System (CNS). Far from it, actually, since *glial cells* or *neuroglia* represent half of the brain and spinal chord volume.

These cells are mostly divided into *oligodendrocytes* (76%), *astrocytes* (17%), and *microglia* (7%), which serve crucial role to maintain the brain in a fully functional state.

Oligodendrocytes are mostly involved in axonal myelination in the CNS, allowing fast and lossless transmission of electric signals over large distances. Astrocytes play a crucial role in calcium propagation, potassium regulation, and are tightly associated to synapses, in a structure called *tripartite synapse*. Microglia are much smaller cells compared to neurons, oligodendrocyte, and astrocytes; they are mostly macrophages and constitute the main active immune defense in the CNS.

Although these cells play a very significant role, we will mostly ignore their presence in this study. In neuronal cultures, oligodendrocytes and microglia are usually scarcely present anyway (axons are not myelinated), so only the presence of astrocytes is really significant and we will only consider their presence by acknowledging that their work in redistributing and buffering ions is done properly and keep the extracellular concentrations homogeneous and roughly constant everywhere.

glial cells play an active role in neuronal networks

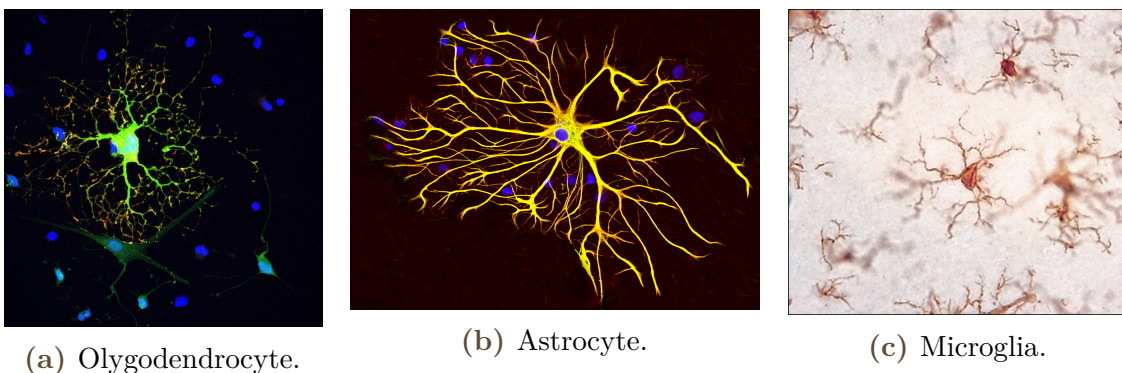


Figure 1.8.: Example of glial cells in the CNS. (a) is from EuroStemCell; (b) is taken from Wikimedia commons, and originally posted by GerryShaw; (d) is from NeuroscienceAssociates.

1.3 Neuronal dynamics

In this section, I will briefly introduce the electrophysiological principles which enable neurons to process and transfer information, and describe how such behavior can be reproduced by concise mathematical models.

1.3.1 The biological reality

As communication between neuronal cells is electro-chemical, the cells must be able to regulate or induce changes in their membrane potential. The potential of this membrane is defined by the imbalance between the concentrations of ions inside the neuron and in the extracellular medium.

To change the value of the membrane potential V_m , the neuron must therefore change the inner ion concentrations. To that end, numerous pumps and passive ion channels are embedded in the membrane to allow or force sodium, potassium, chloride, or calcium to flow in and out of the cell.

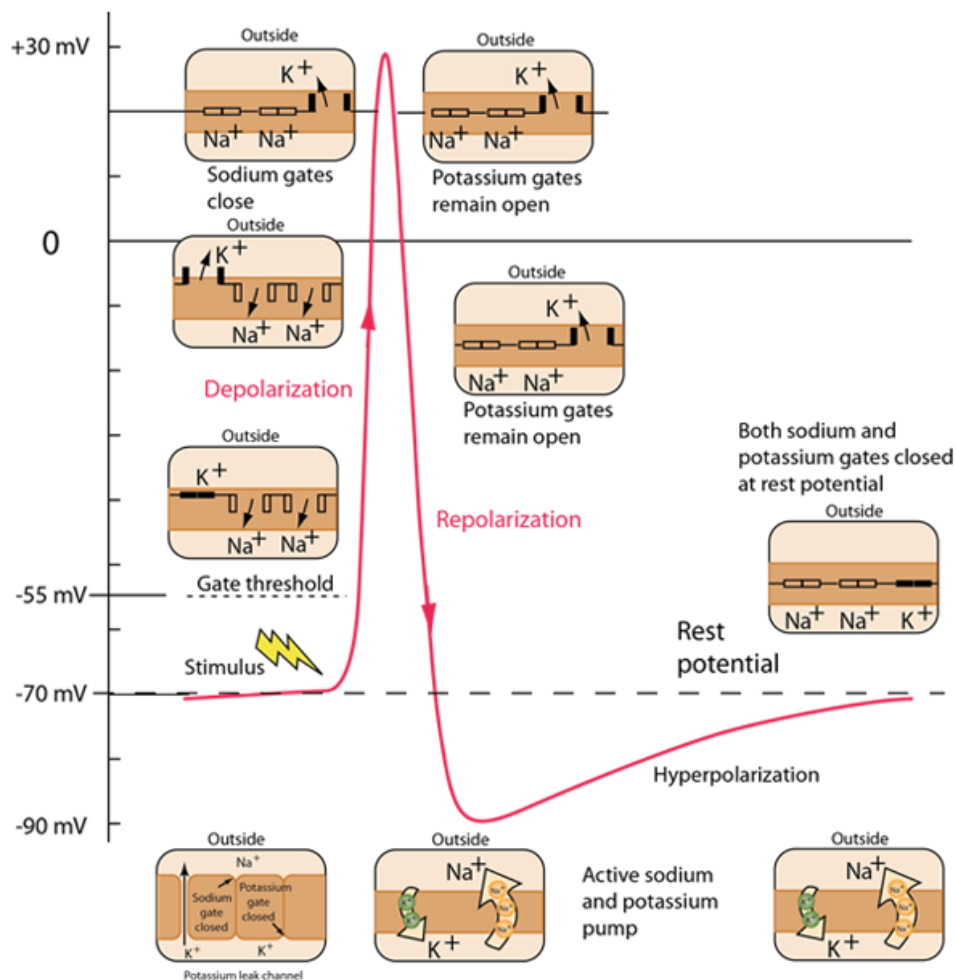


Figure 1.9.: Schematics of the obtention of an action potential by the opening and closing dynamics of the sodium and potassium voltage-gated channels. Rise and fall times of V_m are typically 1 to 2 ms. Image from HyperPhysics.

Sodium (Na^+) currents tend to depolarize the cell towards less negative values of V_m , while potassium (K^+) currents tend to hyperpolarize the cells, bringing V_m to more negative values.

At rest, the neuron typically balances the ion concentration to maintain its potential around -70 to -60 mV. However, when the neuron receives a sufficient amount of excitatory inputs, it locally generates a very significant depolarization which is then actively propagated without loss along the whole axonal length: the *action potential* or *spike*.

Figure 1.9 provides a very simplified view of the mechanisms involved in action potential generation, with the opening and closing of sodium and potassium channels causing the sharp rise and fall of the membrane potential. Here, both channels are called voltage-gated because their opening occurs once the membrane potential crosses a given threshold.

However, other ions also flow in and out of the cell during the action potential. In particular, calcium (Ca^{2+}) ions flow into the cell around the peak of the action potential and is responsible for many crucial mechanisms. As will be describe in “Chemical connections: synapses” (subsection 1.4.1), it enables the release of synaptic vesicles, which conditions the proper transmission of the signal from one neuron to the next.

But calcium also plays a second role which will be of primary importance in the rest of this study. Indeed, not all channels are voltage-gated; some rely on the presence of a chemical molecule to trigger their opening. This phenomenon is present in synapses, but also in the main cell body, where calcium binds to several channel receptors to trigger potassium outflow.

These calcium-gated channels are quite significant because they possess temporal dynamics that span much wider duration than the voltage-gated channels involved during spike generation. They are involved in a phenomenon called After HyperPolarization (AHP), which results, during some time following the spike, in a lower excitability of the neuron. Almost all neurons possess a refractory period which follows the action potential, usually stemming from the slightly slower dynamics of the K^+ -channel which continues to let potassium out for some time after the membrane potential has repolarized to values lower than the resting potential — cf. Figure 1.9. This “standard” phenomenon typically lasts a few milliseconds longer than the spike duration, but remains overall quite short. Calcium-gated potassium channels, however, can remain open for several hundreds of milliseconds, or even on the order of a few seconds, providing a long-term modulation of the neuronal dynamics.

Though the conductance of these long-lasting currents is generally small, they can become quite significant during periods of intense activity, which explains why they will play such a central role in our study of epileptiform bursts of activity in neuronal cultures — cf “The influence of neuronal adaptation” (section 2.2).

1.3.2 Neurons as excitable units

If we simplify its behavior to the core, a neuron can be seen as a simple excitable unit that is characterized by two states: an inactive, resting state, and an active, excited state.

*excitability
partially
characterizes
a neuron*

Depending on its type, a neuron will either spontaneously switch between these two states, the inactive state remaining the most prevalent, or it will require some additional input to be able to transition to the excited state. Regardless of its type, a resting neuron can be forced to switch to the active state when subjected to an external stimulation. The strength of the input that is required to trigger this transition can then be used to characterize the neuron through a property that we will define as its “excitability”.

1.3.3 Simple models for spiking neurons

Together with his book, “Dynamical Systems in Neuroscience” (Izhikevich 2007), this article from Izhikevich 2003 is one of the research materials that inspired me most when I was trying to find where I might fit in scientific research.

This section describes how neurons can be modeled as simple dynamical systems that allow us to visually represent their behavior and understand them both qualitatively and quantitatively.

I will first introduce the 2D neuronal model that will be used throughout the manuscript, then introduce the notions of restlessness and susceptibility to use them on a few examples of typical neuronal activities. I will especially precise the notion of pacemaker neuron, which is characterized by constraints on the neuronal parameters, leading to specific statistical properties on the spiking behavior.

Integrate-and-fire models

Expanding a little the two-state model of an excitable unit, one can describe the transition between the two states by looking at the mechanism explaining most of this transition.

Indeed, if the active state is the short timeframe around the peak of the action potential — cf. Figure 1.9 — then transitions between active and inactive are conditioned by the value of the membrane potential compared to a threshold⁷. Linking the properties of the neuron to equivalent electrical circuits, scientists thus proposed a very simple model⁸, assimilating the neuron to a capacitor associated to a comparator: the neuron “charges” up to a certain value at which it suddenly discharges and sends a spike. The mathematical formulation of this model, called integrate-and-fire models, reads:

$$C_m \dot{V}_m = I(t) \quad \text{if } V_m < V_{th} \quad \text{else } V_m \leftarrow V_r, \quad (1.1)$$

where:

$\dot{V}_m = \frac{dV}{dt}$ is the time derivative of the membrane potential,

C_m is the membrane capacitance,

$I(t)$ is the total input current arriving at the soma at a time t ,

V_{th} is the threshold potential,

V_r is the reset potential.

⁷ In the simple description of the spike generation by only voltage-gated channels.

⁸ see review by Brunel and Van Rossum 2007

Note that during the rest of this study, the membrane potential V_m will simply be written V for simplicity.

The sudden reset of the membrane potential when the threshold is reached marks the emission of an action potential, which is not described by the model. Such models thus require additional equations to account for information transmission between neurons and usually only aim at describing the cell's response to an excitation; we will see in the next section — “Chemical connections: synapses” (subsection 1.4.1) — how to account for information transfer and coupling between cells.

The adaptive Exponential Integrate-and-Fire model

Following the seminal paper of Lappicque on the integrate-and-fire models, the model was properly formulated later (Brunel and Van Rossum 2007), then many other models were developed to describe neuronal dynamics. Not all them followed the integrate-and-fire models framework, starting from the one which is probably the most well-known, the Hugkin-Huxley model (Hodgkin et al. 1952).

However, integrate-and-fire models have several advantages over a priori more realistic, continuous models, notably for simulation and analysis purposes.

Indeed, using such models, the spike times are intrinsically and easily determined; furthermore their low dimensionality enables to visually represent and analyze their dynamics.

This study will thus be performed using an extended version of the simple integrate-and-fire models, introduced by Brette and Gerstner 2005, which builds on the adaptation principles introduced by Izhikevich 2003 and the improved exponential spike generation proposed by Fourcaud-Trocmé et al. 2003⁹.

In this model, the state of the neuron is described by two variables: the usual membrane potential, V , and a second variable, w , which accounts for adaptation currents flowing in and out of the neuron. Because of this, the model is able to account, at least partly, for the AHP mechanisms mentioned above — “The biological reality” (subsection 1.3.1).

The equations of the Adaptive Exponential Integrate-and-Fire (AdExp) model read:

$$\begin{cases} C_m \dot{V} = -g_L(V - E_L) + g_L \Delta_T \exp\left(\frac{V - V_{th}}{\Delta_T}\right) - w + I(t) \\ \tau_w \dot{w} = a(V - E_L) - w \end{cases} \quad \text{if } V \geq V_{peak} \quad (1.2)$$

$$\text{else, if } V > V_{peak}, \text{ then } \begin{cases} V \leftarrow V_r \\ w \leftarrow w + b \end{cases} \quad (1.3)$$

This model is able to reproduce a large set of neuronal dynamics observed *in vitro* and *in vivo*¹⁰ and in particular, neurons displaying spike-triggered adaptation, as well as pacemaker neurons. The wide range of possible dynamics is notably enabled by the presence of two different timescales, one for the adaptation current, τ_w , and another for the membrane potential, given by

$$\tau_m = \frac{C_m}{g_L}, \quad (1.4)$$

with, in general, $\tau_w \gg \tau_m$.

⁹ see also Touboul et al. 2008 for details on the relevance of the exponential spike generation compared to the quadratic model of Izhikevich.

¹⁰ see “Simulating networks of spiking neurons” (Appendix D) and Naud et al. 2008.

Excitability, restlessness, and susceptibility

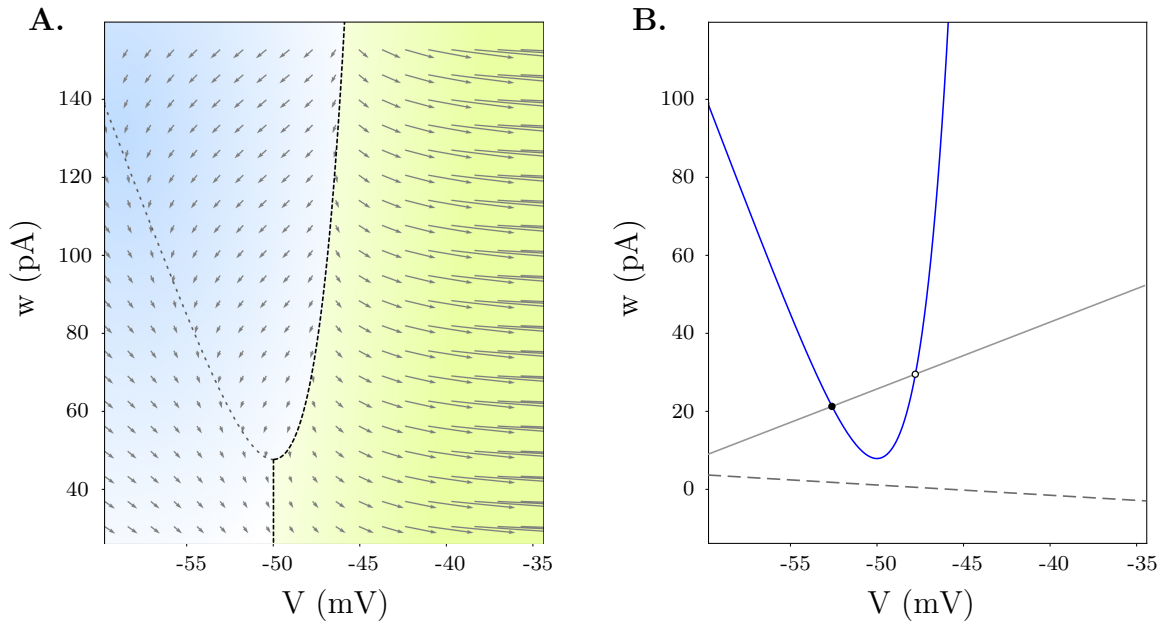


Figure 1.10.: **A.** Visualisation of the susceptibility of a neuron depending on its current state. The susceptibility values are indicated by the color gradient (negative in blue, null in white and positive in green); the limits between the domains is qualitatively given by V_{th} and the leftmost part of the V -nullcline, which is indicated by the black dashed curve. The arrows represent the vector (\dot{V}, \dot{w}) which gives the speed and direction of the flow in phase-space. **B.** The phase space of a resting ($Rl < 0$) and restless ($Rl > 0$) neuron are shown respectively in solid and dashed lines for the w -nullcline. For the resting neuron, the solid w -nullcline intersects the blue V -nullcline in two points, the stable resting point (filled black circle) and the unstable fixed point (empty circle). In the case of the restless neuron, there is no intersection between the dashed w -nullcline and the V -nullcline, hence no resting point and the neuron fires spontaneously in the absence of input.

In the AdExp model, which describes the adaptation currents through a single variable w , the excitability of the neuron can be qualitatively described as “how often and how easily a neuron fires”.

To refine this description, I will define here two dimensionless numbers, the susceptibility, Sc , and the restlessness Rl that will quantify the excitability of a neuron.

Let us first describe the susceptibility Sc as a characteristics of the short-term response of a neuron to an excitation. By short-term, I imply here a response on a timescale dt which is typically smaller than τ_m . At this timescale, the value of the susceptibility Sc will let us determine whether the neuron will spike spontaneously or not. Indeed Sc describes how quickly the membrane potential will increase after the neuron has been subjected to the minimal excitation necessary to make it go over threshold and fire¹¹.

*susceptible
neurons fire
easily*

Let us suppose that, compared to the neuronal timescale τ_m , all the excitation is delivered almost instantly ($\tau_e \ll \tau_m$). In that case, this is equivalent to delivering a

¹¹see “Excitability, restlessness, and susceptibility” (Appendix B) for more details on susceptibility and its underlying hypotheses.

charge Q which will increment the voltage by $\Delta V = \frac{Q}{C_m}$.

In that case, what we want is to find the charge Q necessary to get $V + Q/C_m \geq V_{th}$ and $\dot{V} \geq 0$, with $Q = 0$ if both $V \geq V_{th}$ and $V(V, w) \geq 0$.

We will then define the instantaneous susceptibility of a neuron in a state (V, w) as

$$Sc = \dot{v} - q \quad (1.5)$$

with \dot{v} the dimensionless voltage derivative at $V + \Delta V$, and q the dimensionless charge—see “Neuronal dynamics and the AdExp model” (Appendix A) and Eq. B.11 for the analytic expression.

The susceptibility is therefore an instantaneous variable that does not characterize a neuron, but only its state at a given time. Neurons that are in a state of negative susceptibility will thus require an additional excitation to spike, and that excitation will need to be greater as the magnitude of Sc increases. On the other hand, neurons that are in a state having a positive susceptibility will rapidly spike, even in the absence of an external excitation.

In order to characterize a neuron regardless of its current state, let us introduce the second variable, the restlessness Rl .

This number describes the spontaneous behavior of a neuron: it is negative if the neuron has a resting point and does not fire spontaneously; its is positive if the neuron spikes spontaneously. We will therefore define the restlessness as

*restless
neurons fire
spontaneously*

$$Rl = \begin{cases} Sc(V_{rest}, w_{rest}) & \text{if a resting point exists,} \\ f_0/1\text{Hz} & \text{otherwise.} \end{cases} \quad (1.6)$$

where $Sc(V_{rest}, w_{rest}) < 0$ is the susceptibility at the resting point, and f_0 is the average spontaneous frequency of the neuron in Hz

With that formula, we can divide the neurons in two categories:

- neurons with $Rl \leq 0$, which will need an external excitation to spike,
- neurons with $Rl > 0$, which will spike spontaneously, even in the absence of excitation.

A qualitative illustration of how Sc evolves depending on the state of the neuron, as well as examples of a resting and restless neuron are visible on Figure 1.10.

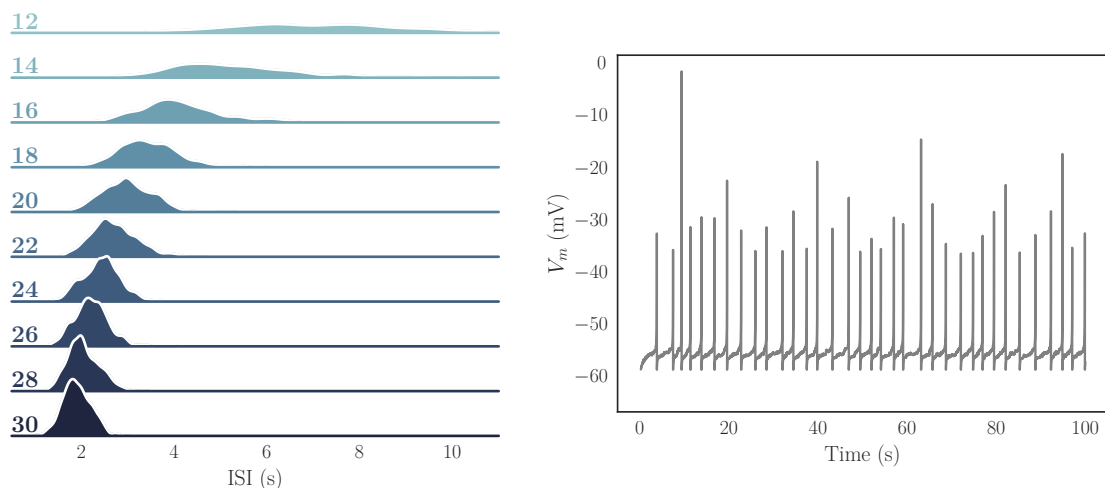
The notion of pacemaker neuron

In this study, neurons qualified as *pacemakers* will play a major role. These neurons are able to regulate their activity to produce very regular spike trains, with a well defined period which is resilient even with respect to significant noise levels.

Using the AdExp model, such neurons can be modeled using negative values for the a parameter. This negative coupling between V and w reproduces the behavior of persistent sodium currents ($I_{Na,P}$), which have been associated to pacemaker behavior (Sipilä et al. 2006; Tazerart et al. 2008).

Such neurons belong to the type I class (Ermentrout 1996); they can fire spikes at arbitrarily low frequencies and their intrinsic dynamics is only slightly affected by noise — see Figure 1.11. However, the specificity of negative a values goes beyond the general properties of type I neurons¹². Indeed, as can be seen on Figure 1.12, the range of Inter-Spike Interval (ISI) that can be obtained with pacemaker neurons is much broader than for simple type I neurons. This difference is, however, mostly quantitative, since these neurons belong to the same class, while it is qualitative if we compare them to type II neurons (Figure 1.13), which display much more irregular spike train and start spiking at finite and not arbitrarily low frequencies.

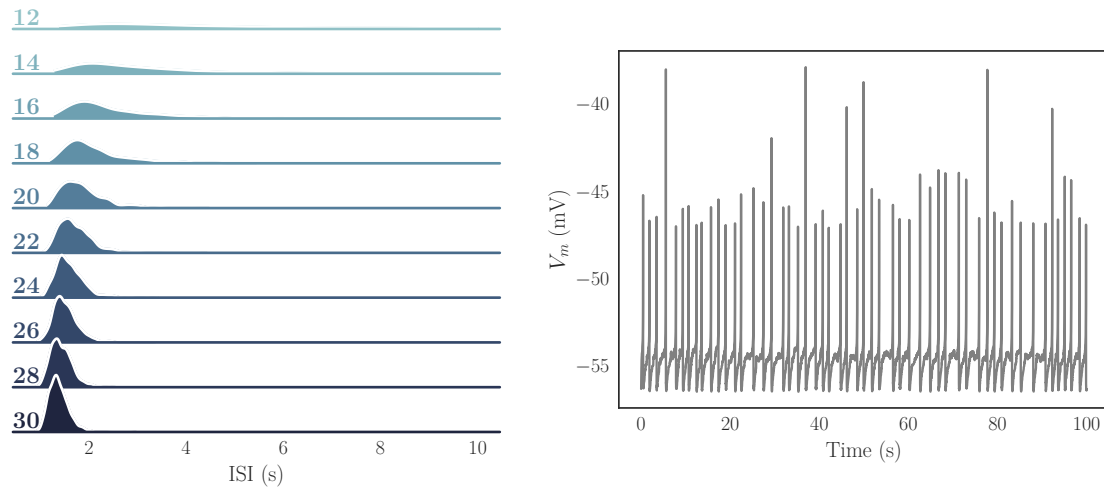
¹² See “Neuronal dynamics and the AdExp model” (Appendix A) for more detailed explanations on the negative a property and pacemaker neurons.



(a) Evolution of the interspike interval (ISI) distribution with noise frequency. The frequency in Hz is given on the left.

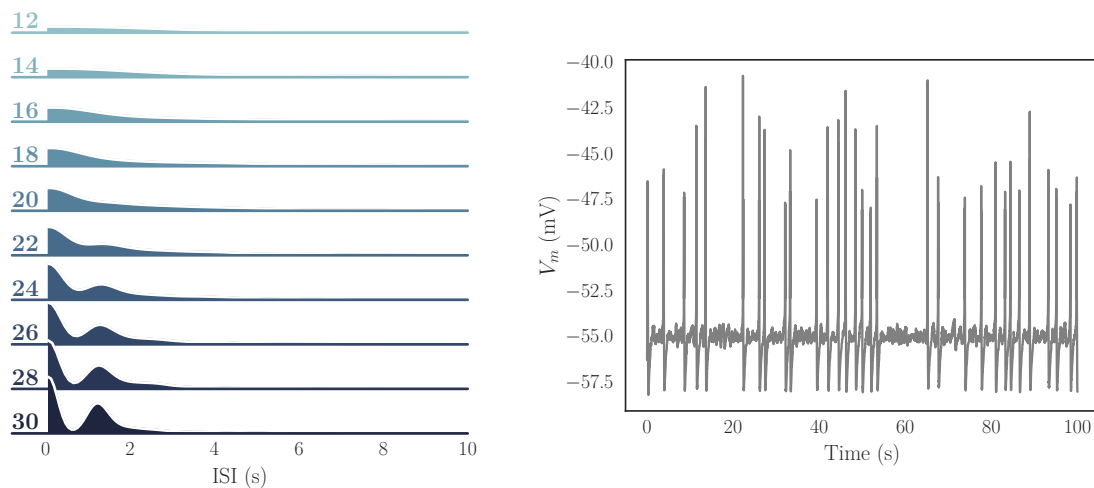
(b) Example of the time evolution of a pacemaker neuron subjected to a 20 Hz Poisson noise.

Figure 1.11.: Response of pacemaker neurons submitted to miniature spiking events following a Poisson distribution. Such neurons display a rather homogeneous activity and do not spike at arbitrarily high frequencies compared to non-pacemaker neurons.



(a) Evolution of the interspike interval (ISI) distribution with noise frequency. The frequency in Hz is given on the left. (b) Example of the time evolution of a type I non-pacemaker neuron subjected to a 20 Hz Poisson noise.

Figure 1.12.: Response of non-pacemaker neurons of type I, submitted to miniature spiking events following a Poisson distribution. Compared to pacemaker neurons, parameters still require some tuning to display such a wide range of firing rates upon variations of the noise, but much less precise than I neurons. Increasing noise rates quickly increase their firing frequency but it remains above a minimal rate, as for pacemaker neurons.



(a) Evolution of the interspike interval (ISI) distribution with noise frequency. The frequency in Hz is given on the left. (b) Example of the time evolution of a type II non-pacemaker neuron subjected to a 20 Hz Poisson noise.

Figure 1.13.: Response of non-pacemaker neurons of type II, submitted to miniature spiking events following a Poisson distribution. Compared to pacemaker neurons, the parameters of these neurons must be tuned very precisely to display such a wide range of firing rates upon variations of the noise. Increasing noise rates quickly makes them fire at high frequency.

1.4 Information transfer: connections between cells

In the previous section, we have seen some properties of intrinsic neuronal dynamics; however, much of the interest of neuronal behavior resides in its evolution from the properties of the single cell to those of the collective behavior once the cells are coupled inside a network.

We will therefore see here how neurons connect together and how these connections influence their dynamics.

1.4.1 Chemical connections: synapses

The main mode of connection between neurons is the chemical synapse, from which a glimpse was given on Figure 1.5.

For functional neuron-neuron connection, a synapse must be formed by the combination of two components¹³, a pre-synaptic site, stemming from the axon of the source neuron, and a post-synaptic site, which can be almost any region of the target neuron's membrane — cf. Figure 1.14. These two components are separated by a small gap of extracellular medium, the synaptic cleft.

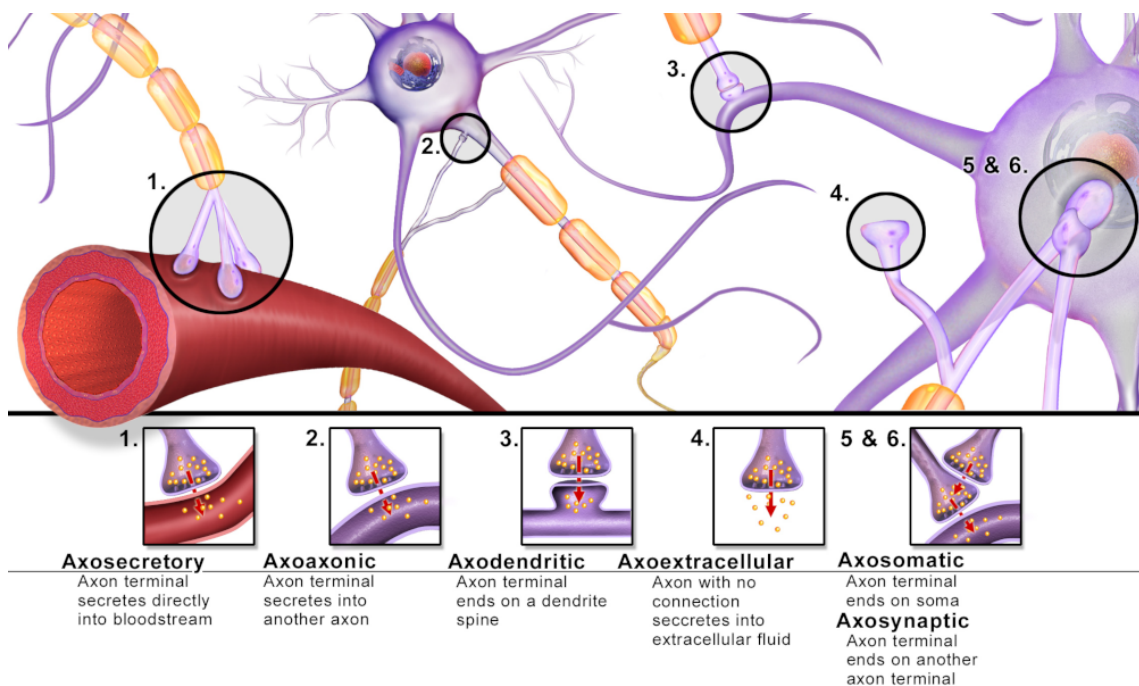


Figure 1.14.: Several synaptic types. Axoextracellular and axosecretory types will not be considered here. Original image from Blausen.com staff (2014). “Medical gallery of Blausen Medical 2014”. WikiJournal of Medicine 1 (2). DOI: 10.15347/wjm/2014.010. ISSN 2002-4436.

Neurotransmission

The pre-synaptic site contains synaptic vesicles, which are filled with *neurotransmitters*. Vesicles can occasionally be released spontaneously, and this phenomenon leads to the arrival of random inputs on the target neuron. Though synaptic noise is

¹³ As mentioned in “Companions: glial cells” (subsection 1.2.3), the reality is usually more complex, as astrocytes tend to interact tightly at the synaptic site to form *tripartite synapses*.

actually of significant importance, and will be mentioned again in “Burst initiation, deterministic or stochastic?” (subsection 2.1.1), it only accounts for a small fraction of the synaptic activity.

Indeed, most of the emission of synaptic vesicles occurs upon the arrival of an action potential at the synapse. The arrival of the spike triggers a local influx of calcium which enables the vesicles to bind to the membrane, fuse with it, and release the neurotransmitters they contain, in a phenomenon called *exocytosis* (Kaeser et al. 2014); this is the *synchronous release*.

The neurotransmitters then diffuse quickly in the synaptic cleft to reach the post-synaptic site, where they bind to specific receptors. Depending on their type, the neurotransmitters will either trigger a depolarization or a hyperpolarization of the membrane. Figure 1.15 shows the example of glutamate, the main excitatory neurotransmitter, which binds to AMPA and NMDA receptors.

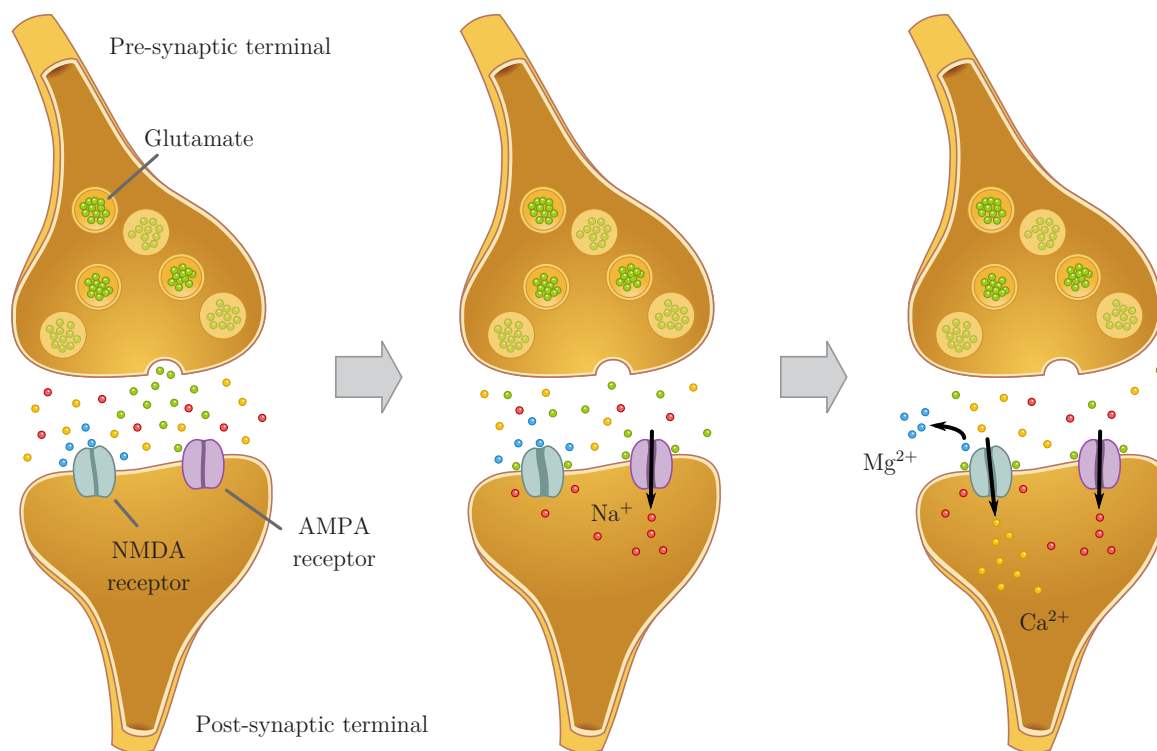


Figure 1.15.: Fast and slow excitatory transmission associated to glutamate. Glutamate binds AMPA and NMDA receptors upon release. This opens the AMPA channels which let Na^+ (red) flow inside the post-synaptic terminal. However, the NMDA channel remains blocked by Mg^{2+} (blue) until the depolarization caused by the sodium influx drives them away from the membrane. At that point the channel is fully activated and Ca^{2+} (yellow) flows in. This explains why NMDA channels activate later than AMPA and why they are considered as both glutamate- and voltage-gated. Image adapted from *LumenLearning* and *The Mind's Machine*.

In excitatory synapses, the fast AMPA receptor opens and let sodium ions flow inwards as soon as glutamate binds with it, leading to a fast local depolarization, which will generally be relayed passively down to the soma. The NMDA receptor, however, has a slower dynamics because it is blocked by magnesium ions, hence the absence of ionic flow when glutamate binds with it. In fact, the NMDA channel requires the additional depolarization induced by the Na^+ flow from the AMPA

channel to push the magnesium away from the membrane and make the channel accessible for calcium ions, which will flow inwards, further depolarize the membrane, then act as second messengers. Overall, upon arrival of a spike at an excitatory synapse, there are two depolarizing contribution that will be felt by the target neuron: a fast one relayed by the AMPA receptor, and a slightly slower one, associated to the NMDA receptor.

However, these two contributions are close enough in terms of timescale so they can be approximated by a single Post Synaptic Current (PSC), which is what will be done in simulations, where the arrival of the spike at time τ will be modeled by an alpha-shaped current:

$$I_s(t) = s \cdot I_0 \frac{t - \tau}{\tau_s} e^{-(t-\tau)/\tau_s} \quad \text{for } t > \tau, \quad (1.7)$$

where

s is the synaptic strength,

I_0 is the unit current 1 pA,

τ_s is the synaptic timescale.

Eventually, not all of the synaptic release events occur during the *synchronous release*, and some vesicles continue to be released at low rates for tens of milliseconds following the main synchronous release; this phenomenon is called *asynchronous release*.

Inhibitory neuron and GABA transmission

Glutamate is the main excitatory neurotransmitter in the CNS, but there is also another crucial type of neurotransmission which is mediated by GABA, and tends to hyperpolarize the target neurons instead of depolarizing them. This neurotransmitter is not expressed in excitatory neurons, which only have glutamate in their synaptic vesicles, but only in inhibitory GABAergic cells. In these cells, the GABA molecules are release by the exocytosis and come to bind on GABA receptors on the target cells, which will let chloride flow into the post-synaptic site, leading to a hyperpolarization of the membrane.

As for glutamate, there are two types of GABA receptors (a and b), with different timescales, but we will neglect these differences in the study.

GABA receptors can be blocked by a chemical antagonist called *bicuculline*, which prevents the opening of the channels, thus the flow of chloride and the hyperpolarization. This molecule will be used during the experiments performed in this thesis to work with fully excitatory networks.

Synaptic depression

Because the finite number of synaptic vesicles that are available at a given time, a synapse cannot transmit an arbitrarily large amount of spikes in a given period.

Indeed, vesicles in the pre-synaptic compartment can be divided into three main pools: a small *readily-releasable pool* (RRP), which will be used during synchronous release, a large *reserve pool*, which is maintained by a constant synthesis of new vesicles, and an intermediate *recycling pool*, which replenishes the RRP after a evoked release.

Thus, since only RRP vesicles are released during synchronous release, if the rate of spike arrival at the synapse is higher than the rate at which the RRP can be replenished, then the synapse will transmit less input after each successive spike, in a phenomenon called *synaptic depression*.

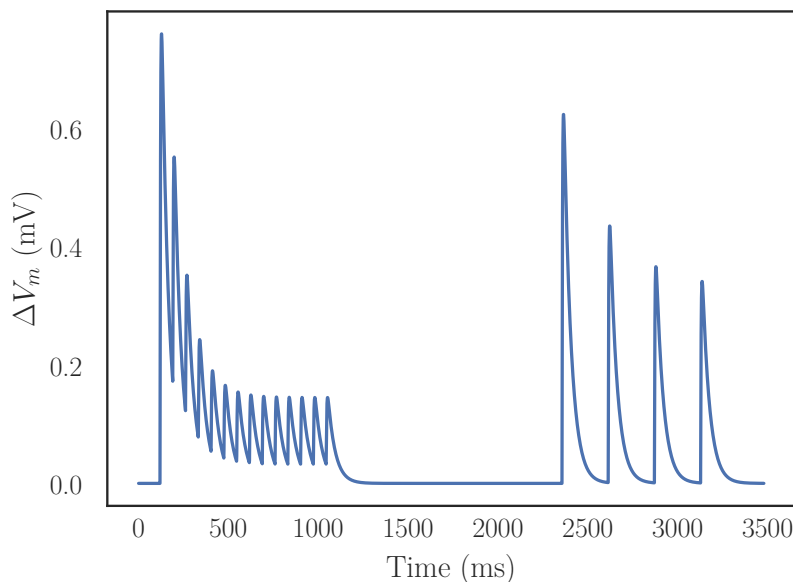


Figure 1.16.: Example of the effect of synaptic depression on the post-synaptic potential obtained at the soma of the target neuron. After each successive solicitation, an additional fraction of the RRP is depleted, leading to a lower current flow in the post-synaptic neuron, in turn lowering the depolarization induced on the target neuron. If the solicitation is at a high rate (left), the RRP is almost completely depleted. It takes a few hundred milliseconds to a few seconds to replenish the RRP, after which the initial amplitude is recovered (first spike of the second series, around 2400 ms). Lower solicitation rates (right) lead to lower depression.

1.4.2 Electrical connections: gap junctions

Besides chemical synapses, another kind of connection exists, where the neurons communicate directly by holes in their membranes through which the ions can flow in both directions. These bidirectional connections (by contrast with the directed synapses), are called *gap junctions*.

As shown on Figure 1.17, gap junctions are formed by channels that connect the cytoplasm of two cells through their membranes. Also called *electrical synapses*, gap junctions are present in the brain, especially among inhibitory interneurons (Galarreta et al. 2001). Gap junctions are strongly involved in neuroglial as well as glia-glia interactions, where they constitute one of the primary mode of information flow.

However, in *in vitro* cultures of neurons, the influence of gap junction seems minimal, since blockade of synaptic transmission abolishes the activity (Penn et al. 2016; Suresh et al. 2016). Furthermore, even the number of neuron-astrocyte gap junctions have been shown to decrease significantly for cultures before the collective activity emerges (Janeiro et al. 1999).

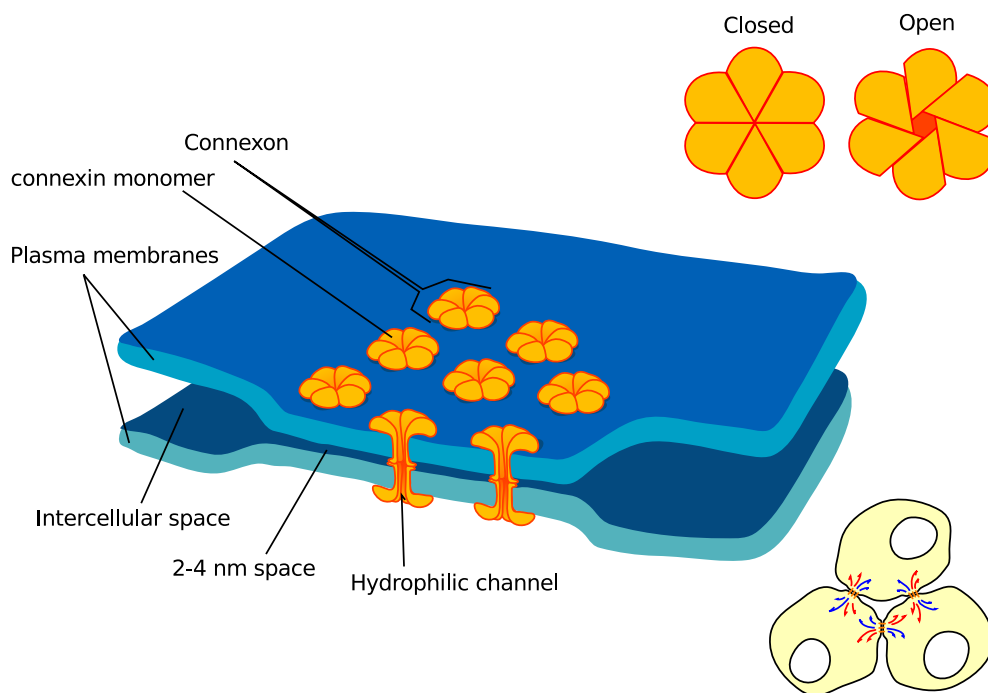


Figure 1.17.: Sketch of a gap junction. Original image by LadyOfHats.

In the rest of this manuscript, we will therefore neglect the role of gap junctions on the activity of all neuronal networks that will be considered.

1.4.3 Other pathways for information transfer

Eventually, apart from direct transmission, the activity of neurons can also be influenced by a large variety of phenomena.

Coming back on glial cells, calcium oscillations mediated by astrocytes may intermittently change neuronal excitability, and astrocytes also play a major role in modulating the efficiency of chemical synapses.

Beyond glial cells, the connections between neurons are not static, but plastic, meaning that they evolve in time, depending on the activity of the neurons. A large body of work is now available on the various mechanisms responsible for the evolution of the connection strength between two neurons; from homeostatic regulation (Turrigiano et al. 2004), to spike-time dependent plasticity and their interactions (Toyoizumi et al. 2014). However, despite recent progress, the sheer complexity of these mechanisms has prevented scientists from obtaining clear and quantitative models to describe this evolution as a general phenomenon, and not as a set of special cases (Markram et al. 2012).

Because of this, and since the timescales over which we study the activity of a network are small compared to those of plasticity mechanisms, all simulation and analyzes will be performed considering the synaptic strengths in the network to be fixed.

1.5 Coupled neurons: network and dynamics

In the previous sections, we have seen the basic behavior of neurons, how they regulate their electrical activity, how they grow, and how they connect together through synapses.

Once the neurons have matured, they will thus form large networks in which the activity of any given neuron will influence that of another, either exciting or inhibiting it.

In the adult brain, this gives rise to a wide variety of activity, or firing patterns, which vary depending on the state of the subject — active, resting, REM sleep. . . Such global patterns of activity are often studied using ElectroEncephaloGraphy (EEG) or functional Magnetic Resonance Imaging (fMRI), which are non-invasive methods. However, these methods have very low spatial and temporal resolutions, so the information obtained already reflects the collective activity of thousands of neurons over several hundred or thousand milliseconds.

In order to study in more details how the collective activity emerges from the detailed interactions of many individual neurons, smaller systems such as the previously mentioned neuronal cultures, more invasive techniques, or genetic engineering are required.

In this thesis, the experimental focus will be on neuronal cultures, because of the relative simplicity of the networks generated on such 2-dimensional setups, and we will therefore focus here on the patterns observed in such structures.

1.5.1 Typical activities of neuronal cultures

In their first weeks of development, neuronal cultures and brain areas display similar types of activity, with sparse overall activity, interspersed with short windows of intense firing (Egorov et al. 2013; Wagenaar et al. 2006). However, these *bursts* of activity recede progressively after the first week postnatal in the brain, while they persist in neuronal cultures over the whole lifespan — see Figure 1.18 for an example.

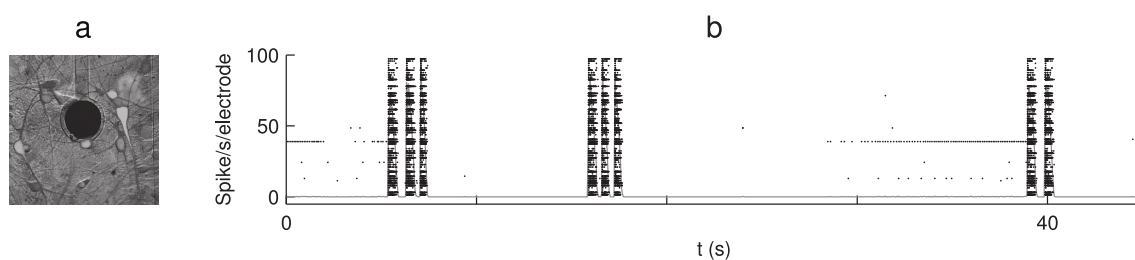


Figure 1.18.: (a) Cortical network on substrate-embedded multielectrode array. The dark circle is an electrode of diameter $30\text{-}\mu\text{m}$. (b) Raster plot showing the spikes recorded at each of the 60 electrodes (black dots) in the system as a function of time. The gray line shows the mean firing rate over 50 ms-time bins. Figure from Masquelier et al. 2013.

Yaghoubi et al. 2018 have shown recently that other types of activity such as asynchronous patterns or intense single-neuron activities could be observed in neuronal cultures, depending notably on the preparation conditions. Yet, decades of research on neuronal cultures (Gross et al. 1993; Kamioka et al. 1996; Okujeni et al. 2017; Opitz 2002; Orlandi et al. 2013; Pasquale et al. 2008) have shown that bursting activity where the whole network becomes active over a period of a few

hundred milliseconds is, by a significant margin, the main type of activity in such systems, regardless of the culturing methods.

1.5.2 Emerging behaviors: synchronization and bursting

Here is where the question of *emergence* comes forth. Indeed, for such a behavior to be systematically occurring in these systems, there should be a reason for it, a rule embedded in the dynamical properties of the neurons or the connections.

However, such a rule can be quite difficult to find, and knowing the properties of an object and the principles governing its behavior does not necessarily mean that predicting its behavior without prior knowledge is possible¹⁴.

Moreover, the predominance of a given behavior does not mean that the emergence of other activities is not possible (Yaghoubi et al. 2018). One of the main goals of this thesis will thus be to provide a general understanding of the phenomena underlying the emergence of collective activity in neuronal cultures in order to provide methods to guide the system towards different types of behavior.

In that respect, our chance is that bursting activity is a special case of *synchronization*, which has been the subject of extensive research, from its simplest description to students discovering dynamical systems (S. Strogatz 2007), to the well-known Kuramoto model (S. H. Strogatz 2000). Furthermore, we will see that adaptive neurons have a dynamics which is similar to that of *relaxation oscillators*, leading to very strong synchronizability (D. Wang 1999).

We will study the mechanisms leading to the collective behavior to understand how its properties depend on the neuronal and network parameters. This will allow us to propose new ways of modulating the bursting activity of neuronal cultures.

¹⁴ As interesting examples, one can have a look at the Langton's ant, or at Conway's game of Life. In both cases, the agents (an ant for Langton, cells for Conway) possess simplistic behaviors, yet they give rise to incredibly complex patterns that are mostly impossible to predict without a comprehensive exploration of all possible situations.

References for chapter 1

- Amini, S. and White, M. K.**, eds. (2013). *Neuronal Cell Culture: Methods and Protocols (Methods in Molecular Biology)*. Humana Press. ISBN: 1627036393 (cit. on pp. 4, 6).
- Arbib, M. A.** (2018). “From cybernetics to brain theory, and more: A memoir”. In: *Cognitive Systems Research* 50, pp. 83–145. ISSN: 13890417. DOI: 10.1016/j.cogsys.2018.04.001 (cit. on p. 7).
- Baj, G. et al.** (2014). “Developmental and maintenance defects in Rett syndrome neurons identified by a new mouse staging system in vitro”. In: *Frontiers in Cellular Neuroscience* 8, February, pp. 1–15. ISSN: 1662-5102. DOI: 10.3389/fncel.2014.00018 (cit. on p. 12).
- Bakkum, D. J. et al.** (2007). “MEART: The semi-living artist”. In: *Frontiers in Neurobotics* 1, November, p. 5. ISSN: 1662-5218. DOI: 10.3389/neuro.12.005.2007 (cit. on p. 4).
- Beaudoin, G. M. J. et al.** (Aug. 2012). “Culturing pyramidal neurons from the early postnatal mouse hippocampus and cortex”. In: *Nature Protocols* 7, 9, pp. 1741–1754. ISSN: 1754-2189. DOI: 10.1038/nprot.2012.099 (cit. on pp. 3, 4).
- Ben-Menachem, E. et al.** (2015). “Surgically implanted and non-invasive vagus nerve stimulation: A review of efficacy, safety and tolerability”. In: *European Journal of Neurology* 22, 9, pp. 1260–1268. ISSN: 14681331. DOI: 10.1111/ene.12629 (cit. on p. 7).
- Brette, R. and Gerstner, W.** (Nov. 2005). “Adaptive exponential integrate-and-fire model as an effective description of neuronal activity”. In: *J. Neurophysiol.* 94, 5, pp. 3637–3642. ISSN: 0022-3077. DOI: 10.1152/jn.00686.2005 (cit. on p. 17).
- Brunel, N. and Van Rossum, M. C.** (2007). “Lapicque’s 1907 paper: From frogs to integrate-and-fire”. In: *Biological Cybernetics* 97, 5-6, pp. 337–339. ISSN: 03401200. DOI: 10.1007/s00422-007-0190-0 (cit. on pp. 16, 17).
- Coles, C. H. and Bradke, F.** (Aug. 2015). “Coordinating Neuronal ActinMicrotubule Dynamics”. In: *Current Biology* 25, 15, R677–R691. ISSN: 09609822. DOI: 10.1016/j.cub.2015.06.020 (cit. on pp. 12, 13, 104).
- Conde, C. and Cáceres, A.** (2009). “Microtubule assembly, organization and dynamics in axons and dendrites.” In: *Nature reviews. Neuroscience* 10, 5, pp. 319–332. ISSN: 1471-003X. DOI: 10.1038/nrn2631. arXiv: NIHMS150003 (cit. on p. 12).
- Costa, L. G., Giordano, G., and Guizzetti, M.**, eds. (2011). *In Vitro Neurotoxicology*. Humana Press. ISBN: 9781617791697 (cit. on p. 6).
- Darville, H. et al.** (2016). “Human Pluripotent Stem Cell-derived Cortical Neurons for High Throughput Medication Screening in Autism: A Proof of Concept Study in SHANK3 Haploinsufficiency Syndrome”. In: *EBioMedicine* 9, pp. 293–305. ISSN: 23523964. DOI: 10.1016/j.ebiom.2016.05.032 (cit. on p. 4).
- Deer, T. R. et al.** (2014). “Effectiveness of Cervical Spinal Cord Stimulation for the Management of Chronic Pain”. In: *Neuromodulation: Technology at the Neural Interface* 17, 3, pp. 265–271. ISSN: 10947159. DOI: 10.1111/ner.12119 (cit. on p. 7).
- DeRosa, B. A. et al.** (2015). “HVGAT-mCherry: A novel molecular tool for analysis of GABAergic neurons derived from human pluripotent stem cells”. In: *Molecular and Cellular Neuroscience* 68, pp. 244–257. ISSN: 10959327. DOI: 10.1016/j.mcn.2015.08.007. arXiv: 15334406 (cit. on p. 5).

- Dichter, M.** (2009). “MODELS | The use of Cell Culture Models to Study Mechanisms Related to Epilepsy and Antiepileptic Drugs”. In: *Encyclopedia of Basic Epilepsy Research*. Elsevier, pp. 808–814. DOI: 10.1016/B978-012373961-2.00322-2 (cit. on p. 6).
- Egorov, A. V. and Draguhn, A.** (2013). “Development of coherent neuronal activity patterns in mammalian cortical networks: Common principles and local heterogeneity”. In: *Mechanisms of Development* 130.6-8, pp. 412–423. ISSN: 09254773. DOI: 10.1016/j.mod.2012.09.006 (cit. on p. 27).
- Ermentrout, B.** (July 1996). “Type I Membranes, Phase Resetting Curves, and Synchrony”. In: *Neural Computation* 8.5, pp. 979–1001. ISSN: 0899-7667. DOI: 10.1162/neco.1996.8.5.979 (cit. on p. 20).
- Fields, D. R.** (2017). URL: <https://www.quantamagazine.org/why-the-first-drawings-of-neurons-were-defaced-20170928/> (cit. on p. 10).
- Fourcaud-Trocmé, N. et al.** (2003). “How spike generation mechanisms determine the neuronal response to fluctuating inputs”. In: *J. Neurosci.* 23.37, pp. 11628–11640. ISSN: 1529-2401. DOI: 23/37/11628[pii] (cit. on p. 17).
- Galarreta, M. and Hestrin, S.** (2001). “Electrical synapses between GABA-releasing interneurons.” In: *Nature reviews. Neuroscience* 2.6, pp. 425–433. ISSN: 14710048. DOI: 10.1038/35077566 (cit. on p. 25).
- Gleeson, P. et al.** (Dec. 2017). “A commitment to open source in neuroscience”. In: *Neuron* 96, pp. 964–965. DOI: 10.1016/j.neuron.2017.10.013 (cit. on p. 8).
- Gross, G. W., Rhoades, B. K., and Kowalski, J. M.** (1993). “Dynamics of burst patterns generated by monolayer networks in culture”. In: *Neurobionics : an interdisciplinary approach to substitute impaired functions of the human nervous system*. Ed. by **Bothe, H.-W., Samii, M., and Eckmiller, R.** North-Holland. ISBN: 978-0-444-89958-3 (cit. on p. 27).
- Harrison, R.** (1907). “Observations on the living developing nerve fiber”. In: *The Anatomical Record* 1, pp. 116–128 (cit. on p. 3).
- Hasler, J. and Marr, B.** (2013). “Finding a roadmap to achieve large neuromorphic hardware systems”. In: *Frontiers in Neuroscience* 7.7 SEP, pp. 1–29. ISSN: 1662453X. DOI: 10.3389/fnins.2013.00118 (cit. on p. 3).
- Hodgkin, A. L. and Huxley, A. F.** (Apr. 1952). “Currents carried by sodium and potassium ions through the membrane of the giant axon of *Loligo*”. In: *The Journal of Physiology* 116.4, pp. 449–472. ISSN: 00223751. DOI: 10.1113/jphysiol.1952.sp004717 (cit. on p. 17).
- Humpel, C.** (2015). “Neuroscience forefront review organotypic brain slice cultures: A review”. In: *Neuroscience* 305, pp. 86–98. ISSN: 18737544. DOI: 10.1016/j.neuroscience.2015.07.086 (cit. on p. 4).
- Ievins, A. and Moritz, C. T.** (2017). “Therapeutic Stimulation for Restoration of Function After Spinal Cord Injury”. In: *Physiology* 32.5, pp. 391–398. ISSN: 1548-9213. DOI: 10.1152/physiol.00010.2017 (cit. on p. 7).
- Izhikevich, E. M.** (Nov. 2003). “Simple model of spiking neurons”. In: *IEEE Transactions on Neural Networks* 14.6, pp. 1569–1572. ISSN: 1045-9227. DOI: 10.1109/TNN.2003.820440 (cit. on pp. 16, 17).
- (2007). *Dynamical systems in neuroscience: the geometry of excitability and bursting*. Ed. by **Izhikevich, E. M.** Cambridge, Mass. London: MIT Press. ISBN: 9780262514200 (cit. on p. 16).

- Janeiro, R. D. et al.** (1999). “Gap-junctional coupling between neurons and astrocytes in”. In: *Proceedings of the National Academy of Sciences of the United States of America* 96.June, pp. 7541–7546 (cit. on p. 25).
- Kaesler, P. S. and Regehr, W. G.** (2014). “Molecular Mechanisms for Synchronous, Asynchronous, and Spontaneous Neurotransmitter Release”. In: *Annual Review of Physiology* 76.1, pp. 333–363. ISSN: 0066-4278. DOI: 10.1146/annurev-physiol-021113-170338 (cit. on pp. 23, 39).
- Kamioka, H. et al.** (Mar. 1996). “Spontaneous periodic synchronized bursting during formation of mature patterns of connections in cortical cultures”. In: *Neuroscience Letters* 206.2-3, pp. 109–112. ISSN: 03043940. DOI: 10.1016/S0304-3940(96)12448-4 (cit. on p. 27).
- Lukojević, M. and Jaeger, H.** (2009). “Reservoir computing approaches to recurrent neural network training”. In: *Computer Science Review* 3, pp. 127–149. ISSN: 15740137. DOI: 10.1016/j.cosrev.2009.03.005 (cit. on p. 3).
- Manninen, T. et al.** (2018). “Challenges in Reproducibility, Replicability, and Comparability of Computational Models and Tools for Neuronal and Glial Networks, Cells, and Subcellular Structures”. In: *Frontiers in Neuroinformatics* 12.May, p. 20. ISSN: 1662-5196. DOI: 10.3389/fninf.2018.00020 (cit. on p. 8).
- Marblestone, A., Wayne, G., and Kording, K.** (2016). “Towards an integration of deep learning and neuroscience”. In: 10.September, pp. 1–41. ISSN: 1662-5188. DOI: 10.3389/fncom.2016.00094. arXiv: 1606.03813 (cit. on p. 2).
- Markram, H., Gerstner, W., and Sjöström, P. J.** (2012). “Spike-Timing-Dependent Plasticity: A Comprehensive Overview”. In: *Frontiers in Synaptic Neuroscience* 4.July, pp. 2010–2012. ISSN: 1663-3563. DOI: 10.3389/fnsyn.2012.00002 (cit. on p. 26).
- Masquelier, T. and Deco, G.** (2013). “Network Bursting Dynamics in Excitatory Cortical Neuron Cultures Results from the Combination of Different Adaptive Mechanism”. In: *PLoS ONE* 8.10, pp. 1–11. DOI: 10.1371/journal.pone.0075824 (cit. on p. 27).
- Mathis, D. M., Furman, J. L., and Norris, C. M.** (Mar. 2011). “Preparation of Acute Hippocampal Slices from Rats and Transgenic Mice for the Study of Synaptic Alterations during Aging and Amyloid Pathology”. In: *Journal of Visualized Experiments* 49. ISSN: 1940-087X. DOI: 10.3791/2330 (cit. on p. 4).
- McCulloch, W. S. and Pitts, W.** (Dec. 1943). “A logical calculus of the ideas immanent in nervous activity”. In: *The bulletin of mathematical biophysics* 5.4, pp. 115–133. ISSN: 1522-9602. DOI: 10.1007/BF02478259 (cit. on p. 7).
- Mekhail, N. A. et al.** (2011). “Retrospective Review of 707 Cases of Spinal Cord Stimulation: Indications and Complications”. In: *Pain Practice* 11.2, pp. 148–153. ISSN: 15332500. DOI: 10.1111/j.1533-2500.2010.00407.x (cit. on p. 7).
- Naud, R. et al.** (2008). “Firing patterns in the adaptive exponential integrate-and-fire model”. In: *Biological Cybernetics* 99.4-5, pp. 335–347. ISSN: 03401200. DOI: 10.1007/s00422-008-0264-7 (cit. on pp. 17, 145, 147).
- Neumann, J. von** (1956). “Probabilistic logics and the synthesis of reliable organisms from unreliable components.” In: *Automata studies*. Ed. by **Shannon, J. C. and McCarthy, J.** Princeton, NJ: Princeton University Press, pp. 43–98 (cit. on p. 7).

- Nordlie, E., Gewaltig, M.-O., and Plesser, H. E.** (Aug. 2009). “Towards Reproducible Descriptions of Neuronal Network Models”. In: *PLoS Computational Biology* 5.8, e1000456. DOI: 10.1371/journal.pcbi.1000456 (cit. on p. 8).
- Okujeni, S., Kandler, S., and Egert, U.** (2017). “Mesoscale architecture shapes initiation and richness of spontaneous network activity”. In: *The Journal of Neuroscience* 37.14, pp. 2552–16. ISSN: 0270-6474. DOI: 10.1523/JNEUROSCI.2552-16.2017 (cit. on p. 27).
- Olah, C. and Carter, S.** (2016). *Attention and Augmented Recurrent Neural Networks*. URL: <http://distill.pub/2016/augmented-rnns> (cit. on p. 2).
- Opitz, T.** (2002). “Spontaneous Development of Synchronous Oscillatory Activity During Maturation of Cortical Networks In Vitro”. In: *Journal of Neurophysiology* 88.5, pp. 2196–2206. ISSN: 0022-3077. DOI: 10.1152/jn.00316.2002 (cit. on p. 27).
- Orlandi, J. G. et al.** (Sept. 2013). “Noise focusing and the emergence of coherent activity in neuronal cultures”. In: *Nature Physics* 9.9, pp. 582–590. ISSN: 1745-2473. DOI: 10.1038/nphys2686 (cit. on pp. 5, 27, 70, 71, 75).
- Pasquale, V. et al.** (2008). “Self-organization and neuronal avalanches in networks of dissociated cortical neurons”. In: *Neuroscience* 153.4, pp. 1354–1369. ISSN: 03064522. DOI: 10.1016/j.neuroscience.2008.03.050 (cit. on pp. 27, 132).
- Penn, Y., Segal, M., and Moses, E.** (2016). “Network synchronization in hippocampal neurons.” In: *Proceedings of the National Academy of Sciences of the United States of America* 113.12, pp. 3341–3346. ISSN: 00278424. DOI: 10.1073/pnas.1515105113 (cit. on pp. 25, 38, 41, 54, 55, 61).
- Potter, S. M. and DeMarse, T. B.** (2001). “A new approach to neural cell culture for long-term studies”. In: *Journal of Neuroscience Methods* 110.1, pp. 17–24. ISSN: 01650270. DOI: 10.1016/S0165-0270(01)00412-5 (cit. on p. 3).
- Renault, R.** (2015). “Emergent design of neuronal devices”. PhD thesis. Université Paris Diderot (cit. on pp. 6, 106, 107).
- Russell, S. J. and Norvig, P.** (1995). *Artificial Intelligence: A Modern Approach*. Vol. 9. 2, pp. 215–218. ISBN: 9780131038059. DOI: 10.1016/0925-2312(95)90020-9. arXiv: 9809069v1 [arXiv:gr-qc] (cit. on p. 2).
- Sakakibara, A. et al.** (2013). “Microtubule dynamics in neuronal morphogenesis”. In: *Open Biology* 3.7, pp. 130061–130061. ISSN: 2046-2441. DOI: 10.1098/rsob.130061 (cit. on p. 12).
- Schlachetzki, J. C. M., Saliba, S. W., and Oliveira, A. C. P. de** (2013). “Studying neurodegenerative diseases in culture models”. In: *Revista Brasileira de Psiquiatria* 35.SUPPL.2, pp. 92–100. ISSN: 15164446. DOI: 10.1590/1516-4446-2013-1159 (cit. on p. 6).
- Schwartz, E. L.** (1993). *Computational Neuroscience*. Bradford Books. MIT Press. ISBN: 9780262691642 (cit. on p. 7).
- Searle, J. R.** (1980). “Minds, brains, and programs”. In: *Behavioral and Brain Sciences* 3.03, p. 417. ISSN: 0140-525X. DOI: 10.1017/S0140525X00005756 (cit. on p. 2).
- Shenoy, K. and Chestek, C.** (2012). *Neural Prosthetics*. revision #124016 (cit. on p. 7).
- Sipilä, S. T. et al.** (2006). “Intrinsic bursting of immature CA3 pyramidal neurons and consequent giant depolarizing potentials are driven by a persistent Na⁺ current and terminated by a slow Ca²⁺-activated K⁺ current”. In: *European Journal*

- of Neuroscience* 23, pp. 2330–2338. ISSN: 0953816X. DOI: 10.1111/j.1460-9568.2006.04757.x (cit. on p. 19).
- Strogatz, S.** (2007). *Nonlinear Dynamics and Chaos*. Ed. by **Strogatz, S.** Studies in Nonlinearity. Sarat Book House. ISBN: 9780813349114 (cit. on p. 28).
- Strogatz, S. H.** (2000). “From Kuramoto to Crawford: exploring the onset of synchronization in populations of coupled oscillators”. In: *Physica D: Nonlinear Phenomena* 143.1-4, pp. 1–20. ISSN: 01672789. DOI: 10.1016/S0167-2789(00)00094-4 (cit. on p. 28).
- Suresh, J. et al.** (2016). “Network burst activity in hippocampal neuronal cultures: the role of synaptic and intrinsic currents”. In: *Journal of Neurophysiology* 115.6, pp. 3073–3089. ISSN: 0022-3077. DOI: 10.1152/jn.00995.2015 (cit. on p. 25).
- Takeda, S. et al.** (2015). “Neuronal uptake and propagation of a rare phosphorylated high-molecular-weight tau derived from Alzheimer’s disease brain”. In: *Nature Communications* 6. ISSN: 20411723. DOI: 10.1038/ncomms9490. arXiv: arXiv:1011.1669v3 (cit. on pp. 7, 92).
- Tazerart, S., Vinay, L., and Brocard, F.** (2008). “The persistent sodium current generates pacemaker activities in the central pattern generator for locomotion and regulates the locomotor rhythm.” In: *The Journal of neuroscience : the official journal of the Society for Neuroscience* 28.34, pp. 8577–8589. ISSN: 0270-6474. DOI: 10.1523/JNEUROSCI.1437-08.2008 (cit. on p. 19).
- Tong, Z. et al.** (2015). “A microfluidic neuronal platform for neuron axotomy and controlled regenerative studies”. In: *RSC Advances* 5.90, pp. 73457–73466. ISSN: 20462069. DOI: 10.1039/c5ra11522a (cit. on p. 7).
- Touboul, J. and Brette, R.** (2008). “Dynamics and bifurcations of the adaptive exponential integrate-and-fire model”. In: *Biological Cybernetics* 99.4-5, pp. 319–334. ISSN: 03401200. DOI: 10.1007/s00422-008-0267-4 (cit. on p. 17).
- Toyoizumi, T. et al.** (2014). “Modeling the Dynamic Interaction of Hebbian and Homeostatic Plasticity”. In: *Neuron* 84.2, pp. 497–510. ISSN: 10974199. DOI: 10.1016/j.neuron.2014.09.036 (cit. on p. 26).
- Trappenberg, T.** (2010). *Fundamentals of Computational Neuroscience*. Fundamentals of Computational Neuroscience. OUP Oxford. ISBN: 9780199568413 (cit. on p. 7).
- Turrigiano, G. G. and Nelson, S. B.** (Feb. 2004). “Homeostatic plasticity in the developing nervous system”. In: *Nature Reviews Neuroscience* 5.2, pp. 97–107. ISSN: 1471-003X. DOI: 10.1038/nrn1327 (cit. on p. 26).
- Wagenaar, D. a., Pine, J., and Potter, S. M.** (2006). “An extremely rich repertoire of bursting patterns during the development of cortical cultures.” In: *BMC neuroscience* 7, p. 11. ISSN: 1471-2202. DOI: 10.1186/1471-2202-7-11 (cit. on p. 27).
- Wang, D.** (1999). “Relaxation Oscillators and Networks”. In: *Wiley Encyclopedia of Electrical and Electronics Engineering* 18.2, pp. 396–405. DOI: 10.1002/047134608X.W2282 (cit. on p. 28).
- Xu, K. et al.** (2015). “Show, Attend and Tell: Neural Image Caption Generation with Visual Attention”. In: *CoRR* abs/1502.03044. arXiv: 1502.03044 (cit. on p. 2).
- Yaghoubi, M. et al.** (2018). “Neuronal avalanche dynamics indicates different universality classes in neuronal cultures”. In: *Scientific Reports* 8.1, pp. 1–11. ISSN: 20452322. DOI: 10.1038/s41598-018-21730-1 (cit. on pp. 27, 28).

Chapter 2

Mechanisms governing epileptiform bursts

How can a phenomenon as widespread as epileptiform bursts, which we described in “Emerging behaviors: synchronization and bursting” (subsection 1.5.2), still remain so elusive when we try to determine its potential causes?

In this case, the problem is mostly due to two main factors: the multiplicity of the potential mechanisms and the complexity of the phenomenon itself, which decomposes in three ill-defined periods, an initiation, a plateau, and a termination phase.

In this chapter, we will discuss the numerous mechanisms that could play a role in the occurrence and shape of network bursts in neuronal cultures. For each mechanism, we will discuss specific observations that could support a causal role in one of the extremal phases (initiation and termination). We will then develop predictive models to evaluate the consequences these mechanisms should have on the bursting properties, which enables us to propose and carry out actual experiments to assess the validity of the model and the likelihood of the associated mechanisms.

Contents

2.1	Possible bursting mechanisms	36
2.1.1	Burst initiation, deterministic or stochastic?	36
2.1.2	Burst termination: adaptation or depression?	38
2.2	The influence of neuronal adaptation	41
2.2.1	A concise model for periodic bursting	41
2.2.2	Shaping bursts through adaptation channels	46
2.3	Statistical properties of bursting behaviors	54
2.3.1	The transition to synchronous bursting	54
2.3.2	Synchronous bursts as percolation events	58
2.3.3	Statistical properties of the interburst interval	59

2.1 Possible bursting mechanisms

A significant difference between what may happen in the brain — e.g. up- and down-states generated by thalamocortical networks (Destexhe 2009) — comes from the fact that cultured networks are isolated: burst of activity cannot stem from the interaction of two different networks, one active and one adaptive, or from the response to external stimuli, but only from the intrinsic dynamics of the neurons or input noise which comes from inside the network.

To understand the phenomena involved in the sporadic activity observed in cultures, three main components must be characterized:

*transition
between up
and down
states*

- What leads a significant fraction of the neurons to become active in a comparatively short time interval? (*initiation*)
- Why is this activity sustained over several hundred milliseconds? (*plateau*)
- What prevents this activity from persisting over longer periods? (*termination*)

relates to

These three phenomena can be qualitatively understood through the description that was developed in “Neurons as excitable units” (subsection 1.3.2). They define the transition of the network between up and down states (Wilson 2008), or, almost equivalently, active and resting states.

*excitation-
excitability
balance*

Indeed, the initiation of the burst can be understood as the moment when the input the neurons receive becomes greater than their excitability; this activity is then sustained as long as the recurrent input remains greater than the excitability and terminates when it goes below it.

For the initiation, this means that either the overall neuronal excitability tends toward infinity, leading to spontaneous activity even with little input, or that enough inputs were received over a short period to go above the finite excitability of some neurons. This distinction is not trivial because the two phenomena interact together, but it is what differentiates pacemaker and noise-driven bursts, and it will be developed in the first subsection.

For the termination, either the excitability decreases as the plateau endures, or the input strength decreases. This phenomenon is easier to understand and can be described by the effect of intrinsic adaptation current versus the activity-driven depletion of synaptic vesicles — Short-Term Depression (STD); it will be developed in the second subsection.

Eventually, the plateau is the easiest phase, consisting of a region where the activity is self-sustained: the first spikes elicited trigger the subsequent ones in an iterative manner.

2.1.1 Burst initiation, deterministic or stochastic?

Let us try to reach a more detailed understanding of the possible mechanisms that might drive the initiation of the bursting activity.

*pacemaker
neurons for
deterministic
periodic
bursting*

A deterministic cause to the burst initiation would be the existence of a subset of neurons which are subjected to a pacemaker mechanism that drives them to spike in a relatively periodic fashion. Coming back to the excitability property, for these neurons, it increases steadily until it reaches infinity with a typical period T , leading the neurons to fire with this same period. Pacemaker neurons can easily synchronize, as mentioned in “Simple models for spiking neurons” (subsection 1.3.3) and lead to

a periodic and significant input inside the network, which could act as a trigger for the transition to the up-state, i.e. the initiation of the burst.

On the other hand, one must not neglect a well characterized phenomenon, which is the presence of synaptic noise, as the spontaneous release of synaptic vesicles (Kavalali 2014; Loy et al. 2014). The neuronal inputs associated to these spontaneous releases are often called miniature Excitatory Post Synaptic Current (mEPSC) or miniature Excitatory Post Synaptic Potential (mEPSP), or simply minis (Sibarov et al. 2015). For each connection between two neurons, these spontaneous events will occur with a base frequency ν_0 ; this means that a neuron having n incoming synapses will receive minis with a total frequency $\nu_n = n \cdot \nu_0$. Because of this constant bombardment of excitatory inputs, some neurons in the network will “spontaneously” fire and the accumulation of these spontaneous spikes in addition to the minis progressively drives the ignition of the whole network.

*minis for
noise-driven
bursting*

Differences between the two mechanisms

At first glance, these two mechanisms have significantly different properties: pacemaker neurons should lead to a more regular activity whereas noise-driven activity could be less periodic. Moreover, pacemaker neurons have no reason to be localized in specific areas of the network and the properties of pacemaker-driven bursts should therefore be less dependent on the network properties. On the contrary, the amount of incoming minis received by a neuron is strongly dependent on its connectivity inside the network, which could lead to a bursting activity displaying stronger correlations to the network structure.

*different
periodicity
and network
influence?*

Disentangling the two phenomena

So far, I have described pacemaker neurons and minis as well-defined and separate mechanisms. Unfortunately, this is not true at all: minis are pervasive, they are always present as soon as synaptic connections are established. This means that, rigorously, synaptic noise should always be considered in a model describing the activity of a neuronal network.

*problem:
synaptic noise
is always
present*

This means that the difference between deterministic and stochastic bursting should come from a quantitative change in the importance of one mechanism relative to the other. Though this is easy for stochastic bursting, where the absence of any pacemaker neuron is a possibility, deterministic bursting will stem from a combination of pacemaker neurons and synaptic noise. In fact, in the pacemaker scenario, the additional input provided by the noise is probably necessary for the neurons to be in a state of spontaneous periodic firing.

How then can we tell these mechanisms apart?

In the following, I will first discuss previous studies that gathered evidence in favor of one phenomenon or the other, then develop some models and simulation framework that will be used to make predictions on the possible differences that might arise depending on the relative strength of a pacemaker mechanism compared to synaptic noise.

Previous experimental and theoretical studies

In the literature, studies reporting on the influence of both mechanisms can be found, most probably because both mechanisms are indeed contributing to the phenomenon.

Thus, a recent study by Penn et al. 2016 shed light on the high regularity of hippocampal neurons, relating it to the influence of a persistent sodium channel, and suggesting that as much as 60% of the cultured neurons might exhibit rhythmic activity patterns.

On the other hand, a paper from (Chever et al. 2016), investigating the role of neuro-glial interactions, showed how the regulation of extracellular potassium by astrocytes influences the importance of the spontaneous synaptic bombardment to which the neurons are subjected, impacting the frequency and duration of epileptiform bursts.

Eventually, two very interesting studies by T. A. Gritsun, Le Feber, et al. 2010 and Baltz et al. 2011, mixing experimental and numerical protocols, compared the influence of bursting pacemaker neurons, random spiking neurons, and synaptic noise as driving mechanisms for bursting events. Both studies concluded that burst profiles were best reproduced by pacemaker neurons. Even though Baltz et al. 2011 further refined the analysis by emphasizing on the importance that pacemaker cells exhibit intrinsically bursting behaviors, adding that older cultures might see an increase in the relative importance of synaptic noise. However, both numerical studies used uniform Poisson noise to model mini and did not take the number of synapses into account.

2.1.2 Burst termination: adaptation or depression?

As for initiation, different mechanisms could lead to the termination of a burst, bringing the network back to the down state.

The two main phenomena that we will discuss here are *adaptation* and *synaptic depression*¹. Indeed, there are two simple ways of preventing the activity from lasting indefinitely: either reduce the excitability of the neurons or reduce the input strength. The former is enforced by adaptation currents and concerns the cells' intrinsic excitability; the latter is obtained through synaptic depression, which reduces the coupling strength between neurons.

Neuronal adaptation

We mentioned adaptation currents in biological neurons – “The biological reality” (subsection 1.3.1) – and in “Simple models for spiking neurons” (subsection 1.3.3) when we described the AdExp model. In this model, all the adaptation is modeled by one slow current w that tends to bring the neuron's membrane potential back towards its resting voltage.

In real neurons, there are many adaptation currents that display a large variety of timescales and origins (Sah et al. 2002). In this study, we will focus on the currents related to After HyperPolarization (AHP), i.e. spike-triggered currents that flow into the cell and hyperpolarize it after the emission of an action potential. This mechanism is modeled by the b step-increment of the slow current w in the AdExp model. As the name “adaptation” suggests, the effect of these currents leads to a form of habituation for the neuron: the excitability of the neuron decreases as the stimulation is repeated, thus its effect on the neuronal behavior diminishes and the

¹ other phenomena such as sodium channel inactivation (Goldin 2003) do not seem to occur in synchronous bursts, and local changes in ion concentrations will not be considered under the hypothesis that glial cells are efficiently maintaining ion concentrations homogeneous.

*act on units
or connections*

*adaptation
currents
reduce
neuronal
excitability*

neuronal response is reduced to get closer to the usual resting behavior (without necessarily reaching it).

Synaptic depression

Contrary to adaptation, synaptic depression does not modify the intrinsic properties of the neurons but rather those of the connections between the cells.

As described in “[Chemical connections: synapses](#)” (subsection 1.4.1), the main type of connection between neurons is the synapse, which contains vesicles filled with neurotransmitters. The release of these vesicles towards the post-synaptic neuron can be triggered by the arrival of a spike, and the amount of released vesicles characterizes the strength of the PSC that will be felt by the target neuron. Thus, reducing the number of released vesicles leads to a decreased strength for signal transfer.

We will therefore focus here on a phenomenon called Short-Term Depression (STD), which concerns the temporary diminution of the coupling strength between neurons because of the repeated arrival of spikes over a short time-period (Neher et al. 2008). This reduction of the synaptic strength stems from the finite number of available vesicles in the readily-releasable pool of the pre-synaptic compartment; indeed, as the arrival of a spike triggers the exocytosis of a fraction of these readily-releasable vesicles, and given that it takes time to replenish the pool, fewer vesicles are available if a second spike arrives before the vesicles have been fully replaced (Kaesler et al. 2014).

STD reduces connections' strength

Underlying reality

In fact, these two phenomena are just two sides of a similar principle that is generally not appearing in neuronal models: the energy cost of the actions that are performed by the neuron.

Indeed, it requires work for the neuron to emit an action potential, then get ready to emit a new one, returning to baseline by actively pumping ions against concentration gradients (Gulledge et al. 2013; Tiwari et al. 2018). Similarly, generating all the vesicles necessary for synaptic transmission is definitely not a cost-free operation. Therefore, adaptation and short-term depression (STD) are just two ways of patching up the models to take into account the fact that, if too much solicitation is applied to it, the neuron cannot keep up and will have to slow down the pace, either by firing less rapidly, transmitting signals at lower intensity, or both.

both mechanisms involve energy costs

Experimental observations

As for the initiation mechanism, both termination mechanisms have been reported to influence the bursting behavior in spontaneously active neuronal networks.

Two experimental studies by Empson et al. 2001 and Sevilla et al. 2006 attested the influence of adaptation currents on the interburst interval and the burst duration. However, these studies were performed on slices, and one of them used 4-aminopyridine and Mg^{2+} -free medium to induce the bursting behavior. Furthermore, these studies used nifedipine to block the slow After HyperPolarization (sAHP), which, as other dihydropyridines, is not very selective with respect to other calcium and adaptation channels (Curtis et al. 2001; Lima et al. 2007) and increases spontaneous release of neurotransmitters (Hirasawa et al. 2003). Given the known influence of mini on the bursting rate, additional experiments would therefore necessary to properly assess the influence of adaptation.

Conversely, the influence of synaptic depletion on bursting events of dissociated neuronal cultures was analyzed by D. Cohen et al. 2011, who demonstrated that the interburst duration displayed a significant dependence on the recovery of synaptic vesicle pools. However, though this effect indeed proves the importance of STD on the bursting behavior, it does not establish any causal relation between STD and burst termination.

2.2 The influence of neuronal adaptation

Adaptation in neurons is a widely represented property, and several studies have mentioned it as a probable candidate in bursting mechanisms Augustin et al. 2013; Compte et al. 2003; Ferguson et al. 2015; Van Vreeswijk et al. 2001.

However, as there was no complete mechanism explaining its role in shaping this phenomenon, we set out to investigate if adaptation alone could account for the dynamics observed experimentally in neuronal cultures.

Our goal was therefore not only to reproduce the bursting dynamics, but also to test if a single mechanism could enable us to reproduce the distinct activities observed by the team of Elisha Moses. Indeed, the results from Penn et al. 2016, showed that the cultures were able to sustain highly synchronized bursts, and that this activity persisted even in the absence of an inhibitory balance, as blocking the inhibitory synapses through bicuculline did not alter the dynamics qualitatively. Moreover, blockade of the persistent sodium current $I_{Na,P}$ led to an almost complete suppression of the activity, hinting at a pacemaker-driven activity.

Eventually, they showed that the network could be brought from an asynchronous activity to this synchronized bursting behavior through a two-step phase transition as calcium concentration was increased, first displaying a fuzzy phase synchronization, followed by a near-zero phase-lag region.

Can we explain bursting and its phase transitions through adaptation alone?

2.2.1 A concise model for periodic bursting

To account for the synchronized bursting activity, the simplest model, given the observations, was to model the neuronal population through adaptive pacemaker neurons: a persistent current would be responsible for the initiation of the up-state, while adaptation would act as a balancing force and prevent the activity from blowing up.

In order to provide the simplest explanation regarding the role that adaptation could play in shaping network bursts, I developed a theoretical and tractable model, first focusing on the simplest homogeneous situation, then progressively increase the complexity. This model can be found in Fardet, Ballandras, et al. 2018 — included in “Bursting and adaptation (Frontiers in Neuroscience 2018)” (section J.3), with details on the theoretical equations in “Self-consistent equations for the bursting behavior” (Appendix C) — while a more intuitive description based on the susceptibility is proposed here.

I will thus show how such a model enables us to understand and predict the bursting properties of an entire neuronal population simply from the average properties of the cells and connectivity.

predict global activity from cell properties

Minimalist

Let us first remove all heterogeneity from the model: we will take all neurons identical, with parameters that lead to a pacemaker and adaptive behavior; furthermore, we will connect them in a fixed-in-degree network, meaning that all neurons receive the same number of connections.

In that situation, if the neurons start in a synchronized state, as they receive the same number of inputs and since there is no noise in the system, they will always

stay synchronous ².

Because of this, we can actually further simplify the system by modeling it through a unique equivalent neuron with an autapse (a self-loop synapse).

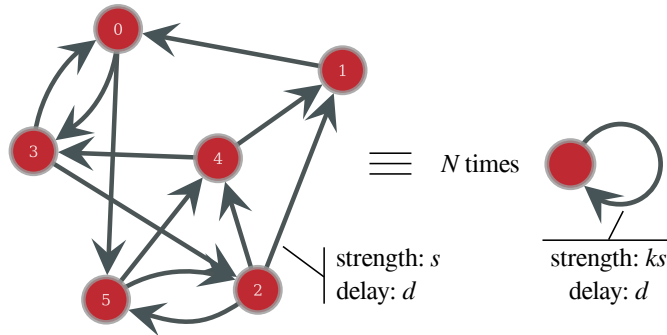


Figure 2.1.: Schematic representation of the equivalence between a fixed-in-degree network containing $N = 6$ synchronous neurons, with in-degree $k = 2$ and connection strength s , and N isolated neurons, with a self-loop connection of strength ks .

Figure 2.1 provides an example for such a network, where each neuron receives incoming connections from two other neurons. In the fully synchronous state, this is equivalent to a single neuron looping on itself with a connection of strength $2s$.

In such a simple system, as in the initial description of a burst, we find again the three characteristic periods for the up-state:

- the *initiation* of the burst is triggered by the progressive depolarisation of the membrane potential due to a persistent current modeling the effect of $I_{Na,P}$ *in vitro*,
- the *plateau* consists of repetitive spiking in the network, as described on Figure 2.2 (the neuron spikes, the action potential propagates until it reaches the target and its arrival on the target excites it; if the excitation is enough, the sequence is repeated),
- the *termination* of the burst once the excitation is not sufficient to make the neuron spike.

Let us now explain this behavior using restlessness and susceptibility — cf. “Excitability, restlessness, and susceptibility” (section 1.3.3). As we chose the parameters to get pacemakers neurons, they have a restlessness that is positive ($Rl > 0$), meaning that they spike spontaneously. Looking at the susceptibility Sc , the spike will occur when Sc also becomes positive, as can be seen on Figure 2.3.

Once these spikes are synchronized (see “Emerging behaviors: synchronization and bursting” (subsection 1.5.2) to understand how this synchronization occurs), all the susceptibilities of the neurons will switch from negative to positive in a short time window; this marks the initiation of the burst.

² Because of the strong synchronizability of relaxation oscillators, to which adaptive neurons belong, this synchronized state is stable and is rapidly recovered after a random perturbation of the network, as shown in “Stability of the synchronized state” (section C.3).

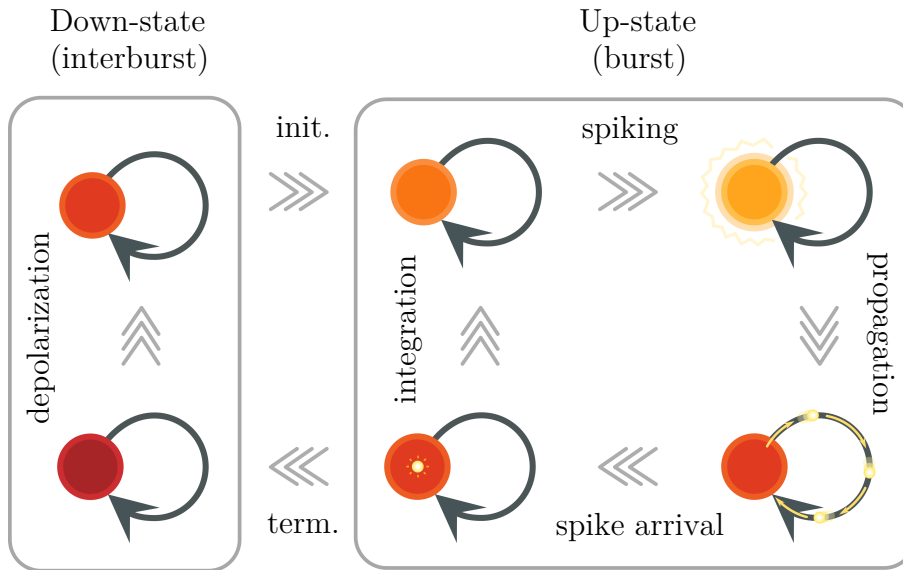


Figure 2.2.: Schematic representation of the two phases of the bursting behavior. On the left, the down-state (interburst) contains the slow process of depolarisation of the neuron from the persistent current. Once the depolarization is sufficient to cross a certain threshold, we switch to the right part, the up-state (burst). The up-state is obtained through the repetition of the spiking, spike propagation and integration periods until the integration is not sufficient to trigger a new spike and we switch back to the left part, to the down state.

During the burst, we can estimate the “excitatory power” of the network as the number of inputs a neuron will receive times the charge Q_s delivered by a single spike. Since all neurons are involved in these bursts, the average number of inputs received by the neurons is simply the average in-degree $\langle k_{in} \rangle$ in the network

$$\mathcal{P}_e \sim \langle k_{in} \rangle Q_s \quad (2.1)$$

*burst lasts
while
 $p_e + \langle Sc \rangle > 0$*

Let us call $p_e = \frac{\mathcal{P}_e}{C_m \Delta T}$ the dimensionless excitatory power; then the plateau will last as long as p_e is greater than $|\langle Sc \rangle|$, i.e. as long as the excitatory power is sufficient to bring the neurons to a positive value of the susceptibility. This condition can be visualized on Figure 2.3.

In the hypothesis that adaptation sculpts the bursting behavior, as the neurons repeatedly fire, the adaptation currents progressively increase (the w variable in the AdExp model), making the neurons less and less susceptible, until the excitatory power of the network is not sufficient to trigger new spikes and the burst terminates.

*w such that
 $p_e + \langle Sc \rangle < 0$
leads to
termination*

Accounting for heterogeneity

What has been described above is a situation where all neurons are perfectly identical and synchronized, and the spike delivery occurs instantaneously. This is obviously not the case in real populations of neurons, where

1. neurons have different properties,
2. they make various numbers of connections,
3. the connection strength is variable and finite,

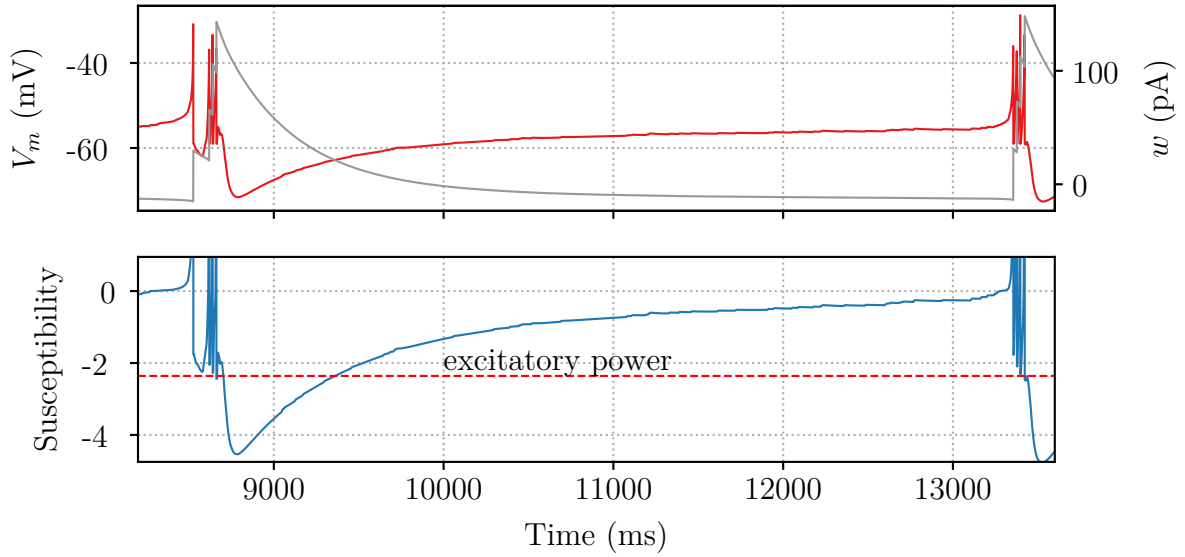


Figure 2.3.: Time course of the membrane potential (red curve) and adaptation variable (grey curve) of one neuron in a heterogeneous bursting network (top). Concurrent evolution of the neuronal susceptibility (bottom). The burst initiation starts as Sc crosses zero and the burst terminates when Sc goes below the network’s excitatory power.

which absolutely prevents perfect synchrony, as shown on Figure 2.5.

In order to take into account the heterogeneity in the connectivity, a simple trick is to model what the input would look like in the case of neurons that produce realistic network bursts. In realistic bursts, the activity is still restricted over a short window, while the remaining time is spent in the down-state; however, instead of being distributed in discrete slices inside the burst, normal spikes are spread more or less homogeneously over the whole burst duration (see Figure 2.5 and “Self-consistent equations for the bursting behavior” (Appendix C) for more details).

We will therefore consider the limit case where the spikes are distributed uniformly inside the burst window T_B . In the limit of a large number of neurons, each cell will receive an almost constant amount of current $I_s^{(c)}$ during the burst, such that

$$I_s^{(c)} = \frac{n_s \langle k_{in} \rangle Q_s}{T_B}. \quad (2.2)$$

The average current is thus simply the total charge delivered during the burst, divided by the burst duration; the total charge being the number of delivered spikes — $\langle n_s \rangle \langle k_{in} \rangle$, with $\langle n_s \rangle$ the average number of spikes emitted by a neuron — times the unit charge Q_s carried by a spike.

In that scenario, the initiation of the burst leads to the addition of a new excitatory current to the neurons, and the burst lasts until the neurons have adapted to this new input.

Termination condition for the adaptation current

As mentioned before, our model poses the adaptation current w as the stabilizing mechanism of the neuronal network, its increase preventing an explosion of the

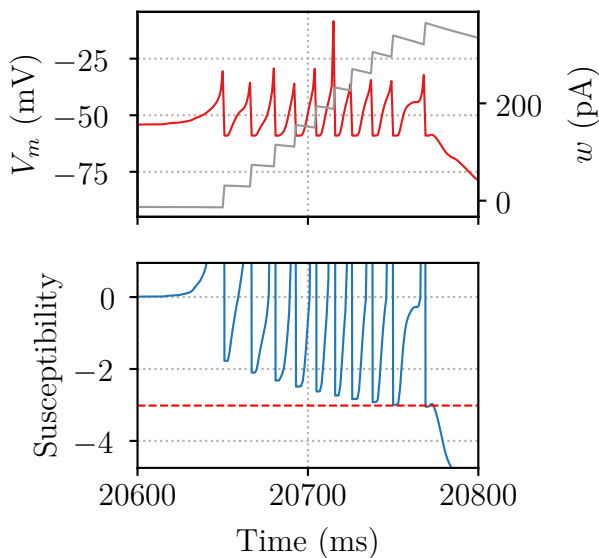
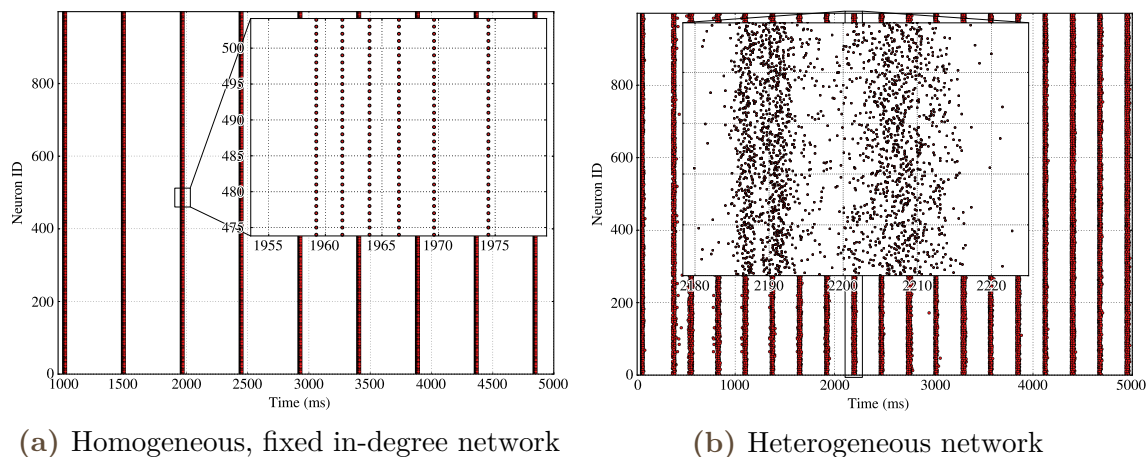


Figure 2.4.: Evolution of the membrane potential (red solid line, top) and adaptation current (grey solid line, top) compared to the susceptibility (blue solid line, bottom) inside a burst. After each spike, the increase of w leads to a decrease of the susceptibility. Burst termination occurs when Sc goes below the network's excitatory power (red dashed line, bottom).



(a) Homogeneous, fixed in-degree network

(b) Heterogeneous network

Figure 2.5.: Rasters of bursting networks. The insets detail the spike distributions inside a burst for a fully homogeneous and a heterogeneous network.

spiking activity. As w increases, the charge that is necessary to make the neurons spike increases conjointly, making the neurons less and less susceptible until the excitatory power of the network is not sufficient to trigger a new spike.

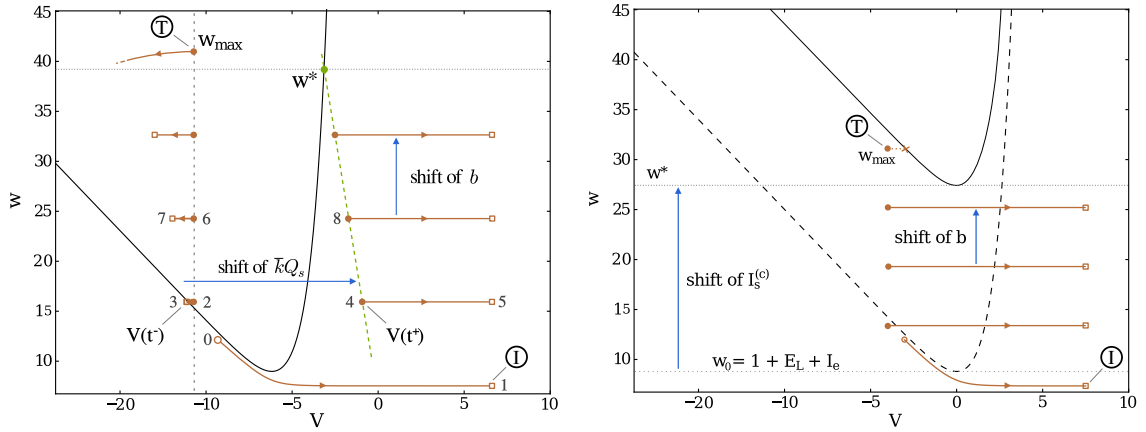
Since the value of w mostly increases through spike-triggered adaptation, modeled by b in the AdExp model, the peak value w_{max} is reached right after the last spike of a burst. Based on this observation, Figure 2.6 details how we can predict the existence of a critical value w^* , such that no new spike can be elicited if $w > w^*$.

Though the precise mechanism varies depending on how we model synaptic coupling³ the basic principle is always preserved: neurons spike if the excitation is strong enough to bring them “above threshold”.

In the AdExp model, this means that they must be able to get either below or to the right of the V -nullcline. Through its b -increment and its negative retroaction on

adaptation eventually prevents threshold crossing

³See the supplemental video of Fardet, Ballandras, et al. 2018 for an example of the time-dependent termination mechanism in more realistic synapses, and “Self-consistent equations for the bursting behavior” (Appendix C) for detailed equations.



(a) Homogeneous, fixed in-degree network. The critical value w^* is given here when the total charge delivered, $\bar{k}Q_s$ is not sufficient to escape the inside of the V -nullcline. (b) Heterogeneous network. The critical value w^* is given here when the trajectory of the spike intersects the $I_s^{(c)}$ -shifted V -nullcline.

Figure 2.6.: Trajectory of the equivalent bursting neuron in dimensionless phase space for Dirac and continuous synapses; the grey numbers indicate the order in which the neuron arrives at the different points in the trajectory. Spiking or jump discontinuities are marked through empty squares while reset points are indicated by full circles. The initiation are marked by circled Is while the burst termination conditions for the homogeneous and heterogeneous descriptions of the bursting behavior are marked by circled Ts.

V , the increase of w prevents both mechanisms by shifting the trajectory upward and speeding up the decay of the potential towards lower values, on the left side of phase space.

The interburst interval

Once the neuronal trajectory is trapped by the V -nullcline, it goes back to lower values of the potential, then the membrane potential begins its slow increase again, along the left branch of the V -nullcline, until it reaches the nullcline's minimum and the initiation starts anew.

During this slow repolarization, the neurons remain in what could be described as a long refractory period while the lingering effect of the adaptation currents keeps the neuronal susceptibility to a low value. This long lasting effect of the adaptation currents is related to slow After HyperPolarization (sAHP) and is related to the value of τ_w in the AdExp model. Thus, the influence of τ_w on the Inter-Burst Interval (IBI) is very significant in our model, as the sAHP mostly dictates the duration of the down-state.

Eventually, as the adaptation variable recovers to its default value, the susceptibility returns to near-zero, then positive values just before the initiation of the next burst.

2.2.2 Shaping bursts through adaptation channels

I will refer to our article (Fardet, Ballandras, et al. 2018) for more details regarding the three different ways in which we have modeled the synaptic coupling of the neurons, the hypotheses underlying the approximations of the neuronal dynamics,

and the consequences that these descriptions have on the population behavior. In a nutshell, these three descriptions allowed us to make relevant predictions regarding the bursting behavior of the population, as can be seen on Figure 2.7.

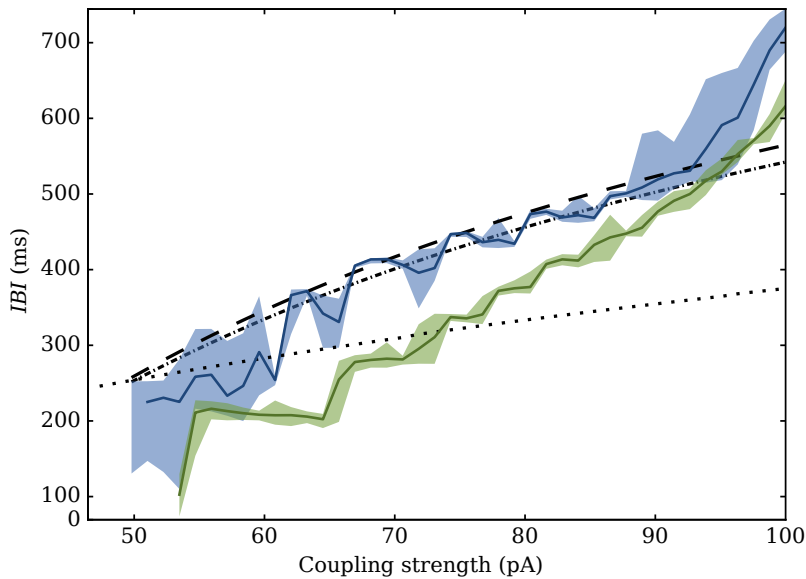


Figure 2.7.: Variation of the IBI depending on maximum value of the PSC (in pA). Values predicted by the equivalent model are shown in dashed, dot-dashed and dotted lines respectively for the Dirac, alpha and continuous models. Simulated values for a Gaussian network with $\sigma_k = 4$ (blue) and $\sigma_k = 20$ (green) are superimposed: the main curve represents the average value, while the filled area marks the 5th to 95th percentiles.

One of the main advantages of this analytic model is that it does not only propose a mechanistic explanation of the bursting behavior, but also predicts the properties of the collective activity based only on the neuronal properties and the average connectivity. Furthermore, linking the parameters of the AdExp model to the biological mechanisms underlying neuronal adaptation, we were able to predict the effect of a blockade of specific adaptation channels on the properties of the network bursts.

Theoretical predictions

Neuronal adaptation channels can be divided into three main categories: slow After HyperPolarization (sAHP), medium After HyperPolarization (mAHP), and fast After HyperPolarization (fAHP). In order to understand the effect of these channels, we mapped them to some of the parameters and phenomena in the AdExp model. This lead to three theoretical predictions (PF, PM, PS) for each of the AHP types.

For instance, fAHP plays an important role in the repolarization of the membrane potential after a spike; in the model, it is thus related to the V_r variable (the reset potential).

Blocking channels responsible for fAHP should therefore be equivalent to increasing the value of V_r . This would lead to an increased excitability of the neurons during the up-state, causing more spikes to be emitted, and at higher rates — see Figure 2.8 (a). Because of the higher activity during a burst, an indirect effect of fAHP blockade should an increase of the sAHP currents, as well as additional synaptic depression, which would lead to increased Inter-Burst Intervals (IBIs).

PF: blocking fAHP increases in-burst activity and lengthens IBIs

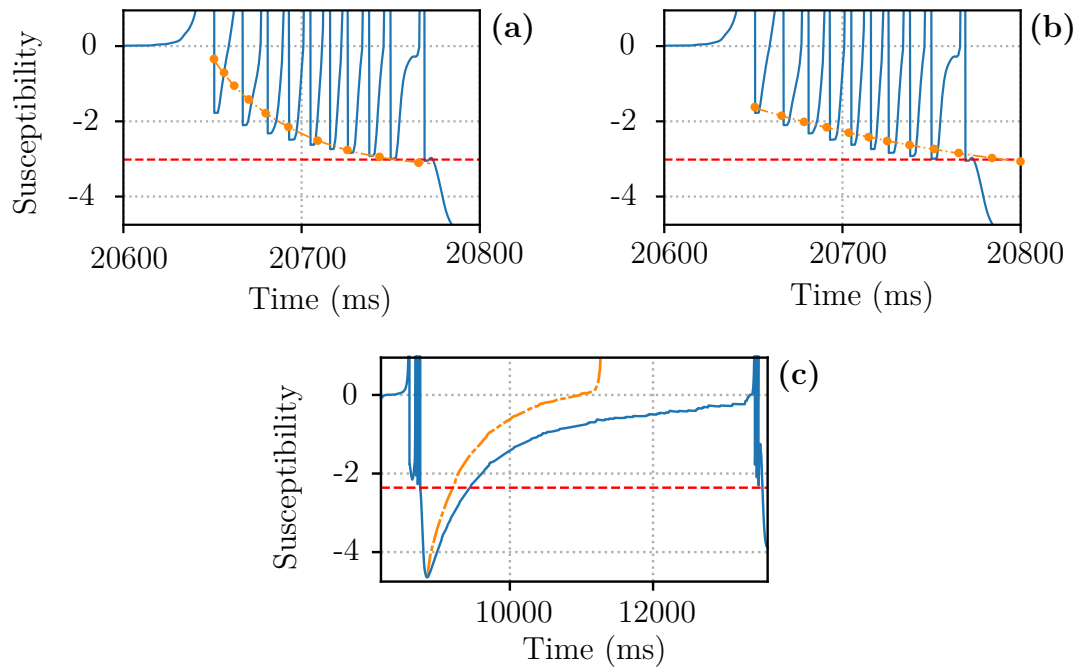


Figure 2.8.: Predicted evolution of the bursting activity under blockade of an AHP currents; susceptibility of simulated activity in “control” conditions is in blue, opposite of the network excitatory power is given by the dashed red line, and predicted shift in the post-spike susceptibility is given by the dash-dotted orange lines, with spike times marked by dots. **(a)** Blockade of *fAHP* through paxilline (increasing V_r in the model) should lead to higher post-spike susceptibility, leading to higher firing rates. **(b)** Blockade of *mAHP* through apamin should reduce medium-term potassium influx, hence reducing the step increase of w in the model, i.e. the step between two consecutive post-spike susceptibility levels. This leads to a lower slope for the decrease of the susceptibility, hence to longer bursts and more spikes but no significant increase in the firing-rate. **(c)** Blockade of *sAHP* through isradipine should remove the long-term influx of potassium post-burst, equivalent to reducing τ_w in the model, thus leading to a faster recovery of the susceptibility, i.e. to shorter interbursts.

Similarly, mAHP produces hyperpolarizing currents whose effect lasts on the order of 100 ms, and that therefore cause (in the model) the progressive decrease in neuronal susceptibility during the burst.

Here, though, we encounter one of the limitations of the AdExp model: since only one adaptation current is present, it is difficult to separate the effects of the slow and medium AHP. However, taking into account that the effect of mAHP is only relevant during the up-state, we will consider here that, as long a τ_w — the typical relaxation time of the adaptation current — is on the order of the burst duration, only the value of b matters to describe the effect of mAHP⁴. Thus, blocking mAHP should lead to lower adaptation inputs, which, as depicted on Figure 2.8 (b) and Figure 2.6, would lead to an increased number of spikes during the burst, though at

PM: blocking mAHP should increase burst duration

⁴Note that we only consider here the effect during the burst: lowering b would obviously also affect the IBI, but separating the effect of medium and slow AHP cannot be done in the framework of the AdExp model, except as a Gedankenexperiment, which is what this prediction is.

a rather similar rate, hence resulting in an increased burst duration. Because the in-burst firing-rate does not increase significantly, it is difficult to predict the indirect effect of mAHP blockade on the IBI. In any case, changes should be less significant than those resulting from fAHP blockade.

Eventually, as for mAHP, we will try to isolate the effect of sAHP by considering that its influence is solely related to the value of τ_w ⁵.

In that perspective, blocking sAHP should lead to a significant decrease of the IBI, as shown on Figure 2.8 (c), regardless of the influence of synaptic depression because both phenomena occur on similar timescales (several hundred milliseconds to a few seconds). Thus, their effects should add up, meaning that weakening one or the other should allow the neuronal susceptibility to increase more rapidly after a burst, allowing for a quicker occurrence of the next burst initiation.

PS: blocking sAHP leads to shorter IBIs

Experimental results

In order to test the theoretical predictions experimentally, I went to Elisha Moses' laboratory at the Weizmann Institute, where I tested the effect of a specific blocker on each of the adaptation currents:

- paxilline, to selectively block fAHP (ReiSS et al. 2006; Sah et al. 2002; Shao et al. 1999),
- apamin, to selectively block mAHP (Empson et al. 2001; ReiSS et al. 2006; Sah et al. 2002),
- isradipine, to selectively block sAHP (Lima et al. 2007; ReiSS et al. 2006).

I analyzed the changes in the collective behavior of cultures that were induced by the blockade of each of the AHP currents. To that purpose, I recorded the activity of primary neuronal cultures from Wistar rats using calcium imaging.

For each of the three blockers, I analyzed the changes induced by the addition to normal (EI) cultures, with functional excitatory and inhibitory synapses, or to excitatory only (E) cultures, where inhibitory synapses had previously been blocked by the addition of bicuculline (40 μ M).

In total, 12 experiments were performed — see “Experimental protocols” (Appendix E) — among which:

- 6 led to results compatible with the theoretical predictions,
- 2 could be explained taking STD into account,
- 2 cultures showed no reaction to bicuculline,
- 1 culture showed no significant reaction to apamin,
- 1 culture showed a different reaction to isradipine, switching to a strongly irregular behavior.

I will leave aside the last four experiments, which cannot be explained at our current level of understanding, and focus on the first eight experiments to see how they relate to our mechanistic description of the bursting behavior.

⁵It is obviously also related to b , however, for a quasi-exponential decay, such as is undergone by w after a burst, reducing the initial value or the timescale has a similar effect regarding the evolution of the delay necessary to reach the minimum value w_{min} .

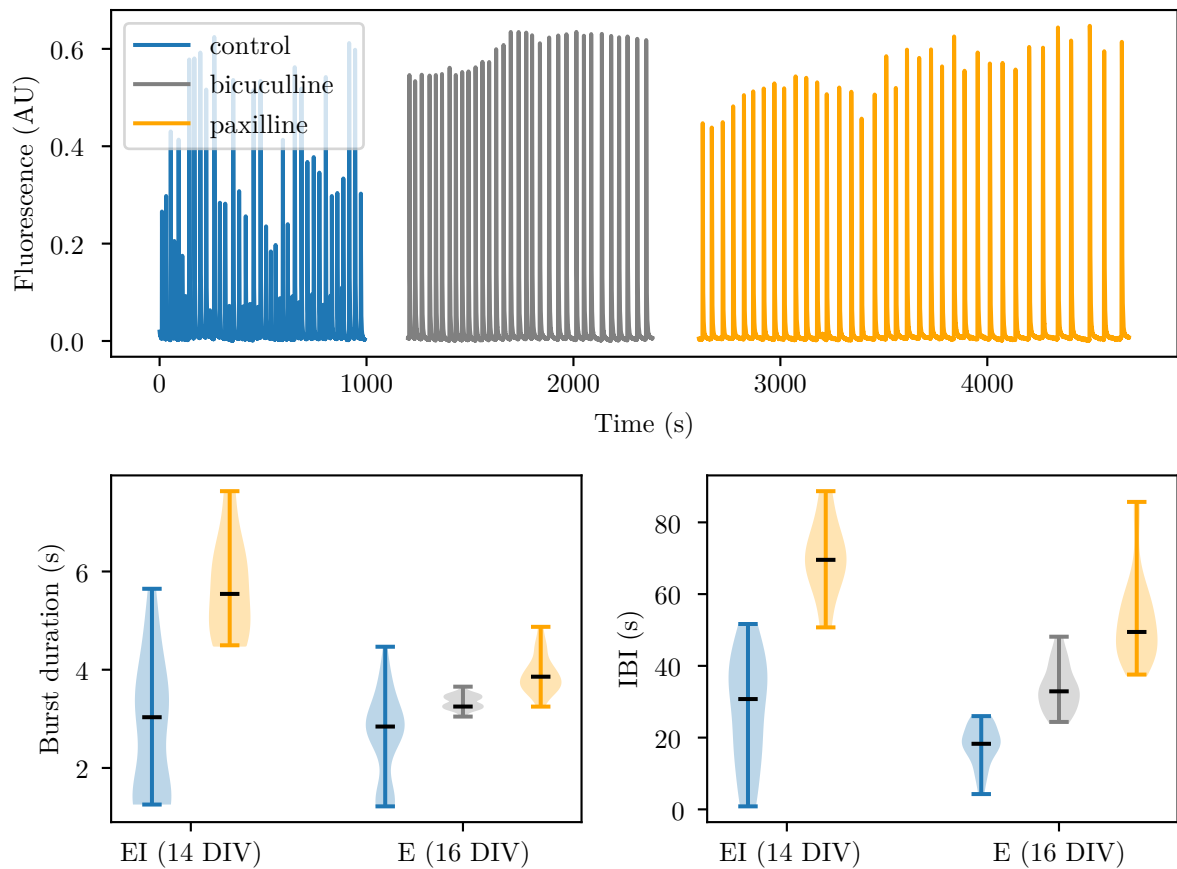


Figure 2.9.: Influence of the fAHP blocker, paxilline, on the bursting activity. (Top) Traces of the calcium fluorescence over time for the 16 DIV culture. (Bottom) Distribution of the burst duration and inter-burst interval (IBI) in the control conditions (blue), after addition of bicuculline (grey), and after addition of paxilline (orange). Median is marked in black. For burst duration and IBIs, p-values using the Kolmogorov-Smirnov and Mann-Whitney rank tests were all smaller than 10^{-5} .

In the case of paxilline (Figure 2.9), the two positive results included both EI (14 DIV) and E (16 DIV) networks. As predicted (PF), addition of paxilline with a final concentration of $2.5 \mu\text{M}$ leads to a significant increase in the Inter-Burst Interval (IBI). In addition to this IBI lengthening, the addition of paxilline also resulted in a significant increase of the burst duration. This effect could indicate that the mAHP is not sufficient to counterbalance the increased excitability, leading to a longer active period in spite of the increased firing rate. However, electrophysiological recordings would be necessary to provide a definite answer to the evolution of the intra-burst activity.

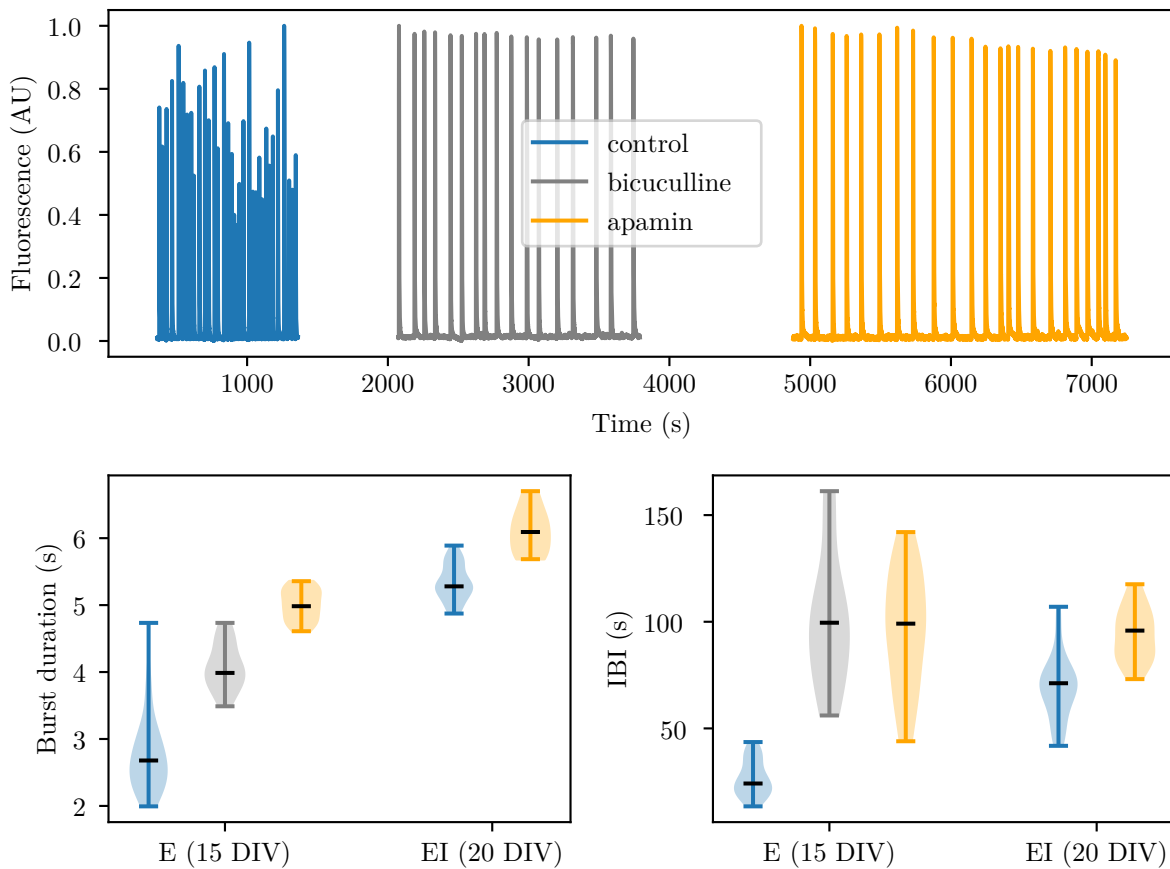


Figure 2.10.: Influence of the mAHP blocker, apamin, on the bursting activity. (Top) Traces of the calcium fluorescence over time for the 15 DIV culture. (Bottom) Distribution of the burst duration and inter-burst interval (IBI) in the control conditions (blue), after addition of bicuculline (grey), and after addition of apamin (orange). Median is marked in black. For burst duration, p-values using the Kolmogorov-Smirnov and Mann-Whitney rank tests were all smaller than 10^{-5} .

Addition of apamin (Figure 2.10, final concentration 200 nM) also led to behaviors that were compatible with the theoretical prediction (PM) for both EI (20 DIV) and E (15 DIV) networks. In both cases, the activity displayed a significant shift towards longer bursts, with no or only slightly significant changes in the IBI.

As shown on Figure 2.11, addition of isradipine (final concentration of $7.5 \mu\text{M}$) led to a significant decrease of the IBI (PS) with no significant change in the burst duration.

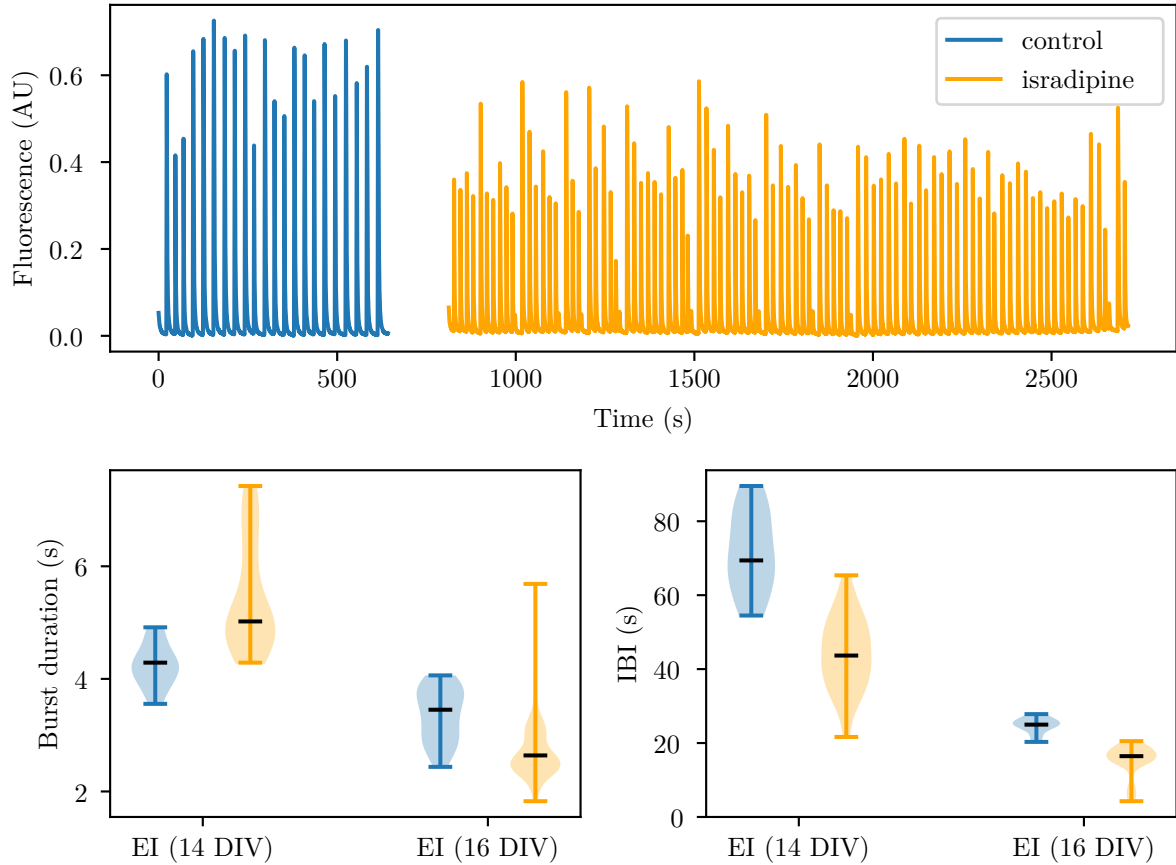


Figure 2.11.: Influence of the sAHP blocker, isradipine, on the bursting activity. (Top) Traces of the calcium fluorescence over time for the 16 DIV culture. (Bottom) Distribution of the burst duration and inter-burst interval (IBI) in the control conditions (blue) and after addition of isradipine (orange). Median is marked in black. For IBIs, p-values using the Kolmogorov-Smirnov and Mann-Whitney rank tests were both smaller than 10^{-6} .

Eventually, two cultures displayed significant qualitative changes in their activity after addition of either apamin or paxilline. Indeed, as shown on Figure 2.12, the bursting behavior switched from a rather regular activity, with little variability in the bursting intensity, to series composed of a “strong” burst, followed by several smaller bursts, which are repeated in time.

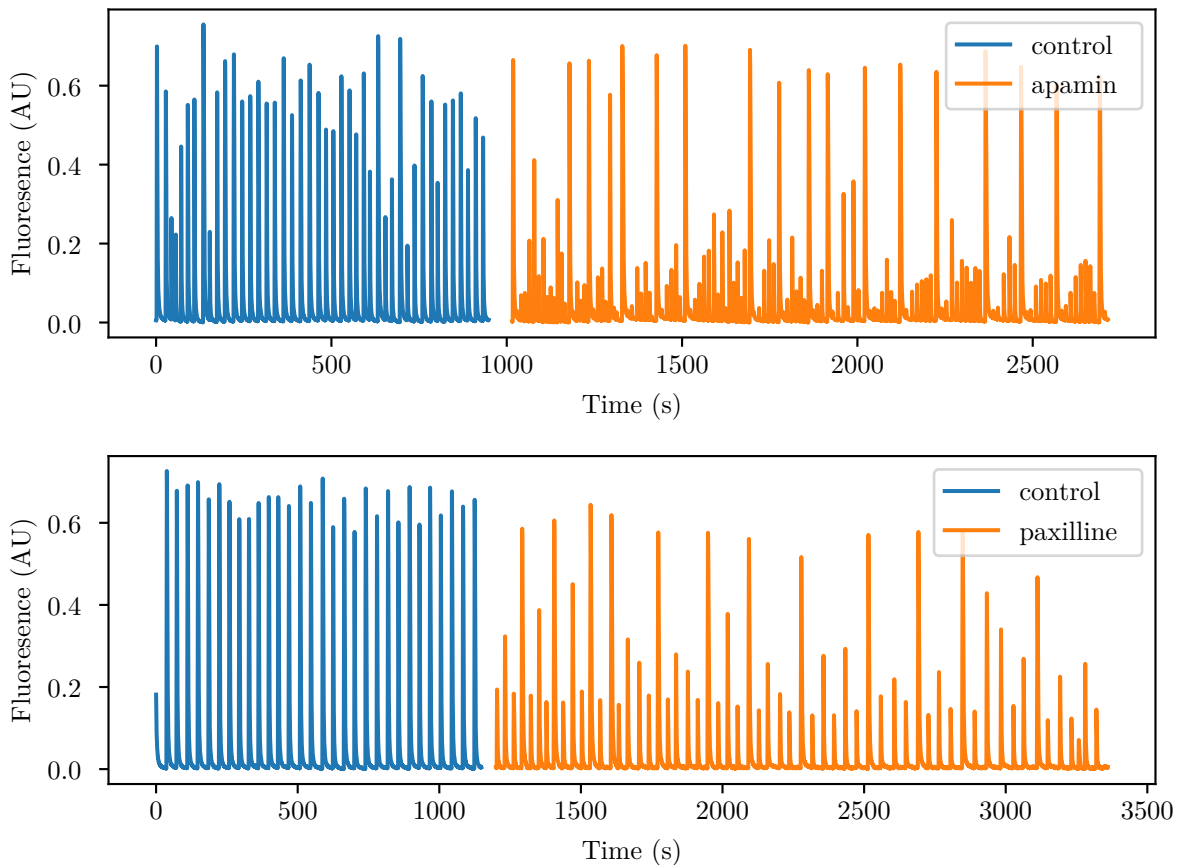


Figure 2.12.: (Top) Reponse of an EI culture (16 DIV) to apamin. (Bottom) Response of an EI culture (16 DIV) to paxilline. In both cases, large (normal) bursts are separated by several smaller bursts.

This behavior looks similar to an effect shown by Loebel et al. 2002 where short-term depression prevents the emergence of “strong” bursts until the vesicle pools have been replenished.

Though further experiments would be necessary to obtain exploitable statistics on the influence of the adaptation channels, these preliminary results are entirely compatible with the hypothesis that cellular adaptation plays a prominent role in shaping network bursts.

*preliminary
experiments
are compatible
with all
predictions*

2.3 Statistical properties of bursting behaviors

Statistical properties of the bursting activities are among the easiest measurements that are experimentally accessible. Indeed, these are “macroscopic” predictions, they involve the whole network, and they are therefore easy to “spot”, compared to specific behaviors in single neurons, and also more reliable given the large variance in biological neuronal networks.

Throughout this manuscript, my goal has been to provide such macroscopic and statistical properties, in order to make experimentally testable predictions. In the case of bursting, the objective is to find out whether there could be some significant statistical differences between pacemaker-driven and noise-driven bursting, as well as between adaptation-based and STD-based termination.

2.3.1 The transition to synchronous bursting

Transition of neuronal networks from asynchronous to synchronous activities has been studied by several groups in the case of balanced networks subjected to external inputs (Brunel 2000; Brunel and Hakim 2008), or as a way of switching between different brain states (Destexhe 2009). However, these modes of synchronization are quite different what is happening in cultures, where the networks are not necessary balanced and are not subjected to external inputs.

Examining the effect of adaptation on the synchronization properties of pairs of neurons have led Ladenbauer et al. 2012 to propose that spike-triggered adaptation might improve low-frequency oscillations in excitatory networks. I will show here that, taking spike-triggered adaptation and its calcium dependency into account, one can explain the progressive transition between an asynchronous and a synchronous bursting state which is observed experimentally.

Experimental observations

In a recent paper, Penn et al. 2016 revealed the existence of a well-defined phase transition in hippocampal cultures, going from asynchronous to phase-locked synchronized burst through the variation of the extracellular calcium concentration.

calcium-induced transition

This transition was progressive: starting with fully uncoupled, asynchronous neurons, they first obtained a “fuzzy” synchronized state, where neurons seem to synchronize their spiking frequency while preserving a broad distribution of the phases. Once calcium concentration exceeded 200 μM , a zero-phase-lag synchrony was obtained, with very sharp initiation for the up-state and almost no interburst activity.

Influence of calcium on neurons and synapses

From a mechanistic standpoint, reducing the calcium concentration can affect four main properties of the neuronal network.

calcium affects both synaptic and neuronal properties

First of all, and most importantly, the diminution of calcium reduces its influx at synapses upon arrival of an action potential, which reduces vesicle release, hence the efficiency of neurotransmission (Neher et al. 2008). At zero calcium, the network is thus effectively disconnected, with a complete removal of the triggered-release; however, the effect of calcium on the spontaneous release — minis — has been reported to be weaker, leading to a relatively smaller variation of the noise rate and amplitude (Williams et al. 2018).

However, apart from synapses, calcium concentration also affects the neuronal behavior. Indeed, all After HyperPolarization (AHP) mechanisms mentioned in the previous sections rely on a spike-driven influx of calcium to trigger the hyperpolarization, meaning that a decrease of calcium would also decrease all AHP-related influence. Diminution of calcium also reportedly increases the excitability of neurons and the combined effect of excitability and AHP changes may lead the neuronal behavior to switch from a spiking to a intrinsically bursting behavior at lower calcium concentrations (Su et al. 2001).

Reproducing the “fuzzy” transition with adaptation

In order to reproduce as faithfully as possible the suspected mechanisms underlying the phase-transition observed by Penn et al. 2016, the effect of changes in the extracellular calcium concentration were modeled in the following way:

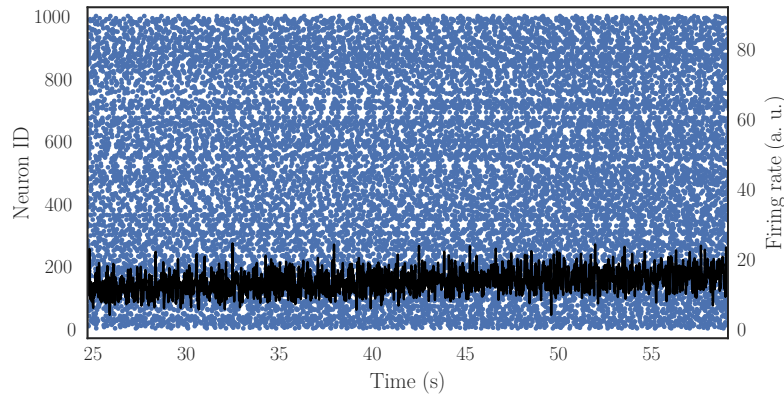
- normalized calcium factor c was defined as $c = [\text{Ca}^{2+}]/1 \text{ mM}$,
- synaptic strength were varied continuously according to $s = c \cdot s_{max}$,
- spike-driven adaptation was set according to the equation $b = b_{min} + c(b_{max} - b_{min})$.

The transition was tested for both spiking pacemaker neurons, with $V_r < V_{th}$, and for neurons that transited between spiking and bursting behaviors depending on the calcium concentration. This change in the behavior was obtained by setting $V_r \gtrsim V_{th}$, such that for high values of b , a single spike is sufficient to bring the neuronal state inside the V -nullcline and prevent bursting sequences. Parameters used for the neurons are given in “Network models and parameters” (section D.2).

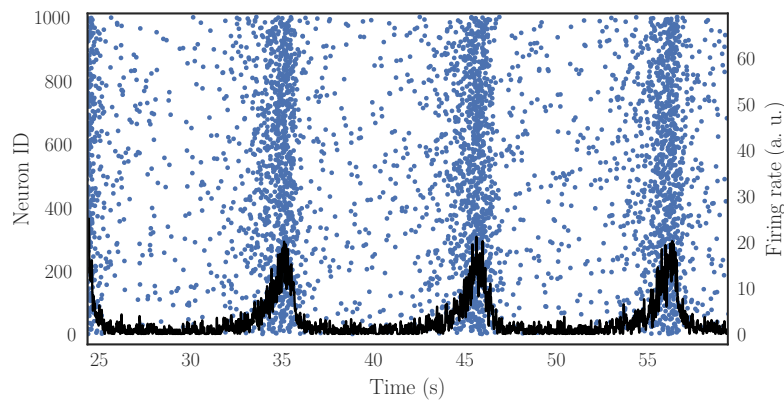
As shown on Figures 2.13 and 2.14, both conditions lead to a progressive transition from asynchronous to zero-lag synchrony which is quite similar to what was observed by Penn et al. 2016. Indeed, at lower calcium, the reduced connectivity and noise lead to sparse activity in the network, the excitatory power being insufficient to trigger many successive spikes. Moreover, the decreased AHP diminishes the relaxation character of neuronal oscillations and reduces their synchronizability, leading to this “fuzzy” synchronization pattern. For higher calcium concentration, the highly synchronized pattern is recovered by the enhanced connectivity and synchronizability, while the restored AHP prevents the activity from diverging during a burst.

The most notable difference lies in the burst termination, which occurs much more rapidly in the simulations compared to the experimental observations. This phenomenon can be attributed to the fact that neither NMDA receptors, nor asynchronous release is incorporated in the model, preventing the occurrence of long-lasting bursts due to slower excitation mechanisms.

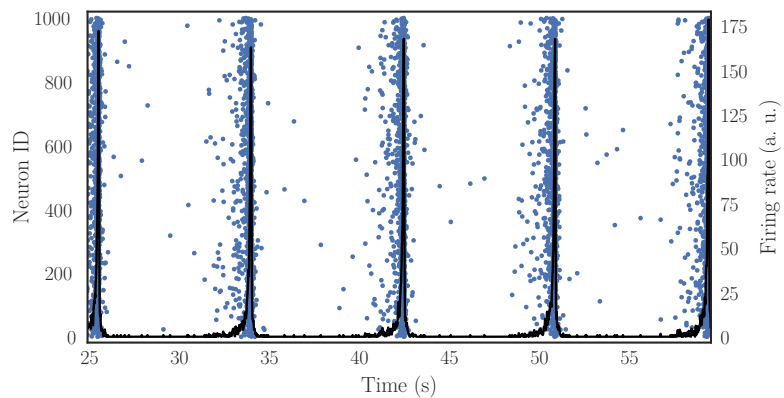
adaptation-based description successfully reproduces the asynchronous, fuzzy, and zero-lag stages



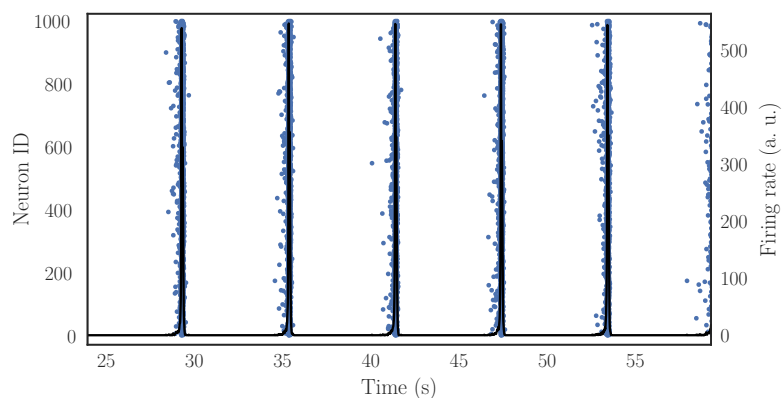
(a) Raster plot of the network for $[Ca^{2+}] = 0 \mu M$.



(b) Raster plot of the network for $[Ca^{2+}] = 100 \mu M$.



(c) Raster plot of the network for $[Ca^{2+}] = 200 \mu M$.



(d) Raster plot of the network for $[Ca^{2+}] = 500 \mu M$.

Figure 2.13.: Evolution of the properties of the culture depending on the simulated calcium concentration for spiking pacemaker neurons. Blue dots mark neuronal spike time while the black curve represents the firing-rate of the whole population in arbitrary units (consistent throughout the figure). Comparing the numerical and experimental results, it appears that both the “fuzzy” transition and the zero-lag synchrony can be recovered. The progressive decrease of the IBI due to the increased level of synaptic noise in the culture is also compatible with the experimental observation.

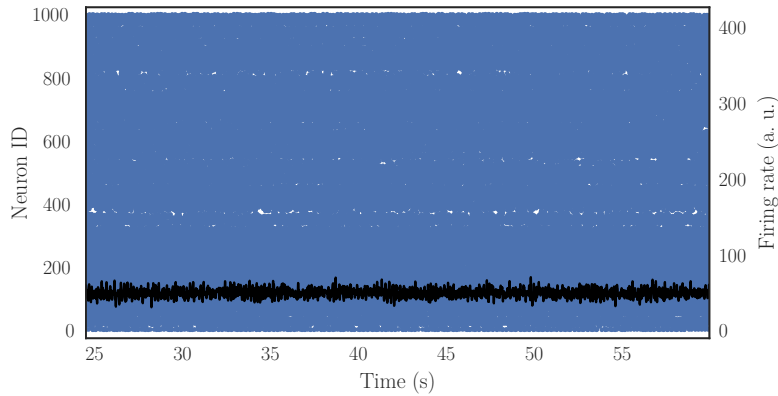
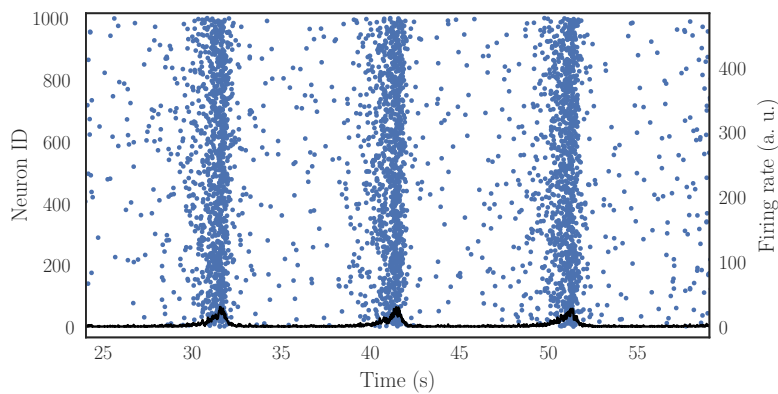
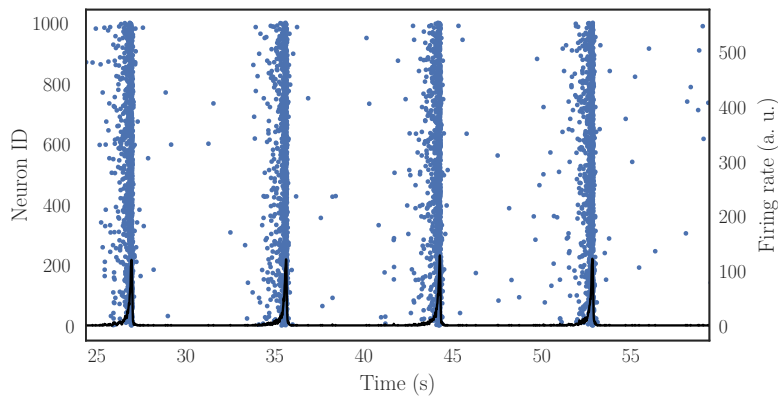
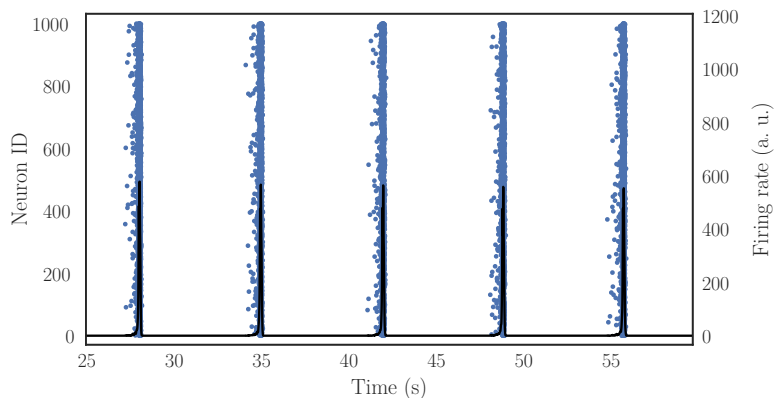
(a) Raster plot of the network for $[Ca^{2+}] = 0 \mu\text{M}$.(b) Raster plot of the network for $[Ca^{2+}] = 100 \mu\text{M}$.(c) Raster plot of the network for $[Ca^{2+}] = 200 \mu\text{M}$.(d) Raster plot of the network for $[Ca^{2+}] = 500 \mu\text{M}$.

Figure 2.14.: Evolution of the properties of the culture depending on the simulated calcium concentration for pacemaker neurons transitioning from intrinsically bursting at low $[Ca^{2+}]$ to adaptive spiking at higher $[Ca^{2+}]$. Blue dots mark neuronal spike time while the black curve represents the firing-rate of the whole population in arbitrary units (consistent throughout the figure). Comparing the numerical and experimental results, it appears that both the “fuzzy” transition and the zero-lag synchrony can be recovered. The progressive decrease of the IBI due to the increased level of synaptic noise in the culture is also compatible with the experimental observation.

2.3.2 Synchronous bursts as percolation events

Is there a generic way to describe bursting? Can we find a framework that would not depend on the specific properties of the units that constitute the bursting network, and may even be independent of the network (at least qualitatively)?

It turns out we can: the initiation of bursting activity in neuronal networks (Breskin et al. 2006; O. Cohen et al. 2010), as well as many other phenomena such as failures in electrical networks, magnetization, and opinion or epidemic spreading, can be described as percolation events.

*burst
initiation as a
generic
percolation
phenomenon*

This is because in all these systems, each unit's behavior can be described as that of a gatherer-comparator: it accumulates the inputs it receives, then “decides” to change its state or not depending on their total value – “changing state” meaning respectively spiking, failing, flipping, changing your mind, or getting sick, in the previously mentioned systems.

A percolation event on a neuronal network is thus a rapid transition from a state where only a small fraction of the neurons are active to a state where almost all neurons are firing or just fired — see Figure 5 in “Review on percolation (IOP Conf. Series 2017)” (section J.1) for a description of this percolation process. This mechanism explains and describes the initiation of a burst as the spread of this active state over the whole network.

This universal behavior enables us to make very general and resilient predictions on the behavior of such units when they are gathered in large assemblies, and this regardless of the detailed mechanisms underlying the response of the units to a stimulation.

Quorum percolation

In that context, Quorum Percolation (QP) has been elaborated to describe the initiation of bursts observed in such cultures as a collective phenomenon, from the point of view of statistical physics rather than dynamical systems.

The introduction of QP was justified by the fact that:

“ In the simplest picture of a spiking neuron, stimuli (inputs) from connected neurons are “integrated” in the target neuron, which fires once a threshold voltage is reached and then propagates the electric signal on to other neurons. Imposing the need for a large quorum of m input nodes to fire leads to a percolation problem, which we term “quorum percolation” (QP). ”

(O. Cohen et al. 2010)

*percolation
has enabled to
deduce
structural
information*

Using this description, several studies (Breskin et al. 2006; O. Cohen et al. 2010; Soriano, Rodríguez Martínez, et al. 2008) managed to show that the evolution of the bursting properties with the number of connections in the network was compatible with an overall Gaussian distribution for the in-degree of the neurons, and that the average value of this Gaussian distribution varied between 60 and 150 neighbors depending on the neurons' origins and density inside the culture.

A review of this model and a discussion of how heterogeneities, delays, and decay affect its properties is proposed in Monceau, Renault, Mérens, Bottani, and Fardet 2017 — included in “Papers” (Appendix J) — as well as a discussion about how this mechanism can also describe the initiation of spontaneous activity in neuronal cultures.

Because these models seemed to reproduce quite faithfully the initiation period of a burst, another study by J.-P. Eckmann et al. 2010 even proposed alternative network structures that would provide a more realistic slope for the temporal recruitment of the neurons, developing the concept of “leader neurons”, which I will comment on in more details in the following chapter.

Extended QP: inhibition and dynamical units

These studies on percolation, confirmed that a sudden shift between two distinct states, associated to the notion of bursting activity in neuronal cultures, is an intrinsic property of random networks containing excitable units: as soon as the number of active units goes above a critical threshold, the activity percolates and spreads to the entire culture.

The robustness of this model to topological disorder in the number of neighbors of the neurons (Mérens et al. 2016), heterogeneity in the firing threshold among the neurons (Monceau, Renault, Mérens, and Bottani 2016), and temporal decay (Renault, Monceau, and Bottani 2013) was also demonstrated by later studies.

We further showed (Fardet, Bottani, et al. 2018) that presence of inhibitory units does not qualitatively affect the behavior but only modulates the threshold value. This is consistent with the fact that burst initiation shows no significant difference in fully excitatory or mixed excitatory/inhibitory networks. In this same publication — included in “Inhibitory and dynamical quorum percolation (Physica A 2018)” (section J.2) — we verified that these predictions were independent of the detailed model used to describe the neurons by showing that the percolation transition could also be reproduced using cells modeled by the AdExp model.

robust against many sources of disorder and independent of the unit’s detailed dynamics

This percolation mechanism, coupled to the relaxation-like behavior of adaptive neurons, explains the high synchronisability of neuronal networks, since differences between neurons are nullified by the fast recruitment of the network, which synchronizes all units.

In this condition, we understand easily why the concept of “leader neurons” became popular. Indeed, the IBI does not correspond to the average value of over all oscillators, as in the Kuramoto model, but is driven by the period of the n th “fastest” neurons, n being the number of active neurons required for percolation to occur.

2.3.3 Statistical properties of the interburst interval

In the introduction — “Simple models for spiking neurons” (subsection 1.3.3) — we have seen that neurons can react differently to similar inputs, and especially how *pacemaker neurons* display more regular behavior compared to non-pacemaker neurons of type I or II.

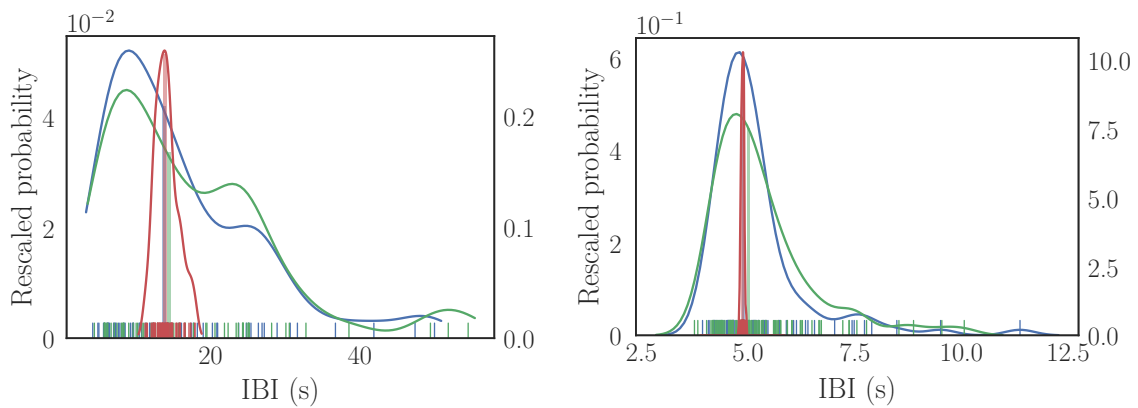
In the following paragraphs, we will see how this increased stability of pacemaker neurons with respect to their intrinsic frequency leads to significant differences in the statistical properties of the bursting activity.

Following other studies on the subject (T. A. Gritsun, Le Feber, et al. 2010; T. Gritsun et al. 2009), we will use these statistical properties to discuss the likelihood of noise versus pacemaker activity as the origin of bursting activity in neuronal cultures.

Bursting activity of homogeneous networks

pacemaker-driven bursts are much more regular

Looking at the distribution of Inter-Burst Intervals (IBIs) in networks where all neurons have identical properties allows to further illustrate the difference between non-pacemaker and pacemaker neurons⁶: as their name indicates, pacemaker neurons display an extremely regular activity, while non-pacemaker neurons of both type I and II generate much more irregular activity. This tendency is further increased as the IBI increases, even though pacemaker neurons retain a rather regular behavior, the variability of the other two types syrockets.



(a) Density estimates for 14-second IBI (b) Density estimates for 5-second IBIs

Figure 2.15.: Kernel density estimate of the IBI distribution for each of the neuronal types. Bursts were obtained for a 1000-neuron network simulated over 1000 seconds with a 15 Hz Poisson noise on the synapses. Individual values of the IBIs are given by the small sticks while density estimates using Gaussian kernel are marked by the solid lines. Median values of the distributions are represented by the vertical lines. Results for pacemaker neurons are in red (median IBI of 13.9 and 4.9 s) and the density is given on the right axes. Type I neurons are in green (median IBI of 14.4 and 4.9 s) and type II neurons are in blue (median IBI of 13.8 and 5.0 s); the densities of both are given on the left axes.

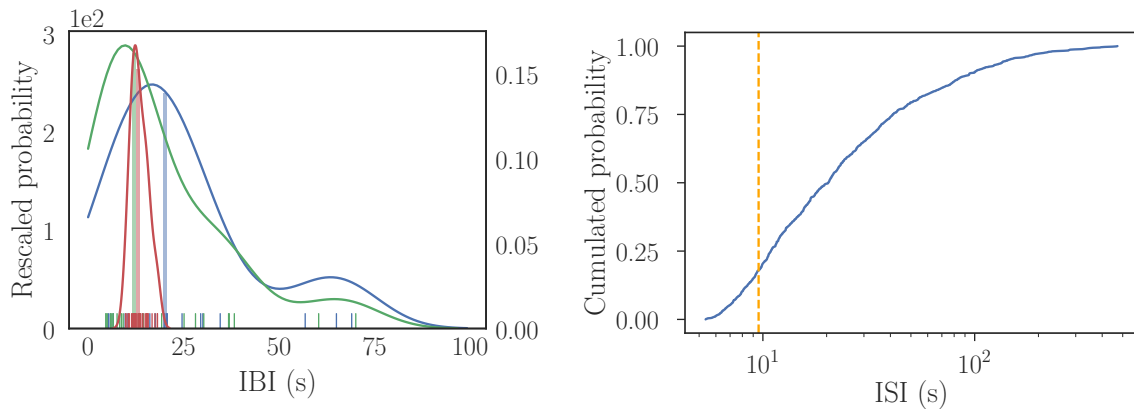
Bursting activity of heterogeneous networks

As shown on Figure 2.16a, adding heterogeneity in the network, by relaxing the constraint that all neurons have identical properties, further increases the variability in the IBI distribution.

This also illustrate the difference between synchronous bursts and a Kuramoto process: looking at the distribution of Inter-Spike Intervals (ISIs) for isolated individual neurons — Figure 2.16b — one can acknowledge the significant difference between the median IBI, which is around 9 s, and the median ISI, which is around 20 s, not accounting for neurons which spiked less than twice over the whole 1000 seconds.

Contrary to Kuramoto phase oscillators which synchronize around the median frequency, our adaptive neurons, as relaxation oscillators, are driven by the fastest group.

⁶ see previous discussion at the end of “Simple models for spiking neurons” (subsection 1.3.3);



(a) Density estimates for ~ 15 -second IBIs in heterogeneous networks

(b) ISI probability of pacemaker neurons compared to their median IBI.

Figure 2.16.: (a) Kernel density estimate of the IBI distribution for each of the neuronal types. Bursts were obtained for a 1000-neuron network simulated over 1000 seconds with minis at an average 15 Hz. Individual values of the IBIs are given by the small sticks while density estimates using Gaussian kernel are marked by the solid lines. Median values of the distributions are represented by the vertical lines. Results for pacemaker neurons are in red (median IBI of 13.2 s) and the density is given on the right axis. Type I neurons are in green (median IBI of 12.0 s) and type II neurons are in blue (median IBI of 20.2 s); the densities of both are given on the left axis. For all neurons, values of a and V_{th} were sampled from Gaussian distributions, with a 0.01 pA and 0.01 mV deviation respectively. This is actually sufficient to produce significant variability in the intrinsic interspike interval of the neurons, when they are taken isolately. (b) shows the cumulated distribution for the pacemaker neurons, which are simulated with the same noise as in (a), but are uncoupled (spikes are not transmitted). The dotted yellow line shows the median interburst, which is significantly different from the average ISI in the network.

Coefficient of variation

In the Supplementary material of their paper, Penn et al. 2016 quantified the variability in the IBI of its hippocampal cultures using a simple measure, the Coefficient of Variation (CV), defined as the ratio between the standard deviation σ of a series, and its mean μ :

$$CV = \frac{\sigma}{\mu}. \quad (2.3)$$

For most of its cultures, the CVs of the IBIs were rather low, with a median around 0.34 for physiological calcium concentrations ($\text{Ca}^{2+} = 1$ mM), and median IBI values between 2 and 8 seconds.

Furthermore, for lower concentrations, they obtain even lower CVs, 0.22 at $\text{Ca}^{2+} = 100$ μM , and 0.09 at $\text{Ca}^{2+} = 200$ μM , both with average IBIs that were higher than 10 s⁷.

⁷note that each of these values correspond to measurements made on a single culture

As can be seen on Figure 2.15, the CV of networks composed of pacemaker neurons is much lower than that networks without pacemakers. In fact, for long IBIs, the regularity of pacemaker neurons allow them to keep the variability to a reasonable range, with a CV of 0.18 on 2.15a, while the variability of the other neurons skyrockets to CVs greater than 0.65. On the other hand, as the interburst decreases, the CVs of non-pacemaker networks become more reasonable (around 0.2), whereas pacemaker neurons display an activity which is much too regular (CV < 0.01).

for long interbursts, pacemaker neurons are necessary to obtain realistic CVs

In order to obtain more realistic activities, with CVs of the same range as those observed in cultures, with various mean IBIs, one must therefore combine pacemaker and non-pacemaker neurons, as shown on Figure 2.17.

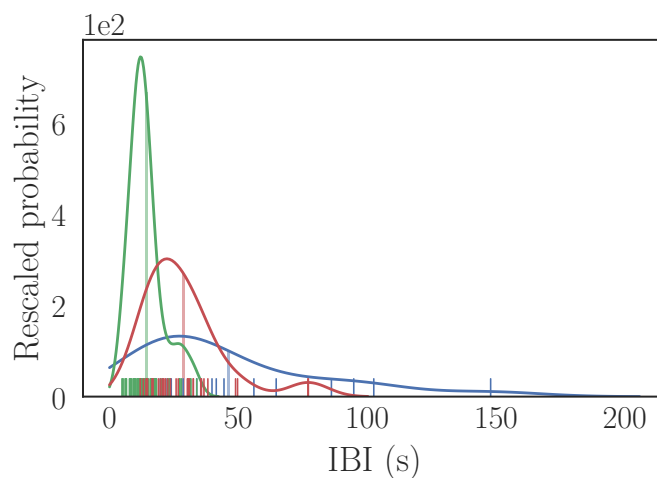


Figure 2.17.: IBI distribution of mixed pacemaker and non-pacemaker type I and II populations, with respective ratios of 20 %, 40 %, and 40 %. Compared to previous results, this enables the obtention of small and large average IBIs with variabilities that are compatible with experimental observations. Fast bursting with an average IBI of 14 s and a CV of 0.46 is shown in green; slower dynamics with an average IBI of 28 s and a CV of 0.54 is in red; slow bursting with a average IBI of 46 s and a CV of 0.76 is shown in blue.

Conclusion on temporal properties

Previous work by T. A. Gritsun, Le Feber, et al. 2010 looked into the profiles of burst dynamics (the rise and decay properties of the firing rate) to analyze the effect of pacemaker neurons on the activity. However, getting precise burst profiles from experimental data is quite tricky, which is the reason why I decided to focus on Inter-Burst Intervals (IBIs), which can be more reliably characterized.

T. A. Gritsun, Le Feber, et al. 2010 concluded that, for cortical cultures, small fraction of pacemaker neurons (between 4 and 16%) led to bursting profiles that are more realistic than those generated purely by noise. Using a different approach based on the statistical variability of the bursting dynamics, I provide additional evidence that inclusion of pacemakers in the population leads to activity patterns that are more compatible with experimental observations.

Overall, and regardless of the detailed neuronal behavior, percolation theory predicts that, for network of excitable units, a threshold exists, above which the activity of individual neurons will spread and recruit the entire network. Because spontaneous activity occurs, either from noise or from pacemaker neurons, experimental observations show the apparition of these percolation events, which lead to a global activity. This activity then self-sustains until some fatigue mechanism leads to its termination. The period of the bursting events is hence dictated by a balance between the intrinsic timescale of the recovery process and the excitation mechanism.

Though further investigation is required to provide a quantitative assessment of the dominant mechanisms (if any), we can already see that the occurrence of spontaneous bursting events appears as almost inevitable in light of the intrinsic neuronal properties... that is, on a homogeneous random network...

References for chapter 2

- Augustin, M., Ladenbauer, J., and Obermayer, K.** (2013). “How adaptation shapes spike rate oscillations in recurrent neuronal networks”. In: *Frontiers in Computational Neuroscience* 7, February, pp. 1–11. ISSN: 1662-5188. DOI: 10.3389/fncom.2013.00009 (cit. on p. 41).
- Baltz, T., Herzog, A., and Voigt, T.** (Sept. 2011). “Slow oscillating population activity in developing cortical networks: models and experimental results”. In: *Journal of Neurophysiology* 106.3, pp. 1500–1514. ISSN: 0022-3077. DOI: 10.1152/jn.00889.2010 (cit. on pp. 38, 75).
- Breskin, I. et al.** (Oct. 2006). “Percolation in Living Neural Networks”. In: *Physical Review Letters* 97.18, p. 188102. ISSN: 0031-9007. DOI: 10.1103/PhysRevLett.97.188102 (cit. on p. 58).
- Brunel, N.** (2000). “Dynamics of sparsely connected networks of excitatory and inhibitory spiking neurons”. In: *Journal of computational neuroscience* 208, pp. 183–208. ISSN: 1573-6873. DOI: 10.1023/A:1008925309027 (cit. on p. 54).
- Brunel, N. and Hakim, V.** (2008). “Sparsely synchronized neuronal oscillations”. In: *Chaos* 18.1, pp. 1–12. ISSN: 10541500. DOI: 10.1063/1.2779858 (cit. on p. 54).
- Chever, O. et al.** (2016). “Astroglial networks promote neuronal coordination”. In: *Science Signaling* 9.410. ISSN: 19379145. DOI: 10.1126/scisignal.aad3066 (cit. on p. 38).
- Cohen, D. and Segal, M.** (2011). “Network bursts in hippocampal microcultures are terminated by exhaustion of vesicle pools”. In: *Journal of Neurophysiology* 106, August 2011, pp. 2314–2321. ISSN: 0022-3077. DOI: 10.1152/jn.00969.2010 (cit. on pp. 40, 73–75).
- Cohen, O. et al.** (Jan. 2010). “Quorum percolation in living neural networks”. In: *EPL (Europhysics Letters)* 89.1, p. 18008. ISSN: 0295-5075. DOI: 10.1209/0295-5075/89/18008 (cit. on p. 58).
- Compte, A. et al.** (May 2003). “Cellular and Network Mechanisms of Slow Oscillatory Activity (<1 Hz) and Wave Propagations in a Cortical Network Model”. In: *Journal of Neurophysiology* 89.5, pp. 2707–2725. ISSN: 0022-3077. DOI: 10.1152/jn.00845.2002 (cit. on p. 41).
- Curtis, T. M. and Scholfield, C. N.** (2001). “Nifedipine blocks Ca²⁺ store refilling through a pathway not involving L-type Ca²⁺ channels in rabbit arteriolar smooth muscle”. In: *Journal of Physiology* 532.3, pp. 609–623. ISSN: 00223751. DOI: 10.1111/j.1469-7793.2001.0609e.x (cit. on p. 39).
- Destexhe, A.** (2009). “Self-sustained asynchronous irregular states and Up-Down states in thalamic, cortical and thalamocortical networks of nonlinear integrate-and-fire neurons”. In: *Journal of Computational Neuroscience* 27.3, pp. 493–506. ISSN: 09295313. DOI: 10.1007/s10827-009-0164-4. arXiv: 0809.0654 (cit. on pp. 36, 54).
- Eckmann, J.-P. et al.** (Sept. 2010). “Leaders of neuronal cultures in a quorum percolation model”. In: *Frontiers in Computational Neuroscience* 4, September, pp. 1–12. ISSN: 16625188. DOI: 10.3389/fncom.2010.00132. eprint: 1009.5355 (cit. on p. 59).
- Empson, R. M. and Jefferys, J. G.** (2001). “Ca(2+) entry through L-type Ca(2+) channels helps terminate epileptiform activity by activation of a Ca(2+) dependent afterhyperpolarisation in hippocampal CA3.” In: *Neuroscience* 102.2,

- pp. 297–306. ISSN: 0306-4522. DOI: 10.1016/S0306-4522(00)00494-2 (cit. on pp. 39, 49).
- Fardet, T., Bottani, S., et al.** (2018). “Effects of inhibitory neurons on the quorum percolation model and dynamical extension with the BretteGerstner model”. In: *Physica A: Statistical Mechanics and its Applications* 499. ISSN: 03784371. DOI: 10.1016/j.physa.2018.02.002 (cit. on pp. 59, 133, 179).
- Fardet, T., Ballandras, M., et al.** (2018). “Understanding the generation of network bursts by adaptive oscillatory neurons”. In: *Frontiers in Neuroscience* 12.FEB. ISSN: 1662453X. DOI: 10.3389/fnins.2018.00041 (cit. on pp. 41, 45, 46, 151, 179).
- Ferguson, K. A. et al.** (2015). “Examining the limits of cellular adaptation bursting mechanisms in biologically-based excitatory networks of the hippocampus”. In: *Journal of Computational Neuroscience* 39.3, pp. 289–309. ISSN: 15736873. DOI: 10.1007/s10827-015-0577-1 (cit. on pp. 41, 74).
- Goldin, A. L.** (2003). “Mechanisms of sodium channel inactivation”. In: *Current Opinion in Neurobiology* 13.3, pp. 284–290. ISSN: 09594388. DOI: 10.1016/S0959-4388(03)00065-5 (cit. on p. 38).
- Gritsun, T. A., Le Feber, J., et al.** (2010). “Network bursts in cortical cultures are best simulated using pacemaker neurons and adaptive synapses”. In: *Biological Cybernetics* 102.4, pp. 293–310. ISSN: 03401200. DOI: 10.1007/s00422-010-0366-x (cit. on pp. 38, 59, 62, 73, 75, 139).
- Gritsun, T. et al.** (Apr. 2009). “Network bursts in cortical neuronal cultures ‘Noise-versus pacemaker’- driven neural network simulations”. In: *2009 4th International IEEE/EMBS Conference on Neural Engineering*. August 2017. IEEE, pp. 626–628. ISBN: 978-1-4244-2072-8. DOI: 10.1109/NER.2009.5109374 (cit. on p. 59).
- Gulledge, A. T. et al.** (2013). “A Sodium-Pump-Mediated Afterhyperpolarization in Pyramidal Neurons”. In: *Journal of Neuroscience* 33.32, pp. 13025–13041. ISSN: 0270-6474. DOI: 10.1523/JNEUROSCI.0220-13.2013 (cit. on p. 39).
- Hirasawa, M. and Pittman, Q. J.** (2003). “Nifedipine facilitates neurotransmitter release independently of calcium channels”. In: *Proceedings of the National Academy of Sciences* 100.10, pp. 6139–6144. ISSN: 0027-8424. DOI: 10.1073/pnas.0936131100 (cit. on p. 39).
- Kaesler, P. S. and Regehr, W. G.** (2014). “Molecular Mechanisms for Synchronous, Asynchronous, and Spontaneous Neurotransmitter Release”. In: *Annual Review of Physiology* 76.1, pp. 333–363. ISSN: 0066-4278. DOI: 10.1146/annurev-physiol-021113-170338 (cit. on pp. 23, 39).
- Kavalali, E. T.** (2014). “The mechanisms and functions of spontaneous neurotransmitter release”. In: *Nature Reviews Neuroscience* 16.1, pp. 5–16. ISSN: 1471-003X. DOI: 10.1038/nrn3875 (cit. on pp. 37, 72).
- Ladenbauer, J. et al.** (2012). “Impact of Adaptation Currents on Synchronization of Coupled Exponential Integrate-and-Fire Neurons.” In: *PLOS Comput. Biol.* 8.4, e1002478. ISSN: 1553-7358. DOI: 10.1371/journal.pcbi.1002478. arXiv: arXiv:1310.2430v1 (cit. on p. 54).
- Lima, P. A. and Marrion, N. V.** (2007). “Mechanisms underlying activation of the slow AHP in rat hippocampal neurons”. In: *Brain Research* 1150.1, pp. 74–82. ISSN: 00068993. DOI: 10.1016/j.brainres.2007.02.067 (cit. on pp. 39, 49).
- Loebel, A. and Tsodyks, M.** (2002). “Computation by ensemble synchronization in recurrent networks with synaptic depression”. In: *Journal of Computational*

- Neuroscience* 13.2, pp. 111–124. ISSN: 0929-5313. DOI: 10.1023/A:1020110223441 (cit. on pp. 53, 161).
- Loy, K. et al.** (2014). “Common strength and localization of spontaneous and evoked synaptic vesicle release sites”. In: *Molecular Brain* 7.1, pp. 1–6. ISSN: Molecular Brain. DOI: 10.1186/1756-6606-7-23 (cit. on p. 37).
- Métens, S. et al.** (Mar. 2016). “Finite-size effects and dynamics of giant transition of a continuum quorum percolation model on random networks”. In: *Physical Review E* 93.3, p. 032112. ISSN: 2470-0045. DOI: 10.1103/PhysRevE.93.032112 (cit. on p. 59).
- Monceau, P., Renault, R., Métens, S., Bottani, S., and Fardet, T.** (2017). “Phase transition approach to bursting in neuronal cultures: Quorum percolation models”. In: *Journal of Physics: Conference Series*. Vol. 905. 1. DOI: 10.1088/1742-6596/905/1/012008 (cit. on pp. 58, 179).
- Monceau, P., Renault, R., Métens, S., and Bottani, S.** (July 2016). “Effect of threshold disorder on the quorum percolation model”. In: *Physical Review E* 94.1, p. 012316. ISSN: 2470-0045. DOI: 10.1103/PhysRevE.94.012316 (cit. on p. 59).
- Neher, E. and Sakaba, T.** (2008). “Multiple Roles of Calcium Ions in the Regulation of Neurotransmitter Release”. In: *Neuron* 59.6, pp. 861–872. ISSN: 08966273. DOI: 10.1016/j.neuron.2008.08.019 (cit. on pp. 39, 54).
- Penn, Y., Segal, M., and Moses, E.** (2016). “Network synchronization in hippocampal neurons.” In: *Proceedings of the National Academy of Sciences of the United States of America* 113.12, pp. 3341–3346. ISSN: 00278424. DOI: 10.1073/pnas.1515105113 (cit. on pp. 25, 38, 41, 54, 55, 61).
- ReiSS, P. and Koert, U.** (Aug. 2006). “Voltage-Gated Ion Channels as Drug Targets. Methods and Principles in Medicinal Chemistry, Vol. 29. Edited by David J. Triggle, Murali Gopalakrishnan, David Rampe and Wei Zheng.” In: *Angewandte Chemie International Edition* 45.33, pp. 5414–5414. DOI: 10.1002/anie.200685419 (cit. on p. 49).
- Renault, R., Monceau, P., and Bottani, S.** (Dec. 2013). “Memory decay and loss of criticality in quorum percolation”. In: *Physical Review E* 88.6, p. 062134. ISSN: 1539-3755. DOI: 10.1103/PhysRevE.88.062134 (cit. on pp. 59, 133).
- Sah, P. and Louise Faber, E. S.** (2002). “Channels underlying neuronal calcium-activated potassium currents”. In: *Progress in Neurobiology* 66.5, pp. 345–353. ISSN: 03010082. DOI: 10.1016/S0301-0082(02)00004-7 (cit. on pp. 38, 49).
- Sevilla, D. F. de et al.** (Aug. 2006). “Calcium-Activated Afterhyperpolarizations Regulate Synchronization and Timing of Epileptiform Bursts in Hippocampal CA3 Pyramidal Neurons”. In: *Journal of Neurophysiology* 96.6, pp. 3028–3041. ISSN: 0022-3077. DOI: 10.1152/jn.00434.2006 (cit. on p. 39).
- Shao, L. R. et al.** (1999). “The role of BK-type Ca²⁺-dependent K⁺ channels in spike broadening during repetitive firing in rat hippocampal pyramidal cells”. In: *Journal of Physiology* 521.1, pp. 135–146. ISSN: 00223751. DOI: 10.1111/j.1469-7793.1999.00135.x (cit. on p. 49).
- Sibarov, D. A. and Antonov, S. M.** (May 2015). “Characteristics of Postsynaptic Currents in Primary Cultures of Rat Cerebral Cortical Neurons”. In: *Neuroscience and Behavioral Physiology* 45.4, pp. 431–439. ISSN: 0097-0549. DOI: 10.1007/s11055-015-0093-9 (cit. on pp. 37, 72).

- Soriano, J., Rodríguez Martínez, M., et al.** (2008). “Development of input connections in neural cultures.” In: *Proceedings of the National Academy of Sciences of the United States of America* 105.37, pp. 13758–13763. ISSN: 00278424. DOI: 10.1073/pnas.0707492105. arXiv: 1008.0062 (cit. on pp. 58, 124).
- Su, H. et al.** (2001). “Extracellular calcium modulates persistent sodium current-dependent burst-firing in hippocampal pyramidal neurons.” In: *The Journal of neuroscience : the official journal of the Society for Neuroscience* 21.12, pp. 4173–4182. ISSN: 1529-2401 (cit. on p. 55).
- Tiwari, M. N. et al.** (2018). “Differential contributions of Ca²⁺-activated K⁺ channels and Na⁺/K⁺-ATPases to the generation of the slow afterhyperpolarization in CA1 pyramidal cells”. In: *Hippocampus* 28.5, pp. 338–357. ISSN: 10981063. DOI: 10.1002/hipo.22836 (cit. on p. 39).
- Van Vreeswijk, C. and Hansel, D.** (2001). “Patterns of synchrony in neural networks with spike adaptation”. In: *Neural Computation* 13.5, pp. 959–992. ISSN: 0899-7667. DOI: 10.1162/08997660151134280 (cit. on pp. 41, 151).
- Williams, C. L. and Smith, S. M.** (2018). “Calcium dependence of spontaneous neurotransmitter release”. In: *Journal of Neuroscience Research* 96.3, pp. 335–347. ISSN: 10974547. DOI: 10.1002/jnr.24116 (cit. on p. 54).
- Wilson, C.** (2008). *Up and down states*. revision #91903. URL: http://www.scholarpedia.org/article/Up_and_down_states (cit. on p. 36).

Chapter 3

Topology and spatio-temporal bursting patterns

In the previous chapter, we gave some details about the evolution of network bursts in time. However, since we are studying 2D cultures, this dynamics is not limited to the temporal realm but also displays specific spatial properties.

In this part, I will therefore try to provide a more complete description of the phenomenon, describing some of the interactions between the temporal, spatial, and structural mechanisms.

After a short overview of previous observations regarding spatio-temporal bursting in cultures, I will show how the access to the spatial data can help provide a more general definition of bursts. Then, I will discuss how different bursting mechanisms lead to different spatio-temporal properties as the interaction between cell and network properties change. We will see how this understanding could further improve our understanding of the primary mechanisms involved in epileptiform bursts.

Contents

3.1	Nucleation centers in experiments and simulations	70
3.1.1	Resilience of the nucleation mechanism <i>in silico</i>	70
3.1.2	Who are the first to fire?	71
3.2	Structure and initiation-termination mechanisms	72
3.2.1	The possible driving mechanisms	72
3.2.2	Influence of the termination mechanism	73
3.2.3	The complex influence of topology	73
3.3	Structural and dynamical properties	75
3.3.1	Topological properties of spatial cultures	75
3.3.2	Burst nucleation in neuronal cultures <i>in silico</i>	78
3.3.3	Limitations of the predictions	86

3.1 Nucleation centers in experiments and simulations

Using calcium imaging at the scale of an entire culture, Orlandi et al. 2013 were able to show experimentally that the occurrence of network-wide bursts was not initiated randomly throughout the culture, but instead was triggered by a nucleation mechanism that occurred only in a few specific areas. This nucleation process occurred only in a small set of localized regions which consistently initiated network bursts over the entire recording. Other groups have also observed or hypothesized the existence of nucleation centers (J. P. Eckmann et al. 2008; Jarvis et al. 2011) and simulations on spatial networks, where the connectivity between neurons is distance dependent, also displayed this nucleation mechanisms. More recently, Lonardoni et al. 2017 used high density CMOS-MEAs to record 4000 neurons over the whole culture, and also observed the presence of nucleation centers from which the activity propagates in a wave-like fashion to recruit the whole network.

Moreover, Orlandi et al. 2013 observed that the propagation of the up-state to the whole network evolved greatly with the age of the culture. While a clear circular propagation from the initiation center could be observed at relatively low speed (often less than 15 mm/s) in cultures less than 12 DIV-old, when the connectivity is still very local, cultures above 20 DIV, with more long-range connections, would display much faster propagation speeds (up to 70 mm/s) and less obvious nucleation centers.

3.1.1 Resilience of the nucleation mechanism *in silico*

We observed the existence of areas that would consistently be responsible for the initiation of network bursts in all simulations. A short overview of these observation will be given in the following paragraphs, while more detailed results and figures will be provided in the rest of this chapter. Parameters for the simulations can be found in “Network models and parameters” (section D.2), subsection “Parameters for “Burst nucleation in neuronal cultures *in silico*” (subsection 3.3.2)”.

The phenomenon was conserved regardless of the heterogeneity of the neuronal population (from identical neurons to highly heterogeneous populations containing four different types of neurons with randomized parameters)¹. Similarly, the size of the network did not affect the nucleation process, and centers were observed for all network sizes considered, i.e. from 1,000 to 50,000 neurons.

However, nucleation centers were significantly affected by the locality of the network: structures with very local connections compared to the network spatial extension, would often present several nucleation centers, whereas structures where connections can span the whole network would typically exhibit only one or two nucleation centers. As such, the existence of nucleation centers seems to be an intrinsic property of networks exhibiting spatial locality.

Taken together with the experimental observation of Orlandi et al. 2013, this fact hints at a significant role played by locality in the emergence of these nucleation centers. This importance of locality in shaping complex behaviors will be further

¹ Only in some rare cases did we observe situations where the nucleation center was “delocalized” all around the periphery of the culture, resulting in centripetal waves that converged towards the center. Because of its rarity and since it had not been reported experimentally, this phenomenon is not treated in this thesis and has been left for future investigations.

*bursts
nucleate in
localized areas*

*nucleation
centers appear
when neurons
make local
connections*

explored at the end of this manuscript, when neuronal devices will be discussed — “Conclusion, towards neuronal devices” (chapter 5).

3.1.2 Who are the first to fire?

The apparent prevalence of locality, compared to neuronal properties, for the obtention of nucleation centers hints at a significant importance of the network structure in the initiation of collective activity. However, despite several claims regarding specific structural properties that “leader” neurons would display (Afshar et al. 2015; J. P. Eckmann et al. 2008; Hernandez-Hernandez et al. 2017), analyses in (Orlandi et al. 2013) and our own simulations did not confirm any of these properties. Moreover, a study by Zbinden 2011 also stressed the importance of neuronal properties to characterize “leader” neurons.

In this chapter, we will analyze the properties of the bursts and their associated nucleation centers depending on the initiation mechanism that causes the bursting behavior. We will focus here on a simple situation where all neurons have identical properties to assess the importance of the network depending on the central mechanism involved in burst initiation.

Because epileptiform activity can occur for a wide range of neuronal biological properties and network structure, the term “leaders” — which is often used to characterize the neurons that fire early at the beginning of the burst — is quite misleading. These neurons indeed initiate the global activity, but they are not necessary for its emergence, and in this sense, they do not *drive* it, nor are there necessarily more active than other neurons. I will therefore refer to them as “first-to-fire neurons”, rather than “leaders”, in the rest of this chapter.

*properties of
nucleation
centers
remain elusive*

3.2 Structure and initiation-termination mechanisms

In this section, we will use the various insights obtained in the previous chapter to draw a more complete portrait of network bursts. Analyzing the different mechanisms that could play a role in structuring the collective activity, we will see how each mechanism relates to the structural properties of the network and why this might explain the difficulty encountered to characterize nucleation centers.

3.2.1 The possible driving mechanisms

In this study, I simulated two main scenarii to model bursting behavior in neuronal cultures:

- systems where the neurons do not have a preferred frequency and are randomly activated by the noisy synaptic bombardment to which they are subjected (*noise-driven bursting*),
- systems where the neurons tend to fire at a specific frequency and for which the noisy synaptic bombardment does not lead to random firing times (*pacemaker-driven bursting*)

As mentioned previously, these two systems are characteristic of the main initiation mechanisms that have been hypothesized to explain the emergence of spontaneous bursting activity.

Noise-driven bursting

Biologically, the noise to which neurons are subjected comes from miniature Excitatory Post Synaptic Currents (mEPSCs), or minis (Kavalali 2014). These minis result from the spontaneous release of synaptic vesicles in the absence of incoming action potential. These events have been shown experimentally to occur randomly at each synapse; taken together over a whole neuron, these events occur with total rates ν which are in the [1, 30] Hz range (Sibarov et al. 2015). Compared to triggered release by action potentials (Bekkers 2003) the quantal release of minis are typically between 1/3rd and 2/3rd of a full spike.

Because spontaneous events arriving at each synapse of the neuron are considered independent, the overall rate ν for one cell is given by

$$\nu = k_{in}\nu_0, \quad (3.1)$$

with k_{in} the in-degree of the neuron and ν_0 the base rate of arrival of minis at a single synapse.

Simulations of noise-driven networks were divided into two categories: 1) control simulations where all neurons received independent realizations of a Poisson noise with the same rate 2) more realistic simulations where the neurons are subjected to a Poisson noise whose rate is proportional to their in-degree, in order to simulate minis.

As detailed afterwards, the presence of noise in the culture tends to increase the variability of the neuronal activity in both cases, though minis introduce additional correlations in the network compared to uniform Poisson noise.

Pacemaker-driven bursting

In the previous chapter, we focused on the influence of pacemaker neurons, i.e. cells with an intrinsic frequency, which, as their name imply, impose this pace to the rest of the culture. As detailed on Figure 2.15 in the previous chapter², this regularity is reflected in the collective activity and tends to reduce the variability of the activity.

However, though we studied the phenomenon in noiseless networks, pacemaker activity can never be found on its own, but, if present, will coexist with synaptic noise.

3.2.2 Influence of the termination mechanism

In the previous chapter “The influence of neuronal adaptation” (section 2.2), we have seen how network bursts could be shaped, and especially terminated, by adaptation currents. Moreover, the preliminary results from experimental blocking of the adaptation channels — “Shaping bursts through adaptation channels” (subsection 2.2.2) — showed that a significant role of adaptation consists in shaping the bursting properties was indeed plausible.

In the literature (D. Cohen et al. 2011; T. A. Gritsun, Le Feber, et al. 2010; Koppert et al. 2011), synaptic depletion is the other mechanism considered as predominant in burst termination. We will discuss here how, in both conditions, the topological properties of the neurons influence their role in the bursting dynamics.

However, it is worth mentioning that — as for noise in the initiation mechanism — synaptic depletion is always present in synapses³ as a physical consequence of the finite rate at which vesicles can be synthesized and conveyed near the presynaptic membrane. The issue here is therefore to find which (if any) of the two mechanisms plays a predominant role during specific parts of the activity. From our experimental results, it is for instance possible that adaptation should dominate the burst termination, while the longer timescale on which synapses recover may dictate most of the IBI duration.

3.2.3 The complex influence of topology

This discussion will mostly be founded on the observation that, in a network composed of identical neurons, the cells which are most active during a burst are those which have the strongest input coupling S , defined, for a neuron i , as

$$S_i = \sum_{j \rightarrow i} s_{ji}, \quad (3.2)$$

where s_{ij} is the total synaptic strength of the connections with presynaptic neuron i and postsynaptic neuron j .

*strongly
connected
neurons fire
more during
bursts*

Hindsight from the adaptation model

When adaptation is the dominant mechanism for burst termination, the most active cells — which fire more spikes during a burst — end up in a state characterized by a higher value of w at the end of the burst.

² see “Statistical properties of the interburst interval” (subsection 2.3.3).

³see also discussion in “Burst termination: adaptation or depression?” (subsection 2.1.2)

Because the influx of potassium in the cell was greater, the time necessary for K^+ to be evacuated, i.e. for w to return to zero, is also increased compared to less active neurons. This means that neurons with the lowest in-degree⁴ will return to a positive susceptibility more rapidly. Because they become susceptible first, the neurons with lowest in-degree, i.e. the least active cells during the up-state, tend to be the first-to-fire in adaptation-terminated bursts.

This fact is especially visible for *pacemaker-driven* bursts, as pacemakers do not a priori occupy specific positions in the network and should not be correlated to specific network properties.

However, if noise is driving the activity, then the influence of the in-degree is quite different, since nodes with higher in-degrees receive larger amounts of minis, which tends to increase their susceptibility more rapidly. This is especially in situations where the IBI is much longer than the recovery time of the susceptibility from adaptation currents. Even with pacemakers, minis are necessarily present and may contribute to an increased excitability of large in-degree pacemakers.

Influence of synaptic depression

Short-Term Depression (STD) is linked to the frequency at which a given connection is solicited. Thus, the synapses that undergo the most significant depletion are those coming from the most active neurons in the network.

As for adaptation, there are thus two scenarii: either 1) the IBI is directly driven by the recovery time of the synapses, or 2) synapses recover fully before the next burst is initiated.

In the first case, it is likely that neurons that will be able to initiate the burst are those whose out-going synapses recovered the most. This basically means synapses that were not over-solicited, meaning that the associated neurons should be among the least active in the burst.

Assessment

Based on our preliminary results — “Shaping bursts through adaptation channels” (subsection 2.2.2) — and hints from previous studies (D. Cohen et al. 2011; Ferguson et al. 2015), it seems probable that burst occurrence should closely follow the end of the recovery period (be it adaptation or depletion). Because of this, the termination mechanism is likely to determine which neurons are the first-to-fire. Since both adaptation and synaptic depletion affect most strongly the neurons that are very active during the burst, the least active neurons are likely to be in the best position to initiate the next up-state.

The presence of minis, which are stronger for neurons with high in-degree tends of course to counteract this influence of the termination mechanism. Yet, if adaptation and STD are indeed the mechanisms dictating the bursting period, first-to-fire neurons might well be, overall, those with lowest input strength.

⁴or the lowest synaptic coupling, in heterogeneous networks

*in “pure
adaptation”
bursts,
first-to-fire
neurons have
lowest input
strength*

*minis counter-
balance
adaptation by
favoring high
in-degrees*

*adaptation
and STD favor
neurons with
low activity...*

*but minis
drive neurons
with high
input strength*

3.3 Structural and dynamical properties

In order to explain why some neurons fire early and drive the rest of the network into the up-state, previous studies tried to reproduce some of the firing rate properties, which led them to attribute specific topological (D. Cohen et al. 2011; Zbinden 2011) or dynamical (Baltz et al. 2011; T. A. Gritsun, Le Feber, et al. 2010) properties to these neurons. In the brain, it has also been suggested that hippocampal bursts *in-vivo* are orchestrated by GABAergic hub neurons (Bonifazi et al. 2009).

However, previous studies on cultures were all based on experimental recordings which included only a tiny fraction⁵ of the network.

In order to investigate the properties of the bursting activity with respect to the network properties of the neurons, the activity of the whole network must be recorded, as was performed by Orlandi et al. 2013 using whole-culture calcium imaging and more recently by Lonardoni et al. 2017 using high density CMOS-MEAs.

In order to model and discuss the results observed in these two studies, I will first introduce the random network model used to model the spatial structure of 2D cultures *in silico*. After a brief analysis of the structural properties of such networks, we will see how, based on the discussion made in “Structure and initiation-termination mechanisms” (section 3.2), we can predict the position of nucleation centers for each bursting scenario. We will then analyze some simulations and discuss how this data can help us evaluate the likelihood of the bursting mechanisms that have been discussed so far.

3.3.1 Topological properties of spatial cultures

In this study, 2D cultures were modeled through Exponential Distance Rule (EDR) networks, which are space embedded random networks similar to Erdős-Renyi networks (Barabási 2016), except that, when testing for the connection probability between two neurons i and j , the probability depends on the Euclidean distance d_{ij} between them:

$$p_{i,j} = p_{ji} = p_0 e^{-d_{ij}/\lambda}, \quad (3.3)$$

where p_0 is a normalization factor to adjust the number of connections in the network, while λ determines the scale of the typical distance between connected neurons in the culture.

This generative model leads to random networks with strong metric correlations, where neighboring neurons tend to cluster together, while forming fewer long range connections with further cells. However, this behavior depends very strongly on the value of λ , and, in the limit $\lambda \rightarrow \infty$, one recovers of course a non-metric Erdős-Renyi network.

In the following, we will see through two main quantities (the clustering coefficient and the betweenness centrality) how locality influences the structures of 2D networks. The clustering characterizes how strongly neurons sharing a common neighbor are connected together; for a neuron i , the clustering coefficient is defined by the fraction of edges that exists among the out-neighbors of i compare to the total number if they were all connected together. The betweenness, on the other hand, quantifies the importance of a connection in propagating information throughout the network by counting how many shortest path go through this specific connection⁶.

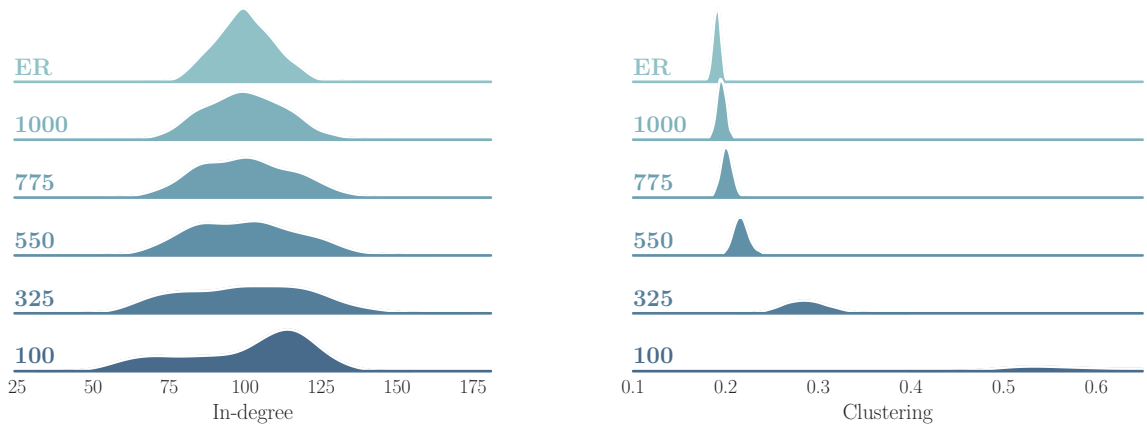
*introducing
space in the
model*

⁵typically 1% or less for old MEA systems in standard cultures

⁶ see “Properties of spatial networks” (section D.3) for additional details and definitions.

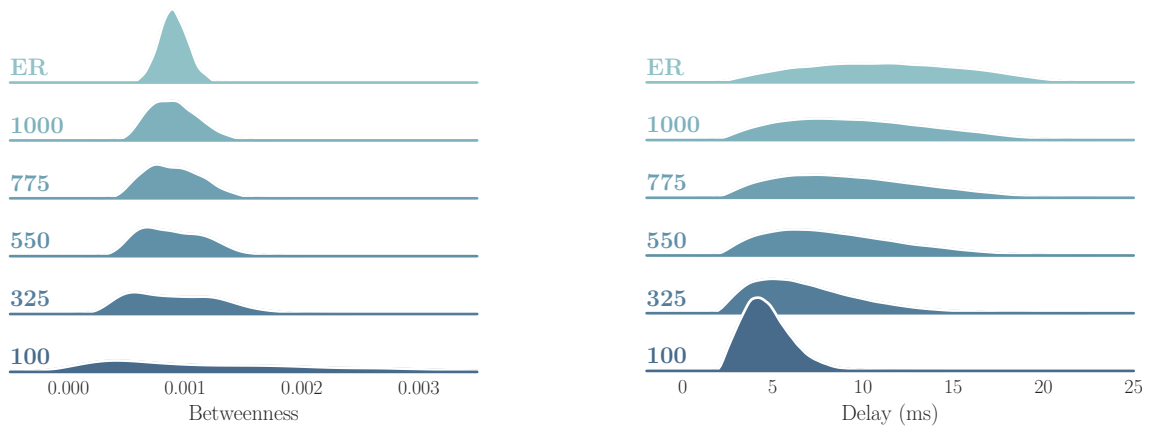
Locality and EDR networks

To generate spatial networks, nodes (neurons) are seeded uniformly in space, then connected together. Because of local heterogeneity in the distribution of the neurons, some regions display higher local densities while other are more sparsely seeded.



(a) Evolution of the in-degree distribution with the spatial scale.

(b) Evolution of the clustering distribution with the spatial scale.



(c) Evolution of the betweenness distribution with the spatial scale.

(d) Evolution of the delay distribution with the spatial scale.

Figure 3.1.: Evolution of the network properties depending on the spatial scale for networks of 1000 nodes contained in a disk of radius 1 mm. Values of λ are given on the left axis; top distribution is always the Erdős-Renyi reference. For all network properties except the delay (obviously), locality, i.e. smaller values of λ lead to greater variability among the nodes.

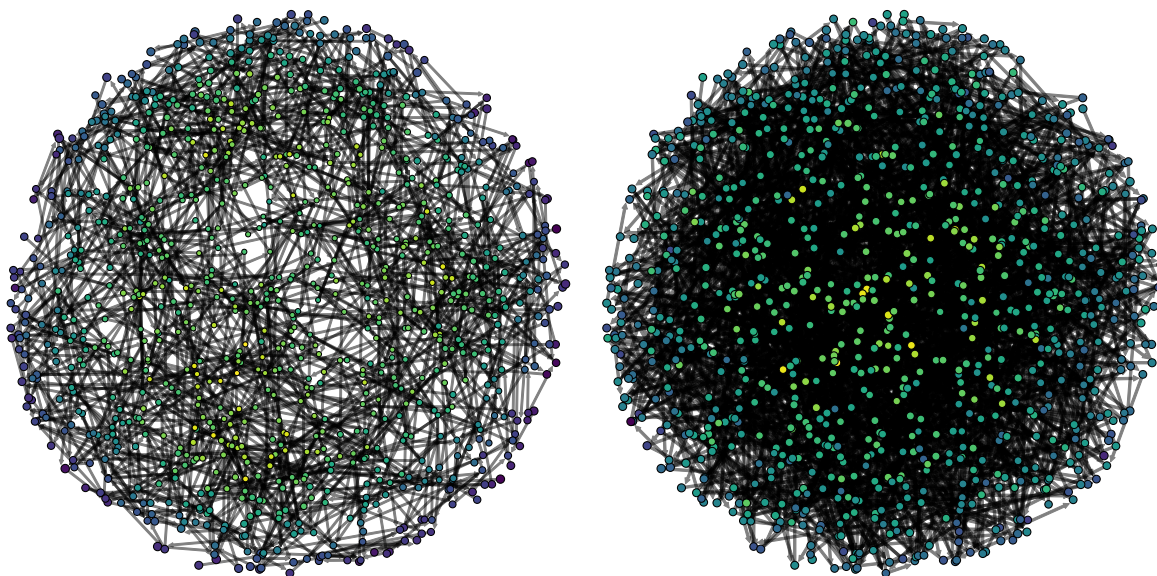
When λ is small compared to the typical length of the environment, heterogeneities between local regions become prominent, hence the widening of the in-degree, clus-

tering, and betweenness⁷ distributions. Indeed, for the in-degree, we see a progressive segregation between nodes in high-density areas (higher in-degree) and low-density regions (low in-degree). The clustering increases significantly but the same phenomenon occurs since low-density regions make only a fraction of all possible connections, which lowers the clustering. The most interesting behavior is probably that of the betweenness probability: as locality increases, nodes having increasingly high betweenness appear while the majority of the population shifts towards low centralities. This behavior is symptomatic of the progressive separation of the network into local dense regions with sparser inter-cluster connectivity, i.e. bottlenecks in the information transfer across the whole culture. Nodes connecting different clusters then start having a more prominent (central) position since shortest-path connecting different regions of the network necessarily go through them.

*locality
increases
structural
heterogeneity
between
neurons*

Circular cultures of various ages

In order to reproduce some of the properties of circular neuronal cultures, their connectivity will be approximated by EDR networks of different λ values depending on their age: low-DIV cultures will be modeled by low- λ networks while older cultures, with more long-range connections, will be modeled by high- λ networks. Complete details about the network models and properties used for simulations can be found in “Network models and parameters” (section D.2).



(a) “Young culture” modeled by an EDR graph with $\lambda = 100 \mu\text{m}$. (b) “Old culture” modeled by an EDR graph with $\lambda = 1 \text{ mm}$.

Figure 3.2.: Spatial and topological visualization of 1000-node EDR networks contained in a disk of radius 1 mm. Node size represents the clustering (higher nodes have higher clustering) while color shows in-degree, from low values in dark violet to high values in yellow. Only one connection in 50 has been kept for better visualization.

⁷ the betweenness of a node quantifies the number of shortest-path in the network that go through that node.

Figure 3.2 shows the evolution of the spatial properties from young (a) to older (b) cultures. A typical property of circular cultures is the presence of high-degree nodes around the center of the culture, where more neurons are present, and high-clustering nodes on the periphery, where the number of neighbors is more limited — hence the high clustering. The strong difference in clustering is especially visible for young cultures, while it homogenizes in older networks.

Predicting the nucleation centers

Based on our discussion in “Structure and initiation-termination mechanisms” (section 3.2), we can now make predictions about the regions that are more likely to act as nucleation centers in the different burst-generation mechanisms:

- for *pacemaker-driven* bursts, where synaptic noise (minis) are not predominant, bursts should be more likely to nucleate on the periphery, where in-degree is low and clustering high, increasing the probability to find clusters of less-active neurons,
- for *noise-driven* bursts, where noisy synaptic inputs initiate the activity, bursts are much more likely to initiate in the center of the culture, where the connectivity is highest.

3.3.2 Burst nucleation in neuronal cultures *in silico*

In order to analyze the spatio-temporal characteristics of the bursting activity in a whole culture, a necessary preliminary step consists of a rapid delimitation of the bursting events, in order to associate all spikes in the recording to a single bursting event.

To that end, the spikes are first converted to a time series representing the firing rate of the whole culture — see “Nucleation centers” (Appendix F) for more details — and the approximate burst times are defined by the highest value of the firing rate. A spike is then considered as satellite of a given burst if it is closer to it than to any other burst, as described on Figure 3.3e.

After the spikes have been attributed to their respective bursts, a clustering algorithm is used to cluster the neurons that have fired before a given timestep: like in a percolation process⁸ active nodes are considered active until the whole culture has been recruited; the ensemble of active nodes is then tested for the presence of clusters — regions where all or almost all nodes have been activated. After the appearance of the first center, this cluster will grow, potentially accompanied by others, until all neurons belong to a cluster. A more visual explanation of the algorithm can be seen on Figure 3.3.

Thanks to the additional information provided by the spatial evolution of the activity, the detection of the first cluster provides a non-arbitrary way⁹ to define the beginning of a burst. To that end, each area assigned to a burst — Figure 3.3e — was divided into time bins of duration given by the average delay in the network. Cluster detection was then performed using the DBSCAN algorithm (Ester et al. 1996) from the scikit-learn python module for each time bin in order to detect

⁸ see “Synchronous bursts as percolation events” (subsection 2.3.2) for more details on percolation processes.

⁹ because the parameters of the clustering algorithm are fully determined by the network structure, there are no arbitrary parameters used in the cluster detection.

clusters of activity in space. To be considered as part of a cluster, an active neuron must have a minimum number of active neighbors k_{min}^{active} within a radius ϵ . Knowing the network structure, the ϵ parameter was thus set to the typical length λ of the EDR model, while the minimum number of active neurons is computed based on the average spatial density of neurons d , and is given by $k_{min}^{active} = \lfloor d * \pi \epsilon^2 - \sqrt{d * \pi \epsilon^2} \rfloor$. This characterizes the number of neurons in the part of the culture with the smallest local density due to the random fluctuations.

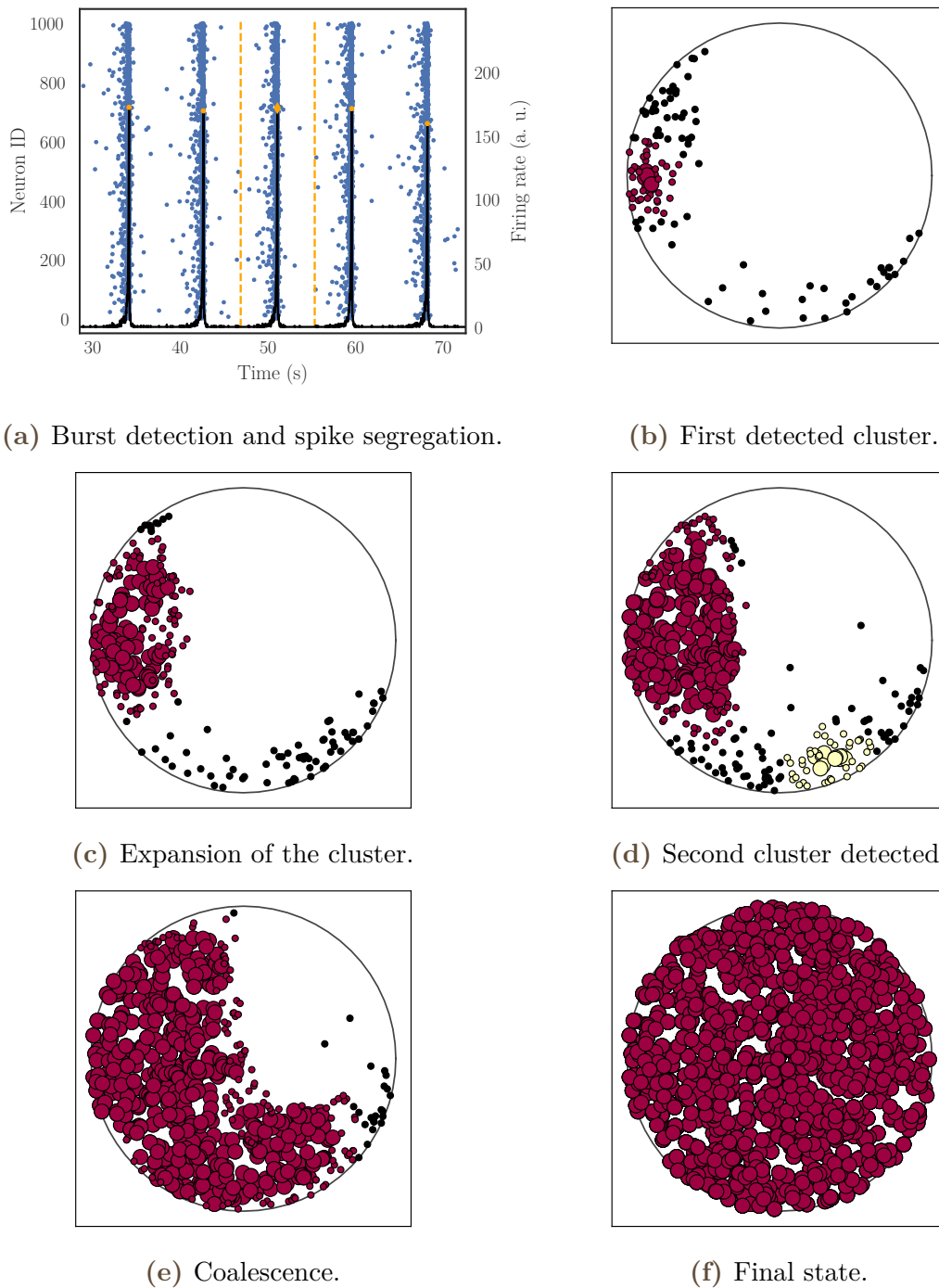
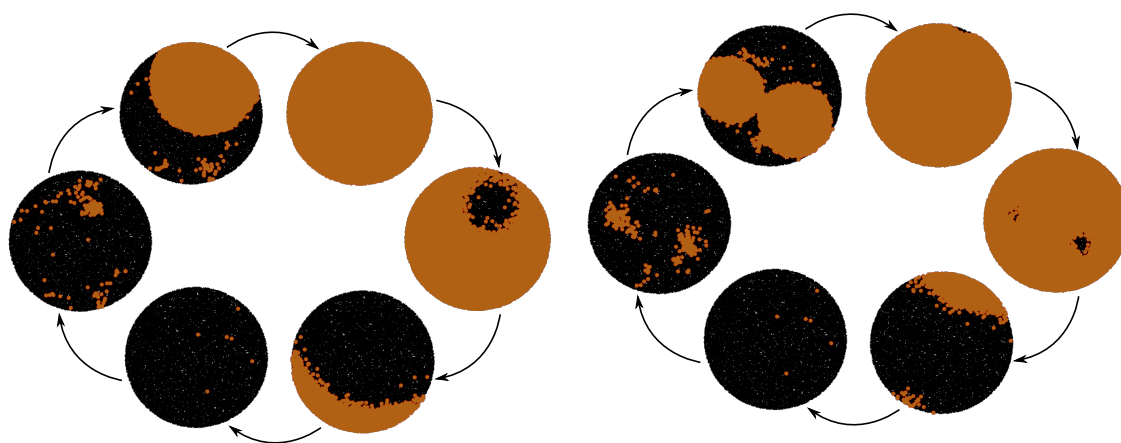


Figure 3.3.: Visualization of the preliminary burst detection (a) and subsequent clustering (b) to (f). (a) From the raster plot (blue dots), the firing rate of the whole population is obtained (black curve). For a given burst, marked by the orange diamond, all spikes closer to it than to the neighboring bursts (orange dots) are associated to that precise bursting event — all spikes between the two dashed orange lines. For these successive spikes, the progressive accumulation of active neurons in the culture is tested through a clustering algorithm. Once a critical density of active neurons is reached, a cluster is detected — (b) red neurons — while other neurons (in black) are still considered as isolated events. In time, the cluster grows (c), potentially coexisting with others (d) until all clusters coalesce (e) and finally encompass the whole culture (f).

Bursting patterns

Though the bursts almost always nucleate from one or several centers, there is great variability in the number, position, and relative importance of these centers.

In most experimental and simulated cultures, only one to three nucleation centers are usually observed. When several nucleation centers are present, no pattern is usually visible in the sequence of the selected centers, and their alternation is seemingly random, though some centers may initiate the activity more often than others. However, simulations of cultures with low connectivity (an average in-degree of 30), displayed a large number of nucleation centers (more than 5) and significant correlation in the initiation sequence, with a given center sometimes activating up to ten bursts in a row¹⁰. Such observation also seem possible in experimental cultures, judging from the recent results of Lonardoni et al. 2017, where up to four or five different nucleation centers — designated by *initiation sites* in the paper.



(a) Burst initiated by one nucleation center. (b) Burst initiated by two nucleation centers.

Figure 3.4.: Temporal evolution of the bursting activity, starting from one (a) or two (b) nucleation centers. Note that the first neurons to transit back to the down-state are usually those around the nucleation centers.

“Age-dependence” of the bursting behavior

General tendencies for the behavior of the nucleation centers can nonetheless be derived from the accumulated observations, and are enumerated in Tables 3.1 and 3.2:

- the number of nucleation centers increases with the locality of the network (many short-range connections lead to many centers),
- concurrently with their decrease in number, the nucleation centers shift towards the center of the culture as connection-range increases.

As mentioned previously, cultures of different DIVs were modeled using EDR networks of different scales and average degree.

¹⁰ these findings are preliminary and are the result of direct observation, since automated tools to characterize and compare burst centers — detecting whether or not two bursting events were initiated by the same center — are yet to be developed.

Young cultures were modeled by networks with short-range connections ($\lambda = 200 \mu\text{m}$) and low in-degrees ($\langle k \rangle = 50$) while older cultures possessed long-range connections ($\lambda = 800 \mu\text{m}$) and higher in-degrees ($\langle k \rangle = 100$). Intermediate cultures were also simulated, with $\lambda = 400 \mu\text{m}$ and $\langle k \rangle = 75$.

Conditions/Age	Young	Intermediate	Old
All	Several	Few	One
Pacemaker-driven	At least two	One or two	One
Noise-driven	One or two	One	One

Table 3.1.: Evolution of the number of nucleation centers depending on the “age” of the culture and on the bursting mechanism.

Conditions/Age	Young	Intermediate	Old
Pacemaker-driven	Border	More centred	Centred
Noise-driven	Almost centred	Centred	Centred

Table 3.2.: Evolution of the location of the nucleation centers depending on the “age” of the culture and on the bursting mechanism. Consistently with the predictions, noise-driven bursts nucleate from the center, where the highest in-degree nodes are localized, while pacemaker-driven bursts are initiated closer to the periphery, where low in-degree nodes are located.

Consistently with the locality dependence of the nucleation centers, one can thus say that young cultures are more likely to display several nucleation centers in the periphery, while older cultures would tend to exhibit a single, more centered initiation site.

Furthermore, these differences in the properties of the nucleation centers also affect the burst profiles. Indeed, for peripheral nucleation centers, the “activity front” — the border of the active area, which delimitates the region where neurons activated from the still quiescent region, as shown on Figure 3.4a — quickly reaches the edge of the culture, meaning that its expansion only occurs as a half-disk, while initiations at the center can expand in all directions. Illustration of this behavior is illustrated on Figure 3.5. Coupled to the fact that propagation speed increases with the amount of long-range connections, this makes burst profiles much sharper for old cultures compared to young cultures: the time necessary to recruit the whole culture diminishes with the age of the culture; conversely, the peak firing rate in the burst increases with age.

First-to-fire neurons and nucleation centers

Most of the time, only one or a few nucleation centers are repeatedly selected to initiate up-states. Because of this strong resilience for a given network and neuronal population, it seems unlikely for nucleation center not to be related to some topological property of the network.

*the position of
the nucleation
center affects
both the
temporal and
spatial
dynamics*

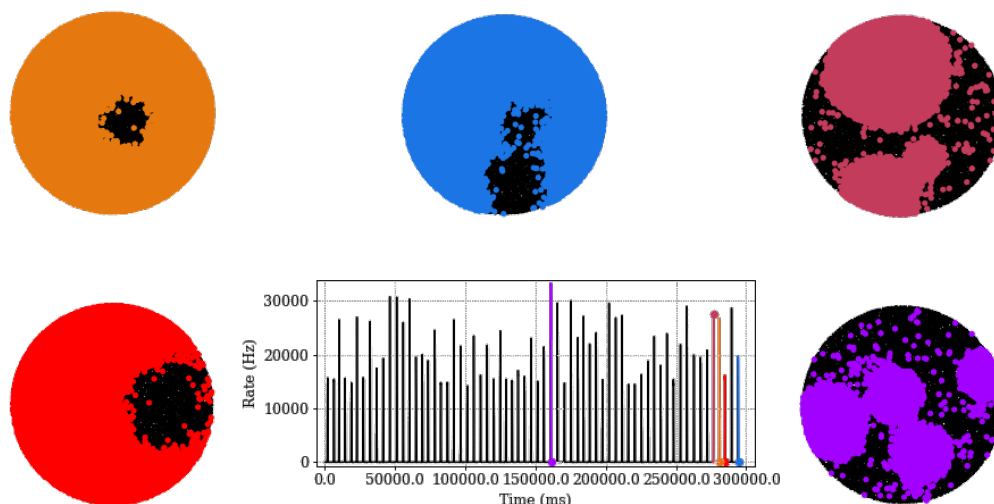


Figure 3.5.: Evolution of the firing rate depending on the number and localization of the nucleation centers. Peak firing rates increases from a single nucleation center on the border (red), two centers with the first one on the border (blue), a single center in the middle (orange), three nucleation centers (purple), and four simultaneous centers (violet). Visualization of the activity on the network is either given at the beginning (full centers) or at the end (empty centers) depending on which displayed better visibility.

Starting from the predictions proposed in the previous section, I investigated the correlations between degree centralities and the first-to-fire property, before extending the analysis to several additional centralities and network properties — see “Predicting nucleation centers by graph centralities” (section F.3) for details on all centralities tested.

The neurons and their associated activity were characterized by three values:

- The average first-to-fire property, quantifying how early a neuron fires with respect to the time at which all neurons have recruited into a burst. For each burst, the first neuron to start is associated the value 1 while the last one is associated the value 0. Intermediate neurons have a value which is proportional to their spike time.
- The first-to-cluster property, characterizing the time at which a neuron is associated to a cluster of active neurons during the percolation process.
- A “nucleator” index, which is a topological property of the network which correlates with the first-to-fire and first-to-cluster properties¹¹.

A surprising feature of the bursting activity which came out of this study was the very strong correlation between the first-to-fire and first-to-cluster properties. Indeed, defining the burst start as the apparition of a first cluster, the first-to-fire neurons are technically “out-of-synch” neurons which precede the bursting event. Yet, these apparently random spikes, which increase in frequency right before the

pre-burst activity is localized around the future nucleation center

¹¹ several nucleator indices will be described in the following, the best nucleator index depending on the properties of the neurons: no “universal nucleator index” was found.

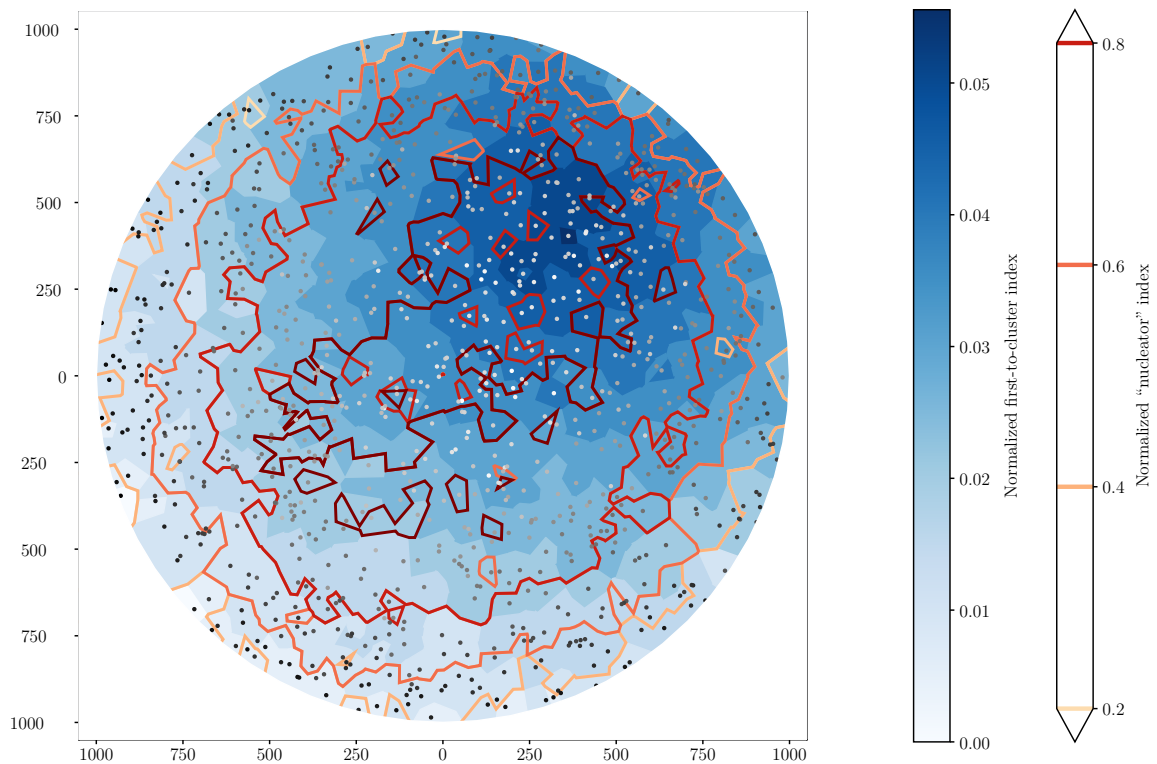


Figure 3.6.: Spatial representation of the bursting properties of an EDR network composed of 2000 adaptive spiking, non-pacemaker neurons. Neurons are represented by the filled circles, colored by their average first-to-fire property over a 500-second simulation: from white for early spiking neurons, to black for the last to fire in the burst. Each node is associated to its Voronoi cell which is colored from dark blue for the first neurons detected in a cluster (the nucleation center), to white for the last to join the percolating cluster. Contour around the Voronoi cell delineate the groups of similar nucleator index, from low values in off-white, to high values in dark red.

start of a burst, are actually statistically localized in close proximity of the future location of the nucleation center, as can be seen on Figures 3.6, 3.7, and 3.8.

As predicted, for networks where the activity is noise-driven, exemplified on Figure 3.6, the nucleation center co-localizes with the area where the nodes have the highest total-degree. In this case, the “nucleator” index consider is thus the normalized value of the degree. Because EDR networks have higher degrees around the center of the culture, nucleation centers tend to be rather centered for non-pacemaker neurons of type I and II, where the activity is purely noise-driven. This effect is especially strong when the noise is correlated to the in-degree (minis), but is still present event for uncorrelated noise, since neurons with higher in-degree are more likely to collect random spikes and become active as a consequence.

Using pacemaker neurons, the localization of the nucleation center depends on the relative importance of the noise compared to the adaptation currents:

*nucleation
position
depends on
neuronal type
and
noise/adapta-
tion
balance*

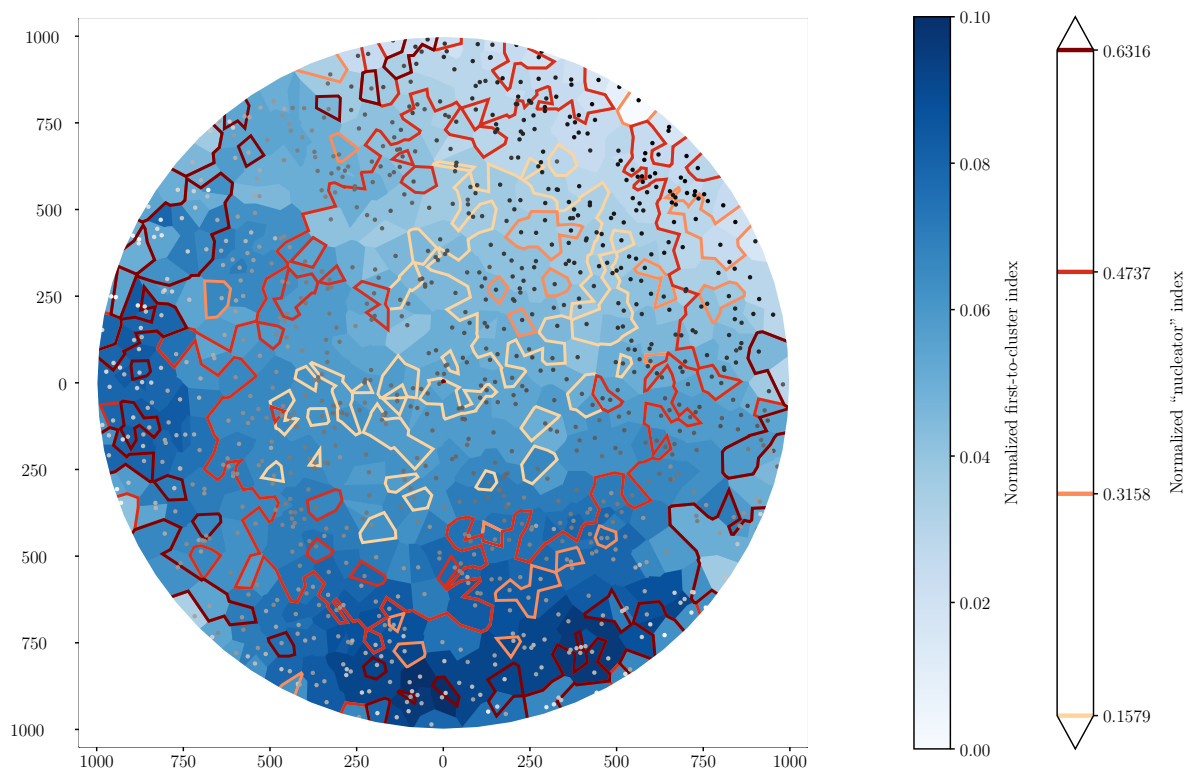


Figure 3.7.: Spatial representation of the bursting properties of an EDR network composed of 2000 pacemaker neurons. Neurons are represented by the filled circles, colored by their average first-to-fire property over a 500-second simulation: from white for early spiking neurons, to black for the last to fire in the burst. Each node is associated to its Voronoi cell which is colored from dark blue for the first neurons detected in a cluster (the nucleation center), to white for the last to join the percolating cluster. Contour around the Voronoi cell delineate the groups of similar nucleator index, from low values in off-white, to high values in dark red.

- if the Inter-Burst Interval (IBI) is mostly dictated by the recovery time of the adaptation current, then first-to-fire neurons tend to be low-in-degree nodes, as shown on Figure 3.7,
- if the IBI is much longer than the recovery time of the adaptation current, then the behavior of the network becomes closer to that of a noise-driven network, since excitatory input need to build up before the neurons start firing again; in that case the nucleation centers shift back towards the interior of the culture, cf Figure 3.8.

In the second case, as for non-pacemaker neurons, the best predictor for the location of the nucleation centers seem to be the total-degree of the neurons (Figure 3.8). However, in the first case, the best “nucleator” index found was very different, since it was given by the combination of the lowest clustering coefficient with the lowest in-degree.

To understand why the combination of both properties might make sense, one must first realize that they actually tend to anti-correlate. Indeed, in the EDR network, the lowest in-degree nodes are located on the periphery of the network, because they have access to a lower number of neighbors, hence their lower connectivity. In addition, this inferior number of available neighbors leads to an increased tendency for neighboring nodes to be connected to one another, which is why peripheral neurons tend to have higher clustering coefficients. Taking the normalized combination of both leads to a “nucleator” index n_j , for node j , given by:

$$n_j = \tilde{c}_j * \tilde{k}_j^{(in)}, \quad (3.4)$$

where \tilde{c}_j is the normalized value of the opposite of the correlation coefficient,

$$\tilde{c}_j = \frac{c_{max} - c_j}{c_{max} - c_{min}}, \quad (3.5)$$

and $\tilde{k}_j^{(in)}$ is the normalized value of the opposite of the in-degree,

$$\tilde{k}_j^{(in)} = \frac{k_{max}^{(in)} - k_j^{(in)}}{k_{max}^{(in)} - k_{min}^{(in)}}. \quad (3.6)$$

This index quantifies a balance between the low connectivity of the neuron and the presence of long-range edges among its connections. Indeed, we know that high-in-degree nodes will take much longer to recover from their superior in-burst firing-rate, which will bring them to very high values of adaptation current w at the end of the burst; first-to-fire neurons are thus more likely to be lower-degree nodes. Yet, if these nodes are too isolated, they will not be able to excite the network sufficiently to initiate the burst. Taking the clustering coefficient into account enables to both prevent the selection of exceedingly small degrees and to make sure that the selected neurons sample more broadly the culture and do not only connect to their local neighbors. In that situation, the neurons that ignite the whole culture are therefore those that maintain an equilibrium between excessive connectivity and excessive local confinement.

Eventually, when neither the noise, nor the adaptation predominates, we obtain an intermediate regime where none of the previous nucleator indices significantly correlates with the nucleation centers.

3.3.3 Limitations of the predictions

Unfortunately, though the predictions of the nucleation centers are based on generic properties which are robust against the model used, the detailed spatiotemporal predictions heavily rely on the predicted properties of the neuronal network. Furthermore, even for a given network model, no universal nucleator index was found, and the best predictions were obtained using different indices depending on the neuronal properties.

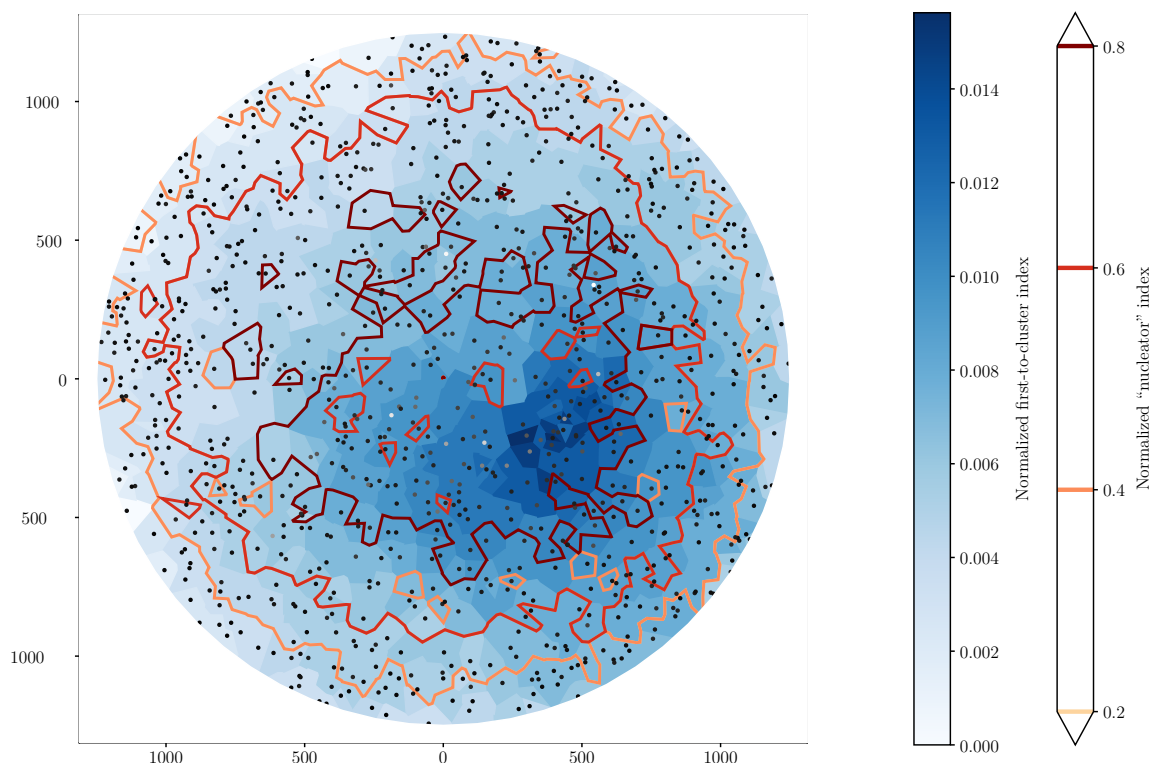


Figure 3.8.: Spatial representation of the bursting properties of an EDR network composed of 2000 pacemaker neurons. Neurons are represented by the filled circles, colored by their average first-to-fire property over a 500-second simulation: from white for early spiking neurons, to black for the last to fire in the burst. Each node is associated to its Voronoi cell which is colored from dark blue for the first neurons detected in a cluster (the nucleation center), to white for the last to join the percolating cluster. Countour around the Voronoi cell delineate the groups of similar nucleator index, from low values in off-white, to high values in dark red.

Though several studies (Barral et al. 2016; Horvát et al. 2016; Lv et al. 2017) have hinted at the validity of simple distance rule models to reproduce properties of spatial neuronal networks, the actual precision of such models and how they behave with respect to boundary conditions near the boundary of the culture is far from obvious. Furthermore, we have postulated here the absence of correlation between neuronal properties and connectivity, which might not be the case, given that neuronal morphology also affects the dynamical properties. Eventually, these models are not optimal to simulate the change of connectivity over time in a single culture, and can only give trends regarding how the behavior statistically evolves with the age of the culture.

We will see in 4.4.2 how these issues can be alleviated, at least partly, using our new simulation platform to grow cultures in a more realistic fashion. However, a final problem remains, which is the issue of the synaptic strength. Indeed, all simulations were performed on networks where all synapses had identical strength, while several studies (Sayer et al. 1990; Song et al. 2005) have hinted at broad distributions for the

synaptic strength. However, without knowing whether synaptic strength correlates to specific network properties, it is quite hard to model their impact, which is why this problem was not tackled in this thesis.

References for chapter 3

- Afshar, G. et al.** (2015). “Enhancing burst activation and propagation in cultured neuronal networks by photo-stimulation”. In: *bioRxiv*. DOI: 10.1101/027177. eprint: <https://www.biorxiv.org/content/early/2015/09/18/027177.full.pdf> (cit. on p. 71).
- Baltz, T., Herzog, A., and Voigt, T.** (Sept. 2011). “Slow oscillating population activity in developing cortical networks: models and experimental results”. In: *Journal of Neurophysiology* 106.3, pp. 1500–1514. ISSN: 0022-3077. DOI: 10.1152/jn.00889.2010 (cit. on pp. 38, 75).
- Barabási, A.-L.** (2016). *Network Science*. Cambridge University Press. ISBN: 1107076269 (cit. on p. 75).
- Barral, J. and Reyes, A. D.** (Dec. 2016). “Synaptic scaling rule preserves excitatory-inhibitory balance and salient neuronal network dynamics”. In: *Nature Neuroscience* 19.12, pp. 1690–1696. ISSN: 1097-6256. DOI: 10.1038/nn.4415 (cit. on pp. 87, 124, 163).
- Bekkers, J. M.** (Dec. 2003). “Convolution of mini distributions for fitting evoked synaptic amplitude histograms”. In: *Journal of Neuroscience Methods* 130.2, pp. 105–114. ISSN: 01650270. DOI: 10.1016/j.jneumeth.2003.09.018 (cit. on p. 72).
- Bonifazi, P. et al.** (Dec. 2009). “GABAergic Hub Neurons Orchestrate Synchrony in Developing Hippocampal Networks”. In: *Science* 326.5958, pp. 1419–1424. ISSN: 0036-8075. DOI: 10.1126/science.1175509 (cit. on p. 75).
- Cohen, D. and Segal, M.** (2011). “Network bursts in hippocampal microcultures are terminated by exhaustion of vesicle pools”. In: *Journal of Neurophysiology* 106. August 2011, pp. 2314–2321. ISSN: 0022-3077. DOI: 10.1152/jn.00969.2010 (cit. on pp. 40, 73–75).
- Eckmann, J. P. et al.** (2008). “Leader neurons in population bursts of 2D living neural networks”. In: *New Journal of Physics* 10. ISSN: 13672630. DOI: 10.1088/1367-2630/10/1/015011 (cit. on pp. 70, 71).
- Ester, M. et al.** (1996). “A density-based algorithm for discovering clusters in large spatial databases with noise”. In: AAAI Press, pp. 226–231 (cit. on p. 78).
- Ferguson, K. A. et al.** (2015). “Examining the limits of cellular adaptation bursting mechanisms in biologically-based excitatory networks of the hippocampus”. In: *Journal of Computational Neuroscience* 39.3, pp. 289–309. ISSN: 15736873. DOI: 10.1007/s10827-015-0577-1 (cit. on pp. 41, 74).
- Gritsun, T. A., Le Feber, J., et al.** (2010). “Network bursts in cortical cultures are best simulated using pacemaker neurons and adaptive synapses”. In: *Biological Cybernetics* 102.4, pp. 293–310. ISSN: 03401200. DOI: 10.1007/s00422-010-0366-x (cit. on pp. 38, 59, 62, 73, 75, 139).
- Hernandez-Hernandez, G. et al.** (Mar. 2017). “Nonlinear signaling on biological networks: The role of stochasticity and spectral clustering”. In: *Physical Review E* 95.3, p. 032313. ISSN: 2470-0045. DOI: 10.1103/PhysRevE.95.032313 (cit. on p. 71).
- Horvát, S. et al.** (2016). “Spatial Embedding and Wiring Cost Constrain the Functional Layout of the Cortical Network of Rodents and Primates”. In: *PLoS Biology* 14.7, pp. 1–30. ISSN: 15457885. DOI: 10.1371/journal.pbio.1002512 (cit. on p. 87).

- Jarvis, S. J., Rotter, S., and Egert, U.** (2011). “Burst initiation and propagation in cortical cultures requires an inhomogeneous connectivity distribution and synaptic rescaling”. In: *BMC Neuroscience* 12.Suppl 1, P85. ISSN: 1471-2202. DOI: 10.1186/1471-2202-12-S1-P85 (cit. on p. 70).
- Kavalali, E. T.** (2014). “The mechanisms and functions of spontaneous neurotransmitter release”. In: *Nature Reviews Neuroscience* 16.1, pp. 5–16. ISSN: 1471-003X. DOI: 10.1038/nrn3875 (cit. on pp. 37, 72).
- Koppert, M. M. et al.** (2011). “Plasticity-modulated seizure dynamics for seizure termination in realistic neuronal models”. In: *Journal of Neural Engineering* 8.4. ISSN: 17412560. DOI: 10.1088/1741-2560/8/4/046027 (cit. on p. 73).
- Lonardoni, D. et al.** (July 2017). “Recurrently connected and localized neuronal communities initiate coordinated spontaneous activity in neuronal networks”. In: *PLOS Computational Biology* 13.7. Ed. by **Battaglia, F. P.**, e1005672. ISSN: 1553-7358. DOI: 10.1371/journal.pcbi.1005672 (cit. on pp. 70, 75, 81).
- Lv, Z. S. et al.** (2017). “Exponential distance distribution of connected neurons in simulations of two-dimensional in vitro neural network development”. In: *Frontiers of Physics* 12.3. ISSN: 20950470. DOI: 10.1007/s11467-017-0602-0. arXiv: 1702.03418 (cit. on p. 87).
- Orlandi, J. G. et al.** (Sept. 2013). “Noise focusing and the emergence of coherent activity in neuronal cultures”. In: *Nature Physics* 9.9, pp. 582–590. ISSN: 1745-2473. DOI: 10.1038/nphys2686 (cit. on pp. 5, 27, 70, 71, 75).
- Sayer, R. J., Friedlander, M. J., and Redman, S. J.** (1990). “The time course and amplitude of EPSPs evoked at synapses between pairs of CA3/CA1 neurons in the hippocampal slice.” In: *The Journal of neuroscience : the official journal of the Society for Neuroscience* 10.3, pp. 826–836. ISSN: 0270-6474 (cit. on p. 87).
- Sibarov, D. A. and Antonov, S. M.** (May 2015). “Characteristics of Postsynaptic Currents in Primary Cultures of Rat Cerebral Cortical Neurons”. In: *Neuroscience and Behavioral Physiology* 45.4, pp. 431–439. ISSN: 0097-0549. DOI: 10.1007/s11055-015-0093-9 (cit. on pp. 37, 72).
- Song, S. et al.** (Mar. 2005). “Highly nonrandom features of synaptic connectivity in local cortical circuits.” In: *PLoS biology* 3.3, e68. ISSN: 1545-7885. DOI: 10.1371/journal.pbio.0030068 (cit. on p. 87).
- Zbinden, C.** (2011). “Leader neurons in leaky integrate and fire neural network simulations”. In: *Journal of Computational Neuroscience* 31, pp. 285–304. ISSN: 09295313. DOI: 10.1007/s10827-010-0308-6. arXiv: 1004.2787 (cit. on pp. 71, 75).

Chapter 4

Accounting for neuronal development

In the previous chapters, almost all simulations were performed with the NEST simulator (Peyser et al. 2017). This open-source software, and others like BRIAN, or NEURON, has proven invaluable to simulate neuronal activity, both on small desktop machines and on large scale supercomputers.

However, there is no such widely-used platform to account for neuronal development and connectivity: even though tools were developed (Koene et al. 2009; Torben-Nielsen et al. 2014; Zubler et al. 2009), they were not as versatile as their “activity” counterparts and their development now seems discontinued. Thus, no simulation platform currently provides access to several models for neuronal development, which hinders theoretical studies of complex neuronal systems and neuronal growth.

In this chapter, I will present a new platform, DeNSE, meant to provide a unifying framework for the study of neuronal development. This software gives access to several existing models for both neuronal elongation and branching, as well as new models, and takes spatial environment into account by modeling the interactions between the neurons and their surroundings.

After a brief introduction of the platform, I will detail the models that were implemented to describe neuronal elongation and navigation through *growth cones* and their behaviors. I will then discuss branching mechanisms and how they interact with elongation models, to finally show how we can move from individual neurons to a fully connected neuronal network.

Contents

4.1	DeNSE, a unifying platform for neuronal growth	92
4.1.1	Existing software, assessment, and objectives	92
4.1.2	Modeling and analyzing developing neurons with DeNSE	94
4.2	Growth cones, steering and interactions	96
4.2.1	Modeling an extending growth cone	96
4.2.2	Beyond the isolated growth cone: interactions	102
4.3	Branching patterns	108
4.3.1	Growth cone splitting	108
4.3.2	Lateral branching	112
4.3.3	Pruning	114
4.4	From neuronal morphologies to neuronal networks	117
4.4.1	A complete neurite tree	117
4.4.2	Coupling neurons: synapses and network	118

4.1 DeNSE, a unifying platform for neuronal growth

When building numerical simulations of neuronal networks, most studies rely on simple network models with characteristic connectivity distributions (e.g. Gaussian, in the case of the homogeneous cultures we studied in the previous chapters, or with small-world, or scale-free properties). Though they might be fine in a number of cases, such model have many flaws if one wants to account for specific properties of the network connectivity.

For instance, countless studies in the brain, as well as many *in vitro* experiments and more theoretical studies in network science (Leyva et al. 2011; Pernice et al. 2013; Tibau et al. 2013) have stressed the significant influence of the network structure on the observed activity. Moreover, several neurodegenerative diseases such as Alzheimer, Parkinson, or Huntington, could be related to the directed propagation of deregulated or misfolded proteins (Takeda et al. 2015), while autistic disorders have been related to altered neuronal arbors, as well as modified spine densities, during development (Courchesne et al. 2005; Kulkarni et al. 2012).

In order to take at least spatial correlations into account, a common first step is to use spatial networks, such as the EDR model we used in “Topology and spatio-temporal bursting patterns” (chapter 3). However, such simple models do not account for the polarization of neurons that often send processes in specific directions, in a strongly non-uniform fashion. Worse, when the networks are embedded in complex non-convex structures, the Euclidean distance used by such generative algorithms cannot provide realistic connectivity between neurons that are separated by distances that are very different from that between their somas.

The DeNSE simulation platform (Development of Neurons in Spatial Environments), presented in this chapter, was developed in order to tackle these issues, which are especially important for the study of neuronal devices, and to provide a generic tool to model neuronal development through biophysical models bringing together different steps of neuronal growth.

4.1.1 Existing software, assessment, and objectives

Between 2009 and 2014, three different simulation platforms were developed to model neuronal growth: NETMORPH (Koene et al. 2009), CX3D (Zubler et al. 2009), and NeuroMaC (Torben-Nielsen et al. 2014).

All three approached neuronal growth from very different perspectives. NETMORPH provided possible branching and elongation processes to obtain a desired morphology through a mathematical description of branching and elongation as stochastic phenomena.

On the other hand, CX3D developed mechanistic axioms to describe the mechanics of migration and extension for large number of neurons, notably to form hierarchically organized networks such as cortical layers.

Eventually, NeuroMaC focused on the importance of interactions in the elongation of neuronal processes, proposing a set of principles that could explain specific morphologies and neuronal circuit organization.

Software limitations

It is almost impossible to determine precisely why a given piece of software was discontinued, and for academic software, this often depends quite significantly on the career evolution of the people involved in their development. However, for the

three simulation platforms we will focus on, regardless of why they now seem to be discontinued, no significant user base was reached, which may have led to new developers investing on them. Let us therefore have a look at the features that might have contributed to this fact, in order to make sure these are properly addressed by DeNSE.

As summarized in Table 4.1, only NeuroMaC respected some “neuroscience standards”, i.e. enabling the user to code in a generic scientific programming language (Python, which is also the main language for neuronal activity simulations) and saving the generated morphologies in the SWC¹ format.

Software	NETMORPH	CX3D	NeuroMaC
Multiplatform	Partly	Yes	Yes
Documentation	.doc file	Online tutorial, google group	Online documentation
Code-sharing	Source code (download only)	Source code (download only)	Yes (GitHub)
Standards	None	Java, XML	Python, SWC
Efficiency	Low speed	Variable	Low speed
Biological mechanisms	Limited	Good	Correct
Versatility	Limited	Limited	Limited

Table 4.1.: Assessment of the three simulators. For practical purposes, I checked whether they could be used on all computers (Linux, Windows or Mac), if they were documented, if the code could be modified and improved by users, if they respected some community standards in the language and the generated files. Regarding the simulator itself, I evaluated how fast it could simulate growing neurons, if the mechanisms underlying growth and branching were modeled in a biologically realistic way, and how versatile the code was (i.e. how many models were implemented and to which extent they could be changed).

Besides the language barrier for NETMORPH and CX3D, the documentations, though quite short and sometimes difficult to understand, were usually sufficient to get started with the software.

I believe that the three projects were discontinued for the following reasons:

- all simulators are quite slow and, except for CX3D, they do not allow to use more than a hundred or a few hundred neurons,
- none of them allows the user to work with different models,

¹A standard format for neuronal morphologies, see

<http://www.neuronland.org/NLMorphologyConverter/MorphologyFormats/SWC/Spec.html>

- the limited biological relevance of the parameters and mechanisms provided in NETMORPH and NeuroMaC restrict their use case to rather theoretical studies.

Overall, it seems that, except for CX3D, which had very specific applications to understand for instance layer formation in the cortex, NETMORPH and NeuroMaC could not provide models and parameters that were close enough to the biological reality. Because of this, they were unable to raise sufficient interest from people focused on the understanding of the biological mechanisms underlying neuronal growth.

On the other hand, though these simulators could have been of interest for people focused on neuronal circuits, their performances were not sufficient to generate the networks involved in such studies, which are usually composed of at least several thousands neurons (for a typical example, see the study of Aimovi et al. 2011 comparing NETMORPH and CX3D).

Objectives for the DeNSE simulator

Based on the previous analysis, the DeNSE simulator was designed with the following specifications in mind:

- the simulator should provide efficient simulations for reasonable network sizes—at least 10,000 neurons,
- models should provide biologically-relevant parameters,
- API should be in Python to respect standards in computational neuroscience and generated morphologies should be saved in standard formats such as SWC,
- the simulator should be versatile—several models for each developmental “feature” such as elongation and branching—and modular—features can be switched on and off, all models can be combined.

Given the complexity of the task, we decided to restrict the scope of DeNSE to bidimensional neurons, in order to focus on *in vitro* studies and neuronal devices.

The design of the DeNSE simulator was thus started using an architecture similar to that of NEST (Gewaltig et al. 2007), using a C++ backend to allow fast and concurrent simulations with OpenMP coupled to a Python frontend through Cython.

4.1.2 Modeling and analyzing developing neurons with DeNSE

Assessment of current capabilities

DeNSE enables to model the development of neurons from the time of the axonal polarization until the end of the growth process. As in NETMORPH and NeuroMaC, the neurons’ positions are fixed; as in NeuroMaC, interactions between the neurons and the environment are considered.

DeNSE can simulate neurons with or without a spatial environment, the former situation being significantly faster as interactions with the environment do not need to be checked.

Though long-range interactions such as chemical gradients would be very interesting in the context of neuron-neuron interactions and might be added to future releases, only mechanical interactions are available in this first version of the simulator.

A simulation with DeNSE

DeNSE is implemented using object-oriented programming; its structure thus reflects the biological hierarchy: a `Neuron` object contains `Neurites`, and each `Neurite` contains `GrowthCone` objects sharing similar properties.

In a simulation, the properties of the neurons, axons, and dendrites are thus passed upon construction, then all growth cones inherit their own neurites' properties.

```
1 import dense as ds
2
3 params = {
4     "growth_cone_model": "run_tumble",
5     "use_uniform_branching": True,
6     "uniform_branching_rate": 0.0002,
7     "sensing_angle": 0.2,
8     "position": (0., 0.),
9     "speed_growth_cone": 0.03
10 }
11
12 dendrite_params = {"speed_growth_cone": 0.01}
13
14 n = ds.CreateNeurons(n=1000, num_neurites=2, params=params,
15                     dendrite_params=dendrite_params)
16
17 ds.Simulate(hours=20.)
18
19 ds.PlotNeuron(show=True)
```

Visualize and analyze the neurons

Neurons were analyzed and visualized using the `neurom`² Python library.

Dendrogram of the neurites were obtained with the `ete3`³ library.

More detailed visualization of the resulting spatial or topological networks were performed respectively with the algorithms included in the DeNSE and NNGT⁴ libraries.

² freely available on GitHub (<https://github.com/BlueBrain/NeuroM>) or via `pip`, see also <http://neurom.readthedocs.io/>.

³ see <http://etetoolkit.org/>, package available via `pip`.

⁴ this is my personal library which is aimed at bridging graph theory and neuroscience; it is freely available on GitHub (<https://github.com/Silmathoron/NNGT>) or via `pip` and the documentation can be found here: <http://nngt.readthedocs.io/>.

4.2 Growth cones, steering and interactions

As mentioned in the introduction — “Neuronal development: from seed to tree” (subsection 1.2.2) — the development of neurons is a complex process through which an almost spherical cell polarizes and evolves into a complex structure composed of long, specialized extensions which connect it to other neighbouring or distant cells (Van Ooyen 2011).

During the extension of the neuronal processes (the *neurites*, one of the main actors is the *growth cone*: this is the “hand-like” structure present at each tip of a neurite, that enables it to sense the surroundings and set the neurite on the “desired” path.

In this section, we will describe the structure of a growth cone, as well as the biological mechanisms involved in its dynamics, before detailing several models that can be used to reproduce its behavior. In the last part, we will focus on how interactions with the rest of the neurite and the environment may affect the dynamics of a single growth cone.

4.2.1 Modeling an extending growth cone Structure and properties of a growth cone

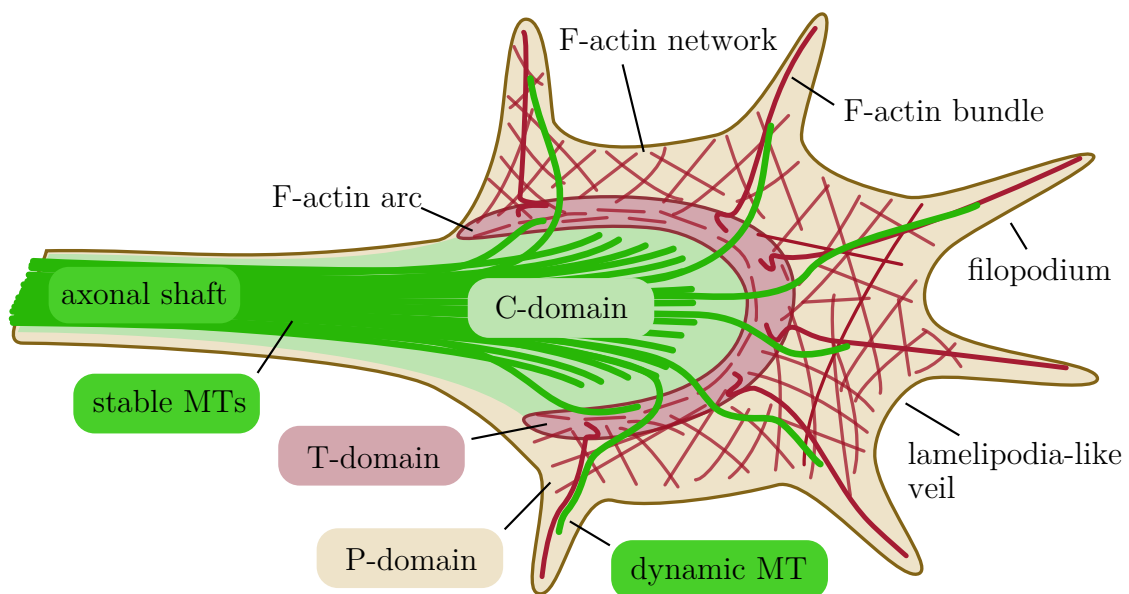


Figure 4.1.: The growth cone leading edge consists of dynamic, finger-like filopodia. They are separated by lamellipodia-like veils consisting of sheets of membrane. The growth cone can be divided into three domains based on cytoskeletal distribution. The central C-domain encloses stable, bundled MTs that enter the growth cone from the axon shaft. The peripheral P-domain contains long, bundled actin filaments (F-actin bundles), which form the filopodia. It also contains mesh-like branched F-actin networks, which give structure to the lamellipodia. Additionally, individual, dynamic, and “pioneering” microtubules (MTs) explore this region, usually along F-actin bundles. Finally, the transition T-domain sits at the interface between the P- and C-domains, where actomyosin contractile structures — called actin arcs — lie perpendicular to F-actin bundles, forming a hemicircumferential ring within the T-domain. Adapted from Lowery et al. 2009.

As can be seen on Figure 4.1, the growth cone is composed of extending protrusions, the *filopodia*, which emerge from a larger body, the *lamelipodia*.

The filopodia are the main sensing organs of the growth cone; they explore the neighboring space and generate the first traction forces that are responsible for the elongation or turning of the growth cone.

Once a traction force has been consistently exerted by a filopodia, a focal adhesion point form on the lamelipodia, below the pulling filopodia. From the focal adhesion, much stronger traction forces can then be applied, stabilizing potential dynamic MTs and leading to the progressive invasion of the other MTs from the C-domain.

Eventually, the large bundle of MTs in the axonal shaft contributes to the rigidity of the extending neurite and determines its general persistence length.

In order to properly account for the whole dynamics of the growth cone, very detailed biomechanical models would be necessary. However, as for neuronal activity, we will use simpler models that capture a number of the main dynamical features of the growth process which is as high as possible.

reproduce characteristics of elongation and turning through simple models

Main characteristics of the trajectory

For all elongation models, the main biological parameter is the persistence length l_p that characterizes the neurite.

This length is defined through the correlation of the neurite's shape: starting from a point \mathbf{r}_0 (associated to an angle θ_0 with Ox) along the neurite, the statistical correlation, at a point \mathbf{r} (associated to an angle θ) along the trajectories of many growth cones in a set of neurons, is given by

$$\frac{\langle \mathbf{r}_0 \cdot \mathbf{r} \rangle}{\|\mathbf{r}_0\| \|\mathbf{r}\|} = \langle \cos(\theta_0 - \theta) \rangle = \exp\left(-\frac{\|\mathbf{r} - \mathbf{r}_0\|}{l_p}\right), \quad (4.1)$$

with $\langle \cdot \rangle$ denoting the ensemble average over the set of growth cones. This correlation decays exponentially with the distance.

l_p : length of straight regions along the path

This length roughly gives the average distance on which the path followed by the neuron can be considered almost as a straight line, i.e. consistently stays along a given angle.

A second characteristic of a growth cone's trajectory is given by its *tortuosity*. For a trajectory linking \mathbf{r}_{first} to \mathbf{r}_{last} via a path \mathcal{C} , the tortuosity is defined as:

$$T = \frac{1}{\|\mathbf{r}_{first} - \mathbf{r}_{last}\|} \int_{\mathcal{C}} \frac{\mathbf{s}}{\|\mathbf{s}\|} \cdot d\mathbf{s}, \quad (4.2)$$

which is the ratio of the total path length and the end-to-end length. As the name indicates, this characterizes how tortuous the path followed by the growth cone is, i.e. how far from its starting point does the growth ends up after "walking" a given distance.

T : how much does it flee the initial point?

Existing models and implementations

The different models implemented in previous simulators vary depending on the properties that they capture. In the simulator, we divide the models into two main categories:

- models related to navigation, or *steering*, i.e. to how the growth cone chooses a new direction at every step,

- models related to elongation (the evolution of the growth cone’s speed in time),
- models related to branching, which will be describe in a later section.

In **NETMORPH**, the steering mechanism is a run-and-tumble model, where the growth cone follows a straight trajectory during “run” periods, interrupted by “tumble” events, where the growth cone makes sudden turns. This model has the benefit of being simple and allows to reproduce desired persistence lengths. Though it might at first be seen as lacking biological relevance (at least to describe growth cones), the run-and-tumble model is actually quite relevant to model the effect of turns caused by a paused, then resumed elongation, as exemplified in Kahn et al. 2016 (Figure 3 in the article). During a pause, the dynamic microtubules (MTs) are disorganized and form bundles before “settling” on a new direction when the elongation resumes.

In **NeuroMac**, the behavior of the growth cone is driven by self-referential forces (SRF), which dictate the new steering direction of the growth cone (Memelli et al. 2013; Torben-Nielsen et al. 2014). Though this mechanical description captures some interesting properties of growth cone navigation and might be especially appealing to physicists, the numerous problems associated to its implementation — see “Self-referential forces” (section G.3) — raise some concerns about its relevance to understanding the behavior of growth cone steering. In order to alleviate these problems, I will propose here a different implementation accounting for the same mechanisms. Like all other steering models in **DeNSE**, the new implementation of the previous “self-referential forces” algorithm is implemented using a probabilistic description and not a force-based one.

In all simulators, the elongation speed was considered constant, which neglects the existence of pausing and retracting periods.

In the following sections, I will therefore describe the models implemented in **DeNSE**, explaining their principle, how they reproduce or improve aforementioned models, and assess how they influence the growth cone motions.

Biological parameters for steering: choosing an angle

As mentioned previously, the *persistence length* of the trajectory followed by the growth cone characterizes the behavior of a neurite and can be affected by various pathologies. However, one can also easily go deeper into the biological details by considering the potential link between the microtubules (MTs) composing the axonal or dendritic shaft of a neurite branch and its persistence length.

Indeed, for a stiff uniform rod — by which a neurite branch can be approximated — the persistence length can be related to the bending stiffness (Peter et al. 2017) by the relation

$$l_p = \frac{B_s}{k_B T} = \frac{EI}{k_B T} = \frac{E\pi a^4}{4k_B T}, \quad (4.3)$$

where

- $B_s = EI$ is the *bending stiffness* or *flexural rigidity*,
- E is the *Young modulus*,
- $I = \pi a^4/4$ is the *area moment of inertia* of a circular rod, with a the cross-section area of the rod⁵.

⁵see https://en.wikipedia.org/wiki/List_of_second_moments_of_area

Model	Parameters	Features
Random walk	l_p	Persistence length
Run-and-Tumble	l_p	Persistence length
SRF	f_{sa}, λ_{sa}	Self-avoidance force and decay scale
	f_{st}, λ_{st}	Soma-tropic force and decay scale
	$f_i (l_p)$	Inertial force (persistence length)

Because the force or the energy necessary to bend a set of rods grows linearly with the number of rods (each rod bends “independently”), the persistence length of a neurite containing m MTs in its shaft is simply $l_p = m \cdot l_{p,MT}$.

However, this persistence length does not account for the fact that discontinuities in the shaft can occur, which, coupled to the active bending of dynamic MTs, can lead to sudden turns on scales which are much lower than the persistence length we computed from the “passive” properties of the neurite.

In the simulator, the user can directly enter the persistence length to any model and the internal parameters will be automatically computed to provide the required behavior — details are provided in “Growth models” (Appendix G). In the case of the simple random walk, this is obtained by setting the standard deviation to

relating l_p to the models’ parameters

$$\sigma = \sqrt{\frac{2vdt}{l_p}}, \quad (4.4)$$

Where v is the speed of the growth cone, and dt is the timestep of the simulation. In the case of the run-and-tumble model, we chose the average distance of a run, l_0 , such that

$$l_0 = \frac{\theta_{max}^2 l_p}{24}. \quad (4.5)$$

where the new angle after each tumble is chosen uniformly in a range $[-\theta_{max}, \theta_{max}]$ around the previous angle.

Elongation, retraction, and pausing

On average, the growth of neurites occurs at an average speed which slowly varies during the different steps of neuronal development. However, experimentally, one observes that, far from displaying a continuous extension, growth cones usually switch between elongation, pausing, and retraction phases during the whole development.

This behavior is handled separately by the “elongation” models, which regulate the evolution of speed during the motion.

Only two elongation models have been included in the simulator so far: (1) a simplistic model with constant speed, which only considers the average elongation speed, without reproducing the three different phases and (2) a more complex model where the speed of the growth cone depends on the amount of a critical resource which is available at the tip.

The first model being rather obvious, I will focus here on the second model which can actually reproduce the elongation, pausing, and retraction phases observed experimentally. Theoretical models describing alternation between these three phases have been introduced in several papers (Hely et al. 2001; Hjorth et al. 2014) which focus either on the influence of tubulin concentration or on other microtubule-associated

proteins. The model introduced here proposes a simpler version of these ideas in order to make it tractable analytically while retaining the global behavior.

In this model, the behavior of the growth cone is related to the amount a of an unbound molecule which is required for the stabilization or elongation of the MTs in the axonal or dendritic shaft. The amount a which is present at the tip depends on the consumption of the growth cone to polymerize or maintain the MTs, and on the advected flux of the molecule in the neurite, based on the total amount of molecule available, A , through the following Langevin equations:

*resource-based
description
reproduces the
different states
of a growing
neurite*

$$\begin{cases} \dot{a} = -a \left(u + \frac{1}{\tau_l} \right) + \frac{A}{\tau_d} + \chi & = -\kappa a + \frac{A}{\tau_d} + \chi \\ \dot{A} = \frac{A_m - A}{\tau_A} - \frac{A}{\tau_d} + \xi & = \frac{1}{\tau} (A_M - A) + \xi \end{cases} \quad (4.6)$$

where:

u is the consumption rate of the molecule by the MTs,

τ_l is the time constant associated to potential leak or degradation of the molecule,

τ_d^{-1} is the advection rate of the molecule along the branch,

τ is such that $\tau^{-1} = \tau_A^{-1} + \tau_d^{-1}$

A_m is the target amount of molecule in the neurite,

$A_M = A_m \tau \tau_A^{-1}$ is the average amount of molecule in the neurite at equilibrium,

τ_A is the characteristic time of the molecular recruitment to the neurite,

χ, ξ drive the fluctuations of a and A , and are defined as Gaussian random variables:
 $\xi \in \mathcal{N}(0, \sigma_\xi)$ and $\chi \in \mathcal{N}(0, \sigma)$.

The boundary condition $a = 0$ is subjected to a no-flux constraint:

$$\forall A, \frac{\partial f}{\partial a}(0, A) = 0, \quad (4.7)$$

with $f(a, A)$ the probability density of the neurite state.

The detailed analysis of the dynamics can be found in “Critical resource and competition” (section G.4) and is summarized on Figure 4.2, where we can see that, on average, the amount of molecule in the neurite converges to A_M , while the amount in the growth cone converges to $\frac{A_M}{\kappa \tau_d}$.

*behavior
(elongation,
retraction, or
stalling)
depends on
the value of a*

We subsequently define the dynamics of the growth cone’s speed v based on the thresholds:

θ_r below which the growth cone retracts,

θ_e above which the growth cone elongates.

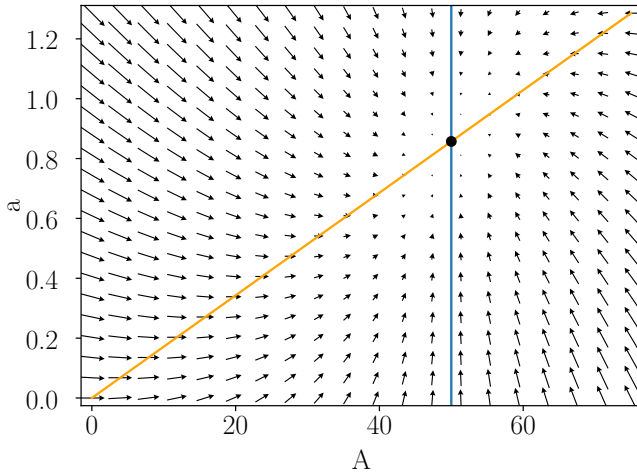


Figure 4.2.: Phase space of the growth cone and neurite state for a single growth cone. Arrows quantify the speed and direction of the motion; A -nullcline is in blue, a -nullcline in orange, and stable fixed point of the average trajectory is given by the black dot. Here $A_M = 50$ and $A_M/(\kappa\tau_d) \approx 0.857$.

such that:

$$v = \begin{cases} \frac{a - \theta_r}{\theta_r} v_r < 0 & \text{if } a < \theta_s \\ 0 & \text{if } \theta_r \leq a \leq \theta_e \\ \frac{a - \theta_e}{a + \theta_e} v_e > 0 & \text{if } \theta_e < a \end{cases} \quad (4.8)$$

where:

v_r is the maximum retraction speed when a growth cone has no resource,

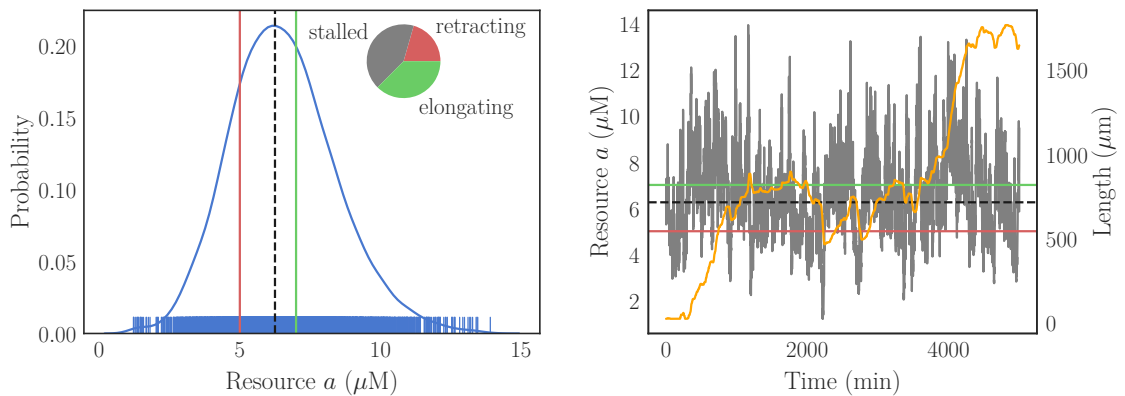
v_e is the maximum elongation speed.

To sum up, in this model, the amount of molecule a that is available at the tip fluctuates around a value that is driven by the total amount A . Depending on the value of a with respect to the two thresholds θ_r and θ_e , the growth cone can switch from elongating to stalling or retracting behaviors — see Figure 4.3.

It is worth noting that the simplicity of the model, as usual, comes at a cost in terms of biophysical relevance since the reaction of the growth cone to changes in the total amount of resource is immediate, as the model does not account for real transport processes. However, I believe that this limitation is acceptable, both because it is the limit case of a reasonable assumption, and in light of the advantages that it provides (making the model, at least partly, solvable). Indeed, immediate response to an average concentration in the neurite, though obviously incorrect, may not be such a bad approximation in the case of proteins whose synthesis could be distributed and with transport speeds that may reach tens of microns per minute (A. Brown 2003). Accounting for transport more precisely would require the implementation of compartmental models which are currently not available in DeNSE.

*model
reproduces
qualitative
behavior*

*with some
intrinsic
limitations*



(a) Distribution of the resource concentration a . (b) Time evolution of the resource (grey) and branch length (orange).

Figure 4.3.: Dynamics of a single growth cone for the critical resource model, where the behavior changes between elongating, retracting, and stalled phases. On both graphs, elongation threshold is given in green, retraction threshold in red, and theoretical average value is the black dashed line, obtained for $a = A_M/(\kappa\tau_d)$.

Termination processes

As any biological object, a neuron cannot grow indefinitely; however, simple random walk models will simply grow indefinitely unless additional checks are implemented. In order to prevent such infinite growth, we included in the models some specific termination conditions, similar to what was done in Memelli et al. 2013. Thus, termination for individual branches occurs when the segment diameter reaches a minimum value⁶.

Termination condition for a whole neurite can also happen when its arbor reaches a specified length, and, similarly, termination of an entire neuron's growth process can be decided via a threshold on its total arbor length.

Eventually a termination mediated by the number of growth cones present in the neurite or neuron can also be set. However, this mechanism has been implemented to prevent memory overflow when branching rates are set to values which are too important and it is not supposed to be used in normal conditions.

4.2.2 Beyond the isolated growth cone: interactions

In the previous paragraphs, we have seen how we can reproduce some of the properties of single growth cones, such as the persistence length or switching behavior between elongation, retraction, or stalling.

However, during most of the development period, the growth cones are not isolated, but, on the contrary, strongly interacting.

In the following paragraphs, I will detail how we can account for the various kinds of interactions that exist between several growth cones, or one growth cone and its environment.

⁶ together with a self-avoidance mechanism, termination when a branch is surrounded by neighboring branches is also being implemented, but is not release-ready yet.

Competing growth cones

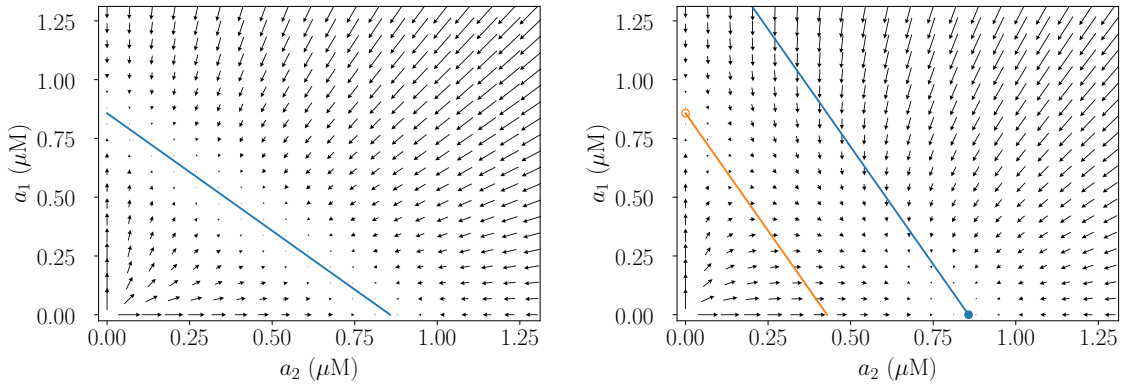
Because the growth cones rely on resources to grow, it can happen that not enough resource is present in the neurite to allow “full speed” elongation of all the growth cones. In such cases, some growth cone might be able to secure more resource for themselves at the expense of other growth cones: one will keep progressing rapidly while others display reduced speed, stalling, or even retraction.

This behavior can partly be accounted for using the previous model of “resource-driven” growth. Indeed, interaction between the growth cones simply modulates the rate at which the resource is received from the neurite. For a growth cone i interacting with other cones j of a neurite, Eq. 4.6 becomes

$$\begin{cases} \dot{a}_i = -\kappa a_i + \frac{A}{\tau_d} \frac{\zeta_i a_i}{\sum_j \zeta_j a_j} + \chi_i \\ \dot{A} = \frac{A_M - A}{\tau} + \xi \end{cases} \quad (4.9)$$

with ζ_i being the weight factor associated to growth cone i .

The addition of this “competition” term introduces interactions between the growth cones as a tip can only get more resource if the amount received by some others is reduced. Considering the transport of the resource to the growth cone the weights $\{\zeta_j\}$ account for the efficiency of the transport and may depend on the branch diameter or the distance to the soma.



(a) Degenerated phase space for identical growth cones ($\zeta_1 = \zeta_2$): nulleclines of both growth cones are fused in a single line. (b) Phase space for $\zeta_2 = 2\zeta_1$: unstable fixed point for 1 (empty circle) and stable fixed point for 2 (filled circle).

Figure 4.4.: Phase space of the quantity of resource for the two growth cones at a constant resource level $A = A_M$ in the neurite. Arrows quantify the speed and direction of the motion. The colorbar represents the number of states in each bin: this is the histogram of the timeseries in (b), and it represents how many times a pair (a_1, a_2) occurred during the simulated time. Here $A_M = 50$ and $A_M/(\kappa\tau_d) \approx 0.857$. As can be seen on (b), when the growth cones have different weights, the only stable state of the system is when the “strongest” cone takes over the whole resource; however, fluctuations allow the exploration of a large area around the two nulleclines (in orange for a_1 and in blue for a_2).

As can be seen on Figure 4.4b, the final stable state of the system, when several growth cones are competing, is necessarily a “winner takes all” state where the growth cone with the largest weight ζ obtains the whole resource.

However, the difference between weights is usually quite small, especially at the beginning of the growth process, where new growth cones have similar diameters and distances to the soma. In a neurite composed of several growth cones having similar weights, a durable metastable state where all cones coexist can be observed because of the region in between the nullclines (orange and blue lines on Figure 4.4b). Indeed, this area is characterized by a slow deterministic dynamics, meaning that the trajectory there can be dominated by a diffusive process due to the noise, as Figure 4.5 illustrates.

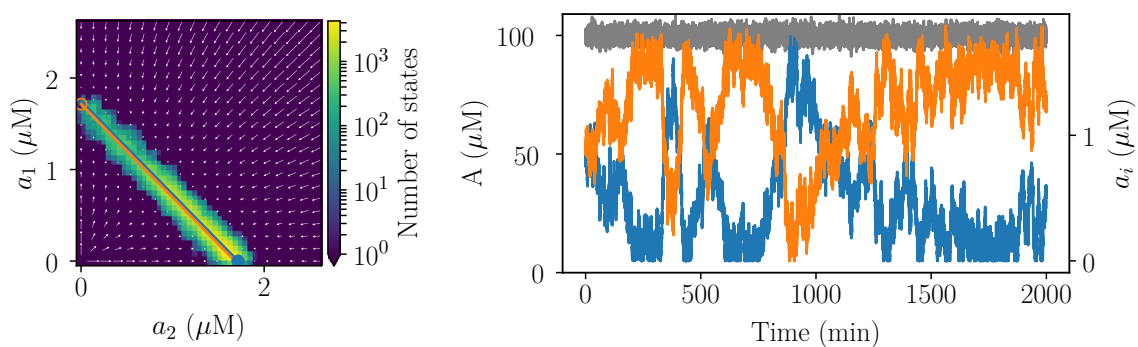


Figure 4.5.: Noise-dominated trajectory for two competing growth cones. Left graph depicts the number of times a particular state of phase-space was visited; Right graph shows the time evolution of the total amount in the neurite (grey line) and in cones 1 (blue) and 2 (orange).

Moreover, beyond that possibility of a noise-dominated trajectory, two growth cones can perfectly coexist, even with strongly different weights, as long as the amount of resource received by each cone supports its elongation. This can be possible because branches having lower diameters, and less MTs in their shaft, will require lower amounts of resource to extend, thus being able to survive with only a small fraction of the available resource.

*coexistence of
elongating
growth cones
is possible*

Sensing the environment

In order to simulate the development of neurons in cultures and complex neuronal devices, it is necessary to account for interactions between the growth cone and the environment it evolves in.

Despite extensive work on the mechanisms involved in the generation of force to steer the trajectory of growth cones, the precise values of the forces exerted (Athamneh et al. 2015) as well as the detailed cytoskeletal dynamics (Cammarata et al. 2016; Coles et al. 2015) still require deeper investigation.

For instance, the lamellipodia is usually the main source of force generation processes through focal adhesions in neural (Rico et al. 2004) and non-neural cells and its role has been shown by studies using optical tweezers (Athamneh et al. 2015) and theoretical models (Craig et al. 2012), other studies (Bornschlögl et al. 2013) consider filopodia as the main pulling actor. Moreover, attempts to quantify the

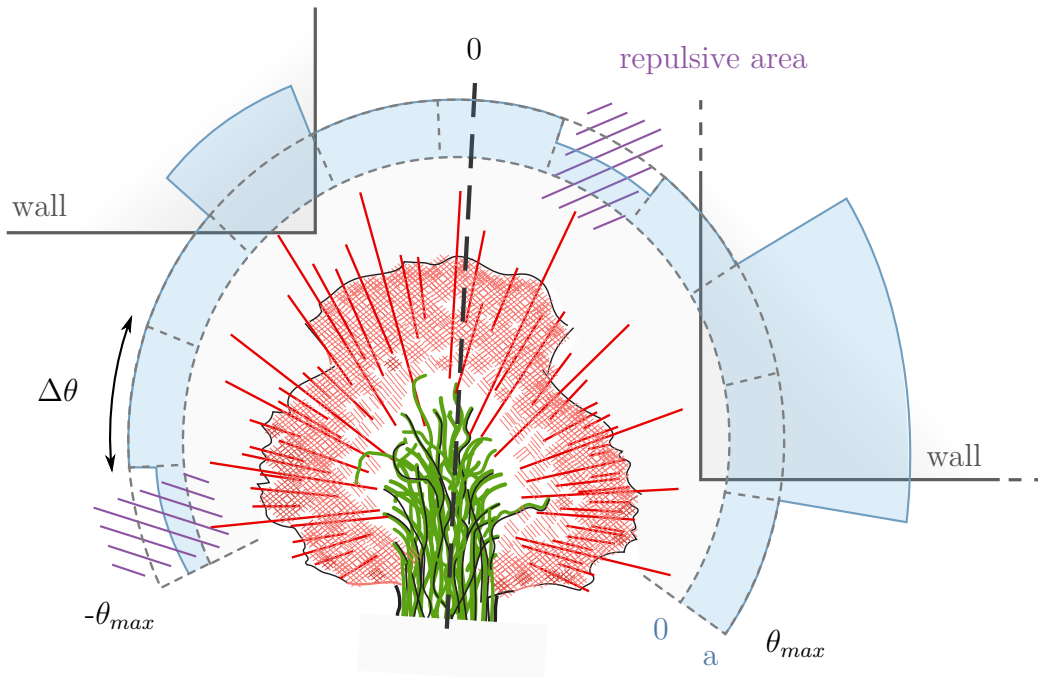


Figure 4.6.: Schematics of the sensing process of the growth cone: filopodia containing bundled actin (straight red line) extend from the lamellipodia and sense/pull on the environment. Each angular region $\Delta\theta$ is then assigned an affinity value in $[0, +\infty[$ which is by default a , the affinity of the current area. In DeNSE, when obstacles, such as walls, or other areas are detected, they increase or decrease the local affinity depending on user-defined parameters. For instance, growth cone usually have a high affinity for walls which they tend to follow, hence the increase of affinity in their direction. Adapted and extended from Grabham 2003.

magnitude of the forces exerted have led to measurements spanning 5 orders of magnitude, from the piconewton (pN) to more than a hundred micronewtons (μN).

However, regardless of the origin of the force generation, the principle of action is usually quite generic:

1. the membrane binds to the environment or other cells through adhesion molecules,
2. these adhesion molecules bind to actin filaments,
3. molecular motors or actin flow generate pulling forces,
4. these forces are transmitted to MTs in the neurite shaft through molecular motors or crosslinkers.

underlying principles for steering emerge from partly understood mechanisms

The amount of force generated then depends on the stiffness of the substrate (Betz et al. 2011) and on the affinity between the growth cone and the surface (Sang et al. 2003; Yu et al. 2008).

In DeNSE, a very qualitative model was implemented in order to account for interactions. First, each growth cone is assigned a number n_f of filopodia that extend from the lamellipodia in well defined directions, ranging from $-\theta_{max}$ to θ_{max} by steps

$$\Delta\theta = \frac{2\theta_{max}}{n_f - 1}.$$

The environment in each direction is assessed by a filopodia and assigned a value which is greater than the default affinity a if deemed “more interesting” than a standard flat substrate, or smaller than a if deemed less interesting.

*growth cones
interact more
or less
strongly with
various
topographical
elements*

The value associated to a given direction typically varies due to:

- a change in the chemistry of the substrate (the value is then the affinity between this specific substrate and the growth cone),
- the presence of a wall, to which most neurites adhere preferentially compared to flat substrates,
- the presence of a step, either doing up, or down, which acts as a potential barrier which is more or less difficult to cross depending on its height.

Moreover, when changing substrate, the affinity of the growth cone is not the only thing that can be modified: the speed of the growth cone, as well as its angular aperture θ_{max} , can also be affected by the substrate properties.

An example of how topographical elements affect the preferential choice of the growth cone is illustrated on Figure 4.6. The set of values sampled by the filopodia leads to a “non-normalized probability distribution”, of integral

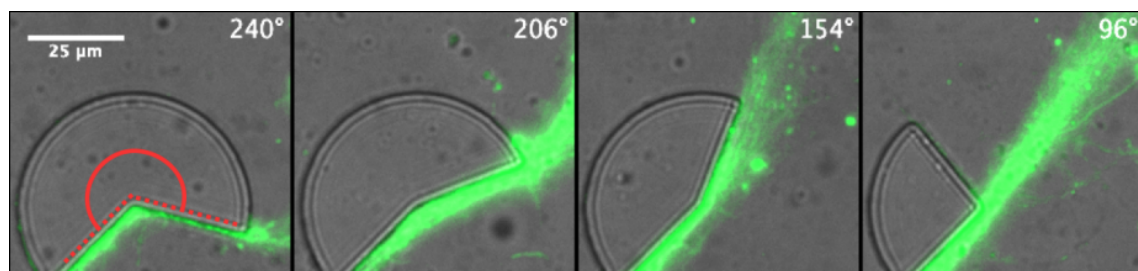
$$I = \sum_{i=1}^{n_f} p(\theta_i),$$

from which the neuron will select at random a direction for its next step. At each step, the growth cone tries to make a step in the preferred direction and succeeds with probability $p = \min(1, I)$, which is why the “probability distribution” is typically “normalized” such that $I_0 = \sum_{i=1}^{n_f} a = 2$ to account for the fact that growth cones grow without problem when half their angular field is blocked. Biologically, this steering through a weighted sampling of the available space can be associated to the preferential invasion of a side of the growth cone by a higher number of MTs (Kahn et al. 2016) when pulling forces facilitate their stabilization. Details on the implementation of the sensing algorithm are provided in “Modeling the environment” (Appendix H).

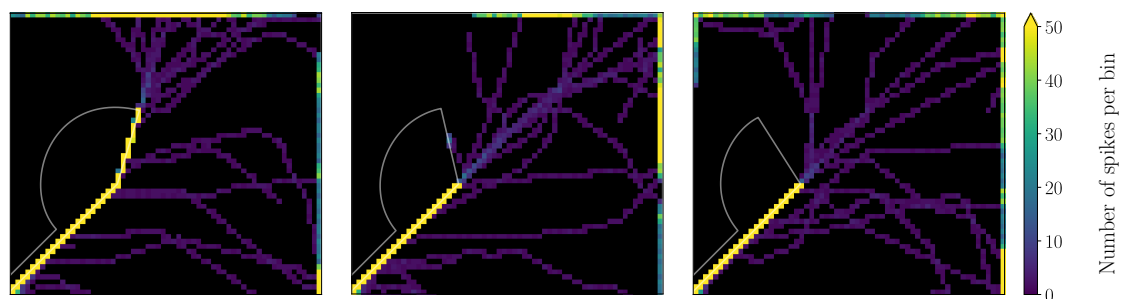
Experiments on the interaction between axons and their environment have been carried out in the team by Renaud Renault (Renault 2015). Through series of setups where only one parameter was varied, he investigated how the behavior of the growth cone evolved in order to quantify the strength of the interactions between the growth cones and the walls. Reproducing these experiments *in silico* allows us to obtain an interval for the value of the wall affinity⁷, as shown of Figure 4.7.

Eventually, growth cones do not only interact with the walls and other artificial obstacles, but also with other neurites and guidance cues. Very different kind of behavior can stem from neurite-neurite interactions, the most striking being self-avoidance (Grueber et al. 2010), fasciculation, and repulsion (L. Wang et al. 2013). Unfortunately, accounting for these interactions in an efficient way requires more advanced spatial algorithms which I did not have time to implement in the initial release of DeNSE, but will be made available in future versions. The inclusion of concentration gradients that might provide guidance to the growth cones requires even more complex description which might be added in a more distant future.

⁷ for reminders, see Figure 4.6



(a) Evolution of the neurite trajectory with the change in angle.



(b) Simulation for decreasing angles, from left to right: 154°, 120°, and 96°.

Figure 4.7.: *In silico* reproduction of the evolution of the trajectory of neurites along a wall, depending on the intensity of the angle change. **(a)** is adapted from Renault 2015 and shows the experimental setup, with the angle marked in red and the neurites shown in green. **(b)** displays simulation of the same setup using DeNSE, with a wall affinity of 1000; density give the number of neurites in each pixel, from more than 50 in yellow, down to one in dark violet and zero in black. Total width is 200 μm on each image.

4.3 Branching patterns

In the previous section, we have seen how the elongation of a branch can be modeled, accounting for their dynamics and interactions with the environment.

However, such models are not sufficient to describe the development of a whole neurite because they do not explain the emergence of new branches, the “arborization” process. Indeed, both axons and dendrites undergo complex branching processes (Gallo 2011; Jan et al. 2010; Lewis et al. 2013) in the course of their development, where new growth cones emerge from existing branches and extend into new ones. Branching mechanisms are widespread phenomena in nature and seem to follow similar principles, even in systems that may be seen as completely different at first (Leonetti 2001).

In this section, we will describe some of the mechanisms through which the complex neuritic arbor is produced, and how they affect the final shape of the neurite tree — cf. Figure 4.8.

In particular, we will focus on four properties to characterize the morphology of the neurites: the number of terminal segments, or *tips*, the total neurite length, the *tree-asymmetry*, and the *Sholl analysis*. These methods are detailed in “Quantifying and analyzing branching patterns” (section I.3), especially the tree-asymmetry measure, which is a properly renormalized version of Van Pelt, H. B. Uylings, et al. 1992.

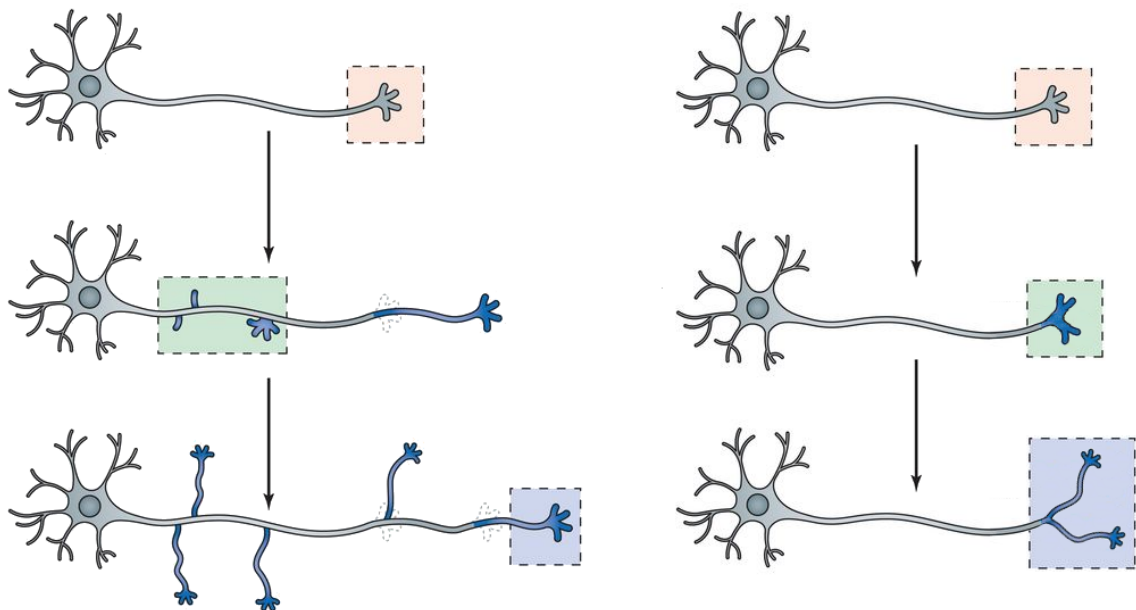


Figure 4.8.: The two main branching modes: lateral branching (left) and growth cone splitting, or bifurcation (right). Image adapted from Lewis et al. 2013.

4.3.1 Growth cone splitting

A first mechanism for the apparition of a new growth cone is the separation of an existing cone into two separate entities. This mechanism is called *growth cone splitting* or *growth cone bifurcation* and has been extensively studied, both experimentally and theoretically (Ooyen 2003; Pelt and H. B. M. Uylings 2002; Wessells et al. 1978).

Biological occurrence

Biologically, the split of a growth cone typically occurs when the dynamical microtubules (MTs) regroup into two separate bundles, one on the right part of the growth cone, the other on the left part.

Two specific situations can facilitate this mechanism:

1. environmental factors, such as multimodal interactions leading to strong pulling in two different directions, either from substrate structure (Withers et al. 2006) or from guidance cues
2. the arrival of an actin wave at the tip (Flynn et al. 2009).

Diameters of the child branches

In a situation where the diameter of a branch triggers the termination of the branch elongation when it goes below a critical value d_{min} , accounting for diameter variation at branching points is of primary importance.

In that perspective, DeNSE implements a power-law rule (Chklovskii et al. 2003; Shefi, Harel, et al. 2004), which defines the relation between the diameters d and d' of the child branches depending on the parent branch diameter d_0 as

$$\left(\frac{d}{d_0}\right)^\eta + \left(\frac{d'}{d_0}\right)^\eta = 1. \quad (4.10)$$

where the exponent η describes the thinning process at branching points (the larger η , the smaller the diameter decrease for large branches).

The model is currently defined as follow: 1) the ratio between the child branches is sampled randomly from a truncated Gaussian distribution $r \in \mathcal{N}(r_0, \sigma)$; 2) the diameter of the first branch is then chosen as

$$d = \frac{d_0}{(1 + r^\eta)^{1/\eta}}, \quad (4.11)$$

then 3) the complementary diameter is taken for the second branch, using

$$d' = (d_0^\eta - d^\eta)^{1/\eta}. \quad (4.12)$$

With that model, it is possible to choose the imbalance between the child branches, with the limit cases $(r_0, \sigma) = (1, 0)$, where child branches always have the same diameter $d_0/2^\eta$, and $(r_0, \sigma) \rightarrow (0, 0)$, where one branch diameter is much larger than the other's.

The van Pelt model

Although not focused on the biological mechanisms, the most advanced models for neurite branching through growth cone splitting is probably due to van Pelt and van Ooyen, notably one which was modestly named “the BEST model”, from the name of the parameters composing it.

Van Pelt and van Ooyen published several articles (Ooyen 2003; Van Pelt, Dityatev, et al. 1997) to provide detailed descriptions of this phenomenon through simple mathematical equations. In Van Pelt, Dityatev, et al. 1997 they proposed the BEST model, accounting for the branching mechanism through growth cone splitting only, via a set of phenomenological.

*bifurcation
events change
both directions
and diameters*

Given a neurite with $n(t)$ terminal segments at a time t , they describe the branching mechanism as the evolution of the number of these terminal segments (Pelt and H. B. M. Uylings 2002), considering that the probability of a growth cone split at time t is $p_s(t)$:

$$\dot{n}(t) = n(t)p_s(t) \quad (4.13)$$

Refining the model, they develop the branching probability for a growth cone characterized by a centrifugal order ⁸ γ , at each timestep i , as:

$$p_i(\gamma) = \frac{B}{N} C_i 2^{-\gamma_i S} n_i^{-E}, \quad (4.14)$$

where:

B is the average number of branching events for a single cone,

E is the competition parameter between the cones,

S is the strength of the order dependence,

T (or N here) is the total duration (number of timesteps).

This model has been further described, generalized, and refined in several papers (Pelt, Ooyen, et al. 2001; Pelt and H. B. M. Uylings 2002), but the basic principles are captured in Equation 4.14. From it, one can show that the number of branching events is limited and decays with time. This model has been including in DeNSE with a slightly modified implementation as the parameter B is given as the average branching rate of a cone.

controlling the asymmetry...

In this model, the typical asymmetry is controlled by the parameter S , which quantifies the likelihood of branching occurrence for growth cones that are already part of a highly branched region of the neurite. Indeed, the centrifugal order γ_i of a cone i characterizes how many bifurcations already occurred while going from the root towards it; thus, the higher the centrifugal order of a cone, the more arborescent its region. For positive S , the model tends to regulate the asymmetry, making growth cones in unbranched regions more likely to branch, while negative values of S will increase spontaneous asymmetry, as illustrated on Figure 4.9a.

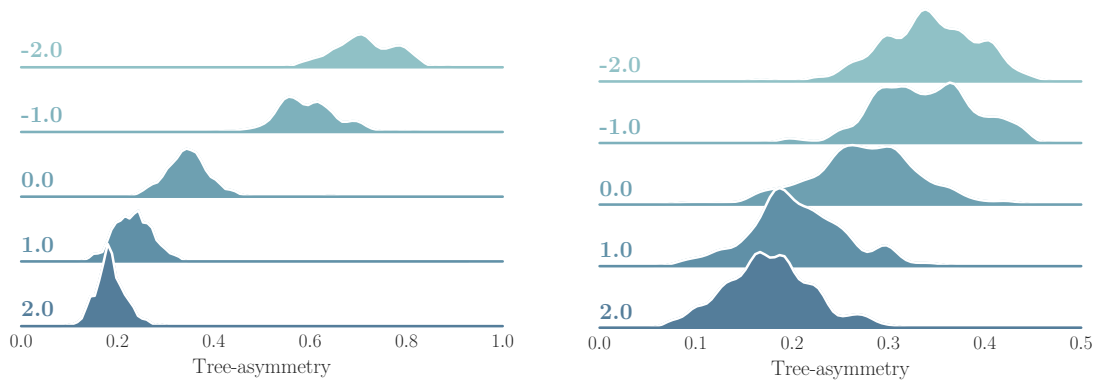
is mostly unnecessary

However, the biological origin of this phenomenon is unclear in the model, and the positive values used for S in papers from van Pelt *et al.* are usually required to obtain more symmetric structures, because their model does not take diameter into account. In DeNSE, it is possible to combine the BEST model and diameter-associated termination, leading to a complete growth model, where branches halt under a critical diameter and new branching occurrences will necessarily occur on the branches which are still active. Because these branches are those with larger diameters, and since (except for pathological cases with $r \rightarrow 0$) this is usually associated to lower branching occurrences, the influence of diameter-associated halt automatically regulates the tree-asymmetry, as shown on Figure 4.9b.

the critical diameter also regulates the branching rate

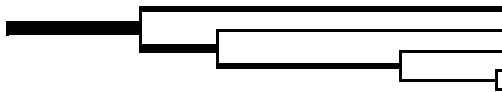
Similarly, the competition parameter E , leading to the progressive decrease of the branching rate in the BEST model, is entirely unnecessary when the growth model takes the diameter into account: as progressive branching events reduce the branches' diameters, they progressively become inactive until none is left.

⁸The centrifugal order is the number of nodes separating the cone from the base of the soma.

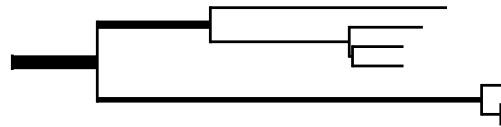


(a) Evolution of tree-asymmetry with S (left values) in the “standard” BEST model.

(b) Evolution of tree-asymmetry with S (left values) accounting for minimal diameter.



(c) Fully asymmetrical dendrogram ($A = 1$) of size 5.



(d) More symmetrical dendrogram ($A \approx 0.52$) of size 7.

Figure 4.9.: Asymmetry properties of trees generated by the BEST model varying the strength S of the order dependence. The distributions were obtained over 300 different neurites. Dendrograms give examples of strongly asymmetrical and more balanced trees, where line thickness depicts the average diameter along the branch. Total length for both neurites is $800 \mu\text{m}$.

Though it reproduces some interesting statistical properties, the BEST model is thus quite artificial, in the sense that 1) it does not provide a mechanistic description of the branching process but uses parameters that are similar to those of generative models (it only aims at obtaining a set of desired properties for the final morphology of the neuron), and 2) some of the parameters introduced are actually not necessary but derive from a minimal diameter constraint which was not taken into account in the model.

Resource- and pull-driven split

In order to provide a model that would be closer to biological phenomena occurring in the neurite, DeNSE includes two mechanisms related to growth cone splitting:

getting closer to biological mechanisms

- a pull-based split when a multimodal pull distribution is present — see “Branching models” (Appendix I),
- a resource-based mechanism, for the competitive model, when the amount of resource in a cone reaches a certain threshold θ_b .

In the resource-based paradigm — cf. “Modeling an extending growth cone” (subsection 4.2.1), once a cone possesses an amount of resource $a > \theta_b$, it displays a

branching rate r_b which is given by

$$r_b(a) = \frac{a - \theta_b}{a + \theta_b} R_b, \quad (4.15)$$

with R_b the maximum branching rate.

The idea behind this description is that, as MTs are stabilized by higher amounts of resource, the probability that two MT-bundles start invading two different parts of the growth cones increases, leading to higher branching probability.

As shown in the previous section, the competitive model has only one stable fixed point where one cone obtains the entire resource content. However, in the case of growth cone splitting, the new cones are often very similar in diameter (Shefi, Golebowicz, et al. 2005), which brings the system quite close to the degenerate case shown on Figure 4.4a. Because of this and of the noise in the resource distribution, the system never remains on the fixed point but explores a (potentially quite large) region around it.

“Growth cone split” (section I.1) gives additional details on the precise analysis of the phenomenon, but the main behavior can be understood qualitatively by crudely approximating the extreme case where, for n growth cones, one gets all the resource while the other $n - 1$ oscillate near their $a = 0$ region. For a level of noise σ , the average value of these low- a cones will scale at least as $\sqrt{\sigma}$, meaning that the average rate r_a at which the winner receives the resource is lower than

$$r_a^{(max)} = \frac{A}{\tau_d} \frac{\zeta_{max} A / (\kappa \tau_d)}{(n - 1) \sqrt{\sigma} + \zeta_{max} A / (\kappa \tau_d)}, \quad \text{hence} \quad \lim_{n \rightarrow \infty} r_a^{(max)} = 0. \quad (4.16)$$

This guarantees that the average branching probability of the most active growth cone will eventually go to zero as the number of growth cone increases.

One of the main interests of this model is that it can be used to couple the elongation and branching mechanisms, allowing us to investigate the consequences of this coupling on the final morphology.

4.3.2 Lateral branching

Besides the bifurcation of a growth cone into two, new growth cones can also emerge directly from the side of existing branches in a phenomenon called lateral, or collateral branching, cf. Figure 4.8.

Biological occurrence

As described in the review of Gallo 2011, collateral branching can occur 1) from the spontaneous protrusion of a filopodium or a lamella from the side of a branch, which matures into a growth cone as new MTs invade it and reinforce the actin network or 2) from an actin deposit left behind by a pausing growth cone. In axons, the lamellar protrusion is strongly associated with actin waves propagating from the proximal segment of the axon towards the extremities.

*branching rate
in resource-
driven split
eventually
goes to zero*

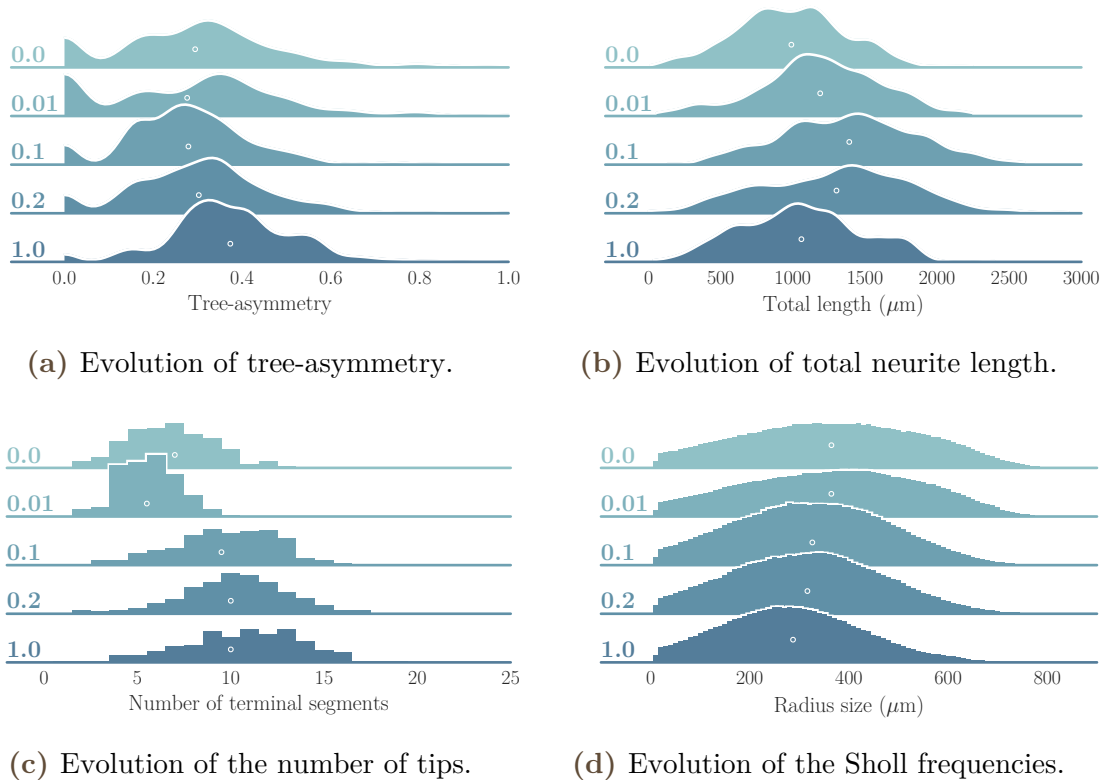


Figure 4.10.: Asymmetry properties of trees generated by the resource-based branching model, varying the strength of the diameter weight on resource acquisition (indicated on the left axis). The distributions were obtained over 300 different neurites. Average values of the distributions are marked by a white circle.

Uniform lateral branching

A first naive model is implemented in DeNSE as a uniform branching model, where new branches emerge randomly and uniformly along the active branches of the neurite tree. These branches develop from a diameter which is a fraction f of the parent’s at the branching point. Despite this apparent uniformity, lateral branching gives rise to strongly asymmetrical structure due to the diameter-based termination process: thin branches inactivate more quickly, leading to a majority of branching occurrences on the wider branches, thus increase the tree-asymmetry, cf. Fig. 4.13a.

Distance-dependent phenomenon

Contrary to what a uniform branching pattern may generate, experimental observations show that lateral branching, either during collateral branching or in the final arborization process, often occurs rather far from the root, and closer to the growth cone (Gibson et al. 2011). In order to account for this fact, and though part of its origin may come from external cues, a second branching model was implemented in DeNSE, where new branches emerge at a distance d from a randomly-chosen growth cone among the active pool⁹, with d following a power-law distribution — see “Lateral branching” (section I.2).

The Front-based Power-Law Lateral (FP2L) branching has several interesting properties:

*uniform and
close-to-the-tip
emergence of
lateral
branches*

⁹meaning that its diameter is greater than d_{min} .

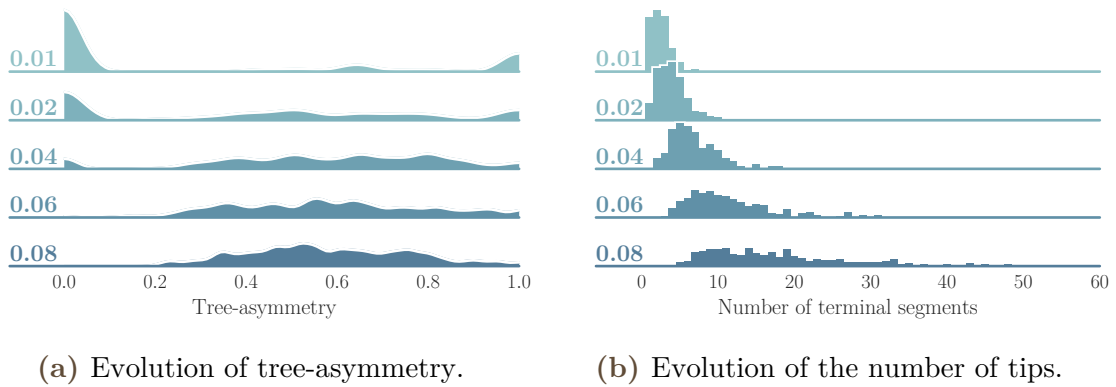


Figure 4.11.: Asymmetry properties of trees generated by uniform lateral branching. Branching rates are given on the left axes, in h^{-1} for a 5 day branching process. For very low branching rates, the over-representation of the trivial 1, 2, and 3-tip structures with asymmetry values 0 and 1 leads to multimodal distributions while higher branching rates and number of terminal segments span the asymmetry space more completely and lead to more unimodal distributions. The distributions were obtained over 300 different neurites.

- Since it stems from areas that are closer to the neurite tips, thus with smaller diameters, FP2L branching leads to smaller branches which stop quicker, and leads to a branching process that is more likely to terminate from diameter-based termination compared to the uniform branching pattern.
- Because it only starts from active growth cones, this model also promotes high asymmetry values; this property is thus conserved, as in the uniform branching pattern.

Coupling with growth cone split

One of the properties of lateral branching is that its occurrence does not affect the diameter of the branch it stems from, but only that of the emerging branch. The new branch starts with a diameter which is a fraction of the parent's diameter. Because of this, neurites generating solely through lateral branching (unless they are modeled through a resource-driven elongation) will take very long to stop growing, leading to unnaturally long neurites with exuberant arborescence.

More biologically plausible structures are therefore preferably obtained when lateral branching is not used as at the final stage of the growth process, but either at the beginning or during an intermediate step, in order to make sure that growth will “properly” terminate.

This effect is nonetheless almost eliminated when using FP2L branching, since the events occur close to the tip, i.e. at lower diameters, and the new branches become inactive more rapidly.

4.3.3 Pruning

Having defined the mechanisms for competition and branching, one logically falls into a last mechanism, called pruning (Oan et al. 2011). Indeed, some branches do not manage to elongate sufficiently: they eventually retract back to the point from which they initially protruded and disappear.

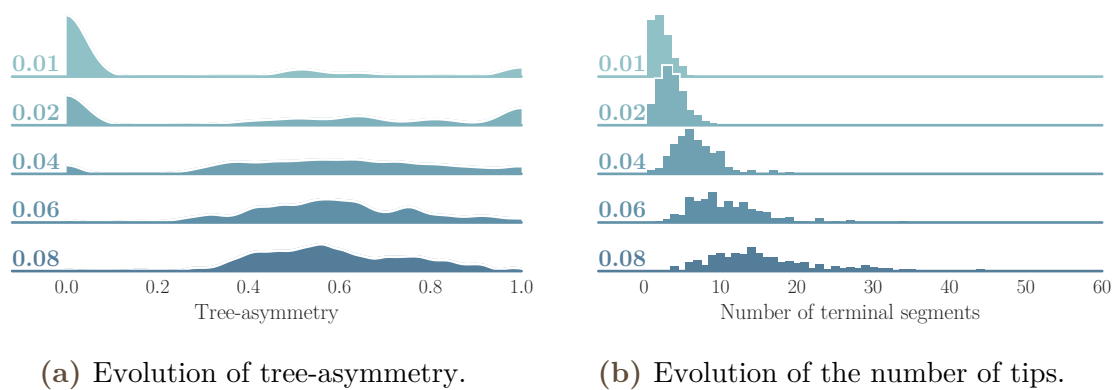
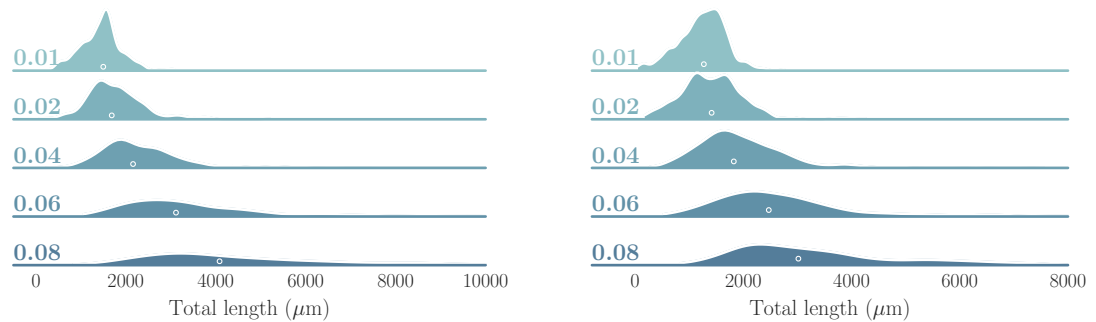


Figure 4.12.: Asymmetry properties of trees generated by FP2L branching. Branching rates are given on the left, in h^{-1} for a 5 day branching process. For very low branching rates, the over-representation of the trivial 1, 2, and 3 tips structures with asymmetry values 0 and 1 leads to multimodal distributions while higher branching rates and number of terminal segments span the asymmetry space more completely and lead to more unimodal distributions. The distributions were obtained over 300 different neurites.

In our model, this behavior is obtained when a growth cones retracts, either from lack of resource, or because of “interaction-based” retraction¹⁰. Once the length of their branch reaches zero, they are pruned, i.e. deleted from the neurite.

¹⁰see “Making the forward step” (section H.2) for details



(a) Evolution of the length for the uniform branching process.

(b) Evolution of the length for the FP2L branching process.

Figure 4.13.: Total length of the neurite tree for a 5 day growth under the uniform and FP2L branching processes. Branching rates are given on the left, in h^{-1} for a 5 day branching process. As predicted from its properties, the FP2L branching algorithm leads to total length that are on average lower than those of the uniform branching (see white circles for average values). Distribution were calculated over 300 neurites.

4.4 From neuronal morphologies to neuronal networks

4.4.1 A complete neurite tree

The development of the entire arborescence of a neurite is a complex process which generally involves all the mechanisms mentioned in the previous section — elongation, growth cone bifurcation, lateral branching, and pruning. These basic ingredients are combined in various proportions depending on the nature of the neurite and the stage of development.

Overall, this makes it almost impossible to describe the general outgrowth of a neurite with a single model, especially at the level of simplification used in the models presented in this study.

In order to reproduce the broad variety of neural shapes that can be found in various brain regions — e.g. for dendritic trees, with number of branches ranging from 10 to 400 (Stuart et al. 1999) — I therefore designed DeNSE to let the user himself separate the growth process into relevant stages.

Multi-step growth

The outgrowth of most neurons can be modeled into a few stages. An initial elongation period with little or no branching events, where the neurites elongate away from the soma until they reach a certain length. Depending on the cell, this period can contain a few bifurcation events that contribute to the development of initial arbor, where neurites do not emerge directly from the soma but rather from a large dendritic trunk.

This initial period is followed by one or several branching periods, composed of many splitting, lateral branching events, or both. As discussed in the previous section — “Branching patterns” (section 4.3) — growth cone splitting or bifurcation can be used to obtain very symmetrical trees, as shown on Fig. 4.14a and 4.15d. More asymmetrical trees can also be obtained through lateral (and especially FLPL) branching events, see for instance Fig. 4.14b and 4.14c.

Eventually, the final period of the development is often composed of a ramification process, preferably modeled in DeNSE by splitting or FLPL branching at low rate to ensure termination, as shown on Fig. 4.14c.

Reproducing realistic morphologies

The multi-step growth procedure was used here to reproduce typical cell morphologies presenting different topological and geometrical properties.

Depending on the initial neurite diameter and on its taper rate, the typical length of the neurite can be regulated, leading to rather short (granule cell, pyramidal and chandelier dendrites) or much more elongated trees (dendrites of the starburst cell, pyramidal axon).

Variability in the branching rates then provides more or less tufted and exuberant arbors.

Specifically, growth cone splitting usually promotes more balanced structures as bifurcation points divide into child branches of comparable width, while lateral branching leads to the development of a well defined trunk (characterized in K. M. Brown et al. 2008 by its *caulescence*) from which smaller branches emerge.

*users can
define time
periods
described by
specific
processes*

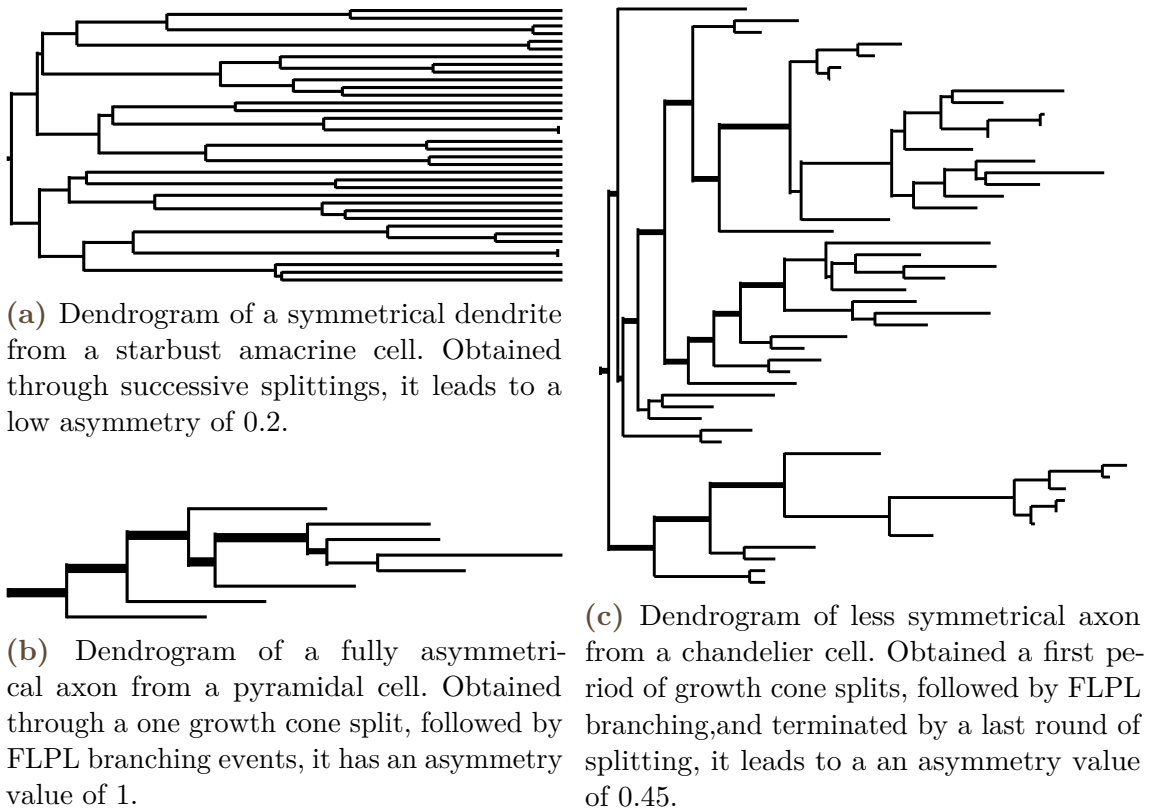


Figure 4.14.: Dendrograms of various cells obtained with DeNSE, through different elongation and branching processes.

Figure 4.15 provides an example in the starburst amacrine cell (4.15d), which is obtained purely through subsequent growth cone splits, while structures like the chandelier and pyramidal cells (4.15a and 4.15b) start with a short period of growth cone splitting, followed by a longer period of elongation and lateral branching.

The main limitation of the DeNSE simulator so far is the absence of self-avoidance and fasciculation (when several cells are involved). This absence is especially visible on the starburst amacrine cell (Fig. 4.15d), for which neurites usually avoid one another very efficiently. These mechanisms are currently being implemented but require a significant amount of work to be computationally efficient.

4.4.2 Coupling neurons: synapses and network

Simple rules for synapse formation

Once morphological types have been selected, DeNSE can be used to grow many neurons in a confined environment such as a culture. However, because of the current limitations of the space-management components of the library, generating synaptic connections on-the-fly is currently not possible¹¹ and is therefore implemented as post-treatment of the generated neuronal population.

Synapses between neurons can then be generated by taking into account the interaction between the axons and dendrites of neighboring cells. Currently, two

¹¹ As for self-avoidance and fasciculation, such interaction mechanisms require an additional grid-based management or other kind of R-tree search methods to provide fast queries of neighboring objects.

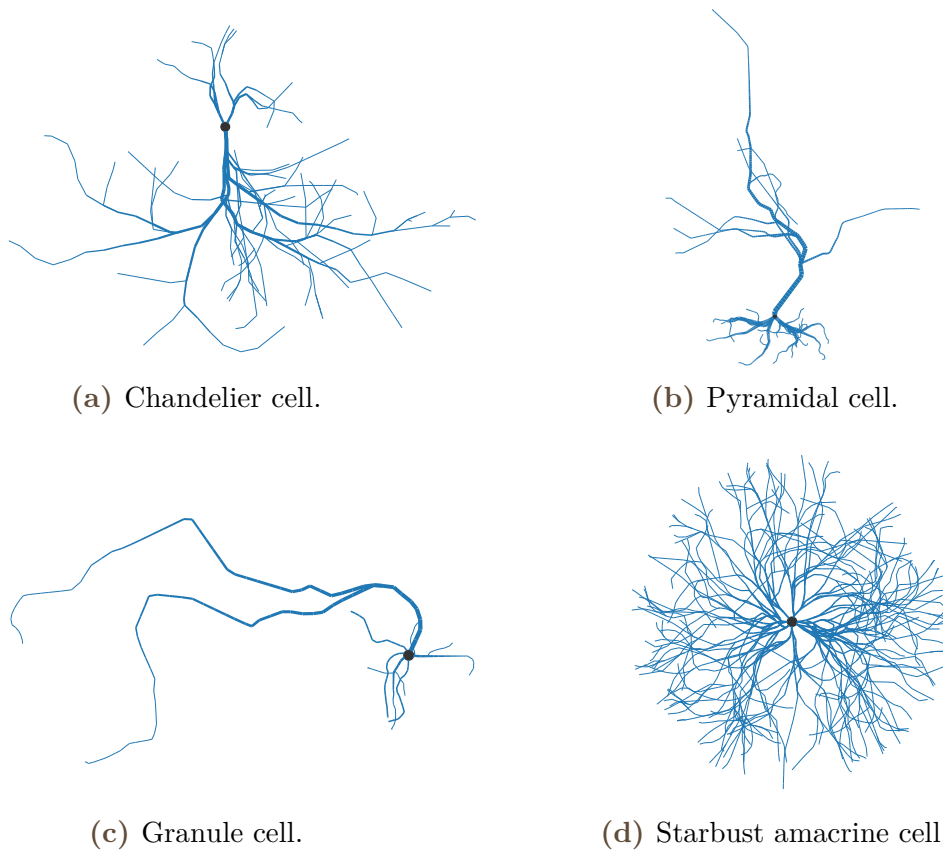


Figure 4.15.: Visualization of four specific cell types generated with DeNSE. The axon is always the longest neurite, except for the starbust amacrine cell, where only neurites are present. Scale is given by the soma size which is $16 \mu\text{m}$ for all cells.

simple generation methods are provided in DeNSE: a very simple crossing test and a slightly more elaborate spine-based method.

The easiest method is simply to check for crossings between axons and dendrites and assign a probability of synapse formation p_s upon crossing. In the case of several connection sites between two neurons, the weights of the connections are summed and the interaction between the neurons is modeled by a single synapse having a weight $w = \sum_k w_k$ and associated to the average delay¹².

A more elaborate and more biologically relevant method consists in taking into account the density of spines along the neurite, as shown on Figure 4.17. To each dendrite is associated a (potentially distance-dependent) spine density ρ . Given that spines reach up to a maximal distance d_{max} , the probability to connect to an existing spine when at a distance $d < d_{max}$ is

$$P(d) = P_0 \frac{d_{max} - d(l)}{d_{max}}, \quad (4.17)$$

where P_0 is an adjustment constant — usually taken as 1.

¹² Because the dendritic tree is usually quite localized compared to the size of the culture, we can actually consider with a good approximation ($\Delta d \leq 1 \text{ ms}$) that delays between connections across the same two neurons are very similar and can be approximated by the mean delay. This allows to consider only simple graphs and not multigraphs, which simplifies the analysis.

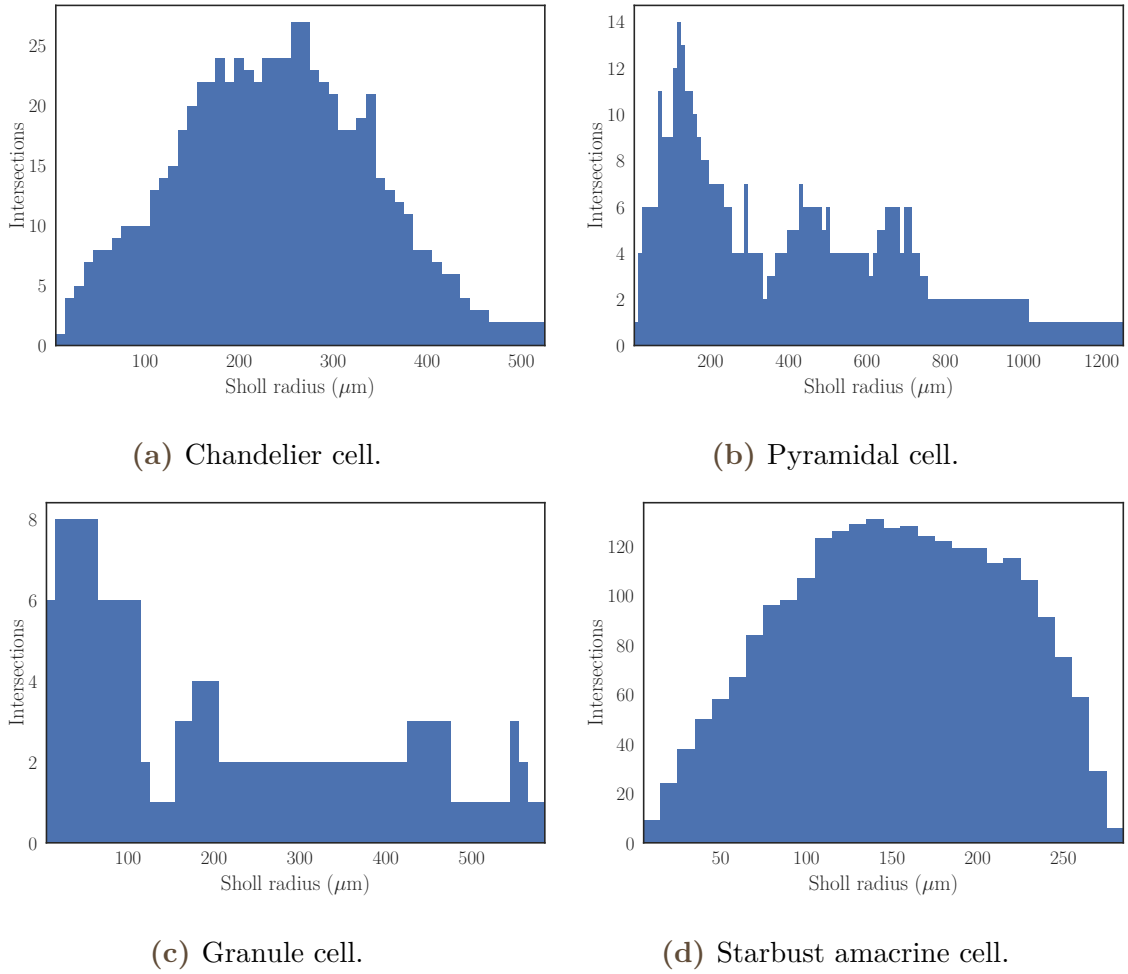


Figure 4.16.: Sholl analysis of four specific cell types generated with DeNSE. The evolution of the number of intersections between the neurites and successive circles centered on the soma allows to quantify the typical reach of the neuron, its branching pattern, as well as its heterogeneity. Thus, the strong isotropy and regularity of the starbust amacrine cell is reflected in its abrupt termination, while significance of the asymmetry between the dendrites and axon of the other three cells transpires in the more or less prominent tail of the distribution.

Thus, for an axon crossing a dendrite’s spine field over a distance l , the number of synapses that will be created is given by:

$$n = \frac{P_0}{l} \int_0^l \frac{d_{max} - d(l)}{d_{max}} \rho(l) dl \quad (4.18)$$

Synapses are actually formed when spines interact with axonal boutons, whose density would also affect the probability of synapse formation. However, the typical density of boutons on axons is usually such that spines can generally reach one bouton for each axo-dendritic crossing (Ikonomic et al. 2007; Zhang et al. 2011), and the overall probability can still be tuned by changing the value of P_0 .

Compared to the crossing method, the “spine-based” algorithm leads to more potential connections since neighboring axons and dendrites can connect, even if they do not cross, as long as they are separated by a distance smaller than d_{max} .

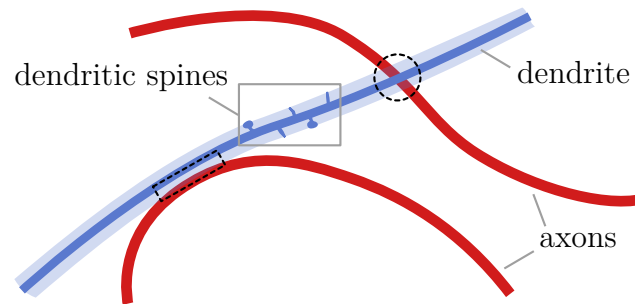


Figure 4.17.: Schematics of the principle of spine-based connectivity. Putative synaptic sites are marked by the dashed black areas. A sketch of spines is shown in the gray inset and approximated in the model by the continuous pale blue area surrounding the dendrite. Note that crossing is not necessary for synapse formation in this model.

Growing neuronal cultures

Culture growth was simulated according to the following procedure:

- 5 days of elongation without branching for the axon, and with low growth cone bifurcation rate for the dendrites,
- 10 days of lateral branching for all neurites, with slightly reduced elongation speed,
- 10 days of final elongation for the axon and of further growth cone splitting for the dendrites, both at reduced speed.

In order to compare the results with the generated EDR networks, the mean connection distance in the culture was computed to obtain the value of λ giving the associated distribution, and the properties of the two networks were then confronted.

This analysis was performed on two networks: one obtained from pyramidal cells, the other from bipolar cells.

General properties of “grown” networks

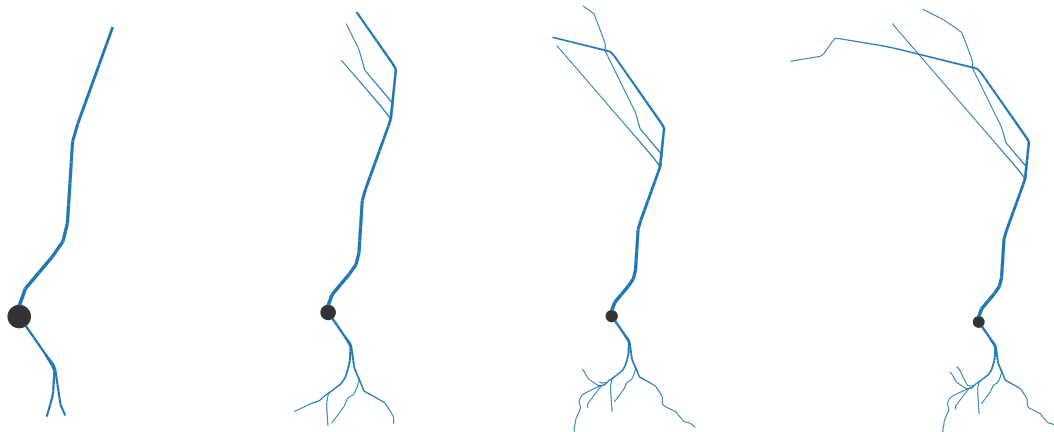
Compared to the EDR model, a significant difference can be seen in the spatial distribution of the in-degree: though central neurons also exhibit rather high degrees, some regions on the periphery also exhibit very high in-degrees. This comes from the fact that growing neurites follow the edge of culture, while not such thing exists in the EDR model. Coming back on the nucleation centers discussed in “Burst nucleation in neuronal cultures *in silico*” (subsection 3.3.2), this implies that the difference between centered initiation points for noise-driven activity and more peripheral nucleation points for pacemaker-driven activity can in fact not be used to differentiate between these two initiation mechanisms.

The spatial distribution clustering coefficient follows a trend which is similar to that of the EDR model, with highest values located on the periphery, and lowest values at the center. However, the actual values observed in both pyramidal and bipolar networks are significantly higher than those of the EDR model which already displayed clustering values that were notably higher than non-spatial random networks.

compared to EDR graphs, grown networks do not exhibit the core-periphery segregation of high-degree neurons

Networks of bipolar cells

Bipolar cells, as shown on Figure 4.18, are a morphological category which is often seen in cultures (Garay et al. 2013), and presents a very specific shape with a rather low space coverage due to its low branching and tortuosity: neurites grow away from the cell in opposite directions, and with little arborization.



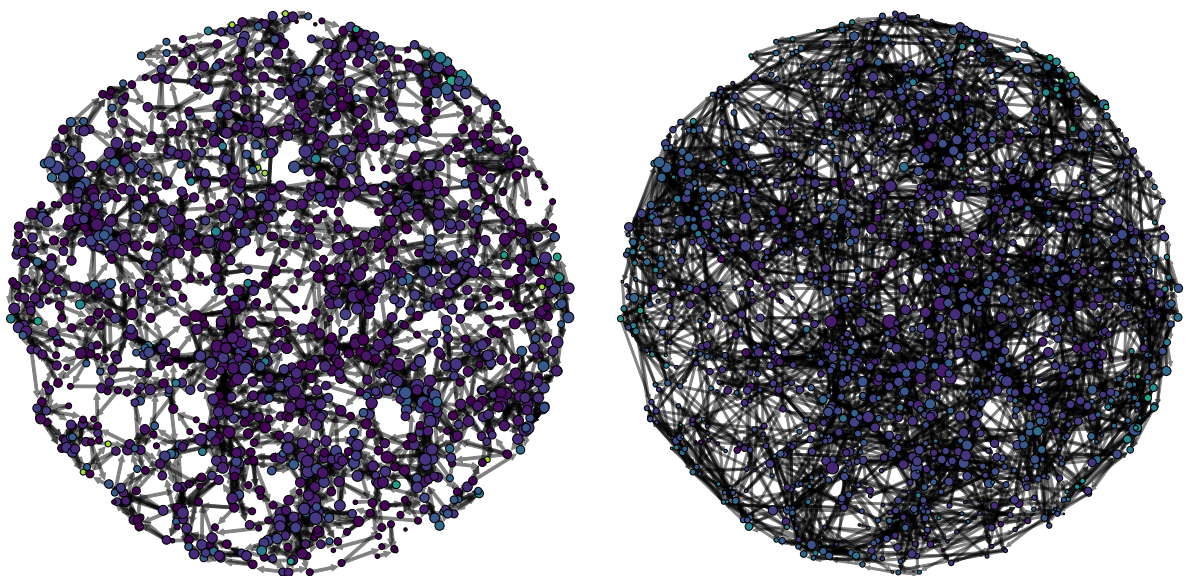
(a) 5 DIV.

(b) 10 DIV.

(c) 15 DIV.

(d) 25 DIV.

Figure 4.18.: Simulated evolution of a bipolar cell in time. Soma size is $8 \mu\text{m}$.



(a) 5-DIV culture of bipolar neurons showing all connections.

(b) 15-DIV culture of bipolar neurons showing one connection in 4.

Figure 4.19.: Simulated growth of a 1500-neuron culture of bipolar neurons over 25 days. Node size shows the relative difference between the in-degree across the network, while color represents the clustering coefficient, from low values in dark purple to yellow for the highest values, through blue and green.

Networks of pyramidal cells

Pyramidal cells — cf. Figure 4.20 — are the main morphological type of excitatory cells in the cortex and the hippocampus. Compared to the previous bipolar cells, they occupy a larger fraction of their surroundings because to their higher neurite number and increased lateral branching.

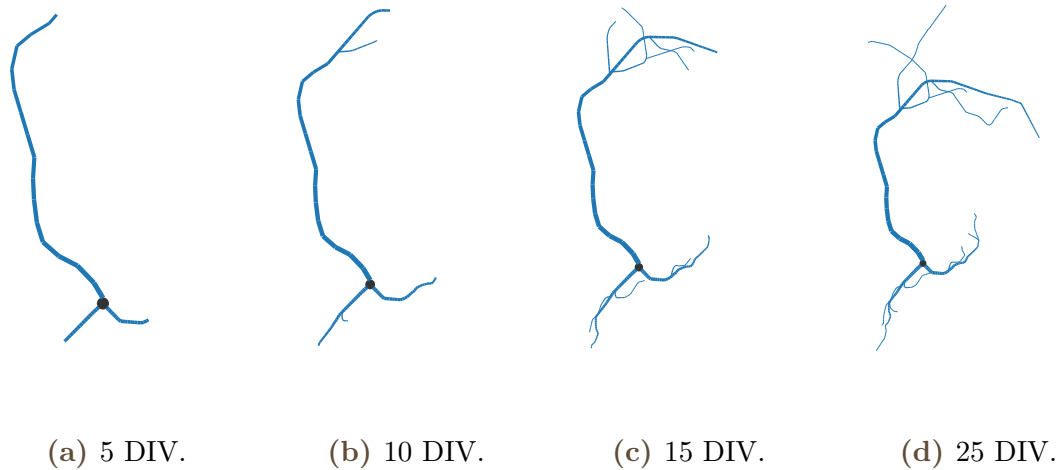
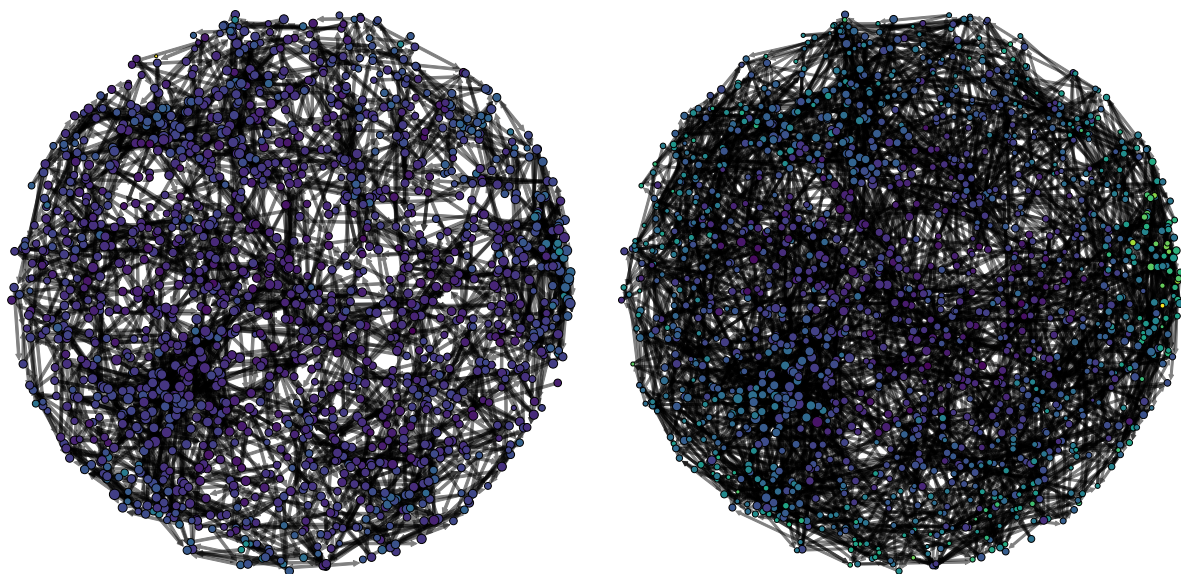


Figure 4.20.: Simulated evolution of a pyramidal cell in time. Soma size is $8 \mu\text{m}$.



(a) 5-DIV culture of pyramidal neurons showing one connection in 5. (b) 15-DIV culture of pyramidal neurons showing one connection in 15.

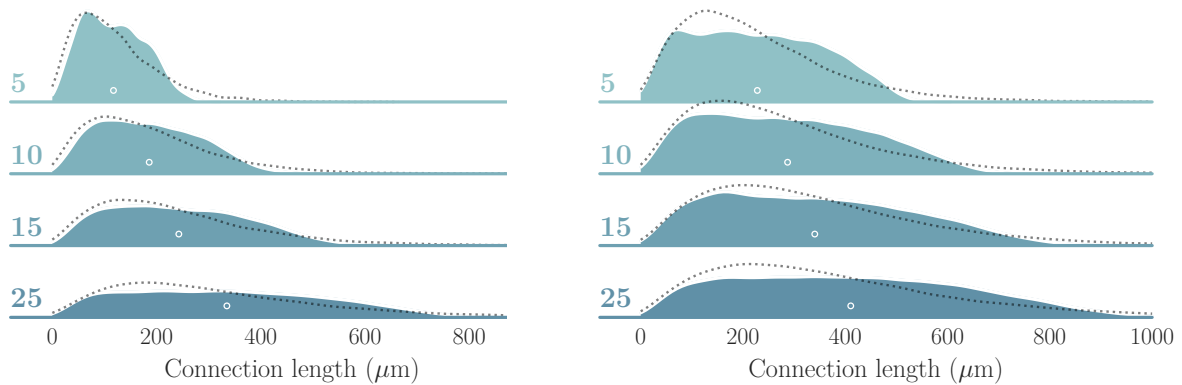
Figure 4.21.: Simulated growth of a 1500-neuron culture of pyramidal neurons over 25 days. Node size shows the relative difference between the in-degree across the network, while color represents the clustering coefficient, from low values in dark purple to yellow for the highest values, through blue and green.

Influence of the cell morphology

Rather unsurprisingly, one observes that the network generated from pyramidal neurons possesses a higher average degree, both because of their superior filling fraction and greater neurite length. This increased degree also leads to higher clustering coefficients, which are significantly greater than those observed in EDR networks.

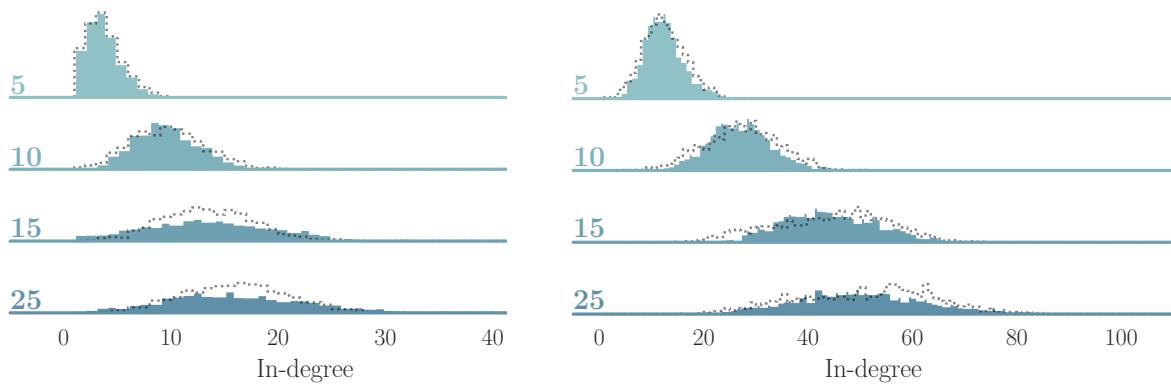
Though the average degree obtained for the bipolar cell is low compared to reported values (Soriano, Rodríguez Martínez, et al. 2008), the degree distribution obtained for the pyramidal neurons is compatible, if on the lower bound of the interval.

Regarding the distance distribution, the values are also compatible with measurements from Barral et al. 2016 which obtain average distances of the order of 400 μm .



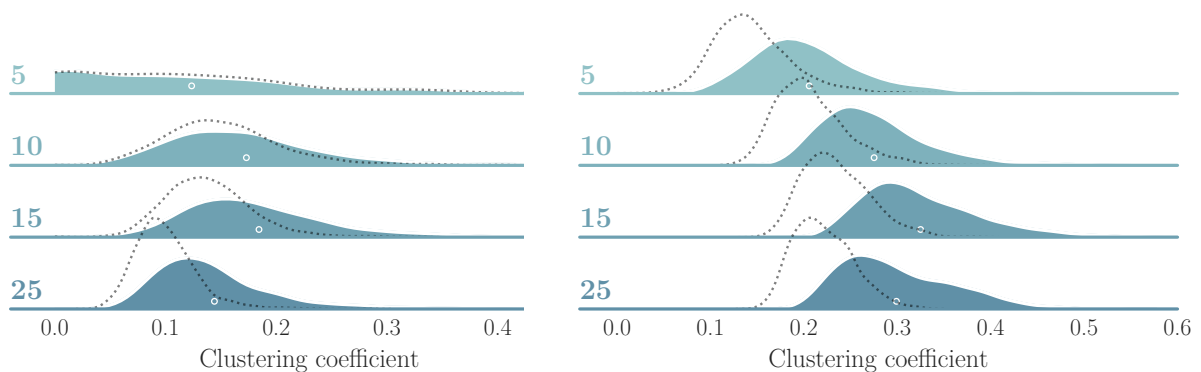
(a) Distance distribution for the bipolar culture.

(b) Distance distribution for the pyramidal culture.



(c) In-degree distribution for the bipolar culture.

(d) In-degree distribution for the pyramidal culture.



(e) Distribution of the clustering coefficient for the bipolar culture.

(f) Distribution of the clustering coefficient for the pyramidal culture.

Figure 4.22.: Comparison of the properties of grown cultures composed of bipolar (left), or pyramidal neurons (right) with respect to those of an “equivalent” EDR network, which is shown by the dotted lines. Average values of the culture properties are marked by the white circles. The age of the culture in DIV is given on the left axis.

References for chapter 4

- Aimovi, J. et al.** (2011). “Modeling of Neuronal Growth In Vitro: Comparison of Simulation Tools NETMORPH and CX3D.” In: *EURASIP journal on bioinformatics & systems biology* 2011, p. 616382. ISSN: 16874153. DOI: 10.1155/2011/616382 (cit. on p. 94).
- Athamneh, A. I. M. and Suter, D. M.** (Sept. 2015). “Quantifying mechanical force in axonal growth and guidance”. In: *Frontiers in Cellular Neuroscience* 9.SEPTEMBER 2015, p. 359. ISSN: 1662-5102. DOI: 10.3389/fncel.2015.00359 (cit. on p. 104).
- Barral, J. and Reyes, A. D.** (Dec. 2016). “Synaptic scaling rule preserves excitatory/inhibitory balance and salient neuronal network dynamics”. In: *Nature Neuroscience* 19.12, pp. 1690–1696. ISSN: 1097-6256. DOI: 10.1038/nn.4415 (cit. on pp. 87, 124, 163).
- Betz, T. et al.** (2011). “Growth cones as soft and weak force generators.” In: *Proceedings of the National Academy of Sciences of the United States of America* 108.33, pp. 13420–13425. ISSN: 0027-8424. DOI: 10.1073/pnas.1106145108 (cit. on p. 105).
- Bornschrögl, T. et al.** (2013). “Filopodial retraction force is generated by cortical actin dynamics and controlled by reversible tethering at the tip.” In: *Proceedings of the National Academy of Sciences of the United States of America* 110.47, pp. 18928–33. ISSN: 1091-6490. DOI: 10.1073/pnas.1316572110 (cit. on p. 104).
- Brown, A.** (2003). “Axonal transport of membranous and nonmembranous cargoes: A unified perspective”. In: *Journal of Cell Biology* 160.6, pp. 817–821. ISSN: 00219525. DOI: 10.1083/jcb.200212017 (cit. on p. 101).
- Brown, K. M., Gillette, T. A., and Ascoli, G. A.** (2008). “Quantifying neuronal size: Summing up trees and splitting the branch difference”. In: *Seminars in Cell and Developmental Biology* 19.6, pp. 485–493. ISSN: 10849521. DOI: 10.1016/j.semcd.2008.08.005. arXiv: NIHMS150003 (cit. on pp. 117, 178).
- Cammarata, G. M., Bearce, E. A., and Lowery, L. A.** (2016). “Cytoskeletal social networking in the growth cone: How +TIPs mediate microtubule-actin cross-linking to drive axon outgrowth and guidance”. In: *Cytoskeleton* 73.9, pp. 461–476. ISSN: 19493592. DOI: 10.1002/cm.21272 (cit. on p. 104).
- Chklovskii, D. B. and Stepanyants, A.** (2003). “Power-law for axon diameters at branch point”. In: *BMC Neuroscience* 4.1, p. 18. ISSN: 14712202. DOI: 10.1186/1471-2202-4-18. arXiv: 0302039 [physics] (cit. on p. 109).
- Coles, C. H. and Bradke, F.** (Aug. 2015). “Coordinating Neuronal Actin/Microtubule Dynamics”. In: *Current Biology* 25.15, R677–R691. ISSN: 09609822. DOI: 10.1016/j.cub.2015.06.020 (cit. on pp. 12, 13, 104).
- Courchesne, E. and Pierce, K.** (2005). “Why the frontal cortex in autism might be talking only to itself: Local over-connectivity but long-distance disconnection”. In: *Current Opinion in Neurobiology* 15.2, pp. 225–230. ISSN: 09594388. DOI: 10.1016/j.conb.2005.03.001 (cit. on p. 92).
- Craig, E. M. et al.** (2012). “Membrane tension, myosin force, and actin turnover maintain actin treadmill in the nerve growth cone”. In: *Biophysical Journal* 102.7, pp. 1503–1513. ISSN: 00063495. DOI: 10.1016/j.bpj.2012.03.003 (cit. on p. 104).

- Flynn, K. C. et al.** (2009). “Growth cone-like waves transport actin and promote axonogenesis and neurite branching”. In: *Developmental Neurobiology* 69.12, pp. 761–779. ISSN: 19328451. DOI: 10.1002/dneu.20734 (cit. on p. 109).
- Gallo, G.** (2011). “The cytoskeletal and signaling mechanisms of axon collateral branching”. In: *Developmental Neurobiology* 71.3, pp. 201–220. ISSN: 19328451. DOI: 10.1002/dneu.20852 (cit. on pp. 108, 112).
- Garay, P. M. et al.** (2013). *CellPlayer 96-Well Kinetic NeuroTrack Assay*. URL: https://www.essenbioscience.com/media/uploads/files/8000-0211-A00%7B%5C_%7D-%7B%5C_%7DCellPlayer%7B%5C_%7D96-well%7B%5C_%7DNeuroTrack%7B%5C_%7DAssay%7B%5C_%7DApplication%7B%5C_%7DNote.pdf (cit. on p. 122).
- Gewaltig, M.-O. and Diesmann, M.** (2007). *NEST (NEural Simulation Tool)*. URL: http://www.scholarpedia.org/article/NEST_%28NEural_Simulation_Tool%29 (cit. on p. 94).
- Gibson, D. A. and Ma, L.** (2011). “Developmental regulation of axon branching in the vertebrate nervous system”. In: *Development* 138.2, pp. 183–195. ISSN: 0950-1991. DOI: 10.1242/dev.046441 (cit. on p. 113).
- Graham, P. W.** (2003). “Microtubule and Rac 1-dependent F-actin in growth cones”. In: *Journal of Cell Science* 116.18, pp. 3739–3748. ISSN: 0021-9533. DOI: 10.1242/jcs.00686 (cit. on p. 105).
- Grueber, W. B. and Sagasti, A.** (Sept. 2010). “Self-avoidance and Tiling: Mechanisms of Dendrite and Axon Spacing”. In: *Cold Spring Harbor Perspectives in Biology* 2.9, a001750–a001750. ISSN: 1943-0264. DOI: 10.1101/cshperspect.a001750 (cit. on p. 106).
- Hely, T. A., Graham, B. P., and Ooyen, A. van** (June 2001). “A Computational Model of Dendrite Elongation and Branching Based on MAP2 Phosphorylation”. In: *Journal of Theoretical Biology* 210.3, pp. 375–384. ISSN: 00225193. DOI: 10.1006/jtbi.2001.2314 (cit. on p. 99).
- Hjorth, J. J. J. et al.** (2014). “Competitive dynamics during resource-driven neurite outgrowth”. In: *PLoS ONE* 9.2. ISSN: 19326203. DOI: 10.1371/journal.pone.0086741 (cit. on p. 99).
- Ikonomovic, M. et al.** (2007). “Superior frontal cortex cholinergic axon density in mild cognitive impairment and early Alzheimer disease”. In: *Archives of neurology* 64.9, pp. 1312–1317. DOI: 10.1001/archneur.64.9.1312 (cit. on p. 120).
- Jan, Y. N. and Jan, L. Y.** (2010). “Branching out: Mechanisms of dendritic arborization”. In: *Nature Reviews Neuroscience* 11.5, pp. 316–328. ISSN: 1471003X. DOI: 10.1038/nrn2836. arXiv: NIHMS150003 (cit. on p. 108).
- Kahn, O. I. and Baas, P. W.** (2016). “Microtubules and Growth Cones: Motors Drive the Turn”. In: *Trends in Neurosciences* 39.7, pp. 433–440. ISSN: 1878108X. DOI: 10.1016/j.tins.2016.04.009 (cit. on pp. 98, 106).
- Koene, R. a. et al.** (Sept. 2009). “NETMORPH: a framework for the stochastic generation of large scale neuronal networks with realistic neuron morphologies.” In: *Neuroinformatics* 7.3, pp. 195–210. DOI: 10.1007/s12021-009-9052-3 (cit. on pp. 91, 92).
- Kulkarni, V. A. and Firestein, B. L.** (May 2012). “The dendritic tree and brain disorders”. In: *Molecular and Cellular Neuroscience* 50.1, pp. 10–20. ISSN: 10447431. DOI: 10.1016/j.mcn.2012.03.005 (cit. on p. 92).

- Leonetti, M.** (2001). *Branching in Nature*. Ed. by **Fleury, V., Gouyet, J.-F., and Léonetti, M.** Berlin, Heidelberg: Springer Berlin Heidelberg. ISBN: 978-3-540-41888-7. DOI: 10.1007/978-3-662-06162-6 (cit. on p. 108).
- Lewis, T. L., Courchet, J., and Polleux, F.** (2013). “Cell biology in neuroscience: Cellular and molecular mechanisms underlying axon formation, growth, and branching.” In: *The Journal of cell biology* 202.6, pp. 837–48. ISSN: 1540-8140. DOI: 10.1083/jcb.201305098 (cit. on p. 108).
- Leyva, I. et al.** (2011). “Synchronization waves in geometric networks”. In: *Physical Review E* 84.6, p. 065101. ISSN: 1539-3755. DOI: 10.1103/PhysRevE.84.065101 (cit. on p. 92).
- Lowery, L. A. and Vactor, D. V.** (2009). “The trip of the tip: understanding the growth cone machinery”. In: *Nature Reviews Molecular Cell Biology* 10.5, pp. 332–343. ISSN: 1471-0072. DOI: 10.1038/nrm2679 (cit. on p. 96).
- Memelli, H., Torben-Nielsen, B., and Kozloski, J.** (Jan. 2013). “Self-referential forces are sufficient to explain different dendritic morphologies.” In: *Frontiers in neuroinformatics* 7, p. 1. ISSN: 16625196. DOI: 10.3389/fninf.2013.00001 (cit. on pp. 98, 102).
- Ooyen, A. van** (2003). *Modeling neural development*. Ed. by **Ooyen, A. van.** MIT Press, p. 339. ISBN: 0262220660 (cit. on pp. 108, 109).
- Oan, R., Su, E., and Shinbrot, T.** (Oct. 2011). “The Interplay between Branching and Pruning on Neuronal Target Search during Developmental Growth: Functional Role and Implications”. In: *PLoS ONE* 6.10. Ed. by **Zheng, J. C.**, e25135. ISSN: 1932-6203. DOI: 10.1371/journal.pone.0025135 (cit. on p. 114).
- Pelt, J. van, Ooyen, A. van, and Uylings, H. B. M.** (2001). “The need for integrating neuronal morphology databases and computational environments in exploring neuronal structure and function”. In: *Anatomy and Embryology* 204.4, pp. 255–265. ISSN: 03402061. DOI: 10.1007/s004290100197 (cit. on p. 110).
- Pelt, J. van and Uylings, H. B. M.** (2002). “Branching rates and growth functions in the outgrowth of dendritic branching patterns.” In: *Network* 13.3, pp. 261–281. ISSN: 0954-898X. DOI: 10.1088/0954-898X/13/3/302 (cit. on pp. 108, 110).
- Pernice, V. et al.** (2013). “The relevance of network micro-structure for neural dynamics.” In: *Frontiers in computational neuroscience* 7.June, p. 72. ISSN: 1662-5188. DOI: 10.3389/fncom.2013.00072 (cit. on p. 92).
- Peter, S. J. and Mofrad, M. R. K.** (2017). “Computational Modeling of Axonal Microtubule Bundles under Tension”. In: *Biophysj* 102.4, pp. 749–757. ISSN: 0006-3495. DOI: 10.1016/j.bpj.2011.11.4024 (cit. on p. 98).
- Peyser, A. et al.** (Oct. 2017). *NEST 2.14.0*. URL: <https://doi.org/10.5281/zenodo.882971> (cit. on p. 91).
- Renault, R.** (2015). “Emergent design of neuronal devices”. PhD thesis. Université Paris Diderot (cit. on pp. 6, 106, 107).
- Rico, B. et al.** (2004). “Control of axonal branching and synapse formation by focal adhesion kinase.” In: *Nature neuroscience* 7.10, pp. 1059–69. ISSN: 1097-6256. DOI: 10.1038/nn1317 (cit. on p. 104).
- Sang, Q. and Tan, S. S.** (2003). “Contact-associated neurite outgrowth and branching of immature cortical interneurons”. In: *Cerebral Cortex* 13.6, pp. 677–683. ISSN: 10473211. DOI: 10.1093/cercor/13.6.677 (cit. on p. 105).

- Shefi, O., Golebowicz, S., et al.** (2005). “A two-phase growth strategy in cultured neuronal networks as reflected by the distribution of neurite branching angles”. In: *Journal of Neurobiology* 62.3, pp. 361–368. ISSN: 00223034. DOI: 10.1002/neu.20108 (cit. on p. 112).
- Shefi, O., Harel, A., et al.** (June 2004). “Biophysical constraints on neuronal branching”. In: *Neurocomputing* 58-60, pp. 487–495. ISSN: 09252312. DOI: 10.1016/j.neucom.2004.01.085 (cit. on p. 109).
- Soriano, J., Rodríguez Martínez, M., et al.** (2008). “Development of input connections in neural cultures.” In: *Proceedings of the National Academy of Sciences of the United States of America* 105.37, pp. 13758–13763. ISSN: 00278424. DOI: 10.1073/pnas.0707492105. arXiv: 1008.0062 (cit. on pp. 58, 124).
- Stuart, G., Spruston, N., and Häusser, M., eds.** (1999). *Dendrites*. Oxford New York: Oxford University Press. ISBN: 0198504888 (cit. on p. 117).
- Takeda, S. et al.** (2015). “Neuronal uptake and propagation of a rare phosphorylated high-molecular-weight tau derived from Alzheimer’s disease brain”. In: *Nature Communications* 6. ISSN: 20411723. DOI: 10.1038/ncomms9490. arXiv: arXiv:1011.1669v3 (cit. on pp. 7, 92).
- Tibau, E. et al.** (2013). “Interplay activity-connectivity: Dynamics in patterned neuronal cultures”. In: *Physics, Computation, and the Mind - Advances and Challenges at Interfaces*. Vol. 1510. AIP Conference Proceedings, pp. 54–63. ISBN: 9780735411289. DOI: 10.1063/1.4776501 (cit. on pp. 92, 136).
- Torben-Nielsen, B. and De Schutter, E.** (2014). “Context-aware modeling of neuronal morphologies.” In: *Frontiers in neuroanatomy* 8.September, p. 92. DOI: 10.3389/fnana.2014.00092 (cit. on pp. 91, 92, 98, 170).
- Van Ooyen, A.** (2011). “Using theoretical models to analyse neural development”. In: *Nature Reviews Neuroscience* 12.6, pp. 311–326. ISSN: 1471003X. DOI: 10.1038/nrn3031 (cit. on p. 96).
- Van Pelt, J., Dityatev, A. E., and Uylings, H. B. M.** (1997). “Natural variability in the number of dendritic segments: Model-based inferences about branching during neurite outgrowth”. In: *Journal of Comparative Neurology* 387.3, pp. 325–340. ISSN: 00219967. DOI: 10.1002/(SICI)1096-9861(19971027)387:3<325::AID-CNE1>3.0.CO;2-2 (cit. on p. 109).
- Van Pelt, J., Uylings, H. B., et al.** (1992). “Tree asymmetry-A sensitive and practical measure for binary topological trees”. In: *Bulletin of Mathematical Biology* 54.5, pp. 759–784. ISSN: 15229602. DOI: 10.1007/BF02459929 (cit. on pp. 108, 178).
- Wang, L. and Marquardt, T.** (2013). “What axons tell each other: Axon-axon signaling in nerve and circuit assembly”. In: *Current Opinion in Neurobiology* 23.6, pp. 974–982. ISSN: 09594388. DOI: 10.1016/j.conb.2013.08.004 (cit. on p. 106).
- Wessells, N. K. and Nuttall, R. P.** (Aug. 1978). “Normal branching, induced branching, and steering of cultured parasympathetic motor neurons”. In: *Experimental Cell Research* 115.1, pp. 111–122. ISSN: 00144827. DOI: 10.1016/0014-4827(78)90408-1 (cit. on p. 108).
- Withers, G. S. et al.** (Sept. 2006). “Effects of substrate geometry on growth cone behavior and axon branching”. In: *Journal of Neurobiology* 66.11, pp. 1183–1194. ISSN: 0022-3034. DOI: 10.1002/neu.20298 (cit. on p. 109).

- Yu, L. M. Y., Leipzig, N. D., and Shoichet, M. S.** (2008). “Promoting neuron adhesion and growth”. In: *Materials Today* 11.5, pp. 36–43. ISSN: 13697021. DOI: 10.1016/S1369-7021(08)70088-9. arXiv: 13697021 (cit. on p. 105).
- Zhang, Z. W., Kang, J. I., and Vaucher, E.** (2011). “Axonal varicosity density as an index of local neuronal interactions”. In: *PLoS ONE* 6.7. ISSN: 19326203. DOI: 10.1371/journal.pone.0022543 (cit. on p. 120).
- Zubler, F. and Douglas, R.** (2009). “A framework for modeling the growth and development of neurons and networks.” In: *Frontiers in computational neuroscience* 3.November, p. 25. DOI: 10.3389/neuro.10.025.2009 (cit. on pp. 91, 92).

Chapter 5

Conclusion, towards neuronal devices

In this final (and brief) chapter, I provide an assessment of the work presented in my thesis on neuronal culture. After discussing how the properties that have proved so useful in neuronal cultures might also be their greatest limitation for the future, I show how the models, tools, and experiments developed here come together to provide leads on a final question: where do we go next?

Contents

5.1	Current limitations of neuronal cultures	132
5.1.1	The unfortunate side-effect of isolation	132
5.1.2	Preventing percolation	133
5.2	Neuronal devices as the next step	133
5.2.1	Directed information flow	134
5.2.2	Development under stimulation	134
5.2.3	Structured networks	135
5.3	Concluding remarks	139

5.1 Current limitations of neuronal cultures

As discussed throughout this manuscript, the major strength of neuronal cultures relies in their simplicity and the ease with which the network and neurons can be monitored, stimulated, or altered. The rather homogeneous and simple network, as well as the isolated nature of the culture have enabled significant progress in our understanding of countless synaptic and cellular mechanisms.

However, when it comes to the diversity of the behavior displayed by neuronal networks, this simplicity is also one of the greatest weakness of homogeneous cultures. Indeed, the stereotypical bursting activity that emerges from such networks acts as an overwhelming attractor and prevents the apparition of more subtle patterns.

This does not mean that synchrony should be avoided at all costs; on the contrary, many synchronous events also play a crucial role in highly complex tasks such as memory consolidation (Benchenane 2006). However, what is desired is a *selective synchrony* (Brette 2012), which would contribute to information encoding, by contrast to the regular and thus rather uninformative process observed in cultures.

If we are to prevent the emergence of this behavior, two main approaches seem to stand out. Indeed, though brain networks also exhibit strong synchronous dynamics in their early developmental stages, or during sleep, mature and awake dynamics evolve away from these purely synchronous states. Comparing brains and culture is of course difficult, given the vast differences in size, heterogeneity, or wiring; however, two differences are easy to notice and are present at all scales: the presence of afferent inputs and the structured (e.g. layered) connectivity.

5.1.1 The unfortunate side-effect of isolation

One of the major issue of the isolated nature of neuronal cultures comes from the fact that neurons cannot live without afferent inputs (Schonfeld-Dado et al. 2011). Thus, in order for the culture to survive, neurons have no choice but to reach a state of self-sustained activity, where they themselves provide the inputs necessary for their survival.

This property is related to the notion of *emergence* mentioned at the beginning of this thesis, and has been investigated in the literature as the *self-organization* of neuronal networks, notably through coupling between growth and activity (T. A. Gritsun, Feber, et al. 2012; Van Pelt, Corner, et al. 1993), then via the evolution of the synaptic strength through plasticity mechanisms (Ocker et al. 2015). In neuronal culture, this notion was often associated to a strong belief that this evolution would spontaneously lead the system towards a critical state (Pasquale et al. 2008; Tetzlaff et al. 2010). Anyhow, the fact is that, over time, cultures indeed mature towards a dynamical state which provides enough inputs to maintain itself; given the strong coupling in the network and the high synchronizability of the units, this kind of activity usually converges to synchronized bursting.

*bursting may
be caused by
the isolated
state of
cultures*

Thus, I propose that the emergence of synchronized bursting is a simple and almost unavoidable side-effect of the requirement for sustained activity coupled with the percolation property displayed by networks of excitable units. To prevent cultures from converging towards this synchronized state, one should therefore either change the isolated nature of the culture, or bring the network below the percolation threshold.

5.1.2 Preventing percolation

As detailed in articles on quorum percolation, there are several ways of preventing the emergence of system-size events:

- reducing the synaptic strength (Soriano, Breskin, et al. 2007),
- reducing the number of neighbours (Renault, Monceau, Bottani, and Métens 2014),
- increasing the proportion of inhibitory neurons (Fardet, Bottani, et al. 2018),
- increasing transmission delays (Renault, Monceau, and Bottani 2013).

Unfortunately, not all of these methods are really suitable experimentally. For instance, though reducing the synaptic weight through partial block of the excitatory synapses is indeed possible, it is both costly, constraining, and only a short-term palliative since the overall synaptic strength and activity in the network will slowly increase to adapt to this constraint. Increasing the number of inhibitory neurons can also be done experimentally, though it requires costly labeling methods and FACS equipment¹; however, similarly to what was mentioned for reduced synaptic weights, the networks simply adapt by scaling up the remaining excitatory connections in order to preserve the bursting behavior. Eventually, increasing the transmission delay would a priori require increasing the average distance between neurons, which, though possible over a limited range, would probably not be sufficient to curb the bursting dynamics.

Overall, the most promising method to prevent percolation is probably to constrain the neurons spatially in order to limit the number of neighbors they can connect to: a limitation of the activity spreading through network patterning and locality constraints.

*percolation
may be
prevented via
network
structuring*

5.2 Neuronal devices as the next step

In order to tackle the limitations of homogeneous neuronal cultures mentioned above, one of the easiest method is to take advantage of the microfluidic capabilities offered by recent technological developments (Feinerman et al. 2008; Renault, Durand, et al. 2016; Taylor et al. 2003). Indeed, these structures enable precise molding of the desired pattern on which the neurons will then be able to develop.

Moreover, the potential of these devices is not limited to “burst prevention”: using the arches developed by Renault, Durand, et al. 2016, it is now possible to build systems where the information is precisely defined, enabling the study of both neuron- and population-level interactions at the same time.

Yet, building these devices, though relatively inexpensive, is still resource- and time-consuming, especially since it can be difficult to predict what the best structure will be to obtain a target connectivity pattern.

I will therefore show here how the tools developed in this thesis can provide a useful insights into the final connectivity obtained inside a given microfluidic structure.

¹ See Renault, Sukenik, et al. 2015, Figure S2 for labelling method using tdTomato. Experimental protocol to isolate GABAergic neurons and obtain cultures with varying fractions — up to almost 100% — of inhibitory neurons were developed as part of the PhD project of Nirit Sukenik, at the Weizmann Institute, and are currently unpublished.

5.2.1 Directed information flow

One of the main focus of neuronal devices has been the design of structure that would allow information to be transferred only in specific directions. Following the seminal paper of Feinerman et al. 2008, with the introduction of neuronal logic gates, several other devices were made using microfluidic techniques.

One of the simplest pattern is of course the neuronal diode, for which an example can be found in Renault, Sukenik, et al. 2015. That kind of device already led to rather efficient selectivity, as shown in the original paper and in recent simulations — cf. Figure 5.1. However, the directivity obtained is not perfect, as can be seen on a reproduction *in silico*, on Figure 5.2.

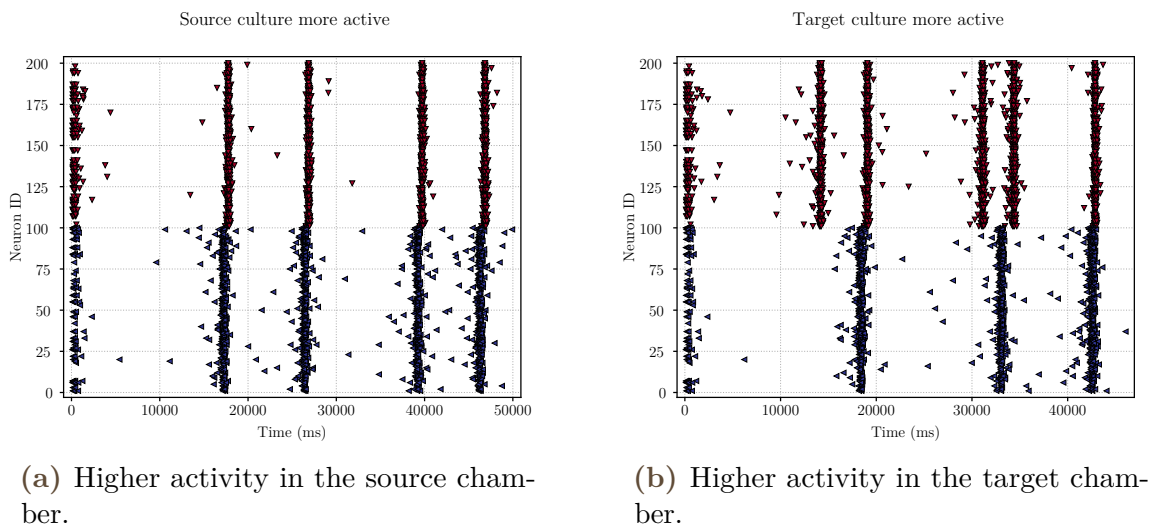


Figure 5.1.: Simulated activity on the diode from Figure 5.2, in two situations: (a) one with higher bursting rate on the source chamber (the one with larger funnel diameter) and (b) another with higher bursting rate on the target chamber (thinner funnel diameter). One can see that activity in the source chamber almost immediately triggers a burst in the target chamber while the reverse is not true, or at least implies much longer delays.

Using the newer arches setup from Renault, Durand, et al. 2016, even higher selectivity can be obtained and simulation using DeNSE also reproduced this selectivity, as shown on Figure 5.3.

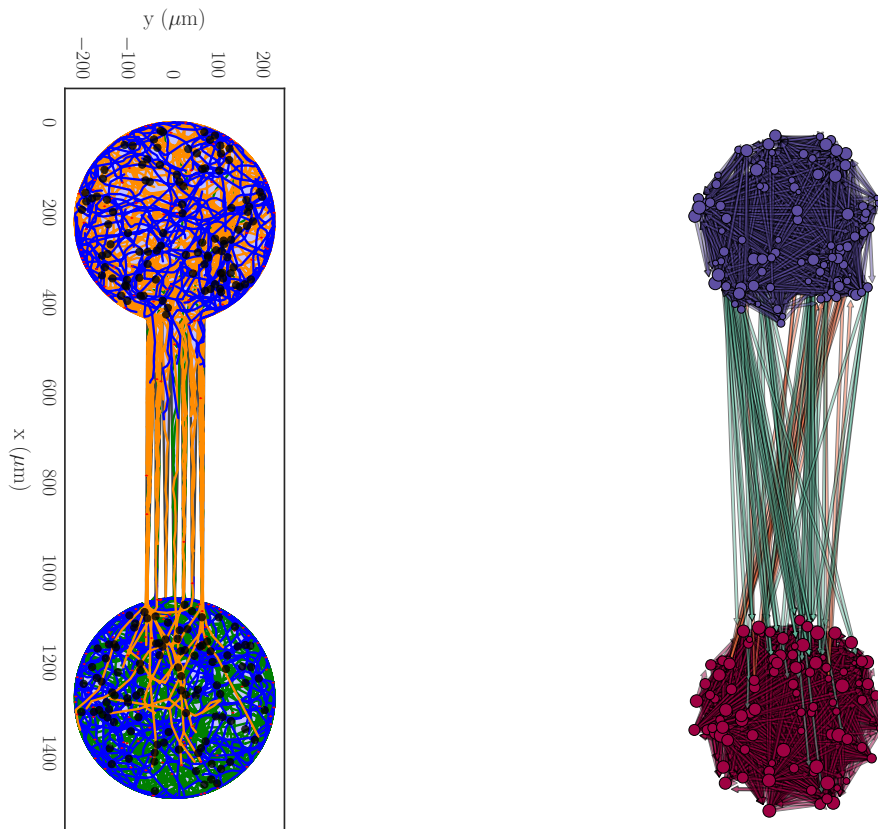
*introducing
causality*

This type of device, though is does not prevent the occurrence of bursting activity, already introduces a new property in the global dynamics: causality. Indeed, the neurons are separated into two non-equivalent populations, with the activity of the “transmitter” neurons remaining unaffected by that of the “receiver” neurons.

5.2.2 Development under stimulation

*growing
non-isolated
cultures to
prevent
bursting*

Beyond potential applications for more precise studies of neuronal communication *in vitro*, the design of neuronal devices with directed connectivity would also provide researchers with a new, more accurate way of investigating the influence of stimulation on the development of neuronal networks.



(a) Device grown with DeNSE

(b) Associated topological network.

Figure 5.2.: Reproduction of the neuronal diode *in silico* with 200 neurons. (a) shows the grown network, with the soma in black, dendrites in blue, axons from the top chamber are in green, axons from the bottom chamber in orange. (b) shows the topological network obtained using the simple crossing method with a probability of connection of 1.

Indeed, such approach was already tested by DeMarse et al. 2016 in a setup using a 2-chamber culture, where one chamber was seeded a few days earlier than the second. However, the setup used in the study was made of symmetrical funnels. Using chambers connected by arches, one could further improve this experiment, first by preventing the newest neurons from projecting to the elder chamber, second, by severing the connection between the chambers and assessing the evolution of the activity in the newest chamber. Indeed, the arches, by preventing projections from the younger chamber to go towards the elder chamber, would enable a separation of the chambers involving only minimal or even no damage to the youngest neurons.

Making the neurons from several chambers project their axons into a single one, it would even be possible to analyze the effect of a progressive decrease of external excitation on the activity of a network.

5.2.3 Structured networks

The previous examples already showed the potential of structuring neuronal connectivity, and in particular of directing the flow of information inside the network. As

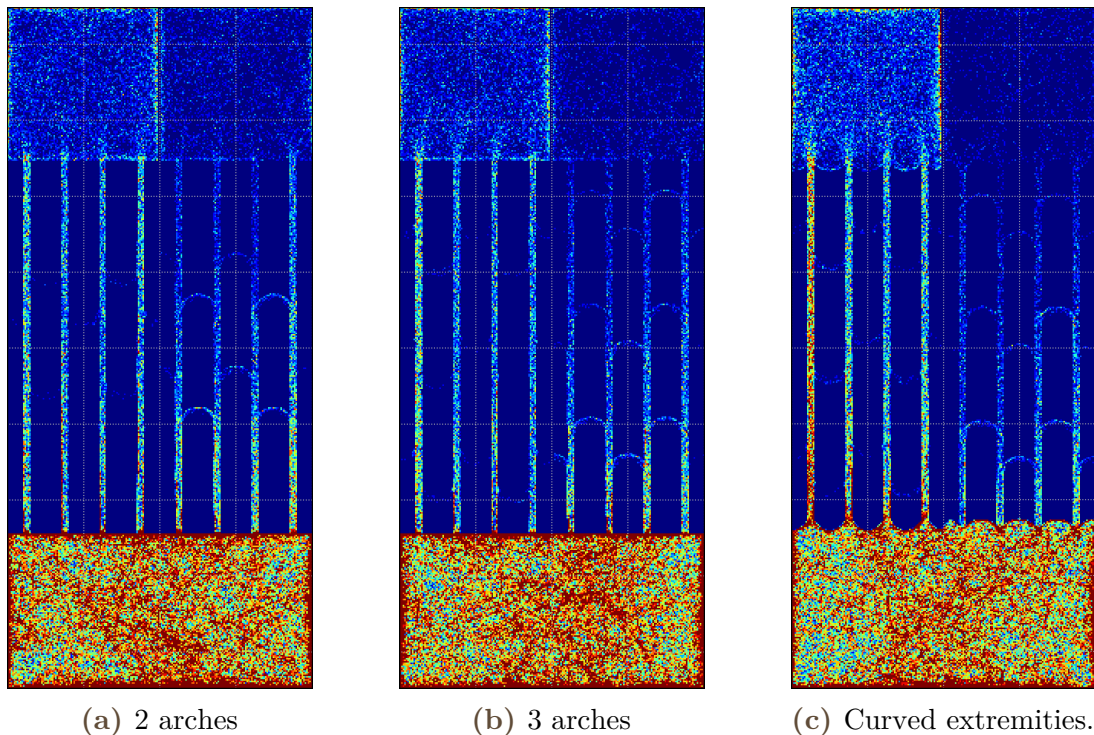


Figure 5.3.: Simulation of the neurite density over the whole device, from high densities in red to low densities in dark blue. Highest density are in the bottom chamber where neurons are initially seeded. The number of axons crossing to the other side decreases progressively with the number of arches — (a) to (b). Convex shape at the entrance helps the axons into the funnels while concave entrance with acute angles prevents them from entering (b).

seen on Figure 5.1, such networks already exhibit activity patterns that cannot be obtained in homogeneous cultures. Yet, though they may be slightly more complex than the stereotypical bursting of “standard” cultures, these activity patterns still only involve synchronous bursting events that span the entire chamber.

To obtain more elaborate firing patterns, it is therefore necessary to change the network structure in greater depth.

Distributed local directivity

The idea behind altering the global and local connectivity of the network was first introduced by Tibau et al. 2013 as a way to force the neurons to connect through complex paths in order to increase the structural and dynamical complexity. This increased complexity prevents the neurons from making long range connections and forces the flow of the activity to follow more complex paths, thus impeding the fast percolation of the activity.

The method relies on the presence of platforms, randomly placed inside the culture, which form islands where neurons are located above the rest on the population, which is on the lower stage — cf. Figure 5.4.

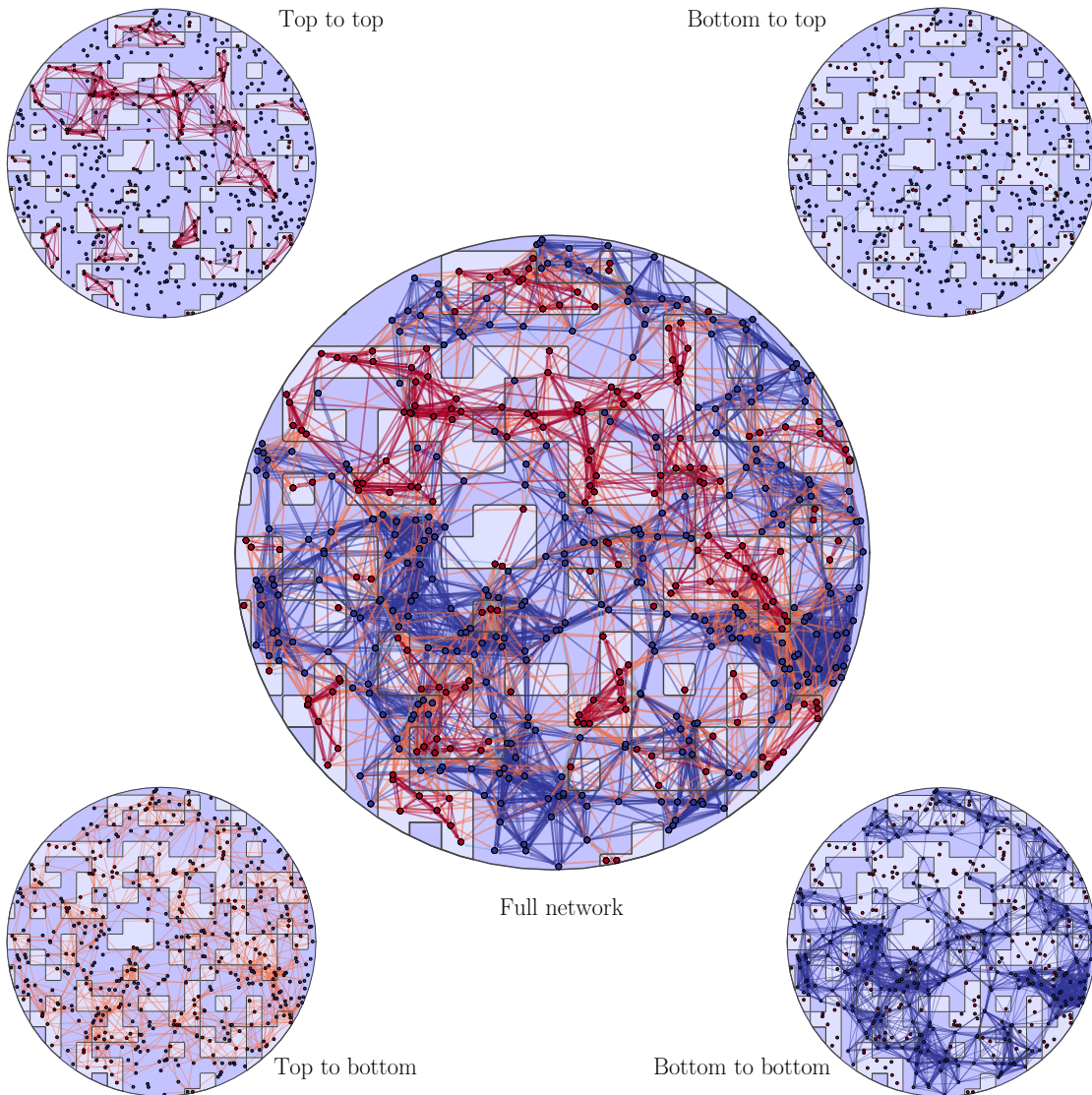


Figure 5.4.: Simulation of a spatial network representing a 2-layer culture. Upper platforms are denoted by lighter blue filling while lower are in darker blue. Neurons on the upper platforms are shown in red, those on the lower platforms are in blue. The four insets show the connectivity between these two groups of neurons and the central representation gives the overlay.

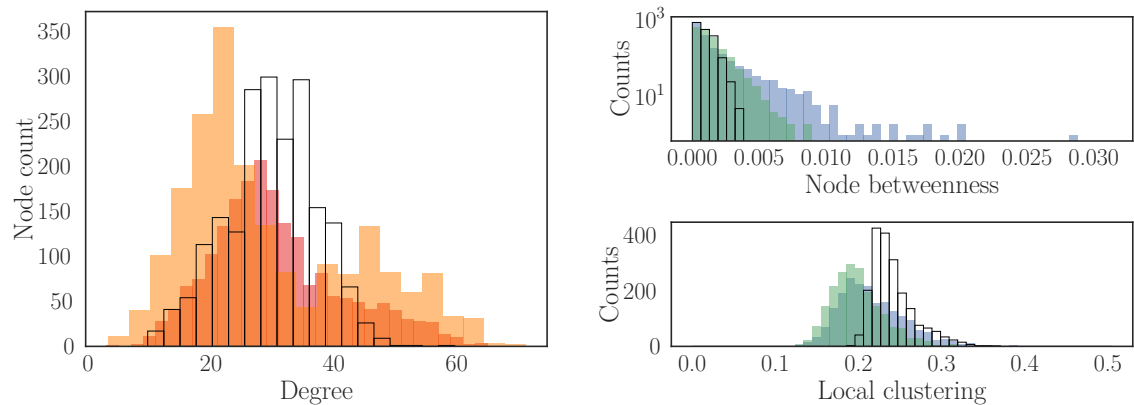
Compared to the previous methods, such a network also leads to a directed connectivity based on these hypothesized mechanisms:

- as the height difference increases, axons from the top are unable to cross the gap,
- while the dendrites of the top-neurons can still descend to the bottom layer, i.e. up to stages a few hundred microns high, bottom-to-top connections can still occur,
- after a few hundred microns, only the axons from the top can reach the bottom layer, resulting in a fully directional top-to-bottom connectivity,
- when the height difference goes above $600 \mu\text{m}$, the two stages are effectively disconnected and coexist without interactions, as might two separate chambers.

Considering the two populations as a whole, the evolution of the connectivity with platform height would therefore appear identical to varying the number of arches in the previous setup. However, in light of the results on “Topology and spatio-temporal bursting patterns” (chapter 3), one notices here that, in contrast with diode-like systems, the 2-layer culture introduces directivity while preserving the locality of the network connections: the two populations are not spatially segregated but tightly intertwined.

For the bottom-neurons, the presence of the platforms constrains their development and prevents them from connecting with as many neighbors as in a homogeneous culture — cf. Figure 5.5a. Top-neurons, however, do not feel this constraint as strongly since they can connect to all neurons on a similar platform, as well as to all bottom neurons in the vicinity. Their only constraint occurs if their axon descends into the bottom area and extends enough to hit another platform.

*distributed
local
constraints to
reduce the
average degree
and help
prevent
percolation*



(a) Degree distribution: in-degree of all neurons in a 2-layer culture in orange, out-degree in red; in-degree of an EDR network with the same number of edges is marked by empty black bars.

(b) Centrality distributions: 2-layer culture is in blue, equivalent EDR network with the same number of edges is in green; standard culture with an average in-degree of 100 is shown by the empty black bars.

Figure 5.5.: Topological properties of the simulated 2-layer culture compared to homogeneous EDR networks.

In short, the connectivity of bottom-neurons is significantly limited spatially, while top-neurons are less affected; this means that transmission of the signal from one part of the culture to the other will often rely on “shortest-path” involving the more central top-neurons, as denoted by the much higher betweenness values of the 2-layer culture on Figure 5.5b. As we will see, the increased locality and the lower degree of such a network results in radically different activity patterns compared to all other setups.

Complexity of the resulting activity

By contrast with homogeneous cultures of the same size, the 2-layer culture displays bursting activity with much longer timescales, as bursts typically last over more than a second — cf. Figure 5.6. Because the activity is more localized, the network does not only display system-size events, but also periods where only part of the culture is active. This enables the occurrence of periods of uninterrupted local and global activity, which may span more than 10 seconds.

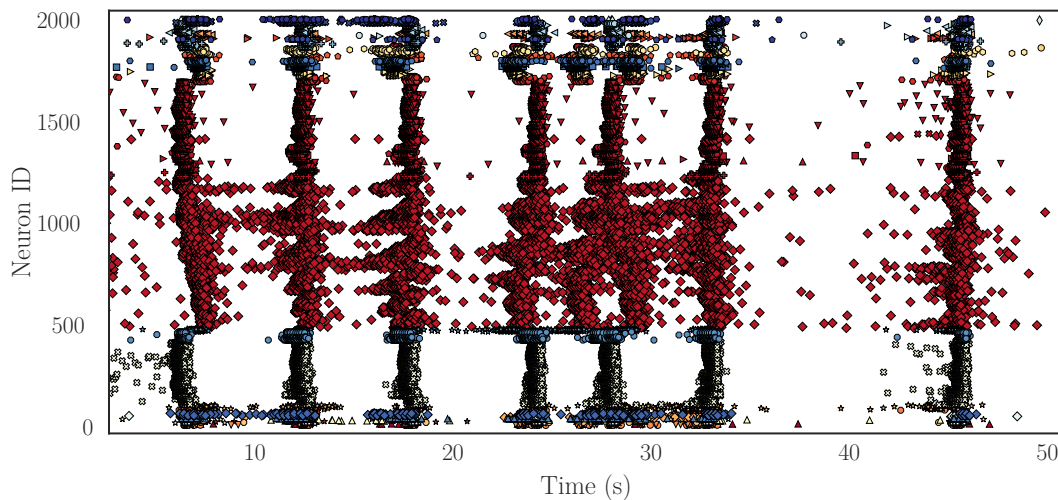


Figure 5.6.: Raster plot of the 2-layer culture. Neurons are grouped by platform (same color) and sorted by increasing x and y position in the culture.

Compared to standard cultures, this activity is therefore more complex, in terms of the variety of timescales and spatial scales involved in the overall activity.

5.3 Concluding remarks

In this manuscript, I presented a set of analytical and numerical tools to reproduce, analyze and characterize the development and activity patterns of neuronal cultures and devices.

From the *susceptibility*-based description of the bursting activity and our simulations on adaptive pacemaker neurons, I was able to predict the influence of adaptation channels on the collective activity. The results from the preliminary experiments that I conducted at the Weizmann Institute are indeed compatible with these predictions and additional experiments may confirm the importance of adaptation in shaping the bursting behavior. Furthermore, these experiments also revealed interesting changes in the activity, which may provide additional insight into the relative influence of adaptation and synaptic depression. Eventually, analysis of the statistical properties of the interburst interval confirmed the study by T. A. Gritsun, Le Feber, et al. 2010 on the increased “authenticity” of bursting activity in network including a fraction of pacemaker neurons.

Moving into a more detailed spatio-temporal study of the nucleation centers in bursting networks, I showed that nucleation centers are consistently observed as soon as locality and spatial correlation are introduced. In addition, analysis of first-to-fire neurons, with the help of Mallory Dazza, revealed that seemingly random activity before burst initiation is in fact concentrated around the nucleation centers. Attempts to characterize the properties of these neurons showed significant correlations with several topological properties depending on the bursting mechanisms involved. However, these properties displayed significant dependence on the boundary conditions that were specific to the EDR model used; because network whose structure was derived from a growth process possessed rather different properties, additional

analysis on such networks would be necessary in order to offer reasonable experimental predictions.

The implementation of the DeNSE simulator, with the support of Alessio Quaresima, enabled the simulation of more realistic cultures with an improved inclusion of the boundary conditions, as growth cones properly interact with the walls delimiting the culture. The development of new models coupling elongation, diameter, and branching, as well as the inclusion and improvement of several existing models, make DeNSE the first growth simulator providing a comprehensive framework to study the development of neurons *in silico*.

Taken together, these results enabled us to discuss some of the limitations of homogeneous neuronal cultures and to propose applications for future neuronal devices. As a proof of concept, the set of examples provided in this last chapter show that DeNSE is able to generate networks *in silico* which display reasonable properties and are able to reproduce the activity of experimental devices.

Though several limitations were apparent throughout the study — especially for DeNSE, which still lacks major mechanisms such as self-avoidance and fasciculation — the extensive analysis provided on the bursting mechanism leads to the conclusion that the emergence of synchronized activity relies on highly resilient and even redundant mechanisms. This explains the resilience and pervasive nature of epileptiform bursts in neuronal cultures and hints at the necessity of new strategies to prevent its apparition: the design of cultures which would grow under external stimulation or the profound modification of the network properties to prevent the percolation of the activity throughout the culture.

Eventually, interesting perspectives ensue from this discussion on the future of neuronal devices. Among them, one may highlight the possibility of studying and modeling structural plasticity, as well as the interplay between growth and activity. In addition, we also rationalized a new paradigm to increase the complexity of neuronal cultures while preserving the quasi-2-dimensionality which constitutes one of their major advantages. Hopefully, future versions of DeNSE, coupled with activity simulators, may prove useful in tackling these challenges and investigating new designs for neuronal devices.

References for chapter 5

- Benchenane, K.** (2006). *Neural Synchrony and Memory In and Out of Sleep*. Second Edition. Vol. 4. Elsevier, pp. 563–583. ISBN: 9780128093245. DOI: 10.1016/B978-0-12-809324-5.21117-6 (cit. on p. 132).
- Brette, R.** (2012). “Computing with neural synchrony”. In: *PLoS Computational Biology* 8.6. ISSN: 1553734X. DOI: 10.1371/journal.pcbi.1002561 (cit. on p. 132).
- DeMarse, T. B. et al.** (Apr. 2016). “Feed-Forward Propagation of Temporal and Rate Information between Cortical Populations during Coherent Activation in Engineered In Vitro Networks”. In: *Frontiers in Neural Circuits* 10. April. ISSN: 1662-5110. DOI: 10.3389/fncir.2016.00032 (cit. on p. 135).
- Fardet, T., Bottani, S., et al.** (2018). “Effects of inhibitory neurons on the quorum percolation model and dynamical extension with the BretteGerstner model”. In: *Physica A: Statistical Mechanics and its Applications* 499. ISSN: 03784371. DOI: 10.1016/j.physa.2018.02.002 (cit. on pp. 59, 133, 179).
- Feinerman, O., Rotem, A., and Moses, E.** (2008). “Reliable neuronal logic devices from patterned hippocampal cultures”. In: *Nature Physics* 4.12, pp. 967–973. ISSN: 1745-2473. DOI: 10.1038/nphys1099 (cit. on pp. 133, 134).
- Gritsun, T. A., Le Feber, J., et al.** (2010). “Network bursts in cortical cultures are best simulated using pacemaker neurons and adaptive synapses”. In: *Biological Cybernetics* 102.4, pp. 293–310. ISSN: 03401200. DOI: 10.1007/s00422-010-0366-x (cit. on pp. 38, 59, 62, 73, 75, 139).
- Gritsun, T. A., Feber, J. le, and Rutten, W. L. C.** (Jan. 2012). “Growth dynamics explain the development of spatiotemporal burst activity of young cultured neuronal networks in detail.” In: *PloS one* 7.9. Ed. by **Wennekers, T.**, e43352. ISSN: 1932-6203. DOI: 10.1371/journal.pone.0043352 (cit. on p. 132).
- Ocker, G. K., Litwin-Kumar, A., and Doiron, B.** (2015). “Self-Organization of Microcircuits in Networks of Spiking Neurons with Plastic Synapses”. In: *PLoS Computational Biology* 11.8, e1004458. ISSN: 1553-7358. DOI: 10.1371/journal.pcbi.1004458 (cit. on p. 132).
- Pasquale, V. et al.** (2008). “Self-organization and neuronal avalanches in networks of dissociated cortical neurons”. In: *Neuroscience* 153.4, pp. 1354–1369. ISSN: 03064522. DOI: 10.1016/j.neuroscience.2008.03.050 (cit. on pp. 27, 132).
- Renault, R., Durand, J.-B., et al.** (2016). “Asymmetric axonal edge guidance: a new paradigm for building oriented neuronal networks”. In: *Lab on a Chip* 16.12, pp. 2188–2191. ISSN: 1473-0197. DOI: 10.1039/C6LC00479B (cit. on pp. 133, 134).
- Renault, R., Monceau, P., and Bottani, S.** (Dec. 2013). “Memory decay and loss of criticality in quorum percolation”. In: *Physical Review E* 88.6, p. 062134. ISSN: 1539-3755. DOI: 10.1103/PhysRevE.88.062134 (cit. on pp. 59, 133).
- Renault, R., Monceau, P., Bottani, S., and Métens, S.** (2014). “Effective non-universality of the quorum percolation model on directed graphs with Gaussian in-degree”. In: *Physica A: Statistical Mechanics and its Applications* 414.m, pp. 352–359. ISSN: 03784371. DOI: 10.1016/j.physa.2014.07.028 (cit. on p. 133).
- Renault, R., Sukenik, N., et al.** (2015). “Combining Microfluidics, Optogenetics and Calcium Imaging to Study Neuronal Communication In Vitro”. In: *Plos One* 10.4, pp. 1–15. ISSN: 1932-6203. DOI: 10.1371/journal.pone.0120680 (cit. on pp. 133, 134, 165).

- Schonfeld-Dado, E. and Segal, M.** (2011). “Activity deprivation induces neuronal cell death: Mediation by tissue-type plasminogen activator”. In: *PLoS ONE* 6.10, pp. 1–5. ISSN: 19326203. DOI: 10.1371/journal.pone.0025919 (cit. on p. 132).
- Soriano, J., Breskin, I., et al.** (2007). “Percolation approach to study connectivity in living neural networks”. In: *AIP Conference Proceedings* 887, pp. 96–106. ISSN: 0094243X. DOI: 10.1063/1.2709591. arXiv: 1007.5016 (cit. on p. 133).
- Taylor, A. M. et al.** (Mar. 2003). “Microfluidic Multicompartment Device for Neuroscience Research ”. In: *Langmuir* 19.5, pp. 1551–1556. ISSN: 0743-7463. DOI: 10.1021/la026417v (cit. on p. 133).
- Tetzlaff, C. et al.** (Dec. 2010). “Self-Organized Criticality in Developing Neuronal Networks”. In: *PLoS Computational Biology* 6.12. Ed. by **Friston, K. J.**, e1001013. ISSN: 1553-7358. DOI: 10.1371/journal.pcbi.1001013 (cit. on p. 132).
- Tibau, E. et al.** (2013). “Interplay activity-connectivity: Dynamics in patterned neuronal cultures”. In: *Physics, Computation, and the Mind - Advances and Challenges at Interfaces*. Vol. 1510. AIP Conference Proceedings, pp. 54–63. ISBN: 9780735411289. DOI: 10.1063/1.4776501 (cit. on pp. 92, 136).
- Van Pelt, J., Corner, M. A., et al.** (1993). “The self-organizing brain: from growth cones to functional networks”. In: *18th International Summer School of brain research*, p. 446. ISBN: 0444818197 (cit. on p. 132).

Appendix A

Neuronal dynamics and the AdExp model

A.1 Pacemaker neurons

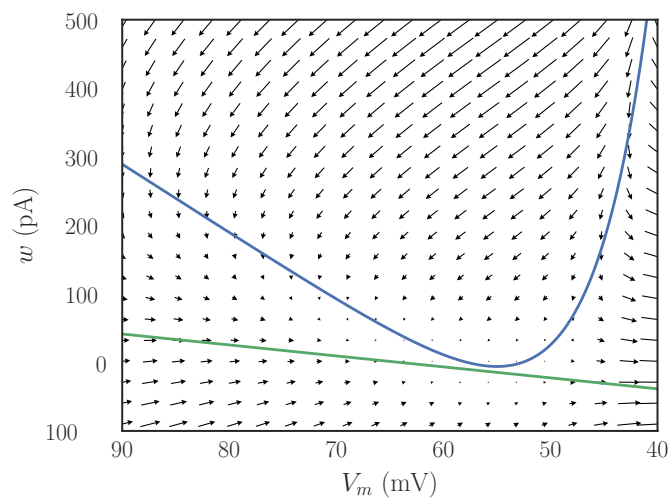


Figure A.1.: Phase space of a pacemaker neuron modeled by the AdExp model ($a < 0$). V -nullcline ($\dot{V} = 0$) is in blue while w -nullcline ($\dot{w} = 0$) is in green. Arrows indicate the values of (\dot{V}, \dot{w}) at each point in phase space.

As shown on Figure A.1, the negative slope of the w -nullcline for pacemaker neurons, can lead to the emergence of an extended ghost of what was the fixed point before the bifurcation. In this area, the derivative of both V and w are very small, generating a “trap” where the neuron remains for a long time and which dampens the effect of external perturbation on the trajectory. This property is what provide pacemaker neurons their strong periodicity and resilience to synaptic inputs and noise.

A.2 Firing patterns

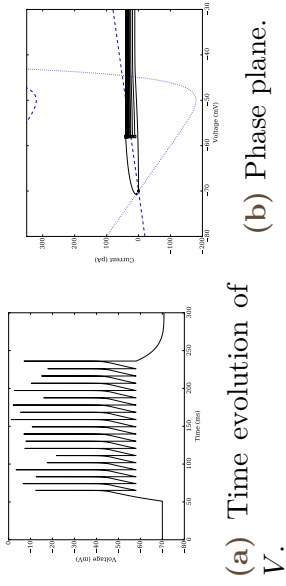


Figure A.2.: Tonic firing

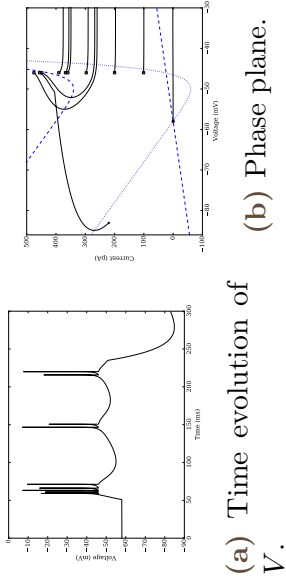


Figure A.5.: Regular bursting

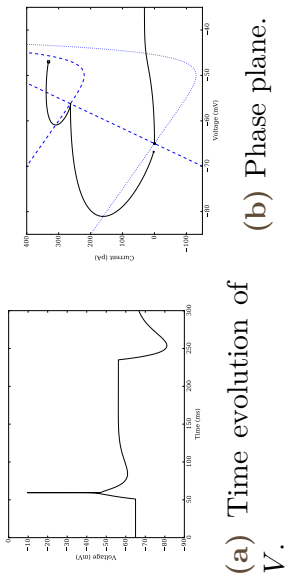


Figure A.8.: Transient spiking

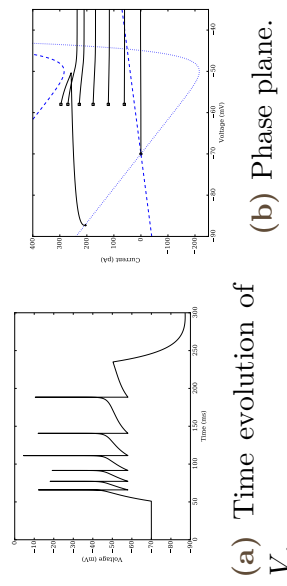


Figure A.3.: Adaptation

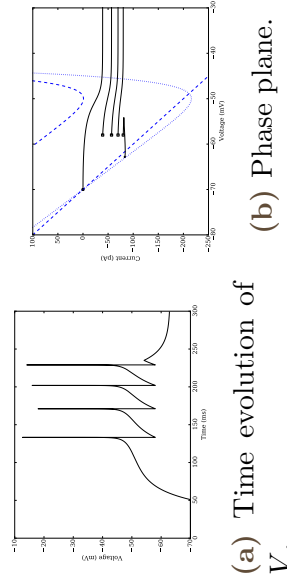


Figure A.6.: Delayed accelerating

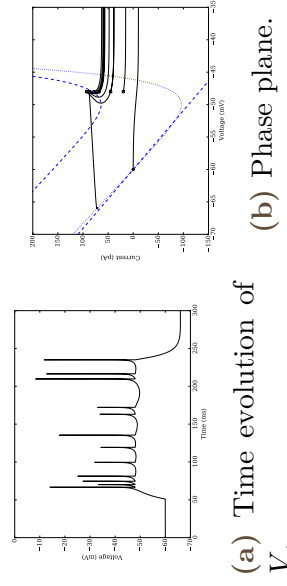


Figure A.9.: Irregular spiking

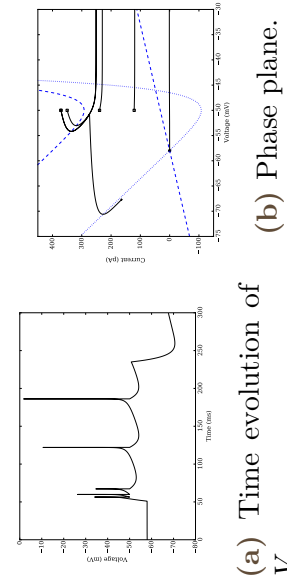


Figure A.4.: Initial burst

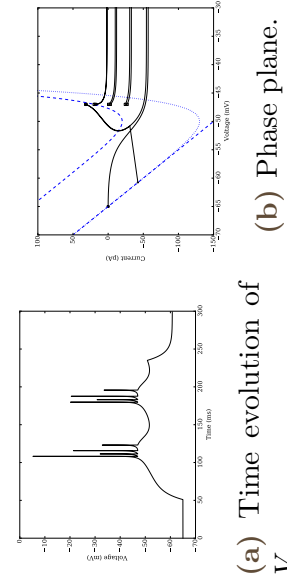


Figure A.7.: Delayed regular bursting

Neurons are excited using a 184 s step-current (from 50 to 234 ms) of amplitude I (see A.1). Starting points are represented by a black square and the final state (after 300 ms of simulation) is marked by a cross.

Figure	Type	C (pF)	g_L (nS)	E_L (mV)	V_T (mV)	Δ_T (mV)	a (nS)	τ_w (ms)	b (pA)	V_r (mV)	I (pA)
A.2	Tonic firing	200	10	-70	-50	2	2	30	0	-58	500
A.3	Adaptation	200	12	-70	-50	2	2	300	60	-58	500
A.4	Initial burst	130	18	-58	-50	2	4	150	120	-50	400
A.5	Regular bursting	200	10	-58	-50	2	2	120	100	-46	400
A.6	Delayed accelerating	200	12	-70	-50	2	-10	300	0	-58	215
A.7	Delayed regular bursting	100	10	-65	-50	2	-10	90	30	-47	110
A.8	Transient spiking	100	10	-65	-50	2	30	90	300	-47	350
A.9	Irregular spiking	100	12	-60	-50	2	-11	130	30	-48	160

Table A.1.: Parameters corrected from Naud et al. 2008 corresponding to Figure A.2–A.9.

Appendix B

Excitability, restlessness, and susceptibility

B.1 Transitions of the AdExp model

In the AdExp model, there are two possible transitions that make a neuron fire spontaneously: a saddle-node bifurcation for $a/g_L < \tau_m/\tau_w$ or an Andronov-Hopf bifurcation for $a/g_L > \tau_m/\tau_w$ (Naud et al. 2008).

In the case of the Andronov-Hopf bifurcation, the transition current or (*rheobase current*) is given by

$$I_{AH} = (g_L + a) \left[V_{th} + \Delta_T \ln \left(1 + \frac{\tau_m}{\tau_w} \right) - E_L - \Delta_T \right] + g_L \left(\frac{a}{g_L} - \frac{\tau_m}{\tau_w} \right) \quad (\text{B.1})$$

whereas in the saddle-node bifurcation, it becomes

$$I_{SN} = (g_L + a) \left[V_{th} + \Delta_T \ln \left(1 + \frac{a}{g_L} \right) - E_L - \Delta_T \right]. \quad (\text{B.2})$$

For I_e greater to the bifurcation current associated to a given parameter set, the neuron will have no equilibrium potential, i.e. it will fire spontaneously.

B.2 Susceptibility

We define the susceptibility of a neuron as the balance between the charge that had to be delivered to make it reach $V \geq V_{th}$ with $\dot{V} \geq 0$ and the speed at which its membrane potential will increase once the charge has been delivered. This leads to:

$$Sc = \dot{v} - q \quad (\text{B.3})$$

with the dimensionless quantities

$$\begin{aligned} \dot{v} &= \frac{\tau_m \dot{V}}{\Delta_T} \\ q &= \frac{Q}{C_m \Delta_T} \end{aligned}$$

It is thus the difference between the post-excitatory derivative of the membrane potential and the excitatory charge that was necessary to reach this “excited” state where the neuron will fire.

The susceptibility Sc of an AdExp neuron can be determined based on the separation of phase space described in Figure B.1¹.

¹ this separation of phase-space is an approximation in the case where the two variables V and w evolve on different timescales, such that $\tau_m \ll \tau_w$ (adiabatic hypothesis); go to the *Limitations* subsection to see when this hypothesis may not hold.

- In the region (a), we have $V \geq V_{th}$ and $\dot{V} \geq 0$, therefore $q = 0$ and $Sc = \dot{v} \geq 0$.
- In (b), we have $\dot{v} \geq 0$, and $q = \frac{V_{th}-V}{C_m \Delta_T}$.
- In (c), we need to reach the right arm of the V -nullcline to get $\dot{v} = 0$, and thus we get $Sc = -q \leq 0$.

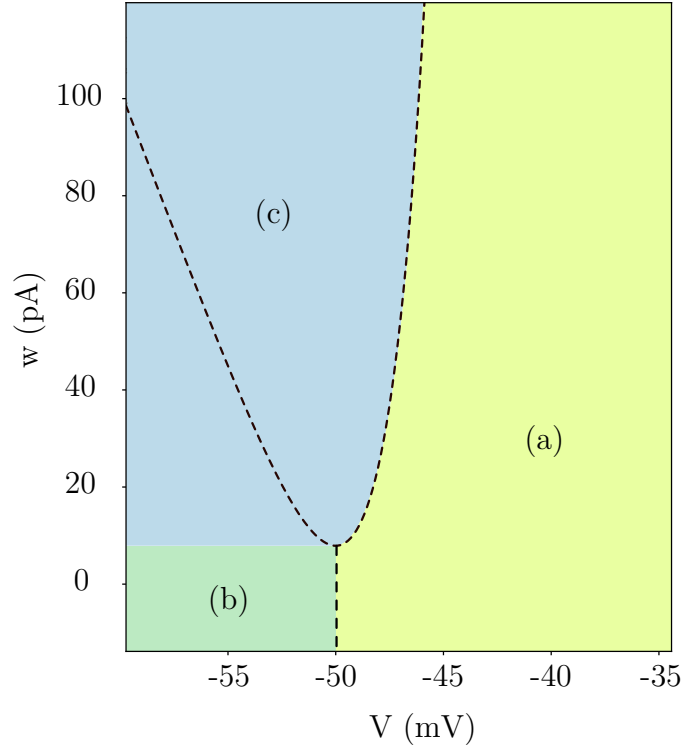


Figure B.1.: The three different regions of phase space for the computation of the susceptibility.

Defining region (b)

Region (b) is defined as the area where $V \leq V_{th}$ and $w \leq w_{min}$, with w_{min} the minimum of the V -nullcline ($V_{NV}(w_{min}) = V_{th}$).

From this, we can compute

$$w_{min} = I_e + g_L (E_L + \Delta_T - V_{th}) \quad (\text{B.4})$$

In this region

$$q = \frac{V_{th} - V}{\Delta_T} \quad (\text{B.5})$$

and the speed in V_{th} is

$$\dot{v} = 1 + \frac{E_L - V_{th}}{\Delta_T} + \frac{I_e - w}{g_L \Delta_T} \quad (\text{B.6})$$

Defining region (c)

The (c) region is the area where $w \geq w_{min}$ and $V \leq V_{VN}^r(w)$, where V_{VN}^r is the curve delimiting the right arm of the V -nullcline.

The equation of the V -nullcline is given by

$$g_L(E_L - V) + g_L\Delta_T \exp\left(\frac{V - V_{th}}{\Delta_T}\right) + I_e - w = 0 \quad (\text{B.7})$$

using the Lambert W function, we can obtain the function giving the right arm as

$$V_{NV}^{(r)}(w) = E_L + \frac{I_e - w}{g_L} - \Delta_T \mathcal{W}_{-1} \left[-\exp\left(\frac{g_L(E_L - V_{th}) + I_e - w}{g_L\Delta_T}\right) \right] \quad (\text{B.8})$$

given that $w \in [w_{min}, \infty[$, the argument of the Lambert W function is always in $[-\frac{1}{e}, 0[$ so the result is always defined using the -1 branch of the Lambert W function.

From this, we can compute the value of q in the (c) region, which leads to:

$$Sc^{(c)} = -q^{(c)} = \frac{V - V_{NV}^{(r)}(w)}{\Delta_T}. \quad (\text{B.9})$$

General equation for the susceptibility

Therefore, the susceptibility can be defined as:

$$Sc = \begin{cases} 1 + \frac{V + E_L - 2V_{th}}{\Delta_T} + \frac{I_e - w}{g_L\Delta_T} & \text{if } V \leq V_{th} \text{ and } w \leq w_{min}, \\ \frac{V_{NV}^{(r)}(w) - V}{\Delta_T} & \text{if } V \leq V_{NV}^{(r)}(w) \text{ and } w \geq w_{min} \\ \frac{E_L - V}{\Delta_T} + e^{(V - V_{th})/\Delta_T} + \frac{I_e - w}{g_L\Delta_T} & \text{otherwise} \end{cases} \quad (\text{B.10})$$

which can be rewritten using the Heaviside Θ function,

$$Sc = \begin{cases} \frac{V_{NV}^{(r)}(w) - V}{\Delta_T} & \text{if } V \leq V_{NV}^{(r)}(w) \text{ and } w \geq w_{min} \\ \frac{E_L - V + 2\Theta(V_{th} - V)}{\Delta_T} + e^{\Theta(V - V_{th})/\Delta_T} + \frac{I_e - w}{g_L\Delta_T} & \text{otherwise} \end{cases} \quad (\text{B.11})$$

Limitations

The adiabatic hypothesis ($\tau_m \ll \tau_w$) is obviously not always valid, and the fact that w varies in time changes the behavior of the neuron with respect to the simple division of phase-space that has been proposed above. Though the variations of w in time make little difference for most of the biologically-relevant values of τ_w , there are some specific regions of phase-space and τ_w values that lead to slightly more complex behaviors.

B.3 Restlessness

Based on the definitions in ‘‘Transitions of the AdExp model’’ (section B.1), we can define the bifurcation current

$$I_e^{(b)} = \begin{cases} I_{SN} & \text{if } a/g_L < \tau_m/\tau_w \\ I_{AH} & \text{if } a/g_L \geq \tau_m/\tau_w \end{cases} \quad (\text{B.12})$$

which leads to

$$\begin{cases} Rl < 0 & \text{if } I_e < I_e^{(b)} \\ Rl \geq 0 & \text{otherwise} \end{cases} \quad (\text{B.13})$$

Appendix C

Self-consistent equations for the bursting behavior

These equations describe the bursting behavior of adaptive spiking neurons in the absence of noise in the system. See also Fardet, Ballandras, et al. 2018 for details.

C.1 Neuronal model (AdEx) and parameters

Dimensionless parameters

The dimensionless parameters are obtained from their dimensional counterparts via the following formulas:

$$\begin{aligned}
 V &= \frac{\tilde{V} - \tilde{V}_{th}}{\tilde{\Delta}_T}, & E_L &= \frac{\tilde{E}_L - \tilde{V}_{th}}{\tilde{\Delta}_T} && \text{(general relation for voltages)} \\
 w &= \frac{\tilde{w}}{\tilde{g}_L \tilde{\Delta}_T}, & I &= \frac{\tilde{I}}{\tilde{g}_L \tilde{\Delta}_T} && \text{(general relation for currents)} \\
 t &= \frac{\tilde{t}}{\tilde{\tau}_m}, & \tau_w &= \frac{\tilde{\tau}_w}{\tilde{\tau}_m} && \text{(general relation for times)} \\
 g_L &= 1 & a &= \frac{\tilde{a}}{\tilde{g}_L} && \text{(general relation for conductances)}
 \end{aligned}$$

C.2 Hypotheses underlying the equivalent model

As the dynamics of w is slow except for its fast spike-triggered increase during the burst, our model is based on a quasi-static hypothesis regarding the subthreshold dynamics of w :

$$\tau_w \gg \tau_m = \frac{C_m}{g_L} = 1. \tag{C.1}$$

C.3 Stability of the synchronized state

Synchronization of relaxation oscillators (a class of periodically active units to which adaptive pacemaker neurons belong) has been extensively studied and is a known asymptotic behavior Bottani 1995; Somers et al. 1993, which has been shown to lead to bursting in the presence of adaptation Van Vreeswijk et al. 2001.

This stability can be observed in simulations, and Figure C.1 shows the immediate recovery of the network bursts after the random perturbation of the network at 250 ms. This perturbation was obtained by sending a 5-ms pulse of current to all neurons, with amplitudes distributed uniformly between 0 and 1 nA.

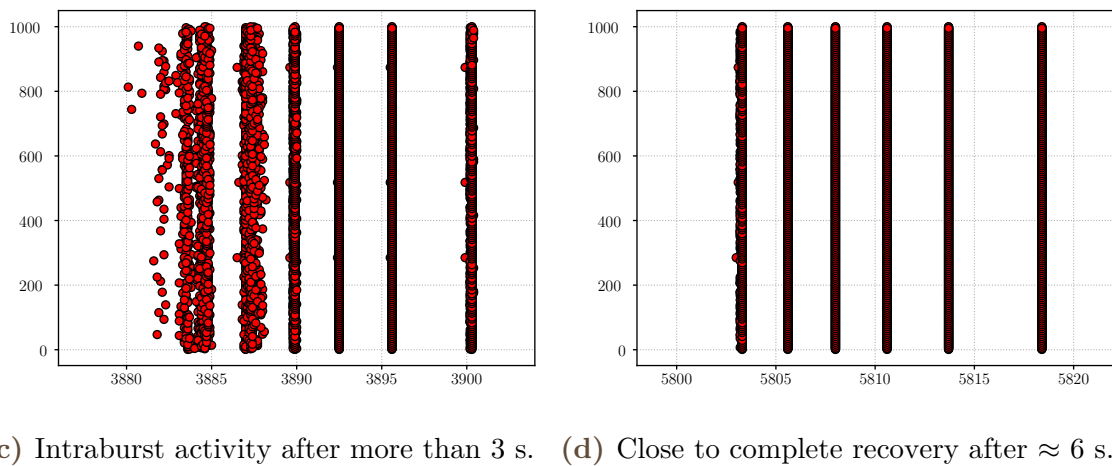
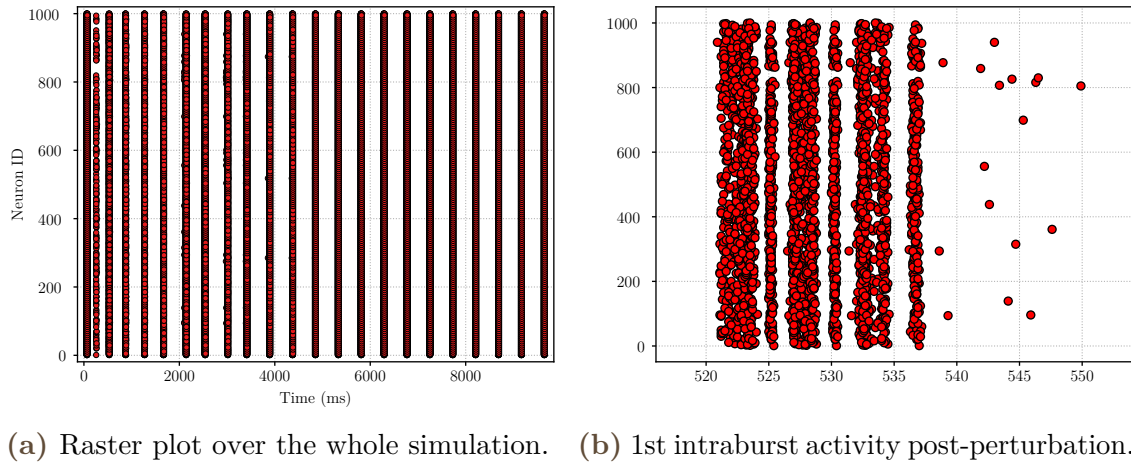


Figure C.1.: Stability of the synchronized bursting state for a 1000-neuron network with respect to an external perturbation of the activity. The bursting behavior is immediately recovered after the perturbation and the intraburst synchrony is progressively recovered over time (time-lag becomes smaller than the simulation timestep – 0.1 ms – after 7 s, making it undetectable).

Neuronal parameters are given below:

```

1 param = {
2     'V_reset': -58.,
3     'V_peak': 0.0,
4     'V_th': -50.,
5     'I_e': 300.,
6     'g_L': 9.,
7     'tau_w': 300.,
8     'E_L': -70.,
9     'Delta_T': 2.,
10    'a': 2.,
11    'b': 60.,
12    'C_m': 200.,

```

```

13     'V_m': -70.,
14     'w': 100.,
15     'tau_syn_ex': 0.2
16 }

```

Neurons are coupled by alpha-shaped currents of peak amplitude 60 pA.

C.4 Linear evolution of V submitted to a constant current

During an ISI, V undergoes a quasi-linear variation which starts right after the reset following a spike (let us simplify the calculations by setting $t = 0$ at this time) and lasts until the effect of the exponential term is no longer negligible.

During this period, the membrane potential behaves as if it were submitted to the linear equation:

$$\frac{dV_l}{dt} = -(V_l - E_L) + I(t) - w. \quad (\text{C.2})$$

For time independent synaptic currents, $I(t) = I$, we obtain – with $V_l(0) = V_r$:

$$V_l(t) = V_r e^{-t} + (E_L + I - w) (1 - e^{-t}). \quad (\text{C.3})$$

C.5 Modeling a burst with instantaneous Dirac synapses

In all this section, the current to which the neurons are subjected is $I(t) = I_0$ at all times and the effect of the spike is instantaneously delivered as a Dirac pulse, i.e. as an equivalent charge Q_s .

Interspike approximation

Between two spikes the slow current w varies slowly enough to be taken constant – see Figure 6 in the main text; therefore the interspike for a given w is called $t_s(w)$. Consider \tilde{a} and \tilde{b} two such spikes, characterized by the times t_A and t_B , the interspike is defined as

$$t_s^{(d)}(w) = t_B - t_A = \int_{t_A}^{t_B} dt.$$

The synaptic delay after which the PSP associated to spike \tilde{a} occurs separates the equation into:

$$t_s^{(d)}(w) = \int_{t_A}^{t_A+d} dt + \int_{t_A+d}^{t_B} dt.$$

Changing variables from t to V for the second term and defining $V_d^+ = V(d^+) \approx V_l(d) + \bar{k}Q_s$ from Eq. (C.2), this becomes:

$$\begin{aligned} t_s^{(e)}(w) &= \int_0^d dt + \int_{V_d^+}^{V_p} \frac{dV}{e^V + E_L + I_e - w} \\ &\approx d + T_{div}^{(d)} \end{aligned}$$

where $V_d = V_l(d)$, from Eq. (C.2), $\alpha = E_L + I_e - w$, $\beta = e^{V_p} + \alpha/2$, $\gamma = \exp(V_d + \bar{k}Q_s) + \alpha/2$, and

$$\begin{aligned} T_{div}^{(d)}(w) &= \int_{e^{V_d + \bar{k}Q_s}}^{e^{V_p}} \frac{du}{(u + \alpha/2)^2 - \alpha^2/4} \\ &= \int_{\gamma}^{\beta} \frac{dx}{x^2 - \alpha^2/4} \\ &= \frac{1}{\alpha} \int_{\gamma}^{\beta} \frac{dx}{x - \alpha/2} - \frac{dx}{x + \alpha/2} \\ &= \frac{1}{\alpha} \ln \left| \frac{(\gamma + \alpha/2)(\beta - \alpha/2)}{(\gamma - \alpha/2)(\beta + \alpha/2)} \right|. \end{aligned}$$

Hence:

$$t_s^{(d)}(w) \approx d + \frac{1}{\alpha} \ln \left| \frac{(2\gamma + \alpha)(2\beta - \alpha)}{(2\gamma - \alpha)(2\beta + \alpha)} \right|. \quad (\text{C.4})$$

Self-consistent equation

Using the linear solution of Eq. C.2 with $I = I_e$, the condition $V(t_{sp}^+) \leq V_{NV}(w)$ translates into:

$$V_r e^{-d} + (E_L + I_e - w)(1 - e^{-d}) + \bar{k}Q_s = V_{NV}(w) \quad (\text{C.5})$$

hence, with $V_{NV} = E_L + I_e - w - \mathcal{W}_{-1}(-e^{E_L + I_e - w})$,

$$w^* = E_L + I_e - V_r + \left[\mathcal{W}_{-1}(-e^{E_L + I_e - w^*}) + \bar{k}Q_s \right] e^d \quad (\text{C.6})$$

where \mathcal{W}_{-1} is the lower branch of the Lambert W function.

Approximative equation for w^*

Once the coupling of the neurons in the network is strong enough¹, the value of w at which the V -nullcline is crossed by the trajectory (see section “Regular networks and Dirac synapses” and Figure 5 in the main text) is located in a region where the shape of the nullcline is dominated by the exponential term. Because of this, even quite significant changes in the value of w^* lead to small changes for $V_{NV}(w^*) \approx \ln(w^*)$ as $w^* = n_s b$ is large.

Thus, $V_{NV}(w^*) \approx C$, which is a constant, and, from Eq. C.5, we get:

$$V_r e^{-d} + (E_L + I_e - w)(1 - e^{-d}) + \bar{k}Q_s \approx C \quad (\text{C.7})$$

hence

$$w^* \approx E_L + I_e + \frac{V_r e^{-d} + \bar{k}Q_s}{1 - e^{-d}} + C. \quad (\text{C.8})$$

¹We call “strong bursting” a situation where $n_s b \gg 1$, with n_s the number of spikes emitted by a neuron during the burst and \tilde{b} the spike-triggered adaptation.

C.6 Bursting in heterogeneous networks: continuous synapses

Interspike approximation

As for the Dirac model, we take

$$\begin{aligned} t_s^{(c)}(w) &= \int_{t_A}^{t_B} dt = \int_{V_r}^{V_p} \frac{dV}{-V + e^V + E_L + I_+ - w} \\ &\approx \int_{V_r}^0 \frac{dV}{E_L - V + I_+ - w} + \int_0^{V_p} \frac{dV}{e^V + E_L + I_+ - w} \end{aligned}$$

Setting $\alpha = E_L + I_+ - w$ and $\beta = e^{V_p} + \alpha/2$, we obtain:

$$t_s^{(c)}(w) \approx \ln \left(\frac{\alpha - V_r}{\alpha} \right) + \frac{1}{\alpha} \ln \left| \frac{(1 + \alpha)(2\beta - \alpha)}{2\beta + \alpha} \right|. \quad (\text{C.9})$$

Self-consistent equation

The upper bound for w is the value $w^* \approx E_L + I_+ - V_r$ at which spiking does not occur anymore, i.e. when the time between two spikes becomes infinite. As w varies by steps of \tilde{b} for individual neurons, the average interspike during the burst, $\bar{t}_s(w^*)$, can be approximated by integrating the exact expression of $t_s(w)$ on $[w_{min}, w^* - \tilde{b}]$, where the integrand does not diverge. To keep the coherence with the other two models, though the total burst duration of the continuous model must be taken as the sum of the spike times plus the delay necessary for the last spike to arrive:

$$T_B = (n_s - 1) \bar{t}_s(w^*) + d \quad (\text{C.10})$$

where

$$\begin{aligned} \bar{t}_s(w^*) &= \frac{1}{w^* - \tilde{b} - w_{min}} \int_{w_{min}}^{w^* - \tilde{b}} t_s^{(c)}(w) dw \\ &= \frac{1}{w^* - \tilde{b} - w_{min}} \int_{w_{min}}^{w^* - \tilde{b}} \left[\ln \left(\frac{\alpha - V_r}{\alpha} \right) \right. \\ &\quad \left. + \frac{1}{\alpha} \ln \left| \frac{(1 + \alpha)(2\beta - \alpha)}{2\beta + \alpha} \right| \right] dw. \end{aligned}$$

In addition, the value of w^* leads to the relation:

$$w^* - w_{min} = I_+ - I_e. \quad (\text{C.11})$$

From Eq. (C.10) and (7) we get

$$d + (n_s - 1) \bar{t}_s(w^*) = \frac{n_s \bar{k} Q_s}{I_+ - I_e}$$

which becomes, using Eq. C.11, and $n_s = (w^* - w_{min})/\tilde{b}$:

$$d + \left(\frac{w^* - w_{min}}{\tilde{b}} - 1 \right) \bar{t}_s(w^*) = \frac{\bar{k} Q_s}{\tilde{b}} \quad (\text{C.12})$$

which leads to the self-consistent equation (8) in the main text.

Note that for this model to make sense with respect to the previous one, we must be able to define an equivalent non-zero burst duration through the interspike, which means that the number of spikes in the burst must be at least two.

C.7 Effect of the last spike

Depending on the model used for the synapses and on the delay regarding spike transmission, the network might feel the effect of the last spike after a time \tilde{d} following the end of a burst.

In the case of the continuous synapses, this delay is already taken into account inside T_B , so we consider that the burst ends directly with the last reset. Thus, we end up at 0 on Figure 4B, with $V_{max}^{(c)} = V_r$. This takes a time $t_{final} = 0$.

For the other two models, the last spark of activity is felt after the delay \tilde{d} . During this delay, the membrane potential decays linearly – cf. Eq. (C.2) – to:

$$V_d = V_l(d) \approx V_r e^{-d} + (E_L + I_e - w)(1 - e^{-d}).$$

In the case of the Dirac synapses, the potential then undergoes an instantaneous shift which leads to the final value $V_{max}^{(d)} = V_d + \bar{k}Q_s$ after $t_{final} = d$. For alpha-shaped synapses, the potential subsequently increases over $4\tau_s$ to reach $V_{max}^{(\alpha)} \approx V_d + 4\tau_s \left(I_e + \frac{\bar{k}ce}{4} + E_L - V_d - w_{max} \right)$ after $t_{final} = d + 4\tau_s$.

To be coherent with the description of the dynamics in time, presented on Figure 4A, we will consider that the global time is $t = 0$ after the last spark of activity dies out and $V(0) = V_{max}$.

C.8 Resting period: interburst dynamics

During the whole interburst (from 0 to 4 on Figure 4A), we consider that V is always small compared to $V_{th} = 0$, i.e. that its dynamics is described by Eq. (C.2) where $I(t)$ simplifies to \tilde{I}_e for all times in $[0; IBI]$, when the effect of the last spike is no longer felt by the neurons.

Note that all subsequent numbers will refer to the circled points marking the different periods on Figure 4.

After the last spike, the system ends up in a highly excited state with $(V, w) = (V_{max}, w_{max})$ – marked 0. In that region, w follows a very simple dynamics which can, at the leading order, be approximated as an exponential decrease from its peak value until it reaches its minimum:

$$\dot{w} \approx \frac{a(\bar{V} - E_L) - w}{\tau_w}. \quad (\text{C.13})$$

This simple equation represents the influence of the average potential $\bar{V} = (V_{min} + V_{max})/2$ felt by w during its decay.

The behavior of V , on the other hand, is slightly more complex and can be divided into three distinct phases: a first, abrupt, decrease of duration T_{down} , followed by a short transition period ending at $T_2 = T_{down} + T_{up}$, then a slow increase until T_I (point 1).

The first period is a rapid decrease dominated by the influence of $w \approx w_{max}$. It is followed by a short period T_{up} (between 1 and 2) where it goes from the V -nullcline to the recovery path (dotted line on Figure 4B).

The resting period can thus be characterized by three values (w_{max} , w_{min} and V_{min}) which strongly influences its duration T_I .

Decrease of V

In order to solve on $[0, T_{down}]$ ($[0; 1]$ region) and get a good approximation for T_{down} , we linearize the slow current. The linearized expression for w is called w_l , the solution of the linearized equation for V is called V_l .

$$w_l(t) = w_{max} + \lambda t.$$

We determine λ by taking the average value $\langle V \rangle = \frac{1}{2}(V_{max} - V_{min}^0)$ in the equation of \dot{w} .

$$w_l(t) = w_{max} + \frac{1}{\tau_w} \left(\frac{a}{g_L} \frac{V_{min} + V_{max} - 2E_L}{2} - w_{max} \right) t.$$

This linearized expression for w is substituted in the right-hand side of Eq. (C.2), its solution with initial condition V_{max} reads

$$V_l(t) = e^{-t} (V_{max} - E_L - I_e + w_{max} - \lambda) + \lambda(1 - t) + E_L + I_e - w_{max}$$

with

$$\lambda = \frac{1}{\tau_w} \left(\frac{a}{g_L} \frac{V_{min} + V_r - 2E_L}{2} - w_{max} \right).$$

Then T_{down} is the time when the derivative of V_l vanishes, it is given by

$$T_{down} = -\ln \left(\frac{\lambda}{\lambda - V_{max} + E_L + I_e - w_{max}} \right). \quad (\text{C.14})$$

Transition from refractory to recovery

After the initial decrease of V , the trajectory passes the nullcline and reaches the recovery path (from 1 to 2). During this portion of the dynamics, $\dot{V} \ll \dot{w}$, so the evolution of w can be considered to happen at constant $V = V_{min}$ at zeroth order. We use this approximation for $w \in [w^{(1)}, w^{(2)}]$. Considering the 1st order, V then slowly evolves to reach the value corresponding to $w^{(2)}$ along the recovery path. From a biological standpoint, this can be seen as the point where the persistent currents and the hyperpolarization-activated currents compensate the effect of the spike-driven hyperpolarizing currents.

$$\dot{w} \approx \frac{1}{\tau_w} [a(V_{min} - E_L) - w]$$

hence, setting $t = 0$ at T_{down} :

$$w(t) \approx a(V_{min} - E_L) + [w^{(1)} - a(V_{min} - E_L)] e^{-t/\tau_w}. \quad (\text{C.15})$$

Putting the solution back into the equation for V and developing around the nullcline point $(V_{min}, w^{(1)})$, we get:

$$\begin{aligned} \dot{V} &= -(V - E_L) + I_e - w \\ &= -(V - V_{min}) - [w^{(1)} - a(V_{min} - E_L)] (1 - e^{-t/\tau_w}). \end{aligned}$$

Changing variables for $V(t) = f(t)e^{-t}$, this leads to:

$$\begin{aligned} \dot{f} &= [V_{min} - (w^{(1)} - a(V_{min} - E_L)) (1 - e^{-t/\tau_w})] \\ \Rightarrow f(t) &= [a(V_{min} - E_L) - w^{(1)}] \left(\frac{\tau_w}{\tau_w - 1} - 1 \right) \\ &\quad + [V_{min} + a(V_{min} - E_L) - w^{(1)}] e^t \\ &\quad + \frac{\tau_w}{\tau_w - 1} [w^{(1)} - a(V_{min} - E_L)] e^{\frac{\tau_w - 1}{\tau_w} t} \end{aligned}$$

hence

$$V(t) = V_{min} + \left[a(V_{min} - E_L) - w^{(1)} \right] \cdot \left[\left(\frac{\tau_w}{\tau_w - 1} - 1 \right) e^{-t} - \frac{\tau_w}{\tau_w - 1} e^{-t/\tau_w} - 1 \right]. \quad (\text{C.16})$$

Recovery period

After the transition which follows the initial decrease of V , we enter the recovery period – interval between points 2 and 3. There, w slowly decreases to its minimum value w_{min} while V increases until the first spike of the following burst. The trajectory stays close to the V -nullcline, on a path where the derivative of both V and w have the same magnitude, i.e, neglecting the nonlinear terms:

$$\frac{\dot{w}}{\dot{V}} \approx \frac{a(V - E_L) - w}{\tau_w(I_e + E_L - V - w)} = \frac{dw_{VN}}{dV} \approx -1$$

which leads to

$$w = \frac{1}{1 + \tau_w} [(a - \tau_w)(V - E_L) + \tau_w I_e] \quad (\text{C.17})$$

or equivalently

$$V = E_L + \frac{1}{a - \tau_w} [(1 + \tau_w)w - \tau_w I_e].$$

During this period, the evolution of w is therefore driven by

$$\begin{aligned} \dot{w} &= \frac{1}{\tau_w} [a(V - E_L) - w] \\ &= \frac{1}{\tau_w} \left[\frac{a}{a - \tau_w} ((1 + \tau_w)w - \tau_w I_e) - w \right] \\ &= -\frac{1 + a}{\tau_w - a} \left(w - \frac{a}{1 + a} I_e \right). \end{aligned}$$

This behavior changes when V reaches $V_{th} = 0$, where the non linear terms become predominant and the dynamics of V , again, becomes much faster than that of w .

Thus, the recovery time is given by:

$$T_R = \frac{\tau_w - a}{1 + a} \ln \left(\frac{w^{(2)} - \frac{a}{1+a} I_e}{w_{min} - \frac{a}{1+a} I_e} \right).$$

Initiation of the burst

After the recovery period, the burst is initiated (point 3 on Figure 4) as the trajectory of the mean-field neuron reaches the minimum of the V -nullcline, i.e. for $w_{min}^0 = 1 + I_e + E_L$ and $V = V_{th} = 0$. Once V reaches 0, the first spike of the burst is initiated, which takes

$$T_{fs} = \int_{t=T_I}^{T_I+T_{fs}} dt = \int_{V=0}^{V_{peak}} \frac{dV}{\dot{V}} \approx \int_{V=0}^{V_{peak}} e^{-V} dV \approx 1. \quad (\text{C.18})$$

Appendix D

Simulating networks of spiking neurons

D.1 Simulation choice and protocols

AdExp implementation

As the exponential term in the differential equation for V is quite difficult to control numerically, I improved the existing implementation of the NEST simulator and provided new current-based synapses, starting from version 2.12.0. The new implementation binds V to be smaller than V_{peak} at all times, and was tested against the solution provided by the LSODAR solver¹, which has been designed to handle directly discontinuous equations. Contrary to the old implementation, this new formulation converges towards the reference solution and is closer to it for any given simulation timestep.

Checking for spurious synchrony

We checked for synchronization artifacts that might come from the grid-based spike delivery in NEST using a custom implementation of the precise (event-based) model of the AdExp neuron, then compared to simulation with varying timesteps. No significant changes (delays or cancellations (Brette, Rudolph, et al. 2007)) were observed, hence all subsequent simulations were performed with timesteps of 0.1 ms, or occasionally 0.5 ms for very long simulations or parameter search.

D.2 Network models and parameters

All network models used in this study are implemented in the NNGT library²

In “Mechanisms governing epileptiform bursts” (chapter 2), both non-spatial Gaussian networks and EDR network were used. In the subsequent chapters, only the EDR and DeNSE-grown networks were considered.

Parameters for the phase transition — “The transition to synchronous bursting” (subsection 2.3.1)

Gaussian networks were generated with an average degree of 100 and subjected to Poisson noise with an average rate of 15 Hz and a peak current given by

$$I_{max}^{(noise)} = \frac{1 + c}{2}. \quad (D.1)$$

¹ see jupyter notebook https://github.com/nest/nest-simulator/blob/master/doc/model_details/aeif_models_implementation.ipynb on the NEST github repository for details.

² a python library aimed at bridging the gap between neuroscience and graph theory; see <http://nngt.readthedocs.io/en/latest/> for details.

Non bursting pacemakers

Bursting to spiking pacemakers

```

1 p_PM_nb = {
2     'E_L': -64.1,
3     'I_e': 23.,
4     'g_L': 10.,
5     'C_m': 250.,
6     'a': -1.5,
7     'V_th': -54.98,
8     'V_reset': -59.,
9     'Delta_T': 5.5,
10    'b': 60.,
11    'tau_w': 350.,
12    'tau_syn_ex': 1.5,
13    't_ref': 3.
14 }
```

```

1 p_B_osc = {
2     'E_L': -64.1,
3     'I_e': 23.,
4     'g_L': 10.,
5     'C_m': 250.,
6     'a': -1.5,
7     'V_th': -54.99,
8     'Delta_T': 5.5,
9     'b': 60.,
10    'tau_w': 350.,
11    'V_peak': 20.,
12    'tau_syn_ex': 1.5,
13    't_ref': 3.
14 }
```

For the bursting pacemakers, the reset potential V_r was randomized following a normal distribution $\mathcal{N}(-53.5, 0.5)$ in order to provide a smooth transition (otherwise all neurons switch from spiking to bursting at the same time).

Parameters for “Burst nucleation in neuronal cultures *in silico*” (subsection 3.3.2)

EDR networks were generated with an average degree of 100 and subjected to minis with a base rate of 0.15 Hz per synapse, such that a neuron of degree 100 will receive mEPSCs with an average rate of 15 Hz. Peak current of the minis is set to a third of the average synaptic strength.

5-second IBI, type II, used with a synaptic coupling of 25 pA

5-second IBI, pacemaker, used with a synaptic coupling of 10 pA

14-second IBI, pacemaker, used with a synaptic coupling of 30 pA.

```

1 p_II_5s = {
2     'I_e' : 0.,
3     'E_L' : -56.4,
4     'V_m' : -56.4,
5     'V_reset' : -53.,
6     'g_L' : 11.,
7     'C_m' : 300.,
8     'b' : 100.,
9     'tau_w' : 500.,
10    'V_th' : -54.935,
11    'a' : 6.,
12    'Delta_T' : 2.,
13    'tau_syn_ex' :
14    ↪ 1.5,
15    't_ref' : 3.
}

```

```

1 p_PM_5s = {
2     'I_e' : 0.,
3     'E_L' : -56.4,
4     'V_m' : -56.4,
5     'V_reset' : -53.,
6     'g_L' : 11.,
7     'C_m' : 300.,
8     'b' : 100.,
9     'tau_w' : 500.,
10    'V_th' : -54.935,
11    'a' : 6.,
12    'Delta_T' : 2.,
13    'tau_syn_ex' :
14    ↪ 1.5,
15    't_ref' : 3.
}

```

```

1 p_PM_14s = {
2     'E_L' : -64.1,
3     'I_e' : 22.5,
4     'g_L' : 10.,
5     'C_m' : 250.,
6     'a' : -1.5,
7     'V_th' : -54.918,
8     'V_reset' : -62.,
9     'Delta_T' : 5.5,
10    'b' : 70.,
11    'tau_w' : 350.,
12    'V_peak' : 20.,
13    'tau_syn_ex' :
14    ↪ 1.5,
15    't_ref' : 3.
}

```

Older simulations, performed during my stay in Japan (JSPS Summer Program 2017) and described in Figures 3.4 and 3.5, used different networks and neuronal parameters, which can be found below.

50,000 neurons were seeded on a disk 6.5 mm in radius, leading to a density around 380 neurons/mm². These neurons were then connected using the EDR model with characteristic distances of either 200, 400, or 800 μm to model different developmental stages. Average degrees were varied between 50 and 150 to also account for the differences in developmental advancement. The weights between all neurons were taken from a lognormal distribution of mean 250. and a scale of 0.5 and the synapses were taken from 'tsodyks2_synapse' with parameters $U = 0.33$, $\tau_{rec} = 1500s$, $u = 0$ and $x = 1$ (Loebel et al. 2002).

The population was composed of 4 neuron types: regular spiking pacemakers, intrinsically bursting pacemakers, adaptive spiking non-pacemakers, fast spiking inhibitory.

Parameters for their resting state (no spontaneous activity) read:

Intrinsically bursting pacemakers

```

1 p_IB_rest = {
2     'E_L': -70.,
3     'V_m': -70.,
4     'I_e': 0.,
5     'g_L': 10.2,
6     'C_m': 300.,
7     'a': -3.5,
8     'V_th': -57.,
9     'V_reset': -53.,
10    'Delta_T': 7.2,
11    'b': 25.,
12    'tau_w': 350.,
13    'V_peak': 20.,
14    'tau_syn_ex': 1.5,
15    'tau_syn_in': 3.,
16    't_ref': 3.
17 }
```

Regular spiking pacemakers

```

1 p_RS_rest = {
2     'E_L': -64.,
3     'V_m': -64.,
4     'I_e': 0.,
5     'g_L': 10.,
6     'C_m': 250.,
7     'a': -1.5,
8     'V_th': -55.,
9     'V_reset': -59.,
10    'Delta_T': 5.5,
11    'b': 80.,
12    'tau_w': 200.,
13    'V_peak': 20.,
14    'tau_syn_ex': 1.5,
15    't_ref': 3.
16 }
```

Adaptive spiking non-pacemakers

```

1 p_AS_rest = {
2     'E_L': -60.,
3     'V_m': -60.,
4     'w': 200.,
5     'V_reset': -60.,
6     'g_L': 9.,
7     'C_m': 300.,
8     'V_peak': 30.,
9     'b': 20.,
10    'tau_w': 300.,
11    'V_th': -56.,
12    'a': 4.,
13    'Delta_T': 2.,
14    'tau_syn_ex': 1.5,
15    'tau_syn_in': 3.,
16    't_ref': 3.
17 }
```

Fast spiking inhibitory

```

1 p_FSi = {
2     'E_L': -60.,
3     'V_m': -60.,
4     'w': 0.,
5     'V_reset': -64.,
6     'g_L': 12.,
7     'C_m': 250.,
8     'V_peak': 30.,
9     'b': 30.,
10    'tau_w': 50.,
11    'V_th': -54.,
12    'a': 1.,
13    'Delta_T': 2.,
14    'I_e': 0.,
15    'tau_syn_ex': 1.5,
16    'tau_syn_in': 3.,
17    't_ref': 2.
18 }
```

Then, a fraction of the excitatory population (usually 5%) was put in a spontaneously active state through both minis of average rate 5 Hz and an increase in their excitability to obtain average spiking rates of 0.1 Hz.

Neuronal parameters for the neuronal devices

For both the 2-stage culture and the neuronal diode, the parameter used were

```

1 p_PM = {
2     'E_L': -64.1,
3     'V_m': -64.1,
4     'I_e': 21.8,
5     'g_L': 10.,
6     'C_m': 250.,
7     'a': -1.6,
8     'V_th': -55.,
9     'V_reset': -59.,
10    'Delta_T': 5.5,
11    'b': 5.,
12    'tau_w': 350.,
13    'V_peak': 20.,
14    'tau_syn_ex': 1.5,
15    't_ref': 3.
16 }
```

with a synaptic strength of 20 pA.

For the more active region of the diode, the following parameters were changed: $a = -1.57$ nS, $I_e = 22.02$ pA, and $E_L = -64.1$ mV.

D.3 Properties of spatial networks

In spatial networks, delays were attributed to the connections based on the distance between the source and target nodes, considering propagation speeds for the action potential in the range [100, 250] $\mu\text{m}/\text{ms}$. This was notably based on the observations of Barral et al. 2016.

Regarding the synaptic strength, no correlation between distance and strength was used since Magee et al. 2000 reported a distance-based scaling leading to almost constant post-synaptic currents at the soma.

Neuronal degree

All networks were generated with average in-degrees between 30 and 100.

Clustering coefficient

The local clustering coefficient c_i is defined as

$$c_i = \frac{|\{e_{jk}\}|}{k_i(k_i - 1)} : v_j, v_k \in N_i, e_{jk} \in E, \quad (\text{D.2})$$

where k_i is the out-degree of node i , and

$$N_i = \{v_j : e_{ij} \in E\}$$

is the set of out-neighbors of node i .

Betweenness

The betweenness centrality of an edge is defined as the number of shortest paths going through it.

For a vertex v , the betweenness centrality $C_B(v)$ is defined as,

$$C_B(v) = \sum_{s \neq t \in V} \frac{\sigma(s, t|v)}{\sigma(s, t)}, \quad (\text{D.3})$$

where V is the set of vertices in the network, $\sigma(s, t)$ is the number of shortest (s, t) -paths, and $\sigma(s, t|v)$ is the number of those paths passing through some vertex v other than s, t .

Appendix E

Experimental protocols

E.1 Culture preparation and feeding procedures

Primary neurons were obtained from Winstar rat embryos at stages E19. All procedures were approved by the Weizmann Institutes Animal Care and Use Committee.

Dissection and papain dissociation of hippocampi was done according to established protocols at the Weizmann Institute (Renault, Sukenik, et al. 2015). Brains from embryos were micro-dissected on ice in L-15 medium without phenol red (Life technologies) supplemented with 0.6% glucose and 0.2% gentamycin. Hippocampi were digested in papain solution (papain 100 units, DNaseI 1000 units, L-Cystein 2 mg, NaOH 1M 15 μ L, EDTA 50 mM 100 μ L, CaCl₂ 100 mM 10 μ L, dissection solution 10 mL) at 37°C for 20 minutes. After digestion, the supernatant was carefully removed and replaced with 10 mL of plating medium (MEM without glutamine supplemented with 0.6% glucose, 1% GlutaMAX, 5% Horse Serum, 5% Fetal Calf Serum and 0.1% B27) supplemented with 25 mg of trypsin inhibitor and 25 mg of Bovine Serum Albumine for 5 min to inactivate the papain. Supernatant was removed, replaced with plating medium and tissues were triturated with fired polished pasteur pipettes.

The medium covering the glass chips was aspirated and the dissociated neurons were seeded in compartment at a density around 5000 neurons/mm². The seeded chips were incubated half an hour in a humidified, 37°C and 5% CO₂ incubator to allow the attachment of neurons to the PLL substrate. Each chip was finally covered by 2 mL of serum-free medium (Neurobasal, B27 4%, GlutaMAX 1% and FCS 1%) and the cultures were placed back into the incubator.

Glial proliferation was stopped 4 days after plating by adding in the medium 20 μ g/mL 5-fluoro-2-deoxyuridine and 50 μ g/mL uridin (Sigma, Israel).

Cultures were fed every day, replacing 0.5 mL of the old medium with new feeding medium containing MEM and HS.

E.2 Calcium imaging

Before imaging, cultures were changed to 2 mL of observation medium containing:

K⁺ at 5.3 mM,

Na⁺ at 144 mM,

Cl⁻ at 155 mM,

Mg²⁺ at 0.81 mM,

Glucose at 39 mM,

Sucrose at 16 mM,

HEPES at 10 mM,

GlutaMAX at 10 mM,

Ca²⁺ at 1 mM,

with addition of 160 μL of NaOH (1 M) to regulate the pH.

One hour before observation, 4 μL of Fluo-4 in DMSO were added and left incubating. After one hour, the medium was removed and replaced with clean observation medium, without Fluo-4.

Observations were subsequently performed on a LEICA TCS SP5 X scanning confocal microscope with a laser excitation at 488 nm. The activity of a 922 μm^2 area in the culture was recorded at 5 Hz using a 10x magnification and a 1.7 zoom.

E.3 Application of the blockers

After control recordings, blockers were added to the medium and left to react for 15 minutes before resuming recordings.

Bicuculline: blocking inhibitory synapses

To record from purely excitatory cultures, 20 μL of bicuculline at 4 mM was added to the 2 mL medium to obtain a final concentration of 40 μM .

Paxilline: blocking fAHP

To block fAHP, 2 μL of paxilline in DMSO (at 2.5 mM) was added to reach a final concentration of 2.5 μM .

Apamin: blocking mAHP

To block mAHP, 10 μL of apamin in water (at 40 μM) was added to reach a final concentration of 200 nM.

Isradipine: blocking sAHP

To block sAHP, 2 μL of isradipine in DMSO (at 7.5 mM) was added to reach a final concentration of 7.5 μM .

Appendix F

Nucleation centers

In order to detect the nucleation centers which contributed to the initiation of bursts of activity in the cultures, the localization of the peak of the bursting activity was first obtained in order to assign each spike in the raster to a given “burst region”. Following this segregation, nucleation centers were obtained using a parameterless clustering method. Eventually, correlation between the nucleation centers and various graph centralities is assessed.

F.1 Preliminary burst delimitation

In order to detect the peak of the bursting activity, the total firing rate of the culture is first obtained by successively convolving the spike times by an exponential and a Gaussian kernel:

$$Fr = \frac{1}{\tau\sigma\sqrt{2\pi}} \sum_i \delta(t - t_i) * \Theta(t - t_i)e^{-t/\tau} * e^{-(t-t_i)^2/(2\sigma^2)}, \quad (\text{F.1})$$

where the exponential kernel preserves the causality of the signal, while the Gaussian kernel avoids the presence of individual peaks in the firing rate and facilitates the detection of a single maximum in the burst.

Values of τ and σ were adapted to provide a single maximum per burst (typically between $\tau \in [4; 20]$ ms and $\sigma = 3\tau$).

Once the burst peaks are detected, all spikes that are closer to it than to any other peak are associated to this burst — see Figure 3.3e in the main text.

F.2 Detection via a clustering algorithm

Once this segregation has been performed, the clustering is implemented by analyzing the spatial distribution of all neurons which activated before a time t .

Setting $t = 0$ at the beginning of a burst region and $t = T$ at the end of this region (dashed orange limits on Figure 3.3e), t is progressively varies from 0 to T and the distribution of the active neurons before time t is assessed to search for clusters.

This clustering search is performed using the DBSCAN algorithm from the scikit-learn library. This algorithm requires two main parameters:

the maximum distance `eps` for two points to be considered as neighbors,

the minimal number of neighbors `min_samples` to be considered as a core point in a cluster.

For the EDR network, and rather similarly for the grown networks, the typical scale of the connectivity — λ , in the EDR case — is half the average distance length in the network, which is the distance which is chosen for **eps** as characterizing the distance between connected neurons. For the number of neighbors, we characterize the degree distribution, which is typically close to normal, and use as typical degree $k_0 = \langle k \rangle - (\langle k^2 \rangle - \langle k \rangle^2)$, which ensures that the minimal connectivity can be reached by most neurons in the network.

F.3 Predicting nucleation centers by graph centralities

Apart from the two centralities presented in the main text¹, the graph centralities tested in this study included:

- the in- and out-degree, which gave results similar to that of the total degree,
- the closeness², which did not correlate to the nucleation centers (NCs), nor to the first-to-fire property (FtF),
- the node betweenness³, which did not correlate to the NCs or the FtF property,
- the subgraph centrality (Estrada et al. 2005) which did not correlate to the NCs, nor to the FtF property,
- the average delay from a node to or from all its neighbors, which did not correlate,
- multiple combination of the normalized centralities above also did not correlate.

¹ see “Burst nucleation in neuronal cultures *in silico*” (subsection 3.3.2).

²see https://en.wikipedia.org/wiki/Closeness_centrality.

³see https://en.wikipedia.org/wiki/Betweenness_centrality.

Appendix G

Growth models

This appendix provides some additional details about the models used for growth cone steering in DeNSE.

G.1 Simple random walker

The simplest model is the random walk, implemented more for reference and null-model purposes than for actual use.

In this model, each of the possible angles given by the filipodia¹ is assigned a probability obtained from a Gaussian distribution which is centered on the current direction angle.

For n_f filopodia spanning an angular aperture $2\theta_{max}$, there are $n_f - 1$ angles that separate the regions assigned to each filopodia; the probability assigned to each filopodia of being chosen as the new direction for the next step is therefore the integral of the Gaussian probability density over that region, i.e. for the filopodia i :

$$P_i = \frac{1}{\sigma\sqrt{2\pi}} \int_{i\Delta\theta - \theta_{max}}^{(i+1)\Delta\theta - \theta_{max}} e^{-\theta^2/(2\sigma^2)} d\theta, \quad (\text{G.1})$$

with $\Delta\theta = 2\theta_{max}/(n_f - 1)$.

As shown by equation 4.4 in the main text, the value of σ can be computed easily from the persistence length.

However, the main issue here is that, in order for a random walk to be independent of the simulation timestep dt , its standard deviation σ must scale as $\sigma = \sigma_0\sqrt{dt}$, where σ_0 is the desired standard deviation associated to the required persistence length. Because of this, in the simple random walk, the typical angular aperture of the growth cone, θ_{max} has to be changed with the timestep. Though this is not a problem per se, it triggers incorrect behaviors when the growth cone interacts with the environment, because this interaction occurs at different angles depending on the timestep, which leads to timestep-dependent results. Consequently, the use of this model is not permitted if a spatial environment is present.

G.2 Run-and-Tumble model

The main model for growth and interactions is therefore the run-and-tumble model — see Kirkegaard et al. 2018 for recent results and list of previous results — since the presence of two parameters (the run length l_0 , and the angular choice θ_{max} during tumbles) enables to uncouple the angular aperture from the persistence length, as shown in equation 4.5 and on Figure G.1. This model is a reference to model planar

¹ see Figure 4.6 in “Beyond the isolated growth cone: interactions” (subsection 4.2.2).

motions, for instance of bacteria, because its two variables l_0 and θ_{max} allow to set the characteristic scale of the persistence length through two mechanisms: the frequency of direction change and the angular width of this change, i.e. the correlation between two successive runs.

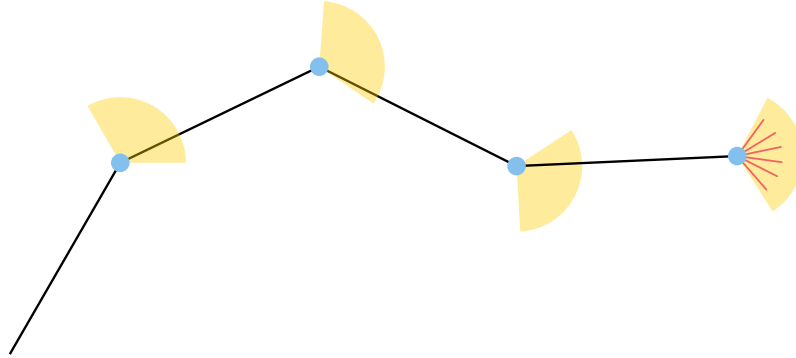


Figure G.1.: Illustration of a run-and-tumble trajectory. The blue circles mark the tumble positions, which are separated by l_0 , while the possible angles for the next run are given by the orange angular are. The filopodia are shown in red on the last position.

Maintaining θ_{max} constant, one can thus provide timestep-independent interactions while ensuring a proper persistence length using the l_0 parameter.

Furthermore, this model also corresponds to the biological reality that the persistence length of the neurite is not related to the flexural rigidity of the microtubules, but rather to active events which trigger ruptures in the axonal or dendritic shaft.

G.3 Self-referential forces

As mentioned in the main text, though the notion of self-referential forces (SRF)² is very interesting, the proposed implementation of these “forces” result in both misleading and error-prone descriptions.

Indeed, the notion of inertial force, to characterize the rigidity³ of the neurite has no physical relevance, mechanical inertia being negligible in those regimes. Considering the mechanism maintaining the neurite’s trajectory almost straight on short distances as an “inertial force” is thus incorrect and may be misleading for non-physicists. If forces are considered, they should be those exerted by the filopodia and lamellipodia, and the work they apply on bending the neurite shaft can then be used to quantify the progressive bending of the growth cone trajectory.

Moreover, the issue of self-referential forces is not limited to the “inertial force”. Indeed, the implementation present in *NeuroMac* (Torben-Nielsen et al. 2014) also models the stochastic deviation from the deterministic force balance using a “stochastic force” term which is added to the deterministic resulting force. Unfortunately, because the stochastic force is directing randomly in $[0, 2\pi[$, the angular distribution obtained for the total resulting force is not unimodal but bimodal, promoting a “broken line” trajectory rather than the smooth evolution observed experimentally.

² as the presence of mechanisms that are intrinsic to the growth cone.

³ visualized by the persistence length of the neurite, as described previously.

To correct this behavior, the SRF implemented in DeNSE considers the resulting force exerted by all filopodia on the C-domain — the center of the growth cone, see Figure 4.1 in “Modeling an extending growth cone” (subsection 4.2.1). Combined to the bending energy of the microtubules in the neurite shaft (equation 4.3), the work of this force gives an effective bending angle that shifts the trajectory.

Similarly, the somatropism is changed to correspond to a mechanism where the growth cone responds to the gradient of a molecule emitted at the soma. This implementation considers that the molecule diffuses around the soma up to a characteristic distance r_0 with a Gaussian profile:

$$C \propto e^{-r^2/(2r_0^2)}. \quad (\text{G.2})$$

The intensity with which each filopodia i senses the gradient is thus proportional to the concentration at the growth cone’s current position, as well as to the cosine of the angle $\Delta\theta_i$ between the filopodia and the direction of the soma. This repulsive contribution is therefore taken into account for all filopodia whose angle with the direction of the soma is lower than 90° and reads:

$$p_{st}(r, \theta_i) = e^{-r^2/(2r_0^2)} \cos(\Delta\theta_i). \quad (\text{G.3})$$

For completeness this algorithm is combined to the run-and-tumble model: the forces account for the progressive turns during runs, where changed is trajectory are prevented by the rigidity of the neurite shaft, while the tumbles account for specific events where the integrity of the shaft is compromised and a new “shaft section” is formed, generating a discontinuity in the neurite’s trajectory.

G.4 Critical resource and competition

As discussed in the main text⁴, conditioning the extension of the growth cone on the amount of a given critical resource which is present at the tip, enables to recover an important property observed *in vitro*, which is the alternation of periods of elongation, retraction, and pausing.

One of the main advantages of the model proposed in equation 4.6 is that it is fully tractable. Deriving the probability density function for the growth cone, one can therefore predict the fraction of time that will be spent in each of the three states.

Solutions for A

The easiest equation to solve is that describing the evolution of the amount of molecule in the neurite, A .

Fokker-Planck

Let $f(A, t)$ be the probability density of A at time t ; we have:

$$\begin{aligned} f(A, t + \Delta t) &= \int f(A - A', t) P_{\Delta t}(A'|t, A - A') dA' \\ &= f(A, t) - f \partial_A \langle \Delta A \rangle - \langle \Delta A \rangle \partial_A f + \frac{1}{2} f \partial_A^2 \langle (\Delta A)^2 \rangle \\ &\quad + \partial_A f \partial_A \langle (\Delta A)^2 \rangle + \frac{1}{2} \langle (\Delta A)^2 \rangle \partial_A^2 f. \end{aligned}$$

⁴ see “Modeling an extending growth cone” (subsection 4.2.1), “Extension, retraction, and pausing”.

Hence:

$$\partial_t f = -\frac{1}{\tau}f + \left(\frac{A_m}{\tau_A} - \frac{A}{\tau}\right) \partial_A f + \frac{\sigma_\xi^2}{2} \partial_A^2 f = \partial_A \left[\frac{1}{\tau} (A_M - A)f + \frac{\sigma_\xi^2}{2} \partial_A f \right] \quad (\text{G.4})$$

with the boundary condition, since $A \geq 0$,

$$\forall t, \partial_A f(0, t) = 0. \quad (\text{G.5})$$

Permanent regime

Once the permanent regime is reached, the Fokker-Plank equation (G.4) becomes:

$$\partial_A \left[\frac{1}{\tau} (A_M - A)f + \frac{\sigma_\xi^2}{2} \partial_A f \right] = 0 \quad (\text{G.6})$$

Hence $\frac{1}{\tau} (A_M - A)f + \frac{\sigma_\xi^2}{2} \partial_A f = 0$ (regularization at $A \rightarrow \infty$).

Thus $\ln(f) = -\frac{1}{\tau\sigma_\xi^2} (A - A_M)^2 + \text{cst}$, which leads to:

$$f(A) = \frac{1}{\sigma_\xi \sqrt{\pi\tau}} \left[\exp\left(-\frac{(A - A_M)^2}{\sigma_f^2}\right) + \exp\left(-\frac{(A + A_M)^2}{\sigma_f^2}\right) \right] \quad (\text{G.7})$$

where $\sigma_f = \sigma_\xi \sqrt{\tau}$.

Average trajectory

The solution of the average variable $\langle A \rangle$ is given by:

$$\langle A \rangle(t) = A_M + (A_0 - A_M)e^{-t/\tau}. \quad (\text{G.8})$$

Solution for one growth cone

$$\begin{cases} \dot{a} = -\kappa a + \frac{A}{\tau_d} + \chi \\ \dot{A} = \frac{1}{\tau} (A_M - A) + \xi \end{cases} \quad (\text{G.9})$$

This leads to the average and squared average:

$$\langle \Delta a \rangle = -\kappa \langle a \rangle \Delta t + \frac{A}{\tau_d} \Delta t + o(\Delta t) \quad (\text{G.10})$$

$$\langle (\Delta a)^2 \rangle = \sigma^2 \Delta t + o(\Delta t). \quad (\text{G.11})$$

Average trajectory

The average equation for A , in turn, leads to (if $\kappa \neq \tau^{-1}$):

$$\langle a \rangle(t) = \frac{A_M}{\kappa\tau_d} + \langle a \rangle_0 e^{-\kappa t} + \frac{\tau}{\tau_d(\tau\kappa - 1)} (A_0 - A_M) e^{-t/\tau} \quad (\text{G.12})$$

or to

$$\langle a \rangle(t) = \frac{A_M}{\kappa\tau_d} + \langle a \rangle_0 e^{-\kappa t} + \frac{A_0 - A_M}{\tau_d} t e^{-\kappa t} \quad (\text{G.13})$$

if they are (we do not consider this case since we will use $\kappa \gg \tau_A^{-1}, \tau_d^{-1}$).

Conditional Fokker-Planck

Let $g_A(a, t) = f(a, t|A)$ be the conditional distribution for a at fixed A .

As for $f(A, t)$ before, we obtain:

$$\begin{aligned} g_A(a, t + \Delta t) &= \int g_A(a - a', t) P_{\Delta t}(a'|t, a - a') da' \\ &= g_A(a, t) - g_A \partial_a \langle \Delta a \rangle - \langle \Delta a \rangle \partial_a g_A + \frac{1}{2} g_A \partial_a^2 \langle (\Delta a)^2 \rangle \\ &\quad + \partial_a g_A \partial_a \langle (\Delta a)^2 \rangle + \frac{1}{2} \langle (\Delta a)^2 \rangle \partial_a^2 g_A, \end{aligned}$$

which gives

$$\partial_t g_A = -\kappa g_A - \left(\frac{A}{\tau_d} - \kappa a \right) \partial_a g_A + \frac{\sigma^2}{2} \partial_a^2 g_A \quad (\text{G.14})$$

$$= \partial_a \left[\left(\kappa a - \frac{A}{\tau_d} \right) g_A + \frac{\sigma^2}{2} \partial_a g_A \right]. \quad (\text{G.15})$$

With the boundary condition ensuring $a \geq 0$,

$$\forall t, A, \quad \partial_a g_A(0, t) = 0. \quad (\text{G.16})$$

Permanent regime

As for A , in the permanent regime we obtain a truncated Gaussian distribution which is centered around $A_M/(\kappa\tau_d)$:

$$\kappa \left(a - \frac{A_M}{\kappa\tau_d} \right) g_A + \sigma^2 \partial_a g_A = 0, \quad (\text{G.17})$$

which leads to

$$g_A(a) = \frac{1}{\sigma} \sqrt{\frac{\kappa}{\pi}} \left[\exp \left(-\frac{(a - A_M/(\kappa\tau_d))^2}{\kappa\sigma^2} \right) + \exp \left(-\frac{(a + A_M/(\kappa\tau_d))^2}{\kappa\sigma^2} \right) \right]. \quad (\text{G.18})$$

From this probability density, we can deduce the fraction of time spent in each of the three states (elongating, retracting, stalled), by computing the integral of g_A on the intervals $[0, \theta_r]$, $[\theta_r, \theta_e]$, and $[\theta_e, \infty[$, which though they involve the error function, can be easily evaluated using any numerical library such as `numpy`.

Several interacting growth cones

Furthermore, for several interacting growth cones, the total amount of molecule present in all the tips also follows the same equation, which enables to qualitatively assess their behavior.

Indeed, in the deterministic limit, if the weight of one of the growth cones is much greater than the other, then one recovers the case of the single growth cone for that neuron, while all other neurons will fluctuate around zero with a deviation σ — see discussion in “Growth cone splitting” (subsection 4.3.1).

In the limit where the deterministic flux is negligible compared to the stochastic fluctuations, then region between the two fixed points is randomly explored.

Limit for the stochastic dynamics is given by:

$$\sigma \gg \frac{A_M}{2\kappa\tau_d} \sqrt{4 \frac{\zeta_1^2 + \zeta_2^2}{(\zeta_1 + \zeta_2)^2} - 2}, \quad (\text{G.19})$$

which goes to zero as ζ_1 and ζ_2 become close.

Appendix H

Modeling the environment

H.1 Principle of growth cone sensing

As shown on Figure 4.6 in the main text, the environment sensing is based on the information gathered by the filopodia in each of their specific direction.

Wall affinity

When a neurite i touches a wall, the affinity in the direction θ_i is set to the user-defined value of the wall affinity, a_w .

If this affinity is greater than the default affinity for the substrate of the current area, then growth cones tend to follow the walls, as shown of Figure 4.7. In the other scenario, if the wall affinity is smaller than the substrate affinity, then growth cones tend to avoid obstacles.

Areas and crossing

DeNSE enables to divide the environment into **Areas** which possess specific properties.

Each area can modulate the growth cones' properties, either increasing or decreasing their speed, angular aperture, or substrate affinity.

Furthermore, areas can have different heights, which affects how growth cones will behave when trying to cross from one area to another.

Overall, for a growth cone trying to cross from area 1 to area 2, the difference in affinity will be compared based on a_1 and a_2 , the two substrate affinities, as well as h_1 and h_2 , their heights.

If h_1 and h_2 are the same, then the probability of crossing to area 2 is simply given by $a_2/(\sum_j a_j)$, with a_j the affinity in the other directions. If $h_2 < h_1$, then the probability of going down to area 2 is modulated by a descent probability p_{down} , to account for the fact that growth cone may also follow the edge. Probability of crossing then becomes $p_{down} \cdot a_2/(\sum_j a_j)$. Eventually, if $h_2 > h_1$, then the height difference Δh between the two areas is tested and the probability is modulated by an exponential decrease with Δh and becomes $a_2 \cdot \exp(-\Delta h/l_c)/(\sum_j a_j)$. Experimentally, it seems that the critical length l_c above which the growth cone can no longer climb up is rather small (a few microns).

H.2 Making the forward step

Testing the total probability

As shown on Figure 4.6, the overall affinities in each direction define a non-normalized probability distribution. The sum of the probabilities in every direction gives the

total step probability P_s . If $P_s \geq 1$, the step is performed; however if $P_s < 1$, then the step is performed with probability P_s — a random number in $[0, 1]$ is drawn and compared to P_s .

Validating the step

Once the step is validated, a direction is chosen based on a sampling algorithm (directions with highest affinity are more likely to be chosen). If the line between the target position and the current position intersects the environment, then the step is forbidden because it would lead the growth cone to leave the inner environment. In that case, the angle is progressively moved toward the closest angle inside the environment, until the line no longer intersects the border of the environment.

Interaction-based retraction

As shown previously, forward moves are not performed systematically, and a growth cone can sometimes stop moving, either because the probability of making a step is too low, or because all possible moves are actually forbidden (they would step out of the environment); in that case, the growth cone is said to be *stalled*. When a growth cone is stalled and cannot perform any forward move, then it has a probability p_r of undergoing an interaction-based retraction. Until this retraction happens, the growth cone remains stalled in its current position.

Appendix I

Branching models

I.1 Growth cone split

Resource- and pull-driven split

Similarly as for the fraction of time spent in the elongating, retracting, and pausing stages that was described in “Critical resource and competition” (section G.4), one can use the analytic probability density function of the amount of resource at the tip of a growth cone to compute its branching probability in time.

As discussed in “Growth cone splitting” (subsection 4.3.1), even in the situation where one growth cone should theoretically obtain the whole resource, the fluctuations in the amount received by the other cones is sufficient to make the remaining resource go to zero. Thus, unless the fluctuation amplitude (given by σ) is on the order of the branching threshold θ_b — which would be biologically unrealistic — the branching rate will eventually go to zero.

In the future, the implementation of a pull-driven split, with the detection of bimodal pull distribution — in the case of two separate areas of high affinity, or two guidance cues — is also planned.

Implementation of the branching times

The resource-driven split is unpredictable and occurs immediately when a growth cone reaches an amount of resource greater than θ_b , if the probabilistic test is positive¹.

Van Pelt branching, on the other hand, occurs at pre-determined times, depending on the base branching rate B and the number of growth cones, as given in equation 4.14.

The branching times are thus sampled from a Poisson process with a rate given by the Van Pelt equation.

I.2 Lateral branching

In the two lateral branching models, the branching events follow a Poisson distribution with a constant rate r_b .

In the case of the uniform branching, a branch is elected randomly to support the emerging growth cone, and a point on this branch is also chosen at random.

For the distance-dependent case, on the other hand, a *growth cone* is selected randomly, and a point on this branch, or on a parent branch going down towards the soma is selected based on a power-law distribution of exponent γ .

¹ because the branching occurs with a probabilistic rate $r_b = \frac{a-\theta_b}{a+\theta_b} R_b$, the algorithm draws a random number $r \in [0, 1]$ and tests whether $r_b \cdot dt > r$.

I.3 Quantifying and analyzing branching patterns

Tree and partition asymmetry

Partition asymmetry: for a tree having T terminal segments (tips), the asymmetry of its structure is recursively defined as the mean of all subpartitions of this tree.

For a given partition of size $n \geq 2$ at a branching point, let us call l and r the size of the two subpartitions such that $n = l + r - 2$ (the common branching point is counted in both subpartitions). The asymmetry a of this partition is then given by:

$$a = \frac{|l - r|}{n}. \quad (\text{I.1})$$

For a complete neurite tree, the global asymmetry is thus given by the average of the $T - 1$ possible partitions:

$$A = \frac{1}{T - 1} \sum_{k=1}^{T-1} a_k. \quad (\text{I.2})$$

The main drawback of this measure, as detailed in (K. M. Brown et al. 2008; Van Pelt, H. B. Uylings, et al. 1992), is that its value does not vary in $[0, 1]$, but in $[0, a_{max,T}]$, with $\lim_{T \rightarrow \infty} a_{max,T} = 1$.

However, it is possible to compute $a_{max,T}$ analytically, because in the most asymmetric case, one of the subpartitions is always of size 2:

$$a_{max,T} = \frac{1}{T - 1} \sum_{k=1}^{T-1} \frac{2(T - k) - 2}{2(T - k)} \quad (\text{I.3})$$

$$= 1 - \frac{1}{T - 1} \sum_{k=1}^{T-1} \frac{1}{T - k} \quad (\text{I.4})$$

$$= 1 - [\psi^{(0)}(T) + \gamma], \quad (\text{I.5})$$

with:

$\psi^{(0)}$ the digamma function,

$\gamma = -\psi^{(0)}(1)$ the Euler–Mascheroni constant.

In this thesis, all asymmetry values for trees composed of T tips were therefore renormalized by $a_{max,T}$, in order to always have an asymmetry of 1 to characterize the most asymmetric trees, regardless of their size.

Sholl analysis

The Sholl analysis (Sholl 1953) consists in looking at how many branches of a neuron or neurite are present at a given distance from the soma. By plotting the number of intersections between concentric circles starting from the soma and a neuron's or neurite's arbor, one can thus characterize how the number of branches evolves with the distance to the soma. The histograms of the number of intersections at a given distance then convey intuitively some of the characteristics of the branching patterns involved, as show on the Figures in “A complete neurite tree” (subsection 4.4.1).

Appendix J

Papers

This chapter contains the papers that were published during my PhD, concerning the percolation of activity in bursting neuronal networks (Fardet, Bottani, et al. 2018; Monceau, Renault, Mérens, Bottani, and Fardet 2017), as well as a detailed model on the influence of adaptation on synchronous bursting (Fardet, Ballandras, et al. 2018). A more intuitive and visual description of Fardet, Ballandras, et al. 2018 is detailed in “A concise model for periodic bursting” (subsection 2.2.1).

J.1 Review on percolation (IOP Conf. Series 2017)

This paper reviews the results obtained by the Quorum Percolation (QP) model to describe the response of a neuronal network to an external excitation. It further describes how variability in the neuronal properties and the presence of decay (accounting for the neuronal relaxation during the transmission delay) do not prevent the occurrence of the percolation phenomenon. Eventually, I discuss how the percolation formalism may also prove useful to describe activity patterns that are not triggered externally, but result from the intrinsic activity of the neuronal network.

Phase transition approach to bursting in neuronal cultures: quorum percolation models

P Monceau^{1,2}, R Renault¹, S Méstens¹, S Bottani¹ and T Fardet¹

¹Laboratoire Matière et Systèmes Complexes, UMR 7057 CNRS, Université Denis Diderot-Paris 7, 10 rue A. Domon et L. Duquet, 75013 Paris Cedex, France.

²Université d'Evry-Val d'Essonne, France.

E-mail: Pascal.Monceau@univ-paris-diderot.fr

Abstract. The Quorum Percolation model has been designed in the context of neurobiology to describe bursts of activity occurring in neuronal cultures from the point of view of statistical physics rather than from a dynamical synchronization approach. It is based upon information propagation on a directed graph with a threshold activation rule; this leads to a phase diagram which exhibits a giant percolation cluster below some critical value m_C of the excitability. We describe the main characteristics of the original model and derive extensions according to additional relevant biological features. Firstly, we investigate the effects of an excitability variability on the phase diagram and show that the percolation transition can be destroyed by a sufficient amount of such a disorder; we stress the weakly averaging character of the order parameter and show that connectivity and excitability can be seen as two overlapping aspects of the same reality. Secondly, we elaborate a discrete time stochastic model taking into account the decay originating from ionic leakage through the membrane of neurons and synaptic depression; we give evidence that the decay softens and shifts the transition, and conjecture that decay destroys the transition in the thermodynamical limit. We were able to develop mean-field theories associated with each of the two effects; we discuss the framework of their agreement with Monte Carlo simulations. It turns out that the critical point m_C from which information on the connectivity of the network can be inferred is affected by each of these additional effects. Lastly, we show how dynamical simulations of bursts with an adaptive exponential integrate-and-fire model can be interpreted in terms of Quorum Percolation. Moreover, the usefulness of the percolation model including the set of sophistication we investigated can be extended to many scientific fields involving information propagation, such as the spread of rumors in sociology, ethology, ecology.

Keywords: Phase transitions general studies, neural networks, percolation, complex networks.

1. Introduction

In vitro cultures of dissociated neurons have turned out to be a powerful tool in investigating fundamental questions in several scientific fields. From a conceptual point of view, compelling issues comprise the nature of biological computations, the mechanisms of information spreading throughout networks, and the understanding of collective behaviors [1], as these questions could bring new elements to the understanding of neuronal computation and to the field of artificial intelligence. Moreover, neuronal cultures are suitable for pharmaceutical drugs experimentation and have been useful in studying neurodegenerative diseases [2]. Lastly, populations of neurons could be the basic units in designing computational devices involving real living cells [3]. Experimentally, such cultures can be obtained by seeding dissociated neurons extracted from



rodent embryos on a suitable substrate; axons and dendrites grow in such a way that neurons self-organize after a few days into a quasi two-dimensional network [4]. The cells can be maintained alive several weeks and display sustained electric activity. Let us recall that there are about 10^{11} neurons in the human brain, each of them being connected to 7 000 others on average through synapses; hence, it is a very complex network where neurons are organized in localized computational units connected according to a well defined hierarchical structure. However, *in vitro* cultures establish very different connectivity patterns during their growth [3] since they are characterized by a higher level of randomness. The neuronal cultures we are interested in hold between 10^3 and 10^5 neurons with typical densities between 500 and 5 000 neurons per mm^2 , each of them connected via a number of synapses falling between 20 and 200. These changes in connectivity and scale which could at first glance appear as a loss from a neurobiologic point of view are largely compensated by the benefits associated with *in vitro* experimentation. The recent development of techniques such as micro-electrode arrays (MEA), [5] optogenetics and calcium imaging [6, 7] enables the experimentalists to carry out quantitative measurements inaccessible *in vivo*. Furthermore, more precise control over the system can now be attained: physicochemical parameters such as extracellular ionic concentrations can be modified [8], drugs can be injected [4], neurons can be electrically or optically excited. Microfabrication techniques are now also used to structure the connectivity between sub-populations by constraining mechanically the axon growth with obstacles or designed channels [3] in order to build *in silico* models of brain structures or build neuronal devices designed for specific functions [9]. Both *in vitro* and *in vivo*, neuronal rhythms are a widespread phenomenon observed at many temporal and spatial scales. Synchronized periodic bursts of spiking activity emerge spontaneously in cultures of dissociated neurons from rodent hippocampus and cortex [8, 10], depending on their density and age. Furthermore, bursts can be triggered by initially activating a fraction of neurons. Rather than describing collective behaviors observed in living neuronal networks grown *in vitro* in terms of synchronization [11, 12], the Quorum Percolation model (QP) tackles the issue of population wide activation from the point of view of statistical physics. The Quorum Percolation model, derived from bootstrap percolation, has been specifically designed to describe activity bursts observed in such cultures [13]. Under its original form, it is a discrete time dynamics model of information propagation on a directed graph, built up according to a simplification of the most relevant biological features: the neurons, located at the nodes of the graph, are two state systems whose activation is governed by a threshold (Quorum) rule. A burst is seen as a discontinuity in the activity of the network, interpreted as the occurrence of a giant excited cluster. We further refined the model by introducing the following biological relevant developments:

- (i) Modulation of the neurons excitability. As a matter of fact, neuronal cultures exhibit some variability in the neuron excitability; we study the modifications induced in the behavior of a Quorum Percolation model by taking into account an uncorrelated Gaussian variability of the neuronal thresholds.
- (ii) Decay of the subthreshold neuron voltage. The decay accounts for ionic leakage through the membrane of neurons, since they do not behave as perfect capacitors; we take it into account in a Quorum Percolation with Decay (DQP) where we model the decay by a discrete time disintegration process of the membrane potential of the neurons.

2. Phase diagram and critical behavior of the original quorum percolation model

The networks we deal with includes N neurons, where each of them is a two-level system which can be either active or at rest. A directed network is constructed by randomly choosing, for each neuron i , k incoming links among the $N - 1$ other neurons according to an in-degree probability distribution p_k . Experimental results and their interpretation through the original

Quorum Percolation model suggest that the connectivity of mature *in vitro* cultures can be approximated by a random oriented graph with Gaussian distribution of incoming links [10]; hence, in the following, we will restrict ourselves to such networks, where \bar{k} denotes the mean value of p_k and σ_k its standard deviation. The construction of such networks does not require information on the geometrical location of neurons in the physical space. Thus, we deal with percolation on a random graph without taking in account any spatial metric. Starting at time $t = 0$ from an initial state of the network where a given fraction f of randomly chosen neurons is set active, information spreads through the network according to an excitability threshold rule. A neuron i becomes active if a given number m (called quorum) of its k incoming neighbors are active. The activation process of the network is described by a discrete-time dynamics with a step Δt during which each neuron integrates the signals sent by its incoming neighbors. A discrete variable $V_i(t)$ – accounting for the membrane potential – is assigned to each neuron i . The transition from one time step to the next obeys the following rules:

- (1) Every neuron i activated between $t - \Delta t$ and t sends at time t one signal to each of its neighbors through its outgoing links; no further signals will be sent by such an activated neuron at later times. Each sent signal has the same weight and is associated to an integer increment equal to +1.
- (2) The variable $V_i(t)$ of each target neuron at rest is incremented by the sum of the inputs received at time t .
- (3) If $V_i(t)$ is greater than or equal to the activation threshold m , the neuron i fires, which means that it switches from the resting state (at time t) to the active state (at time $t + \Delta t$).
- (4) Once a neuron has been activated, it remains in the active state until the end of the process.

The macroscopic activity state of a network at time t is the fraction of its active neurons. Once a random network, and a random initial state have been drawn, the discrete-time dynamics described above is deterministic, monotonically increasing, and leads to an equilibrium state of the network characterized by a final fraction Φ of active neurons. Explicit simulations aim at directly calculating the response Φ of a finite-size network of N neurons, from an initial excitation parametrized by the fraction f of initially activated nodes. Given a set of parameters $\{\bar{k}, \sigma_k\}$, and m , a Monte-Carlo run consists of the following steps:

- (i) A random directed network \mathcal{G} is constructed according to the incoming links probability distribution p_k .
- (ii) A fraction f of neurons is randomly activated.
- (iii) The discrete time process described above goes on until the number of active neurons stops increasing, i.e. when the stationary state has been reached.

The average value of Φ is then calculated over several runs. A typical phase diagram is shown on Fig. 1 where two regimes can be distinguished as m varies, for fixed values of \bar{k} and σ_k . Such a phase diagram provides a good description of experiments carried out in the group of E. Moses [4, 13]. Below some critical value m_C , the final fraction of activated neurons presents a discontinuity when we vary the control parameter f (the initial fraction of activated neurons), whereas it remains continuous above m_C . The sudden jump occurring at f^* in the global activity Φ is associated with a percolation transition on the network \mathcal{G} , where a very small variation of f results in the appearance of a giant cluster, whose normalized size g is given by the difference between the lower and upper values of ϕ at the discontinuity. Once p_k is fixed, following the usual concepts of percolation on lattices [14], the normalized mean cluster size $\langle g \rangle$ can be considered as an order parameter whose behavior in the vicinity of m_C is given by a power law: $\langle g \rangle \sim \left(\frac{m_C - m}{m_C} \right)^\beta$.

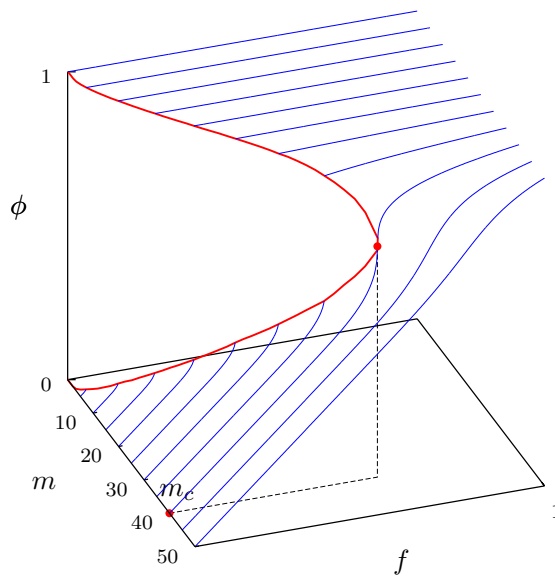


Figure 1. Phase diagram of the Quorum Percolation model, for a Gaussian "in-connectivity" with $\bar{k} = 50$ and $\sigma_k = 10$. When the quorum m is smaller than m_C , a jump in the fraction of active neurons Φ occurs when increasing the fraction f of initially activated neurons from zero. The height $\langle g \rangle$ of the jump at the discontinuity is the normalized size of the percolation giant cluster.

As a main result, it should be noticed that the critical behavior of $\langle g \rangle$ provides information on the connectivity of the network [10, 13]. It is tricky to calculate the critical exponent β , since the quorum percolation model is discrete; however we were able to derive an extension of the QP model to continuous values of m with the help of a mean-field approach in good agreement with Monte-Carlo simulations [15, 16]. A numerical resolution of the associated highly nonlinear self-consistent equation led to a value very close to the classical mean-field exponent $\beta = 1/2$ when p_k is Gaussian. This value, associated with a Gaussian distribution of incoming links, is in agreement with experimental results. Furthermore, the critical value has been shown to depend on \bar{k} and σ_k as $m_C \approx \bar{k} - 1.3\sigma_k$. Hence the position of the critical point provides quantitative information on the mean value and width of the Gaussian connectivity distribution.

3. A quorum percolation model with quorum variability

Unlike the original QP model where the quorum takes the same value over the whole set of neurons, we introduce disorder on the excitability by randomly setting each node's quorum to an integer value according to some probability distribution \mathcal{P}_m – with no correlation to other network properties. Thus, the Monte-Carlo algorithm described in section 2 includes an additional stage just after the first one, where such a disorder on the quorums is implemented. ϕ must be averaged over the three sets of associated configurations, that is a set of initial configurations associated to f , a set of quorums related to \mathcal{P}_m and a set of networks realizations based on p_k .

3.1. Mean-field theory

An alternative approach for calculating ϕ can be deduced from a mean-field treatment: the probability for a neuron to be active at equilibrium corresponds to the probability to be either active through initial stimulation or to be activated during the QP discrete time process; the activation probability of a neuron – given m and k – can be approximated by a binomial process depending upon ϕ . Since the activation of a neuron can occur only if at least m incoming links are linked to active neighbors, such an activation probability reads $\sum_{l=m}^{\infty} \binom{k}{l} \Phi^l (1 - \Phi)^{k-l}$. In the end, we obtain the following self-consistent equation:

$$\frac{\Phi - f}{1 - f} = \sum_{m=1}^{\infty} \mathcal{P}_m \sum_{k=m}^{\infty} p_k \sum_{l=m}^k \binom{k}{l} \Phi^l (1 - \Phi)^{k-l} = \sum_{k,m} \Pi(m, k) \sum_{l=m}^k \binom{k}{l} \Phi^l (1 - \Phi)^{k-l} \quad (1)$$

where the right-hand term accounts for the total activation probability $\mathcal{P}^{act}(\Phi)$ of a neuron of the network. The solutions of the self-consistent equation (1) are given by the intersection points of $\mathcal{P}^{act}(\Phi)$ with the line of slope $1/(1 - f)$ passing through the point of coordinates (1, 1) in the $\{\Phi, \mathcal{P}_m^{act}(\Phi)\}$ plane. Assuming that \mathcal{P}_m and p_k are Gaussian probability distributions with respective average values \bar{m} and \bar{k} and variances σ_m and σ_k , the self-consistent equation involves a truncated bidimensional Gaussian probability distribution. As a first result, it turns out that the qualitative behavior of the solutions for Φ is close to the one observed in the absence of disorder. When numerically solving equation (1) in the physically meaningful range [0,1] of f , two regimes can be distinguished: For m smaller than a critical value m_C now depending on the additional parameter σ_m , there is a range $f \in]f_0, f^*[$ where three different real values of Φ satisfy (1). For $m > m_C$, a single real value of f satisfies (1). Since the QP process requires Φ to be an increasing function of f , the physical behavior of Φ resolves the existence of an unstable branch below m_C in this range by a discontinuity at f^* associated with the appearance of the giant cluster; the normalized size of this cluster is equal to the difference between the lower Φ^- and the upper Φ^+ solutions of equation (1) at the border between the two regimes. Situations showing the evolution of the jump in Φ for two different values of σ_m are displayed on Fig. 2.

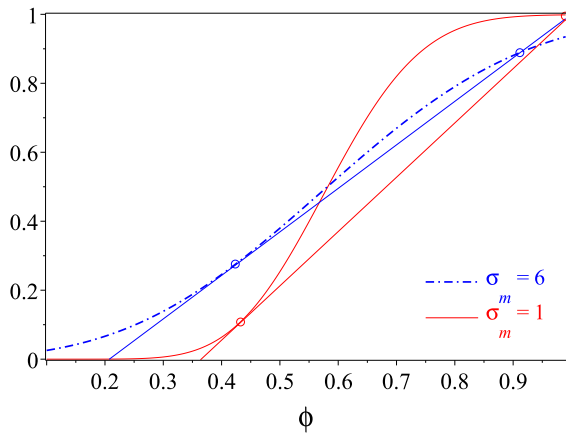


Figure 2. Evolution of $\bar{\mathcal{P}}^{act}(\Phi)$ for $\bar{k} = 25$, $\sigma_k = 3$ and $\bar{m} = 15$ and two different values of σ_m . The open circles represent the intersections of the curves $\bar{\mathcal{P}}^{act}(\Phi)$ with the lines \mathcal{D} of slopes $1/(1 - f)$ giving the two solutions ϕ^- and ϕ^+ of equation (1) associated with the percolation clusters.

3.2. Simulation results

Results reported on Fig. 3 provide a picture of the main conclusions that can be drawn out from a large set of Monte Carlo simulations and numerical resolutions of equation (1).

- (i) There is a good agreement between the mean-field and Monte Carlo approaches at least within the range of physical parameters involved in the quantitative description of neuronal cultures with Gaussian in-degree.
- (ii) For a fixed value of \bar{m} , increasing the variance σ_m shifts the position of the jump in Φ towards lower values of f and reduces the size of the giant cluster (unless \bar{m} is “too small”, in which case a slight bump can appear in the variation of g with σ_m).
- (iii) \bar{m} being fixed, a large enough amount of disorder (σ_m) on the excitability can destroy the percolation transition ($\sigma_m = 32$ on Fig. 3).

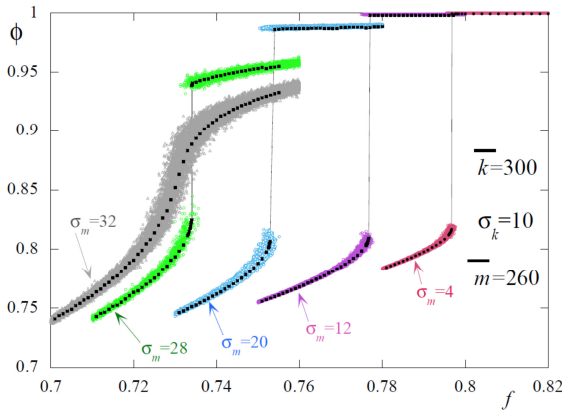


Figure 3. Evolution of the activity of the network when increasing σ_m at a fixed value of \bar{m} obtained by explicit simulations with $N = 100\,000$ neurons (clouds of points) and self-consistent equation (black dots). Notice the agreement between the two approaches and the vanishing of the percolation transition when the disorder width σ_m is large enough.

- (iv) The position of the critical point m_C depends not only on \bar{k} and σ_k , but also on σ_m ; as long as the jump in ϕ survives, m_C decreases when σ_m increases.

An interpretation of some of the preceding conclusions can be done by looking at the truncated bidimensional Gaussian probability distribution $\Pi(m, k)$ involved in the activation probability. The initially excited nodes are uniformly drawn over the whole distribution, but the nodes liable to be involved in the network activation must satisfy $m \leq k$ in order to be excitable; hence, they lie under the bisecting line in the (m, k) plane. Two competitive effects arise when increasing σ_m from zero: a fraction of nodes, associated with the part of $\Pi(m, k)$ below \bar{m} becomes more easily excitable, while the other fraction becomes less easy or even – when they cross the bisecting line – impossible to excite. The neurons below \bar{m} are responsible for the shift of $\langle f^* \rangle$: the ignition mechanism of the giant cluster needs a smaller fraction of initially excited nodes, but a larger spread of activity throughout the network since $(\Phi^- - \langle f^* \rangle)$ increases with σ_m as shown in the example displayed Fig. 3. Moreover, as can be seen on Fig. 2, the sigmoids associated with the activation probability $\mathcal{P}^{act}(\Phi)$ become less steep when σ_m increases, leading to smaller values of the slope of the line tangent to this curve at the point Φ^- , hence to a decrease in f^* . Since Monte Carlo simulations showed that we can rely on the mean field theory to describe a Quorum Percolation with excitability disorder, a prolongation to non integer values of m with the help of Beta functions enables to investigate properly the critical region [15]. As a main result a normal form treatment of the prolonged self-consistent equation leads to the same power law behavior as in the case without disorder, that is $\langle g \rangle \propto \left(\frac{m_C(\sigma_m) - m}{m_C(\sigma_m)} \right)^{1/2}$. Nevertheless it is worth noticing that m_C depends on the additional parameter σ_m ; hence the relation $m_C \approx \bar{k} - 1.3\sigma_k$ cannot be used to infer the values of the connectivity parameters.

3.3. Finite size analysis of the fluctuations

A detailed study of finite-size effects is of great interest from an experimental point of view, since measurements are always carried out on finite neuronal populations. A finite-size scaling in the vicinity of the critical point cannot be done from the standard point of view of percolation [14], since it relies on a comparison between the linear size of the network and some correlation length, quantities which do not make sense in the present case of percolation on a graph, where the dimensionality of the system and the metric are not defined. Recalling that, in the presence of quorum disorder, the physical quantities calculated from Monte Carlo simulations are averaged over three sets of configurations, special attention must be paid to the study of sample to sample fluctuations. Moreover, such fluctuations which are linked to self-averaging properties can exhibit very unusual properties in the vicinity of a critical point [17, 18]. A large set of parameters $\{\bar{k}, \sigma_k, \bar{m}, \sigma_m\}$ has been investigated by means of intensive Monte Carlo simulations

for different sizes ranging from $N = 10^3$ to $N = 2.5 \times 10^6$. As a main result we found that the relative fluctuations decrease as power laws of the network sizes: $\langle \Delta g \rangle / \langle g \rangle \sim N^{-\gamma}$ and $\langle \Delta f^* \rangle / \langle f^* \rangle \sim N^{-\zeta}$ and that fluctuations of the order parameter f are always larger than the fluctuations of the jump positions; moreover, the fluctuations in g increase as \bar{m} increases, approaching the critical value m_C as expected from a second order phase transition. On the other hand, the fluctuations in g and f^* increase as the threshold disorder σ_m is increased (for a given value of \bar{m}), the exponents associated with the power laws exhibit an universal character, since no significant difference in these exponents can be brought out from the set of simulations we carried out: $\zeta = 0.495(10)$ and $\gamma = 0.29(15)$. Therefore, a finite-size analysis of the fluctuations does not enable the direct detection of disorder on the quorum. Let us recall that, in the case of networks with a linear size L in a D dimensional space, a quantity \mathcal{O} is said to be strongly self-averaging if $[\langle \Delta \mathcal{O} \rangle / \langle \mathcal{O} \rangle]^2 \sim 1/N = L^{-D}$ and weakly self-averaging if $[\langle \Delta \mathcal{O} \rangle / \langle \mathcal{O} \rangle]^2 \sim L^{-a}$ where $0 < a < D$ [17]. Hence, it turns out that f^* is practically strongly self-averaging since $[\langle \Delta f^* \rangle / \langle f^* \rangle]^2 \sim N^{-1}$ whereas the order parameter is weakly self-averaging independently of the physical parameters, in particular the threshold disorder.

3.4. Subcritical behavior: disorder-independent fixed points

We investigated the effects of threshold disorder on the behavior of the network activity for values of \bar{m} and σ_m such that no percolation occurs anymore. An example of the results obtained by Monte Carlo simulations is shown on Fig. 4.

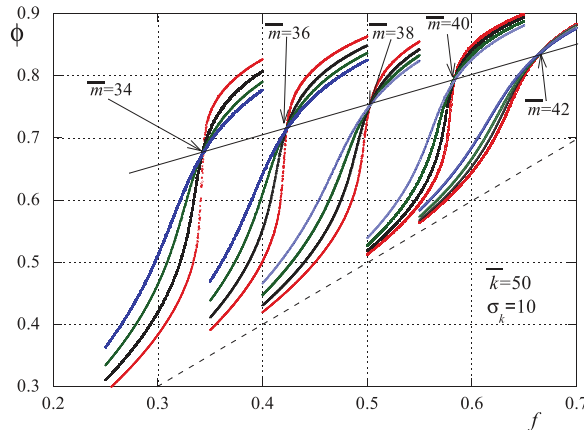


Figure 4. Disorder independent fixed points in the supercritical region with $\bar{k} = 50$, and $\sigma_k = 10$ for different values of \bar{m} indicated inside the figure and each time four different values of σ_m (increasing from red to blue): [11, 14] when $\bar{m} = 34$, [9, 12] when $\bar{m} = 36$, [7, 10] when $\bar{m} = 38$, [3, 6], when $\bar{m} = 40$, [2, 5], when $\bar{m} = 42$. The dotted line corresponds to $\Phi = f$.

The most striking result is the emergence of disorder independent fixed points: the mean activity of the network, for a given \bar{m} and a given f_{FP} is independent of the width of the threshold distribution over a large range of σ_m . Furthermore, it turns out that the activity Φ_{FP} at the fixed point and f_{FP} follow a universal law, since they line up along the straight line $\Phi_{FP} = \frac{1}{2}(1 + f_{FP})$ independently of \bar{k} and σ_k . Hence the fixed points occur right when the activation probability is equal to $\frac{1}{2}$. This can be interpreted if we remember the evolution of $\mathcal{P}^{act}(\Phi)$ with σ_m : the evolution observed on Fig. 2 has the same profile when Eq. (1) has a single solution. Below Φ_{FP} , an increase in σ_m enhances the activity propagation, while it has the opposite effect above. Therefore, the two competitive effects, arising between the more easily and less easily excitable populations when σ_m is varied, balance exactly at the fixed point.

3.5. Discussion: connectivity, excitability and disorder

With regard to experiments carried out on neuronal networks, m was tuned by drugs [13] and \bar{k} and σ_k deduced from simulations fitting the experimental data in the critical region assuming an uniform excitability. Since the critical value of the quorum depends on σ_m , the hypothesis that no threshold disorder is present can lead to wrong estimations of the connectivity parameters

of the network. The results reported in section 3 show that the excitability and connectivity distribution widths quantified by σ_k and σ_k are intricately connected. There is some kind of equivalence between connectivity and excitability, which was noted by J. P. Eckmann et al. [19]. In fact, as already pointed out in the case of neuronal cultures, connectivity and excitability can be seen as two overlapping aspects of the same reality: the addition of synaptic blockers – used to increase the control parameter m – can also be interpreted as a weakening of the network functional connectivity [4, 13]. This is locally reflected in the model: a node whose threshold goes from m to $m + 1$ when introducing disorder needs a larger number of incoming links to fire. Roughly speaking, what matters in describing the qualitative behavior of the model is the ratio of excitability to connectivity \bar{m}/\bar{k} . However, the accessible physical quantities that can be brought out from experiments involve averaging processes from which the detailed respective roles of the connectivity driven by p_k and the excitability driven by \mathcal{P}_m are very difficult to discriminate.

4. A quorum percolation model with decay

The membrane of biological neurons can be compared to a capacitor that supports electric potential difference through ionic charge separation. Active neighbors will inject ionic currents into this capacitor, changing the electric potential difference across the membrane until it eventually passes a threshold value (associated with m in the framework of the QP model) when the neuron fires. This membrane is not a perfect capacitor as it is continuously leaking ions; hence, without new input, the membrane potential decays exponentially to its resting value with a time constant τ . In the limit where the time interval between each received signals is much larger than τ , they won't add up at all. The state of a real neuron is thus not only determined by the number of received signals, but also by their arrival times. We take into account the decay by building an extended model, (called DQP for Decay Quantum Percolation) in which each discrete accumulated signal can disintegrate independently with a probability $d \in [0, 1]$ at each step of the percolation process. Thus, the evolution of the neuronal activity is described by a discrete time stochastic process with a step Δt involving two competitive mechanisms: the reception of new signals sent by activated neurons and the decay of the accumulated signals with a characteristic time τ . The quorum is here assumed to be the same for all neurons.

A scheme of The Monte Carlo DQP process is provided on Fig. 5, and goes as follow:

- (1) Every neuron j activated between $t - \Delta t$ and t sends at time t one signal to each of its out-neighbors; no further signals will be sent by such an activated neuron at later times. Each sent signal has the same weight and is associated to an integer increment equal to 1.
- (2) The variable $V_i(t)$ of each target neuron at rest is incremented by the sum of the number of signals it has received at time t .
 - If $V_i(t)$ is greater than or equal to the activation threshold m , the neuron i switches from the state at rest (at time t) to the state active (at time $t + \Delta t$).
 - If $V_i(t)$ is smaller than m , each integer element of this potential is submitted to a Bernoulli trial of parameter d (with $0 \leq d \leq 1$) and is disintegrated if the trial is positive; the potential of the neuron at rest has decayed from its value $V_i(t)$ to $V_i(t + \Delta t)$.
- (3) Once a neuron has been activated it remains in such a state until the end of the process.

A DQP Monte Carlo run follows the same algorithm as the one described in section 2, where the discrete process of the item (3) is replaced by the process in item (2). Thus, it is as if the sum of accumulated signals decays on average exponentially with a time constant $\tau = -\Delta t / \ln(1 - d)$, within a time step Δt . If we normalize the time constant τ to the duration of an iteration *in vitro*, that is, the minimal time interval necessary to transmit activity from a neuron to another inside a culture, we can reckon the value of the decay parameter d . Taking into account the action

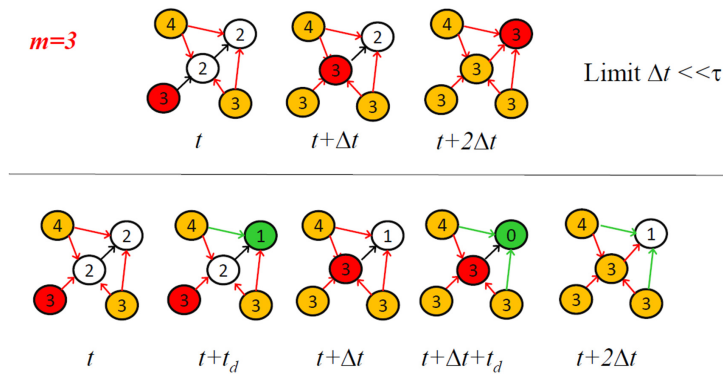


Figure 5. Mechanism of DQP model (below); the QP model is recalled above. At time t , the red neuron (left down) is activated; the orange ones (left up and down right have been activated before). At $t + t_d$, the green one (up right) encounters a decay; its potential is decreased from 2 to 1. The network is updated at $t + \Delta t$: the central neuron is activated. At $t + \Delta t + t_d$ the upper right neuron encounters once more a decay, and its potential is decreased from 1 to 0; in its updated state at $t + 2\Delta t$ it receives a signal from the centered neuron, but it is not in the same state as in the absence of decay (when $\Delta t \ll \tau$).

potential duration and propagation speed, the size of a typical culture and the synaptic delay, we can estimate that Δt lies between 1 and 10 ms and d between 0.1 and 0.01. Nevertheless, from a mean-field point of view, we were able to establish a recursive relation enabling us to fully describe the stochastic dynamics in the presence of decay [22]. The striking point is the idea that everything goes on as if the decay changes the connectivity of the network all along the process. At time t let us consider a neuron with k incoming neighbors, a potential $V_i(t) = s$ and x active neighbors ($x \geq s$ according the DQP rules); this neuron has undergone $(x - s)$ decrements due to the decay. Hence it is as if $(x - s)$ among the k incoming links had been erased. This remark enables to define a time dependent effective connectivity according to the Quorum Percolation without decay; this neuron will behave as a neuron experiencing an effective connectivity defined as $k_{eq} = k - (x - s)$. Details on the derivation of this recursive relation based on this equivalence can be found in [22].

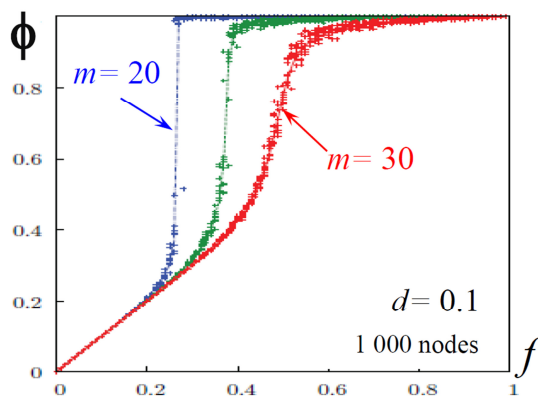


Figure 6. Comparison of a network calculated by Monte Carlo simulations (lines) and numerical resolution of the mean-field algorithm (dots); points of the same color correspond to 10 different equivalent Monte Carlo simulations. $\bar{k} = 50$, $\sigma = 10$, $d = 0.1$

Fig. 6 displays typical results where the agreement between Monte Carlo simulations and the mean-field approach can clearly be seen even when the size of the network is rather small. The effect of the decay is shown on Fig. 7 where Monte Carlo simulations are gathered together.

As a main result, the decay softens the transition, reduces the apparent size of the discontinuity, and shifts its position towards higher values of f .

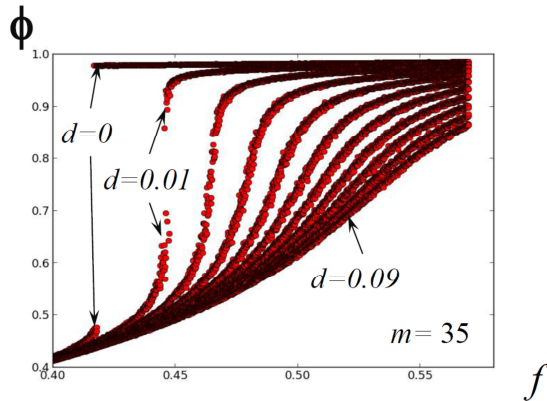


Figure 7. Evolution of the activity of a network when increasing the decay d at m constant calculated by Monte Carlo simulations. Note the decrease of the apparent size of the discontinuity with d and the vanishing of the transition if d is large enough; m_C should be equal to 0.58 without decay. $\bar{k} = 50$, $\sigma = 10$, $m=35$.

The size of the discontinuity g as a function of m was previously used [13] to infer connectivity in real neuronal networks; since decay is part of the physics of these networks, we wanted to evaluate to what extent the decay parameter d was changing those results. The value of the step ϵ between successive values of f is crucial in evaluating the size of the discontinuity; when dealing with Monte Carlo simulations on networks with N neurons, the increment in f associated with a single neuron imposes a lower bound $1/N$ for ϵ . For a given value of m , we define the apparent size of the discontinuity $g_\epsilon(m)$ as the maximum value of the difference $[\Phi(f + \epsilon) - \Phi(f)]$ with respect to f . In order to characterize properly the transition in the thermodynamical limit, when $N \rightarrow \infty$, numerical calculations of $g_\epsilon(m)$ are done in the framework of the mean-field approach; hence the evolution of $g_\epsilon(m)$ as a function of ϵ can be studied with ϵ as small as wished, approaching the real size of the discontinuity. Surprisingly, when d is non-zero, continuously decreasing ϵ leads to a steady gradual reduction of $g_\epsilon(m)$: $\forall m, \lim_{\epsilon \rightarrow 0} g_\epsilon(m) = 0$. The convergence is faster when the decay d is strong and the m/\bar{k} ratio is high, but the phenomenon was observed in every computationally accessible case, as long as d was non-zero. This strongly suggests that $g_\epsilon(m)$ always converges towards 0 when $d > 0$ and $m > 1$.

Thus, the main result of our set of computations is the conjecture that the critical point expected from the classical QP model in the thermodynamical limit vanishes in the framework of the DQP model. It also reveals how the distinction between continuous and discontinuous transitions depends both on the size of the network and the accuracy in the control of external stimulation; consequently the decay, although being part of the networks dynamics, may remain unnoticed. Lastly, a consequence of the shift in the apparent size of the discontinuity is that a model which does not take decay into account leads to an underestimation of m_C , introducing a bias in the estimation of the network connectivity parameters, since the relation $m_C \approx \bar{k} - 1.3\sigma_k$ does not hold anymore when $d \neq 0$.

5. Percolation in dynamical situations of bursting cultures

The QP model was initially designed to study bursting activity in neuronal cultures; we will discuss here how it can be applied, beyond the study of “forced” systems, to analyze spontaneous activity in neuronal cultures. We simulated networks of oscillatory excitatory neurons using the adaptive exponential integrate-and-fire model [23]. Each neuron is connected to others from a Gaussian distribution of average 100 and standard deviation 5, and the spikes are transmitted between neurons with a constant delay of 1 ms. Figure 8 shows the simulated activity, which is composed of periodic bursts with a specific inner structure. A burst is indeed composed of a succession of *synchronous burst slices* (SBS) which are the base units that we will describe, using the introduced formalism, as several distinct percolation events. Let us first describe

and explain how a burst is initiated, develops and terminates. Burst initiation comes from the intrinsic behavior of the neurons which are oscillators [8]: their membrane potential slowly depolarizes under the influence of a persistent sodium current $I_{Na,p}$ until a first spike is initiated. After an initial synchronization of the population due to phase reset and positive feedback [24], the first spikes of a burst occur concomitantly in a relatively short time period (e.g. 4510–4512 ms) and involve a large fraction of the population. This initial SBS acts as the intrinsic counterpart of the external excitation in the Quorum Percolation model since it is what activates the first neurons of the following SBS (the [4514–4516] ms slice on the inset). Thus we obtain a series of SBSs, each initiated by the input of the previous one. Moreover, the successive SBSs get wider and more sparse because of adaptation mechanisms and fatigue, which increase the quorum necessary for one neuron to activate. Since the effect of the SBS is spread over several milliseconds, taking decay into account, we eventually reach a point where the cumulative effect of the previous SBS is no longer sufficient for neurons to reach their increased quorum and the burst terminates.

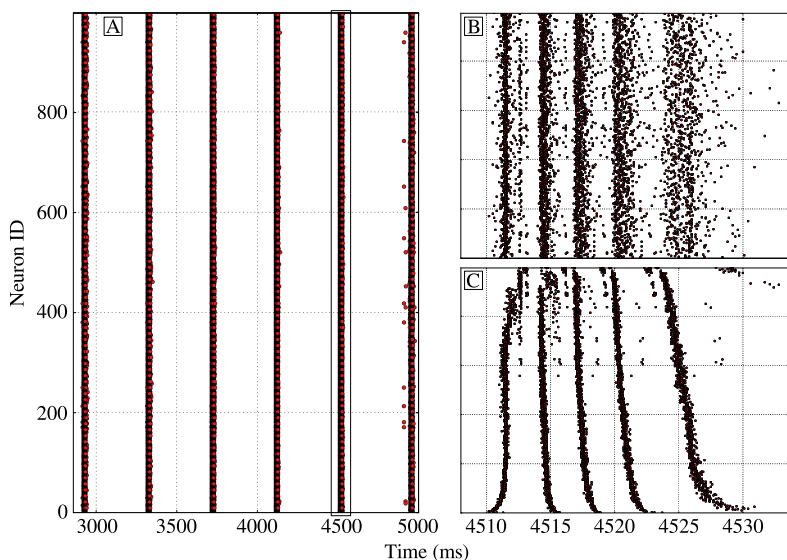


Figure 8. **A:** spike raster of a 1000-neuron network with Gaussian in-degree distribution $\mathcal{N}(100, 5)$, displaying periodic spiking behavior. **B:** detailed dynamics of 5th burst (boxed), with the successive SBSs. **C:** same time-window as **B** but with neurons ordered by increasing in-degree; we can clearly see the activity propagate between groups with different connectivity profiles.

The detailed structure of the burst becomes apparent if we sort the neurons based on their in-degree. Figure 8 C represents the same time window as **B** and shows how strongly the spiking times of the neurons correlate to their in-degree. Indeed, higher-degree nodes will reach their quorum more easily, thus firing earlier than the rest of the network. This effect becomes more significant as the average quorum increases; on the last SBS of **C**, we can clearly see the sigmoidal shape as the percolation front propagates from the higher to the lower in-degree nodes. Eventually, it should be stressed that, though the percolation formalism helps us understand the inner structure of the burst, only the last SBSs can be described as a “pure” percolation phenomenon. This can be understood from the 2nd SBS: because of the extension of the 1st SBS, the resulting “initially activated fraction” is not clearly defined and it looks like two percolation processes are interfering. We can see that the structure becomes clearer on the last SBSs where the activity of the whole population occurs on a unique and longer timescale, in a decreasing in-degree order, and follows the initial activation of the highest in-degree neurons.

6. Conclusion

We elaborated extensions to the original Quorum Percolation model by introducing two additional neurobiological properties; we studied their effects on the activity of the networks. In each case, we were able to construct a mean-field theory in good agreement with Monte Carlo

explicit simulations within a wide parameter range, which is specified in this paper. The central idea that enabled us to derive these mean-field approaches is the mapping of the network onto equivalent ones related to the original QP model, but exhibiting a different connectivity. A main point is the close relation between excitability and connectivity, between decay and connectivity. These two effects impact the position of the critical point in a manner that can remain unnoticed. Hence deciphering the functional connectivity of the network using percolation methods is more difficult than expected. Yet, the study of bursts with the help of a two dimensional dynamical model gives evidence that the ideas of percolation are worth being kept in mind within such a framework. At last, although the Quorum Percolation models we set out in this paper have been designed to describe what triggers burst of activity in neuronal networks, they are also relevant in other scientific fields (propagation of rumors, ecology, sociology...) involving information propagation throughout networks with a threshold rule.

Acknowledgments

This work was granted access to HPC resources of IDRIS (Orsay) under the allocation 2015057043 made by GENCI (Grand équipement national de calcul intensif). We are grateful to Elisha Moses, Yaron Penn for helpful discussions.

References

- [1] J P Eckmann, O Feinerman, L Gruendlinger, E Moses 2007 J Soriano, and T Tlusty, *Phys. Rep.* **449** 54
- [2] S Stern, M Segal and E Moses 2015 *EBioMed.* **2** (9) 1048
- [3] R Renault 2015 *Emergent design of neuronal devices* PhD thesis, Université Paris Diderot
- [4] I Breskin, J Soriano, E Moses and T Tlusty 2006 *Phys. Rev. Lett.* **97**, 1
- [5] G W Gross, B K Rhoades, D L Reust, F U Schwalm 1993 *J. Neurosci. Methods* **50** 131
- [6] K R Gee, K A Brown, W N Chen, J Bishop-Stewart, D Gray, and I. Johnson 2000 *Cell Calcium* **27** 97
- [7] R Renault, N Sukeinik, S Descroix, L Malaquin, J L Viovy, J M Peyrin, S Bottani, P Monceau, E Moses and M Vignes 2015 *PLoS ONE* **10** 4: e0120680
- [8] Y Penn, M Segal, E Moses 2016 *PNAS* **113** (12) 3341
- [9] R Renault J B Durand J L Viovy and C Villard *Lab Chip* **16** 2188
- [10] J Soriano, M Rodriguez Martinez, T Tlusty and E Moses 2008 *PNAS* **105** (37), 13758
- [11] E M Izhikevich 2007 *Dynamical systems in neuroscience* (Cambridge Massachusetts: MIT Press)
- [12] F A Rodrigues, T K D M Peron, Peng Ji, J Kurths 2016 *Phys. Rep.* **610** 1
- [13] O Cohen, A Keselman, E Moses, M Rodriguez Martinez, J Soriano, and T Tlusty 2010 *Eur. Phys. Lett.* **89** 18008
- [14] D Stauffer and A Aharony 1994 *Introduction to percolation theory* (London: Taylor and Francis)
- [15] R Renault, P Monceau, S Bottani and S Métens 2014 *Physica A* **414** 352
- [16] S Métens, P Monceau, R Renault and S Bottani 2016 *Phys. Rev. E* **93** 032112
- [17] S Wiseman and E Domany 1998 *Phys. Rev. Lett.* **81** 22
- [18] P Monceau 2011 *Phys. Rev. E* **84** 051132
- [19] J P Eckmann, E Moses, O Stetter, T Tlusty and C Binden, *Front. Comput. Neurosci.* **4**, 132
- [20] M Isokawa 1997 *Brain Res.* **1**(2) 114
- [21] J R Geiger, J Lübke, A Roth, M Frotscher, and P Jonas 1997 *Neuron* **18**(6) 1009
- [22] R Renault, P Monceau, and S Bottani 2013 *Phys. Rev. E* **88** 062134
- [23] R Brette and W Gerstner 2005 *J. Neurophysiol.* **94**(5) 3637
- [24] S Bottani 1996 *Phys Rev E* . 1996 textbf 54(3) 2334-2350.
- [25] F Lombardi, H J Herrmann, D Plenz and L De Arcangelis 2014 **8** *Frontiers in Neuroscience* doi: 10.3389/fnys.2014.00204
- [26] V S Sohal and J R Huguenard 2003, **2003** : 8978-8988;

J.2 Inhibitory and dynamical quorum percolation (Physica A 2018)

The following paper uses an extension of the initial Quorum Percolation (QP) model to assess how the presence of inhibitory neurons in the network would affect the percolation process. In a second part, I show that the percolation transition is also obtained for networks where the units are modeled through a dynamical description (the AdExp model) and include time-delays in the information propagation mechanism.

Both these results highlight the fact that the initiation of a bursting event can indeed be describe as a percolation process and that it is qualitatively independent of the presence of inhibitory neurons.

Effects of inhibitory neurons on the Quorum Percolation model and dynamical extension with the Brette-Gerstner model

Tanguy Fardet^{a,*}, Samuel Bottani^a, Stéphane Métens^a, Pascal Monceau^{a,b}

^a*Laboratoire Matière et Systèmes Complexes, UMR 7057 CNRS, Université Denis Diderot-Paris 7, 10 rue A. Domon et L. Duquet, 75013 Paris Cedex, France.*

^b*Université d'Evry-Val d'Essonne, France.*

Abstract

The Quorum Percolation model (QP) has been designed in the context of neurobiology to describe the initiation of activity bursts occurring in neuronal cultures from the point of view of statistical physics rather than from a dynamical synchronization approach. This paper aims at investigating an extension of the original QP model by taking into account the presence of inhibitory neurons in the cultures (IQP model). The first part of this paper is focused on an equivalence between the presence of inhibitory neurons and a reduction of the network connectivity. By relying on a simple topological argument, we show that the mean activation behavior of networks containing a fraction η of inhibitory neurons can be mapped onto purely excitatory networks with an appropriately modified wiring, provided that η remains in the range usually observed in neuronal cultures, namely $\eta \lesssim 20\%$. As a striking result, we show that such a mapping enables to predict the evolution of the critical point of the IQP model with the fraction of inhibitory neurons. In a second part, we bridge the gap between the description of bursts in the framework of percolation and the temporal description of neural networks activity by showing how dynamical simulations of bursts with an adaptive exponential integrate-and-fire model lead to a mean description of bursts activation which is captured by Quorum Percolation.

*Corresponding author

Email address: tanguy.fardet@univ-paris-diderot.fr (Tanguy Fardet)

Keywords: quorum percolation, inhibitory neurons, neuronal cultures, dynamical model

1. Introduction

Neuronal rhythms are widespread oscillating phenomena, both *in vivo* and *in vitro*, which were observed over many temporal scales [1]. Hitherto, the fundamental mechanisms underlying their occurrence is far from being fully understood and is the subject of a significant research activity; it involves several scientific fields, from fundamental biology, information theory [2], physics of dynamical systems and critical phenomena [3] to graph topology [4] and massive parallel computation [5, 6]. The human brain is a very complex network, with about 10^{11} neurons [7], each of them connected to 1000–15000 others. Moreover, it is organized in localized computational units connected according to a well defined hierarchical structure. Thus, although investigation and imaging techniques enabling to record the cerebral activity *in vivo* are making significant progress [8, 9], the mere size and complexity of the brain makes its whole description and understanding a far-sighted goal. Complementary to observations and experiments on real brains, *in vitro* experiments on dissociated neuronal cultures are an invaluable tool in investigating the fundamental questions on neuronal dynamics set above. Such cultures are usually obtained by seeding dissociated neurons extracted from rodent embryos, or alternatively neuronal stem cells, on a suitable substrate. Though similar monitoring can be performed on brain slices, we will focus on the activity of dissociated cultures, where axons and dendrites grow in such a way that neurons self-organize after a few days into a two-dimensional network exhibiting a high level of randomness [10]. As a matter of fact the connectivity between neurons is described by probability distributions. These neuronal cultures hold between 10^3 and 10^5 neurons with typical densities between 500 and 5 000 neurons per mm^2 , each of them connected via a number of synapses falling between 20 and 200 [11]. These changes in connectivity and scale compared to a brain could, at first glance, appear as

a loss from a neurobiologic point of view; yet, they are a key feature for the complementary approach of *in vitro* experimentation to study neuronal activity and growth. Quantitative measurements of the neural activity inaccessible *in vivo* can be carried out with the help of micro-electrode arrays (MEA) [12], optogenetics, and calcium imaging [13].

Synchronized periodic bursts of spiking activity have been regularly observed in dissociated neuronal cultures [14, 15] and appear as a fundamental emergent spatio-temporal property of neuronal populations. Bursts of activity can also be artificially triggered by externally activating a fraction of neurons. The Quorum Percolation model (QP) has been elaborated to describe the initiation of bursts observed in such cultures as a collective phenomenon, from the point of view of statistical physics rather than dynamical systems [16]. Under its original form the QP model does not take into account the presence of inhibitory neurons. However, a general description of collective behaviors in neural networks requires the integration of inhibitory neurons in the QP model, since it has been pointed out that they can play a role in the structure of bursts [17, 18]. We devoted recently several studies to extend the original QP model by including additional biological relevant properties and modulation of the neuronal activity: the decay of the neuronal voltage accounting for ions leakage through the neuron membrane [19], variability in the quorum accounting for a modulation of the neuronal excitability threshold [20], finite size scaling and the derivation of a normal form around the critical point together with a preliminary study of the incorporation of inhibitory neurons [21]. In this last paper, we suggested that under specific conditions, the mean characteristics of the burst activation of networks with inhibitory neurons are the same as the ones of purely excitatory networks with different effective connectivity. The first goal of this paper is to provide a deeper investigation of the mapping between the presence of inhibitory neurons and an equivalent purely excitatory reduced connectivity. We point out what should be learned from the mean field approach, we characterize the connectivity features of the purely excitatory network accounting for a fraction of inhibitory neurons, we quantify its equivalence domain and derive a

relation between the critical point and the fraction of inhibitory neurons. As
60 inhibitory neurons are commonly assumed to play a modulating role of neu-
ronal activity and spatio-temporal coordination, we investigate the validity of
our previous conclusions in a dynamical setting. Thus, the second goal of this
paper is to show that the key features of Quorum Percolation captured by the
simple, discrete model with inhibition are preserved in a fully dynamical model
65 based on biologically more refined description of neurons and synapses, namely
the adaptive Exponential Integrate-and-Fire model [22]. However, it should be
noticed that the dynamics of the activity cannot be captured by IQP and QP
models, since they deal with equilibrium properties of the short time onset of
bursts.

70 **2. The original Quorum Percolation model**

The original Quorum Percolation (QP) model is a discrete-time cellular
automaton describing the propagation of information on a graph through a
minimal set of rules for activation cascades in neuronal populations. Since neu-
ronal communication through synapses is directional, the neuronal population
75 is represented by a directed graph connecting neurons located on the vertices.
Specifically introduced to describe the onset of activity bursts observed in small,
in vitro cultures [16], the model is based on a non spatial graph considering only
the node connectivities and constructed by randomly choosing, for each neuron
 i , k incoming links among the $N - 1$ other neurons according to an in-degree
80 probability distribution p_k . It is worth noticing that such a random description
of the incoming links probability relevant in the case of cultures of dissociated
neurons grown in an *in vitro* environment does not work anymore in the case
of neuronal cultures that have grown *in vivo* like brain slices or animal visual
cortex [23].

85 In the QP model, each neuron i is represented by a discrete variable $V_i(t)$
which accounts for the membrane potential, and by a neuronal state – at rest
or active – with activation governed by a threshold rule. A neuron is activated

between $t - \Delta t$ and t if its potential becomes greater or equal to some activation threshold m ; once activated, it sends signals to its outgoing neighbors. As the
90 models represents only one activation wave, an activated neuron remains so and sends no further signals in the following steps. After a time step Δt , each neuron i integrates the signals it received by incrementing its potential $V_i(t - \Delta t)$ by the sum of the inputs from its incoming neighbors activated during the elapsed time interval. All the signals are taken identical and associated to an integer
95 increment equal to $+1$, which sets the scale for the threshold value m . The network is stimulated at time $t = 0$ by an initial excitation of the network, performed by activating a given fraction f of randomly chosen neurons.

The activity of the network at time t is given by the fraction of active neurons $\phi(t)$, increasing with t , and converging towards a stationary value $\Phi(f, m)$ after a few time steps, dependent on the initial active fraction f and the threshold m . As first reported by Cohen *et al.* [16] the surface $\Phi(f, m)$ (noted simply Φ in the following) defines a phase diagram as shown on Fig. 1, where two regimes can be distinguished depending on m . Below some critical value m_c , Φ presents a discontinuity at some value $f^*(m)$ when the control parameter f is varied, whereas it remains continuous above m_c . The sudden jump occurring at $f^*(m)$ is associated with a percolation phenomenon on the network, where a very small variation of f results in the appearance of a giant cluster, whose normalized size is given by the difference between the lower and upper values of Φ at the discontinuity. Despite its simplicity the phase diagram of QP model captures the key behavior observed in experiments in the group of E. Moses [11, 16] on induction of activity in neuronal cultures which exhibits the same emergence of a giant cluster depending on neuronal excitability. Following the usual concepts of percolation on lattices [24] for the second order transition between the presence and absence of a percolation phenomenon, the amplitude of the jump $\langle g \rangle$ is considered as the standard order parameter, whose behavior in the vicinity of m_c follows a power law:

$$\langle g \rangle \sim \left(\frac{m_c - m}{m_c} \right)^\beta. \quad (1)$$

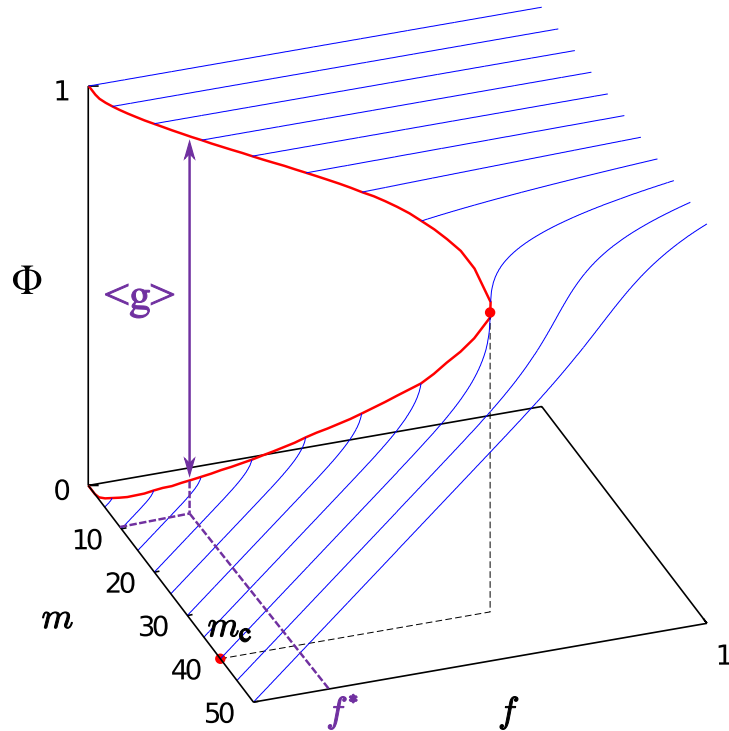


Figure 1: Phase diagram of the Quorum Percolation model, for a Gaussian in-degree distribution with a mean $\bar{k} = 50$ and a standard deviation $\sigma_k = 10$. When the quorum m is smaller than m_c , a jump in the fraction of active neurons Φ occurs when increasing the fraction f of initially activated neurons from zero. The height $\langle g \rangle$ of the jump at the discontinuity is the normalized size of the giant percolation cluster.

Since m is discrete, it is difficult to extract a precise critical value of β from the behavior of $\langle g \rangle$, mainly because the uncertainty over the value of m_c is at least of 1 unit. We overcame such an hurdle by carrying out an extension of the quorum percolation mean-field theory to non integer values of m and we showed [25] that a Gaussian distribution p_k of incoming links leads to $m_c = \bar{k} \left(1 - a \left(\frac{\sigma}{\bar{k}} \right) + b \left(\frac{\sigma}{\bar{k}} \right)^2 \right)$ where \bar{k} is the mean value of the number of incoming links and σ the width of p_k ; for values of \bar{k} lying in the range of experiments on mature cultures, we found that $a \in [1.27, 1.30]$ and $b \in [1.56, 1.59]$. Moreover we showed that the value of β for such incoming links distributions is compatible

with $\beta = 1/2$.

Defined as above the model is only related to the topological relationships between nodes and does not take into account spatial properties from localization of neurons in space. Hence, no metric is involved and the percolation cannot be described with respect to a given dimensionality as in the usual case of lattices [24]. As showed by Tlusty and Eckmann [26] for small dense neuronal cultures as those used for the global activation experiments, the spatial embedded neuronal network is in practice a fully randomly connected one. For large cultures, as for instance those investigated by Orlandi *et al.* [27] activity propagation fronts are observed and a spatial metric has to be considered for the study of the neuronal culture dynamics. Furthermore, it has recently been shown on the basis of another statistical physics model of neuronal cultures, the random field Ising model, that metric correlations induce strong deviations from the mean field [28].

3. A quorum percolation model with inhibitory neurons: IQP

3.1. Main features of the IQP model and comparison with experiments

Let us now assume that a fraction η of neurons, drawn at random, is inhibitory. As in the original model, the network is wired in such a way that, for each neuron, the number of incoming links follows a probability distribution p_k ; however, we now set every outgoing link of an inhibitory neuron to “inhibitory”. We account for these neurons in the following way: when an inhibitory neuron fires, it sends a signal equal to -1 instead of $+1$ through its outgoing links, thus decrementing the potential of each target. Hence, a neuron becomes active if the number of its active excitatory incoming neighbors e minus the number i of its active inhibitory ones is greater than the quorum: $(e - i) \geq m$. A sketch explaining the progress of the Quorum Percolation with inhibitory neurons (IQP) is provided in Fig. 2. It should be noticed that, unlike the QP model, the potential of a neuron is no more a monotonous increasing function of the time t associated with the discrete time kinetics, but the fraction of active neurons

(inhibitory and excitatory) necessarily increases with t because of the threshold rule. Running Monte-Carlo simulations to compute the stationary activity Φ involves (i) constructing a random network \mathcal{G} of N neurons according to the incoming links probability distribution p_k , (ii) declaring a fraction η of neurons
 140 inhibitory according to an uniform random distribution, (iii) activating a fraction f of the neurons regardless of their excitatory or inhibitory nature and (iv) processing the quorum activation rule until the number of active neurons stops increasing.

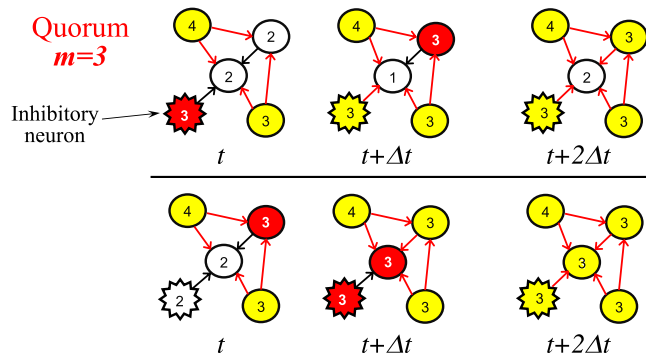


Figure 2: Arrows represent the directed axonal links between neurons. The neurons associated with the light grey (yellow) color are active (i.e. they already fired) while the white ones are at rest and the red ones are just firing at the indicated time. One inhibitory neuron is represented as a dented circle. Upper figure: at time t , the inhibitory neuron fires (because of external inputs which are not represented here); thus the potential of its outgoing neighbor, in the center, shifts from 2 to 1. Let us suppose that, at time $t + \Delta t$ the upper right neuron fires (also because of external inputs not represented here); the potential of its outgoing neighbor is incremented by one, leading to the state represented at $t + 2\Delta t$. The bottom figures show that the order in which the neurons fire matters in the presence of inhibitory neurons. If we assume that the right upper corner excitatory neuron fires before the left down inhibitory one (because of another history of external inputs than on the first row) the central neuron now activates, while it will never fire before the end of the process in the example above.

We carried out explicit Monte Carlo simulations of the IQP model for Gaussian incoming links distributions involving 100 000 neurons, four values of
 145 $\bar{k} \in \{25, 50, 75, 100\}$, ten values of η ranging from 0.05 to 0.2, and three different values of σ in each case; these ranges were chosen to be consistent with

the experimental estimations [11, 16]; in each case, the value of Φ as a function of f was averaged over 29 different network configurations. A selection of some of these explicit IQP simulations are shown as solid red lines in Fig. 3 to Fig. 4 for networks with different mean connectivity as a function of η .

Our main result is that, for η under 25 percent (i.e. less than a quarter of the whole population is inhibitory), the presence of the inhibitory neurons does not change the qualitative behavior of the quorum percolation phase diagram: for a given value of η , jumps in the activity will occur, provided that m is smaller than a critical value m_c , which depends on η .

Furthermore, Fig. 5 shows the influence of η for a fixed value of the threshold m and fixed values of the connectivity parameters $\{\bar{k}, \sigma\}$. Indeed, when the ratio η of inhibitory neurons is increased, the position f^* of the jump in Φ is shifted towards greater values of the initial activity, while its size g is decreased (until it possibly vanishes). Hence, when inhibition increases for a given firing threshold and a given connectivity, a more important fraction of initially activated neurons is necessary to trigger the percolation.

Communication between neurons involves chemical signaling at the synaptic level: neurotransmitters present in the pre-synaptic domain are released by vesicle exocytosis and bind to receptors located in the post-synaptic domain. This release is triggered by electrical signaling conveyed by action potentials, and is the biological equivalent of the update of a node's potential by its active neighbours. In neuronal networks, both excitatory and inhibitory synapses are present, the latter being associated to $GABA_A$ (Gamma-aminobutyric acid) receptors. These receptors can be hindered, and even blocked by adding specific drugs. Using bicuculline in the culture medium to block $GABA_A$ receptors Soriano *et al.* [14] compared the activations of fully excitatory networks and of untreated mixed excitatory and inhibitory cultures and observed that the presence of inhibitory neurons decreases the threshold for the percolation phenomenon compared to the purely excitatory case. Such an experimental result is very well described in the framework of the IQP model and predicted by our simulations.

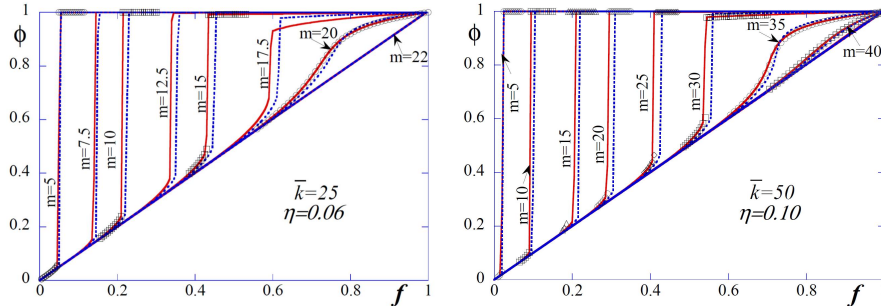


Figure 3: Comparison between explicit IQP Monte Carlo simulations (solid red lines), solutions of the mean-field equation around the jumps (open black symbols), and QP simulations of the equivalent purely excitatory network obtained through $\bar{k}_{eq} = \bar{k}(1 - 2\eta)$ (blue dotted lines). $\bar{k} = 25$, $\sigma = 2.5$ and $\eta = 0.06$ (left) $\bar{k} = 50$, $\sigma = 5$ and $\eta = 0.10$ (right).

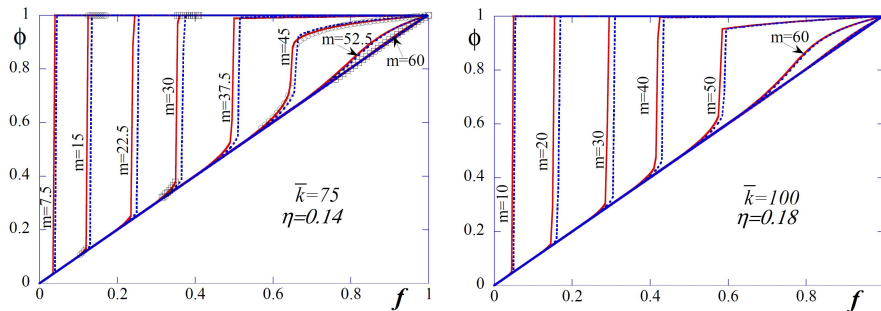


Figure 4: Comparison between explicit IQP Monte Carlo simulations (solid red lines), solutions of the mean-field equation around the jumps (open black symbols), and QP simulations of the equivalent purely excitatory network obtained through $\bar{k}_{eq} = \bar{k}(1 - 2\eta)$ (blue dotted lines). $\bar{k} = 75$, $\sigma = 7.5$ and $\eta = 0.14$ (left) $\bar{k} = 100$, $\sigma = 10$ and $\eta = 0.18$ (right).

3.2. Mean-field theory

An alternative approach for calculating the stationary fraction of active neurons Φ can be deduced from a mean-field leading to a self-consistency equation [21]. Indeed Φ is also the probability for a neuron to be active at equilibrium and it corresponds to the probability to be either active through initial stimulation or to be activated during the IQP discrete signal propagation process. This activation probability of a neuron in the cascade depends itself upon Φ and can be approximated by binomial processes given m and p_k . In order to obtain

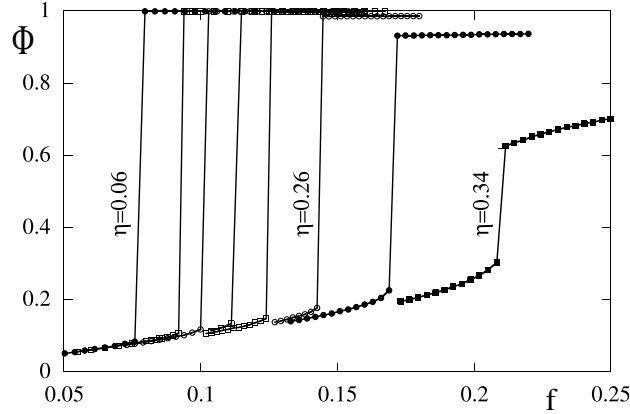


Figure 5: Evolution of the jump in the activity when the ratio η of inhibitory neurons increases from 0.06 (leftmost jump) to 0.34 (rightmost jump) in steps of 0.04. These values are obtained via the mean-field equation, for a fixed threshold $m = 10$ and fixed parameters $\{\bar{k} = 50, \sigma = 0.05\}$ for the network connectivity.

this self-consistency equation, we first partition the set of neurons according to their number k of incoming links and consider a neuron of the network with k_e excitatory and k_i inhibitory incoming links (k is fixed). The probabilities that $Y = e$ excitatory neurons among k_e and $Z = i$ inhibitory ones among k_i are active read respectively $\mathcal{P}_{ex}(Y = e) = \binom{k_e}{e} \Phi^e (1 - \Phi)^{k_e - e}$ and $\mathcal{P}_{in}(Z = i) = \binom{k_i}{i} \Phi^i (1 - \Phi)^{k_i - i}$. The probability for the target neuron to exceed the quorum (to have $e - i \geq m$) can be calculated by noticing that an activation occurs if $Z = i$ only if $Y \geq m + i$. Hence the activation probability of this neuron can be written as the double sum: $\mathcal{P}(e - i \geq m) = \sum_{i=0}^{k_i} \mathcal{P}_{in}(Z = i) \sum_{e=m+i}^{k_e} \mathcal{P}_{ex}(Y = e)$. Now, the probability that a neuron with k incoming links has k_i inhibitory ones reads $P(k_i|k) = \binom{k}{k_i} \eta^{k_i} (1 - \eta)^{k - k_i}$, assuming that η is also the fraction of inhibitory incoming links, as we will discuss further. In the end, the self

consistency equation can be written:

$$\Phi = f + (1 - f) \sum_{k=m}^{\infty} p_k \sum_{k_i=0}^{k-m} \binom{k}{k_i} \eta^{k_i} (1 - \eta)^{k-k_i} \sum_{i=0}^{k_i} \binom{k_i}{i} \Phi^i (1 - \Phi)^{k_i-i} \sum_{e=m+i}^{k-k_i} \binom{k-k_i}{e} \Phi^e (1 - \Phi)^{k-k_i-e}. \quad (2)$$

180 We compared the results of our Monte-Carlo simulations for 100 000 neurons with the values of Φ provided by the resolution of equation (2) focused on the vicinity of the jumps, in some cases showed in Fig. 3 and Fig. 4. This extension of the range of our investigation with respect to [21] where only 10 000 neurons populations were simulated shows in a robust way a very good agreement between the two approaches; we checked that this agreement increases with the
185 size of the network because of finite size effects, since the mean-field approach is expected to hold in the infinite limit. The agreement is remarkable as the mean field approach is not designed to take into account temporal correlations while strictly speaking, the actual IQP process is sensitive to them. Indeed, Fig. 2 shows that the order in which a neuron receives signals can come into play
190 whereas it does not matter in the absence of inhibitory neurons. Nevertheless, a reason why the mean field actually works is that the order of activation hardly comes into play in the information propagation process but when the state of the neurons are close to firing, that is just below the quorum.

195 3.3. Mapping of the IQP model on purely excitatory networks

A close look at the IQP rules suggests that a neuron with k incoming links, k_i of them being inhibitory, could in average behave as a neuron with $k - 2k_i$ purely excitatory incoming links: each inhibitory neuron can be viewed as canceling one of the excitatory. This can be for example observed for the central
200 neuron in the sketch of the upper row of Fig. 2: starting from a value of its potential equal to 2, it ends with the same value since the inhibitory and excitatory inputs compensate each other: it is as if the links with the left down and the upper right neurons had been erased. The robustness of the agreement of

the IQP mean-field theory with Monte-Carlo simulations suggests that such an
 205 observation may be averaged over the whole network. We therefore expect that
 a mixed excitatory and inhibitory network with a mean number \bar{k}_i of inhibitory
 incoming links and $\bar{k} - \bar{k}_i$ excitatory ones should lead to the same stationary
 state as a purely excitatory network with $\bar{k} - 2\bar{k}_i$ mean incoming links. In order
 to check this hypothesis, we ran additional Monte-Carlo simulations: Assum-
 210 ing that $\bar{k}_i = \eta\bar{k}$, we simulated for each set $\{\bar{k}, \sigma, \eta, m\}$ already investigated in
 the framework of the IQP model, an associated QP set $\{\bar{k}_{eq} = \bar{k}(1 - 2\eta), \sigma, m\}$
 without inhibitory neurons. Some typical results are reported in Fig. 3 and Fig.
 4, where comparisons of the activity computed by the two processes are shown.
 As shown on these figures, the stationary response of the mixed excitatory and
 215 inhibitory networks to a given external excitation f is indeed remarkably close
 to the one of the associated purely excitatory network with the equivalent re-
 duced number of incoming links. From these figures, we can notice that the
 differences between the two approaches depend on m and f : They are more
 pronounced when m increases and in the vicinity of the jump, where the perco-
 220 lation process makes the fraction Φ of active neurons undergo a steep variation,
 from a value just above f to a value close to 1. However a quantitative analysis
 of these differences can be achieved from a global point of view by computing
 a (renormalized) Minkowski distance between the IQP and the associated QP
 response over the whole excitation range as:

$$\Delta = \frac{1}{N} \sqrt{\sum_{i=1}^{i=N} (\Phi(f_i) - \Phi_{eq}(f_i))^2}, \quad (3)$$

225 where a subscript i must be added to the initial value of the excitation
 parametrized by f to define properly Δ ; f_i runs from 0 to 1, and i from 1 to $N =$
 200. $\Phi(f_i)$ and $\Phi_{eq}(f_i)$ denote respectively the original IQP activity and the QP
 activity on equivalent excitatory networks averaged over 29 configurations, as
 responses to an excitation parametrized by f_i ; since $\Phi(f_i) \in [0, 1]$, Δ lies between
 230 zero for identical global responses and one for maximal disagreeing responses.
 Fig.6 and Fig. 7 show the evolution of Δ in the $\eta - m$ plane. These results call

for the following comments: obviously, if m is greater than k_{eq} the differences between IQP and QP are negligible because the activation probability are very low, since Φ and Φ_{eq} are very close to f all over the range $[0, 1]$. For a given value of η the differences between the two approaches exhibit a maximum at an intermediate value of the quorum, while for a given value of m , the difference increases with η , excepted if m is too low. Lastly the meaningful scale of the discrepancies decreases as the mean connectivity \bar{k} of the network increases.

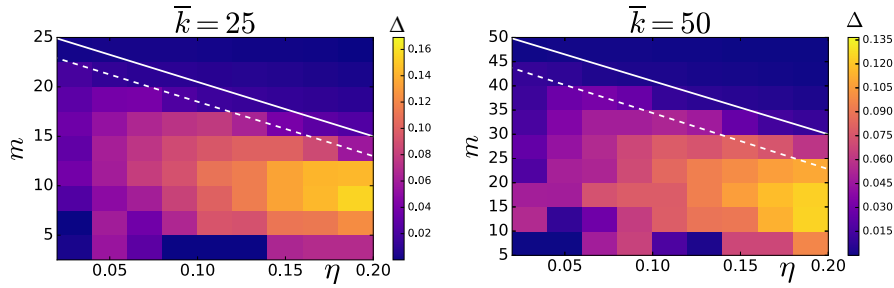


Figure 6: Minkovski distances Δ between the IQP model and the equivalent QP model without inhibitory neurons as a function of m and η for $\bar{k} = 25$ and $\bar{k} = 50$. The solid white lines represent k_{eq} and the dotted ones m_c as a function of η .

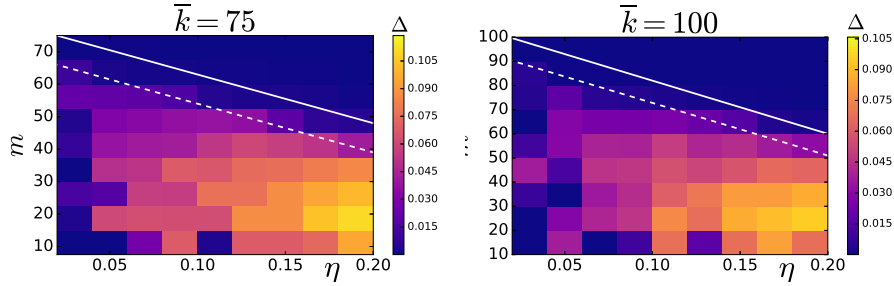


Figure 7: Minkovski distances Δ between the IQP model and the equivalent QP model without inhibitory neurons as a function of m and η for $\bar{k} = 75, \sigma = 7.5$ and $\bar{k} = 100, \sigma = 10$. The solid white lines represent k_{eq} and the dotted ones m_c as a function of η .

Besides the global comparison of the QP and IQP model, we carried out a local analysis by investigating a physical quantity describing the critical behavior: the order parameter. Typical results are shown in Fig. 8 where values of

the order parameter (averaged over 29 configurations in each case) calculated from simulations of the IQP model are compared with values extracted from the equivalent QP model. As long as η is below 10%, the mean relative differences in the two approaches $\langle \frac{\delta g}{g} \rangle$ remain below 7%. We can retrieve a slight increase in the differences and in the relative differences $\langle \frac{\delta g}{g} \rangle$ as η is increased and an increasing agreement as \bar{k} increases. It should be noticed that these results take into account uncertainties on the calculation of $\langle g \rangle$; these uncertainties grow very quickly when getting close to the critical point and the comparisons are no more meaningful. As a matter of fact, when linking these results with the ones set out in the last subsection, we can conclude that an important part of the differences in Minkowski distances (Fig. 6 and Fig. 7) stems from the shift in the position of the jump rather than its height.

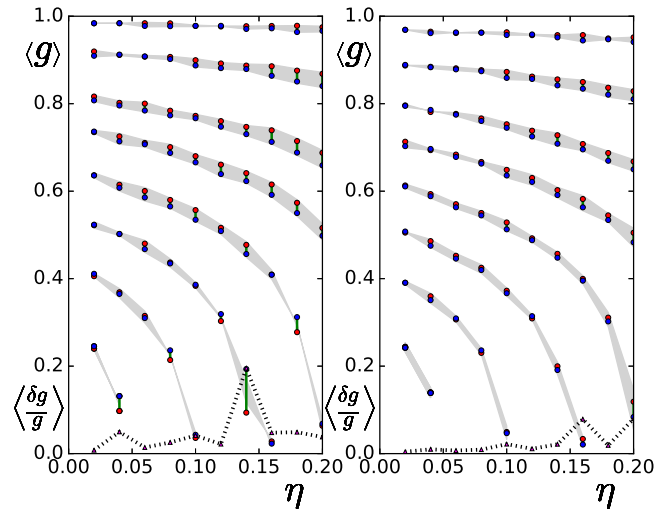


Figure 8: Evolution of the order parameter $\langle g \rangle$ calculated from the IQP model (red circles) and the equivalent QP one (blue circles) as a function of η in the cases where $\bar{k} = 50$ (left) and $\bar{k} = 100$ (right) for 8 different values of m ranging from $0.9\bar{k}$ to $0.2\bar{k}$ from bottom to top. The shaded area accounts for the differences between the two approaches and the dotted line follows the mean relative deviations between them for different values of η .

3.4. Critical point of the IQP model

255 We carried out an additional set of simulations of the IQP model by steps
of 1 unit in m in order to estimate the critical values $m_c(\eta)$ of the quorum as a
function of η for the four different values of the mean incoming links numbers
already investigated. We were able to estimate $m_c(\eta)$ within an uncertainty of 1
unit for \bar{k} equal to 25 and 50 and an uncertainty of 2 units for \bar{k} equal to 75 and
260 100. The results are shown in Fig. 9 where a linear decrease of the values of the
critical point $m_c(\eta)$ with η can be seen. Such a result can be nicely interpreted
in the framework of the mapping set out in the last subsection. When going
back to the analytical expression of the critical point obtained in the framework
of a continuous extension of the QP model [25], $m_c = \bar{k} \left(1 - a \left(\frac{\sigma}{\bar{k}} \right) + b \left(\frac{\sigma}{\bar{k}} \right)^2 \right)$
265 and plugging the value of the equivalent network mean number of incoming links,
we obtain to leading order in σ/k_{eq} :

$$m_c(\eta) = m_c(\eta = 0) - 2\bar{k}\eta, \quad (4)$$

where $m_c(\eta = 0) = (\bar{k} - a\sigma)$. Results of the fits of the lines observed on
Fig. 9 are set out in Table I; as a main result, the evolution of the critical point
 $m_c(\eta)$ with the fraction of inhibitory neurons extracted from IQP simulations is
270 predicted by the QP theory applied to the equivalent network with a remarkable
agreement. $m_c(\eta)$ gives a relation between the two parameters characterizing
the the total distribution of incoming links (excitatory and inhibitory) $\{\bar{k}, \sigma\}$
and the fraction of inhibitory neurons. Let us notice that it is a little bit
different from the results obtained by Soriano et al. [14] in a situation where p_k
275 is Poissonian: they showed that that the critical values m_{cE} for a mixed network
made fully excitatory by addition of bicuculline in the culture and m_{cEI} for the
mixed network are linked by the approximated relation $\frac{m_{cEI}}{m_{cE}} = 1 - \frac{\bar{k}_I}{\bar{k}_E}$ where
 \bar{k}_E and \bar{k}_I designate the mean numbers of excitatory and inhibitory incoming
links of the mixed network.

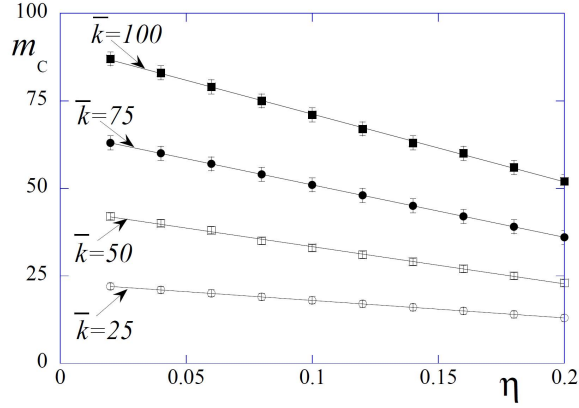


Figure 9: Evolution of the critical point m_c as a function of η for the four different values of \bar{k} investigated with $\sigma = 0.1\bar{k}$

\bar{k}	$m_c(\eta = 0)$	$m_c(\eta)$ (fits)
25	21.7	$23 - 50\eta$
50	44.3	$44 - 106\eta$
75	64.4	$66 - 150\eta$
100	88.8	$90 - 194\eta$

Table 1: Results of the fits of the four straight lines represented on Fig. 9; values of the critical points calculated from the continuous extension of the QP model are recalled in the middle column of the table

280 4. Validity of the quorum percolation paradigm in a dynamical frame- work

As percolation is sufficient to describe the initiation of bursts, it should be investigated if properties of the basic theoretical percolation models remain valid in more realistic situations. As mentioned previously, percolation phenomena,
285 with and without inhibition, have been experimentally validated by the match of the original minimal model to the experimental observations on neuronal cultures by the group of E. Moses [11, 14, 16]. This significant evidence of

quorum percolation phenomenon in living neuronal networks concerned how-
ever only the single response of a neuronal population to an external activation
290 signal of increasing strength. Although it would be surprising for a percolation
process to happen only in this circumstance, its occurrence during the long-
term activity of a neuronal culture remains to be characterized. This question
is specifically relevant when focusing on networks with inhibitory neurons, as
inhibition plays a role on the temporal correlations of neuronal activity in a
295 population. Thus, this last section is devoted to the investigation of quorum
percolation in the framework of a dynamical model of neuronal networks. We
show on a generic example that the percolation description remains relevant to
describe the initiation of a burst of activity inside a population of dynamical
neurons, then discuss how this phenomenon can also be observed in simulations
300 of spontaneous neuronal activity.

Similarly as for the IQP model, we use and generate a random network \mathcal{G}
with Gaussian distribution p_k of incoming links characterized by \bar{k} and σ . Each
node is now described by a differential equation model that realistically describes
the membrane potential variation in time and spikes. The input links are rep-
resented by terms in the neuronal state differential equation that describe the
positive (for excitation) or negative (for inhibition) time varying post-synaptic
potential of synapses. We chose here the adaptive Exponential Integrate-and-
Fire (aEIF) model [22] because of its compromise between simplicity and biolog-
ical relevance. In this model, the dynamical evolution of a neuron is described
by two variables – its membrane potential V and a slow adaptation current w
– which are governed by the following equations:

$$\begin{cases} C_m \frac{dV}{dt} = -g_L(V - E_L) + g_L \Delta_T \exp\left(\frac{V - V_{th}}{\Delta_T}\right) - w + I \\ \tau_w \frac{dw}{dt} = a(V - E_L) - w \end{cases} \quad (5)$$

$$\text{if } V > V_{peak} \quad \begin{cases} V \leftarrow V_r \\ w \leftarrow w + b \end{cases} \quad (6)$$

all neuronal parameters are defined in [22]. Hence we will only mention the two
most relevant in this study, which are E_L , the resting potential of an isolated

neuron, and V_{th} , the “threshold” potential, which marks the beginning of a spike initiation, generated by the diverging exponential. The difference $V_{th} - E_L$ is therefore closely related to the quorum defined in the IQP model. The connection from any neuron A to a second neuron B is implemented using alpha-shaped post-synaptic currents (PSCs) in the input term I which leads, if a spike occurs at $t = 0$, to a subsequent current of the form

$$I_s(t) = s_{AB} \frac{I_0}{\tau_s} t e^{-t/\tau_s}, \quad (7)$$

where s_{AB} is the dimensionless synaptic strength and $I_0 = e \cdot 1pA$ is a normalization constant which sets the peak value of the PSC to $s_{AB} pA$. Inhibitory inputs correspond to negative s_{AB} and we declare a fraction η of the neurons as inhibitory (all outgoing synapses have negative strengths) according to a uniform random distribution. The numerical simulations were carried out using the NEST neuronal simulator [6].

We aim first at reproducing the quorum percolation with this dynamical model. In order to perform the same numerical experiment as in the quorum percolation Monte-Carlo runs, we adapted an equivalent protocol to the dynamical model : (i) a random fraction f of all neurons is activated via a large post-synaptic current that brings them above their “threshold” and induces their simultaneous firing; (ii) the simulation is pursued until the number of active neurons stops increasing (in practice, because of the relaxation from the leak conductance, simulations are performed on a 100-*ms* time window, which is long enough for all activity to occur given our sets of neuronal parameters). In order to be as close as possible to the original experiment, the neurons are set so that their refractory period after a spike is equal to the simulation time (ensure they fire only once), and the axon transmission delay is set to one simulation timestep, i.e. 0.1 *ms*. For this first part, the units are all implemented with parameters for adaptive spiking neurons, though this has no significant impact on the involved timescale.

Parameters	f^* (IQP)	f^* (Sim.)
$\bar{k} = 25, m = 5$	0.05	[0.06; 0.08]
$\bar{k} = 25, m = 10$	0.18	[0.19; 0.21]
$\bar{k} = 25, m = 15$	0.45	~ 0.45
$\bar{k} = 75, m = 9$	0.04	[0.045; 0.05]
$\bar{k} = 75, m = 15$	0.11	[0.11; 0.115]
$\bar{k} = 75, m = 30$	0.29	[0.31; 0.32]
$\bar{k} = 75, m = 45$	0.52	~ 0.54

Table 2: Comparison between the values of the critical fraction of initially active neurons f^* obtained by the IQP or the dynamical simulations for $\eta = 0.05$. Interval for the dynamical simulation is given by the “jump” values for the 5th and 95th percentiles. For the last row in each \bar{k} set, the dynamical simulation displayed a smooth transition, so the value given is the position of the inflexion point.

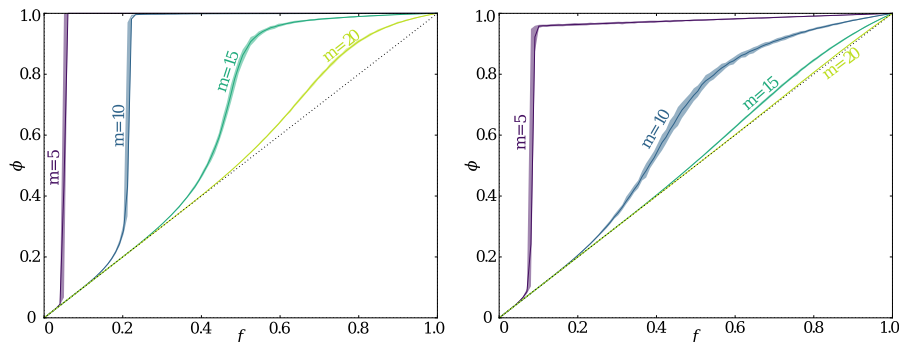


Figure 10: Simulated phase transition for inhibitory fractions of 5% (left) and 25% (right) – averaged over 50 runs for each curve to quantify the fluctuations. For the simulations, 10 000 neuron networks were generated with Gaussian in-degree distributions ($\bar{k} = 25$ and $\sigma_k = 5$). The average transition curve is represented by the solid lines (with increasing quorums $\{5, 10, 15, 20\}$ from dark purple to light green) and the filled area is delimited by the 5th and 95th percentiles, i.e. it contains 90% of the simulated datapoints. The dashed line marks the $\Phi = f$ curve. As in the mean-field model, increasing the inhibitory fraction leads to a sharp decrease in the critical quorum value: $10 < m_c < 15$ for $\eta = 0.05$ whereas $5 < m_c < 10$ for $\eta = 0.25$.

330 In the dynamical simulations, the quorum m was evaluated as the number
of simultaneous spikes necessary to make a neuron fire (see Appendix for a more
detailed explanation on how its precise value is obtained). The resulting activity
of the total population can be seen on Fig. 10. Comparison with Fig. 3 and Fig.
4 shows significant resemblance in the qualitative, as well as in the quantitative
335 behavior of the phase transition. As for the mean-field model, an increase in the
fraction η of inhibitory neurons leads to a decrease of both the size g of the jump
and the final fraction of active neurons Φ . The tendency for the critical value
of the quorum to be lower in the dynamical simulations can be easily explained
by the combination of the leak conductance and the PSC decrease over time,
340 as detailed in a previous percolation model including decay [19]. Beside this
small offset, the excellent agreement of the positions where the jump occurs,
detailed in Table 2, confirms that the simple IQP percolation model captures
the behavior of a more sophisticated dynamical model and is thus relevant to
describe the ignition of a burst of activity in a network of coupled neurons.

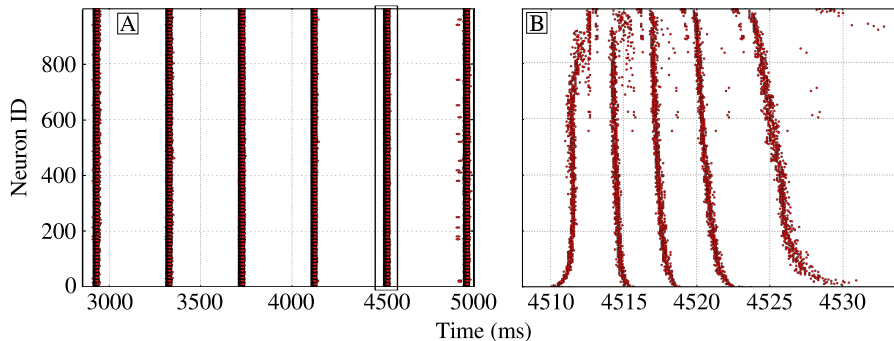


Figure 11: **A.** Spike raster of a 1000-neuron network with Gaussian in-degree $\mathcal{N}(100, 5)$ displaying a spontaneous and periodic bursting behavior. **B.** shows the inset of the left raster with the detailed dynamics of the successive SBSs. Neurons ordered by increasing in-degree.

345 Eventually, as can be seen on Fig. 11, the percolation paradigm is perfectly
relevant to describe some of the successive network events that occur inside a
network burst, for spontaneously active neural networks. Spontaneous bursting
activity is a common phenomenon in neuronal networks [27, 15] and the IQP

can therefore be a useful tool to investigate the properties of this spontaneous
350 behavior.

On Fig. 11 **A**, the simulated activity is composed of periodic bursts which themselves present a precise substructure as a succession of *synchronous burst slices* (SBS), shown on 11 **B**. These are the basic activity blocks that can be described through the percolation formalism. Indeed, after the first spontaneous slice, each subsequent SBS is triggered by the previous one. Because the
355 excitability of the neurons decreases as the burst progresses, this corresponds to a succession of percolation events with increasing values of the quorum. After the last SBS, the value of the quorum becomes greater than m_c so no new percolation can occur and the burst terminates.

360 5. CONCLUSION

In this paper, we set out an extension of the Quorum Percolation model with a Gaussian distribution of incoming links (QP) including a fraction η of inhibitory neurons (the IQP model). Furthermore, we showed how the mean stationary activation of bursts in a network with inhibitory neurons can be
365 mapped onto an equivalent purely excitatory network endowing an appropriate and different wiring. We provided a quantification of the agreement between the QP and IQP approaches and showed that the agreement is good in usual neuronal cultures, where $\eta \lesssim 20\%$. Thus, on the issue of large scale response of quorum percolation, mixed inhibitory and excitatory Gaussian random net-
370 works with mean input connectivity \bar{k} and fraction η of inhibitory neurons, have a purely excitatory Gaussian random network equivalent with a mean incoming links connectivity $(1 - 2\eta)\bar{k}$. This enabled us to calculate the critical point of the IQP model as a function of η . Lastly, we gathered together the approaches coming from the fields of percolation theory and dynamical systems in order to
375 check how the percolation paradigm remains meaningful for the interpretation of a network response to excitation in a biologically more realistic model taking time explicitly into account. We built indeed a dynamical version of the IQP

model using Brette-Gestner adaptative exponential neurons and alpha-shaped synapses. We showed that Quorum Percolation occurs also in the more sophisticated dynamical framework so that, despite their apparent simplicity, QP and IQP models are an appropriate approach for bursts onset in neuronal cultures.

6. Appendix

All dynamical simulations were performed using the NEST simulator [6] with the `aeif_psc_alpha` model (present on the master branch of the GitHub repository or in release versions strictly higher than 2.11.0) and static synapses.

The neurons were set to adaptive spiking using the neuronal and synaptic parameters detailed in Table 3.

Neuronal parameter	C_m	g_L	E_L	V_{th}	I_e	Δ_T	a	τ_w	t_{ref}
Value	200	9	-60	-50	0	2	2	600	100
Synaptic parameter	$\tau_{s,exc}$	$\tau_{s,inh}$	d						
Value	0.2	0.2	0.1						

Table 3: Neuronal and synaptic parameters used in the simulations. The units are as follow: capacitance in pF , conductance in nS , voltage in mV , current in pA and time in ms . d is the spike transmission delay.

In order to obtain a desired quorum m , the synaptic strength between neurons was tuned according to the following procedure:

- Send m spikes, each with strength s , on a neuron, and increase s until the post-synaptic neuron fires, which occurs for a synaptic strength s_m^* .
- Repeat the process for $m - 1$ spikes; this results in a second value s_{m-1}^* .
- use the synaptic strength $s_m = \frac{s_m^* + s_{m-1}^*}{2}$ for all connections in the network.

This value of the synaptic strength is important if we want to compare quantitatively the predictions of the mean-field model to the simulations. Indeed, in the simulations, the evolution of the state V_i of neuron i is progressive, and a spike

is not necessarily triggered immediately after the excitation. More precisely, at the critical value s_m^* for which the neuron starts spiking when it receives m spikes, the emission of this spike can take an infinite amount of time (critical
400 slowing down). The choice of s_m as the average value between s_m^* and s_{m-1}^* is therefore important to ensure that the neuron will fire rapidly enough (with a characteristic timescale τ_s) after the reception of m spikes, and thus be in a situation which is comparable to that of the mean-field model.

The networks were generated using the nngt library using the igraph back-
405 end.

7. ACKNOWLEDGEMENTS

This work was granted access to HPC resources of IDRIS (Orsay) under the allocation 2016057701 made by GENCI (Grand équipement national de calcul intensif).

- 410 [1] D. Purves, Neuroscience, Oxford University Press, 2012.
URL <https://books.google.com/books?id=B5YXRAAACAAJ>
- [2] J. P. Eckmann, O. Feinerman, L. Gruendlinger, E. Moses, J. Soriano, T. Thusty, The physics of living neural networks, Physics Reports 449 (1-3) (2007) 54–76. [arXiv:1007.5465](https://arxiv.org/abs/1007.5465), [doi:10.1016/j.physrep.2007.02.014](https://doi.org/10.1016/j.physrep.2007.02.014).
- 415 [3] E. M. Izhikevich, Dynamical systems in neuroscience, 2007.
URL <http://mitpress.mit.edu/item.asp?tttype=2&tid=11063&mlid=600%5Cnpapers://e5fa1263-0213-4cdb-b4d1-93aaa9302477/Paper/p2818>
- [4] S. N. Dorogovtsev, a. V. Goltsev, J. F. F. Mendes, Critical phenomena in
420 complex networks, Reviews of Modern Physics 80 (4) (2008) 1275–1335.
[arXiv:0705.0010](https://arxiv.org/abs/0705.0010), [doi:10.1103/RevModPhys.80.1275](https://doi.org/10.1103/RevModPhys.80.1275).
- [5] H. Markram, E. Muller, S. Ramaswamy, M. W. Reimann, M. Abdellah, C. A. Sanchez, A. Ailamaki, L. Alonso-Nanclares, N. Antille, S. Arsever,

- 425 G. A. A. Kahou, T. K. Berger, A. Bilgili, N. Buncic, A. Chalimourda,
 G. Chindemi, J. D. Courcol, F. Delalondre, V. Delattre, S. Druckmann,
 R. Dumusc, J. Dynes, S. Eilemann, E. Gal, M. E. Gevaert, J. P. Ghobril,
 A. Gidon, J. W. Graham, A. Gupta, V. Haenel, E. Hay, T. Heinis, J. B. Her-
 nando, M. Hines, L. Kanari, D. Keller, J. Kenyon, G. Khazen, Y. Kim, J. G.
 King, Z. Kisvarday, P. Kumbhar, S. Lasserre, J. V. Le Bé, B. R. C. Mag-
 430 alhães, A. Merchán-Pérez, J. Meystre, B. R. Morrice, J. Muller, A. Muñoz-
 Céspedes, S. Muralidhar, K. Muthurasa, D. Nachbaur, T. H. Newton,
 M. Nolte, A. Ovcharenko, J. Palacios, L. Pastor, R. Perin, R. Ranjan,
 I. Riachi, J. R. Rodr\`iguez, J. L. Riquelme, C. Rössert, K. Sfyraakis,
 Y. Shi, J. C. Shillcock, G. Silberberg, R. Silva, F. Tauheed, M. Telefont,
 435 M. Toledo-Rodriguez, T. Tränkler, W. Van Geit, J. V. D\`iaz, R. Walker,
 Y. Wang, S. M. Zaninetta, J. Defelipe, S. L. Hill, I. Segev, F. Schürmann,
 Reconstruction and Simulation of Neocortical Microcircuitry, *Cell* 163 (2)
 (2015) 456–492. doi:10.1016/j.cell.2015.09.029.
- [6] M.-O. Gewaltig, M. Diesmann, NEST (NEural Simulation Tool), *Scholar-*
 440 *pedia* 2 (4) (2007) 1430.
- [7] S. Herculano-Houzel, *The Human Advantage: A New Understanding of
 How Our Brain Became Remarkable*, MIT Press, 2016.
 URL <https://books.google.com/books?id=XkzECwAAQBAJ>
- [8] M. E. Raichle, A brief history of human brain mapping, *Trends in Neuro-*
 445 *sciences* 32 (2) (2009) 118–126. doi:10.1016/j.tins.2008.11.001.
- [9] P. Guevara, D. Duclap, C. Poupon, L. Marrakchi-Kacem, P. Fillard, D. Le
 Bihan, M. Leboyer, J. Houenou, J. F. Mangin, Automatic fiber bundle
 segmentation in massive tractography datasets using a multi-subject bundle
 atlas, *NeuroImage* 61 (4) (2012) 1083–1099. doi:10.1016/j.neuroimage.
 450 2012.02.071.
 URL <http://dx.doi.org/10.1016/j.neuroimage.2012.02.071>
- [10] L. Millet, M. U. Gillette, Over a Century of neuron culture: From the

Hanging drop to Microfluidic devices, *Yale Journal of biology and medicine* 4 (85) (2012) 500.

- 455 [11] I. Breskin, J. Soriano, E. Moses, T. Tlusty, Percolation in living neural networks, *Physical Review Letters* 97 (18) (2006) 1–4. [arXiv:1007.5143](https://arxiv.org/abs/1007.5143), [doi:10.1103/PhysRevLett.97.188102](https://doi.org/10.1103/PhysRevLett.97.188102).
- [12] G. W. Gross, B. K. Rhoades, D. L. Reust, F. U. Schwalm, Stimulation of monolayer networks in culture through thin-film indium-tin oxide recording electrodes., *Journal of Neuroscience methods* 50 (1993) 131.
- 460 [13] R. Renault, N. Sukenik, S. Descroix, L. Malaquin, J.-L. Viovy, J.-M. Peyrin, S. Bottani, P. Monceau, E. Moses, M. Vignes, Combining Microfluidics, Optogenetics and Calcium Imaging to Study Neuronal Communication In Vitro, *Plos One* 10 (4) (2015) 1–15. [doi:10.1371/journal.pone.0120680](https://doi.org/10.1371/journal.pone.0120680).
URL <http://dx.plos.org/10.1371/journal.pone.0120680>
- 465 [14] J. Soriano, M. Rodríguez Martínez, T. Tlusty, E. Moses, Development of input connections in neural cultures., *Proceedings of the National Academy of Sciences of the United States of America* 105 (37) (2008) 13758–13763. [arXiv:1008.0062](https://arxiv.org/abs/1008.0062), [doi:10.1073/pnas.0707492105](https://doi.org/10.1073/pnas.0707492105).
- 470 [15] Y. Penn, M. Segal, E. Moses, Network synchronization in hippocampal neurons, *Proceedings of the National Academy of Sciences* (2016) 201515105 [doi:10.1073/pnas.1515105113](https://doi.org/10.1073/pnas.1515105113).
URL <http://www.pnas.org/lookup/doi/10.1073/pnas.1515105113>
- [16] O. Cohen, A. Keselman, E. Moses, J. Soriano, T. Tlusty, Quorum percolation in living neural networks 89 (January) (2010) 1–6. [doi:10.1209/0295-5075/89/18008](https://doi.org/10.1209/0295-5075/89/18008).
URL <http://www.iop.org/EJ/abstract/0295-5075/89/1/18008?rss=2.0>
- 480 [17] V. S. Sohal, J. R. Huguenard, Inhibitory interconnections control burst pattern and emergent network synchrony in reticular thalamus., *J Neuros*

23 (26) (2003) 8978–8988. doi:23/26/8978[pii].

URL <http://www.ncbi.nlm.nih.gov/entrez/query.fcgi?cmd=Retrieve{&}db=PubMed{&}dopt=Citation{&}list{&}uids=14523100{&}5Cnhttp://www.ncbi.nlm.nih.gov/pubmed/14523100>

- 485 [18] F. Lombardi, H. J. Herrmann, D. Plenz, L. De Arcangelis, On the temporal organization of neuronal avalanches., *Frontiers in systems neuroscience* 8 (October) (2014) 204. doi:10.3389/fnsys.2014.00204.

URL [http://journal.frontiersin.org/article/10.3389/fnsys.2014.00204/abstract{&}5Cnhttp://www.pubmedcentral.](http://journal.frontiersin.org/article/10.3389/fnsys.2014.00204/abstract{&}5Cnhttp://www.pubmedcentral.nih.gov/articlerender.fcgi?artid=4211381{&}tool=pmcentrez{&}rendertype=abstract)

- 490 [nih.gov/articlerender.fcgi?artid=4211381{&}tool=pmcentrez{&}rendertype=abstract](http://www.pubmedcentral.nih.gov/articlerender.fcgi?artid=4211381{&}tool=pmcentrez{&}rendertype=abstract)

- [19] R. Renault, P. Monceau, S. Bottani, Memory decay and loss of criticality in quorum percolation, *Physical Review E - Statistical, Nonlinear, and Soft Matter Physics* 88 (6) (2013) 1–8. doi:10.1103/PhysRevE.88.062134.

- 495 [20] P. Monceau, R. Renault, S. Métens, S. Bottani, Effect of threshold disorder on the quorum percolation model, *Physical Review E* 94 (1) (2016) 1–8. doi:10.1103/PhysRevE.94.012316.

- [21] S. Métens, P. Monceau, R. Renault, S. Bottani, Finite-size effects and dynamics of giant transition of a continuum quorum percolation model on random networks, *Physical Review E* 93 (3) (2016) 032112. doi:10.1103/PhysRevE.93.032112.

500 URL <http://link.aps.org/doi/10.1103/PhysRevE.93.032112>

- [22] R. Brette, W. Gerstner, Adaptive exponential integrate-and-fire model as an effective description of neuronal activity, *J. Neurophysiol.* 94 (5) (2005) 3637–3642. doi:10.1152/jn.00686.2005.

505 URL <http://www.ncbi.nlm.nih.gov/pubmed/16014787>

- [23] S. Song, P. J. Sjöström, M. Reigl, S. Nelson, D. B. Chklovskii, Highly nonrandom features of synaptic connectivity in local cortical circuits, *PLoS Biology* 3 (3) (2005) 507–519. doi:10.1371/journal.pbio.0030068.

- 510 [24] D. Stauffer, A. Aharony, Introduction to percolation theory, 1994.
- [25] R. Renault, P. Monceau, S. Bottani, S. Mérens, Effective non-universality of the quorum percolation model on directed graphs with Gaussian in-degree, *Physica A: Statistical Mechanics and its Applications* 414 (m) (2014) 352–359. doi:10.1016/j.physa.2014.07.028.
- 515 URL <http://linkinghub.elsevier.com/retrieve/pii/S0378437114005974>
- [26] T. Tlustý, J. P. Eckmann, Remarks on Bootstrap Percolation in Metric Networks, *JOURNAL OF PHYSICS A: MATHEMATICAL AND THEORETICAL* 42 (2009) 1–11. arXiv:0902.3384, doi:10.1088/1751-8113/42/20/205004.
- 520 URL <http://arxiv.org/abs/0902.3384>
- [27] J. G. Orlandi, J. Soriano, E. Alvarez-Lacalle, S. Teller, J. Casademunt, Noise focusing and the emergence of coherent activity in neuronal cultures, *Nature Physics* 9 (9) (2013) 582–590. doi:10.1038/nphys2686.
- 525 URL <http://dx.doi.org/10.1038/nphys2686><http://www.nature.com/doifinder/10.1038/nphys2686>
- [28] L. Hernández-Navarro, J. G. Orlandi, B. Cerruti, E. Vives, J. Soriano, Dominance of Metric Correlations in Two-Dimensional Neuronal Cultures Described through a Random Field Ising Model, *Physical Review Letters* 118 (20) (2017) 1–5. doi:10.1103/PhysRevLett.118.208101.
- 530

J.3 Bursting and adaptation (Frontiers in Neuroscience 2018)

This paper gives a more detailed mathematical description of the bursting model developed in “A concise model for periodic bursting” (subsection 2.2.1). It provides a description of the different results obtained through the description of synapses by either instantaneous Dirac synapses, “continuous” synapses, and alpha-shaped current synapses. From these results, theoretical predictions regarding the effect of adaptation channels (AHP) on the global dynamics are then proposed. These predictions were later tested experimentally and preliminary results are discussed in “Shaping bursts through adaptation channels” (subsection 2.2.2).

References to the supplementary material can be directly obtained in “Self-consistent equations for the bursting behavior” (Appendix C).



Understanding the Generation of Network Bursts by Adaptive Oscillatory Neurons

Tanguy Fardet^{1*}, Mathieu Ballandras¹, Samuel Bottani¹, Stéphane Métens¹ and Pascal Monceau^{1,2}

¹ Laboratoire Matière et Systèmes Complexes, UMR 7057, Université Paris Diderot, USPC, Paris, France, ² Department of Physics, Université d'Evry-Val d'Essonne, Evry, France

OPEN ACCESS

Edited by:

Matteo Barberis,
University of Amsterdam, Netherlands

Reviewed by:

Alexey Goltsov,
Abertay University, United Kingdom
Frederic Von Wegner,
Universitätsklinikum Frankfurt,
Germany

*Correspondence:

Tanguy Fardet
tanguy.fardet@univ-paris-diderot.fr

Specialty section:

This article was submitted to
Systems Biology,
a section of the journal
Frontiers in Neuroscience

Received: 03 October 2017

Accepted: 17 January 2018

Published: 06 February 2018

Citation:

Fardet T, Ballandras M, Bottani S,
Métens S and Monceau P (2018)
Understanding the Generation of
Network Bursts by Adaptive
Oscillatory Neurons.
Front. Neurosci. 12:41.
doi: 10.3389/fnins.2018.00041

Experimental and numerical studies have revealed that isolated populations of oscillatory neurons can spontaneously synchronize and generate periodic bursts involving the whole network. Such a behavior has notably been observed for cultured neurons in rodent's cortex or hippocampus. We show here that a sufficient condition for this network bursting is the presence of an excitatory population of oscillatory neurons which displays spike-driven adaptation. We provide an analytic model to analyze network bursts generated by coupled adaptive exponential integrate-and-fire neurons. We show that, for strong synaptic coupling, intrinsically tonic spiking neurons evolve to reach a synchronized intermittent bursting state. The presence of inhibitory neurons or plastic synapses can then modulate this dynamics in many ways but is not necessary for its appearance. Thanks to a simple self-consistent equation, our model gives an intuitive and semi-quantitative tool to understand the bursting behavior. Furthermore, it suggests that after-hyperpolarization currents are sufficient to explain bursting termination. Through a thorough mapping between the theoretical parameters and ion-channel properties, we discuss the biological mechanisms that could be involved and the relevance of the explored parameter-space. Such an insight enables us to propose experimentally-testable predictions regarding how blocking fast, medium or slow after-hyperpolarization channels would affect the firing rate and burst duration, as well as the interburst interval.

Keywords: bursting, adaptation, neuronal networks, synchrony, oscillators

INTRODUCTION

Network bursting is an intermittent collective behavior that occurs spontaneously in neuronal populations. It is characterized by long quiet periods, with almost no spike emission, punctuated by brief periods of intense spiking activity, where the whole network displays high firing rates—most neurons emit at least 2 closely-packed spikes. This particular pattern is then repeated, with varying regularity, over long time intervals.

Such periodic and synchronized activity has been observed as an emergent phenomenon in large neuronal populations, both in brain regions (Meister et al., 1991; Blankenship and Feller, 2009; Rybak et al., 2014) and unperturbed neuronal cultures (Wagenaar et al., 2006; Stegenga et al., 2008; Penn et al., 2016). It has been investigated as a plausible candidate for rhythmogenesis (Ramirez et al., 2004), but also in various disorders such as epilepsy (Derchansky et al., 2008) or Parkinson's disease.

Recent experiments by Penn et al. (2016), studying dissociated neuronal cultures where the chemical environment was precisely controlled, provide evidence that the majority of hippocampal pyramidal neurons are self-sustaining oscillators. These oscillators spontaneously synchronize to give birth to a very regular network bursting phenomenon.

Starting from these results and others (Ramirez et al., 2004; Suresh et al., 2016), we propose here a detailed understanding of the synchronized network bursting dynamics that explains and reproduces other experimental observations (Sipilä et al., 2006; Masquelier and Deco, 2013; Orlandi et al., 2013) of bursting on a variety of different timescales and with inter-burst intervals (IBIs) ranging from less than 1 s up to several minutes. We focus specifically on the characterization of the synchronized attractor and do not consider the transient synchronization process from an asynchronous to a synchronized phase. Indeed, synchronization of pulse-coupled oscillators is a known asymptotic behavior (Somers and Kopell, 1993; Bottani, 1995), which has been shown to lead to bursting in the presence of adaptation (Van Vreeswijk and Hansel, 2001). This was confirmed in all our simulations, regardless of the precise neuronal parameters, as long as they corresponded to adaptive oscillatory neurons. By oscillatory, we mean that a single neuron will spike periodically if uncoupled and considered independently.

Let us insist on the fact that collective bursting, giving rise to “network bursts,” should not be confused with the individual behavior observed at the cellular level for “bursting” or “chattering” neurons. Though they share similar intervals of rapid firing followed by long quiet periods (Connors and Gutnick, 1990; Sipilä et al., 2006), hence the common name, collective bursting can stem from radically different mechanisms and occur on different timescales (see Supplementary S1.3). Here, population-wide bursts are a specific synchronized behavior emerging from the interaction of oscillating, adaptive-spiking neurons which do not display intrinsic bursting behavior when considered independently but only emit single spikes.

The periodic activity of the intrinsically oscillatory neurons present in culture populations and brain regions is assumed to rely on leak currents which affect their excitability (Suresh et al., 2016). More specifically, the persistent, non-inactivating, sodium current $I_{Na,p}$ (Golomb et al., 2006; Penn et al., 2016) and the H-current I_h (Lüthi and McCormick, 1998) are the prime candidates for this intrinsic depolarization. Adaptation, on the other hand refers to the capacity of a neuron to change—here, more precisely, to lower—its excitability in response to continuous or repeated excitation, such as a step-current in electrophysiological experiments, or the intense synaptic input received from its neighbors during a collective burst. Adaptive neurons indeed display periodic firing with a spiking frequency that progressively slows down from its initial high frequency value. The biophysical processes mediating adaptation are thus distinct for the origin of the rhythmic behavior which they modulate, and several potassium currents are considered for this frequency adaptation, like the muscarinic K^+ (I_M) current or the Ca^{2+} activated K^+ currents (I_{AHP}) (Sah and Louise Faber, 2002; Golomb et al., 2006).

We show here that adaptive spiking is a sufficient condition for network bursting, confirming what was suggested by previous studies (Van Vreeswijk and Hansel, 2001; Masquelier and Deco, 2013; Ferguson et al., 2015), and that intrinsically bursting or chattering neurons are not required. Indeed, we focus on the role of adaptation to explain why, as observed in the experiments, the presence of inhibitory neurons is not necessary to obtain regular collective bursting dynamics. Likewise, though short-term synaptic plasticity might play a role in shaping the dynamics (Gritsun et al., 2010; Masquelier and Deco, 2013), we also demonstrate that it is not required to reproduce characteristic timescales of this dynamics.

METHODS

We first describe the models used for the different units composing the system (neurons, synapses and network structure). Based on these, we derive an effective model which remains almost completely tractable, so that most of the properties of the collective dynamics can be predicted analytically. This model is based on successive approximations which were validated by numerical experiments: by dividing the cyclic behavior into several subdomains, we isolate regions where the activity can be solved under different approximations. The final solution is thus composed of the concatenation of these different approximations. We also used these simulations to verify and extend the predictions of our analytic equivalent model.

Neuronal Model

We chose the adaptive Exponential Integrate-and-Fire (aEIF) model (Brette and Gerstner, 2005) because of its compromise between simplicity and biological relevance. The dynamical evolution of a neuron is described by two variables, its membrane potential \tilde{V} , and a slow adaptation current \tilde{w} , which are governed by the following equations:

$$\text{if } \tilde{V} \leq \tilde{V}_{peak} \quad \left\{ \begin{array}{l} \tilde{C}_m \frac{d\tilde{V}}{dt} = -\tilde{g}_L(\tilde{V} - \tilde{E}_L) + \tilde{g}_L \tilde{\Delta T} e^{\frac{\tilde{V} - \tilde{V}_{th}}{\tilde{\Delta T}}} \\ \quad - \tilde{w} + \tilde{I}_e + \tilde{I}_s \\ \tilde{\tau}_w \frac{d\tilde{w}}{dt} = \tilde{a}(\tilde{V} - \tilde{E}_L) - \tilde{w} \end{array} \right.$$

$$\text{else if } \tilde{V} > \tilde{V}_{peak}, \quad \text{then} \quad \left\{ \begin{array}{l} \tilde{V} \leftarrow \tilde{V}_r \\ \tilde{w} \leftarrow \tilde{w} + \tilde{b} \end{array} \right. \quad (1)$$

where \tilde{C}_m is the membrane capacitance, \tilde{g}_L is the leak conductance of the neuron, \tilde{E}_L is its resting potential, $\tilde{\Delta T}$ affects both the slope and the strength of the spiking current, \tilde{V}_{th} is the threshold potential, $\tilde{\tau}_w$ is the adaptation timescale, \tilde{a} gives the strength of subthreshold adaptation, \tilde{b} gives the intensity of the spike-triggered adaptation, and \tilde{V}_r is the reset potential. \tilde{V}_{peak} is the spike cutoff for the model. \tilde{I}_e is an external current to which the neuron can be submitted.

The main difference of this model compared to the well-known integrate-and-fire model is the presence of the

second variable, the current \tilde{w} , which modulates the neuronal excitability. The synaptic input received by a neuron is represented by the variable \tilde{I}_s , which is usually time dependent. The neuronal adaptation can be either subthreshold, through the coupling between \tilde{V} and \tilde{w} via \tilde{a} , or spike-driven, from the step increments of size \tilde{b} that \tilde{w} undergoes after a spike.

The exponential spike generation present in the aEIF model is more realistic than the hard threshold of the original Integrate-and-Fire model, which leads to unrealistically fast spiking during bursts. The soft threshold of the Izhikevich model (Izhikevich, 2007), which also includes adaptation and could have been a possible choice, is similar to that of the aEIF model and would be analytically more tractable. However, it generates a divergence which is not sharp enough, thus leading to overly long interspikes and induces an undesired influence of the cutoff value (V_{peak}) on the neuronal dynamics (Touboul, 2009). Despite its non-analytic nature, this feature of the aEIF model was therefore critical to capture the inter-spike dynamics inside bursts.

In this study, and in accordance with the experimental observations for several types of pyramidal neurons, we use only neuronal parameters leading to adapting neurons which exhibit periodic spiking. This state is reached through the persistent current \tilde{I}_e , which drives their progressive depolarization and makes them spike periodically; setting $V_r < V_{th}$ ensures that the neurons are not intrinsically bursting, as described in Naud et al. (2008).

Contrary to the resting state, where one stable and one unstable fixed point exist (points where both $\dot{\tilde{V}}$ and $\dot{\tilde{w}}$ are zero), the periodic activity occurs after these two points disappear through a bifurcation, as described in Brette and Gerstner (2005) and Touboul and Brette (2008), when I_e becomes high enough. In this spiking regime, no fixed point is present in phase space, which allows the neuron to depolarize until V_{peak} before being reset to V_r , thus following a discontinuous limit cycle. Illustration of the resting and spiking behaviors can be found on Figures S2, S3, while biologically-relevant values of the parameters used for the aEIF model can be found in Table S1, in the Supplementary Material.

For these parameter sets, we have $\tilde{\tau}_w \gg \tilde{\tau}_m = \frac{\tilde{C}_m}{\tilde{g}_L}$, as the typical timescales for the continuous variation of \tilde{w} relate to medium and slow after-hyperpolarization, which occur over hundreds of milliseconds (Sah and Louise Faber, 2002).

During the rest of the study, we use the dimensionless version of the model:

$$\begin{cases} \dot{V} &= -(V - E_L) + e^V - w + I_e + I_s \\ \tau_w \dot{w} &= a(V - E_L) - w \end{cases} \quad (2)$$

$$\begin{cases} \dot{V}_i &= -(V_i - E_L) + e^{V_i} - w_i + I_e + \underbrace{\sum_{j \rightarrow i} \sum_{t_j} s_{ji} \cdot (t - t_j - d) \Theta(t - t_j - d) e^{-\frac{t - t_j - d}{\tau_s}}}_{I_{syn,i}(t)} \\ \tau_w \dot{w}_i &= a(V_i - E_L) - w_i \end{cases} \quad (5)$$

Details for the change of variables can be found in the first section of the Supplementary Material, “Neuronal model

and parameters.” From then on, all equations involve only dimensionless variables and parameters.

Synaptic Model

The coupling strength between a pre-synaptic neuron j and a post-synaptic neuron i , such that $j \rightarrow i$, is represented by the total charge Q_s transmitted from j to i . This charge is passed dynamically through the ion channels of the synapses, which we represent here by an alpha-shaped post-synaptic current (PSC) (Roth and van Rossum, 2009). If neuron j spikes at time t_j , the triggered PSC is felt by i , after a delay d_{ji} , and is described by:

$$\begin{aligned} I_s(t) &= \Theta(t - t_j - d_{ji}) I_{ji}(t - t_j - d_{ji}) \\ &= s_{ji} I_0 \cdot (t - t_j - d_{ji}) \Theta(t - t_j - d_{ji}) e^{-\frac{t - t_j - d_{ji}}{\tau_s}}. \end{aligned} \quad (3)$$

Where s_{ji} is the strength of the synaptic connection from j to i , τ_s is the characteristic synaptic time, $\Theta(x)$ is the Heaviside step function, such that $\Theta(x) = 0$ if $x \leq 0$ and $\Theta(x) = 1$ if $x > 0$, and $I_0 = \frac{1pA}{\tilde{g}_L \Delta T}$ is the unit current which we set in this way to be coherent with the conventions of the NEST simulator (Kunkel et al., 2017). As such, the total charge delivered to i reads:

$$Q_{s,ji} = \int_0^\infty I_{ji}(t) dt = s_{ji} I_0 \tau_s^2. \quad (4)$$

Network Models

This study is based on two non-spatial random network models: a fully homogeneous network with fixed in-degree which is useful to introduce the equivalent model, and more heterogeneous Gaussian in-degree networks which are supposed to be representative of connectivity in dissociated cultures (Cohen et al., 2010). Both random networks are generated in the same way by drawing a number k_i (in-degree) of incoming connections originating from randomly chosen other neurons in the population. In the case of fixed in-degree networks, the in-degree k_i is fixed and identical for each neuron. For Gaussian random networks, k_i is drawn for each neuron from a Gaussian distribution with mean value \bar{k} and standard deviation σ_k . Note that the fixed-in-degree networks can be seen as the limit case of the Gaussian ones when the variance goes to zero. The out-degree distributions are binomial and identical in both cases. All networks were generated using the graph-tool or igraph backends of the NNGT library.

All transmissions between neurons in the network are subjected to the same delay d and have the same synaptic strength s , which means that the complete dynamical system describing the network is given, for each neuron i , by:

Where $\{j \rightarrow i\}$ is the set of neurons j that are presynaptic neurons for i and $\{t_j\}$ is the set of spike times for neuron j .

Numerical Simulations

All dynamical simulations were performed using the NEST simulator (Kunkel et al., 2017) with the `aEIF_psc_alpha` model implementation, that we developed, and which corresponds to the Equations (2, 3) presented above. Neurons were set to adaptive spiking using the neuronal and synaptic parameters detailed in Table S1 and were connected using `static_synapses`, i.e., without plasticity, but including a delay d in the spike transmission. Simulations were started from a population of neurons in an asynchronous random state, with their state variable \tilde{w} following a normal distribution of average value 50 pA and standard deviation 10 pA. The runs were performed on networks containing 1,000–100,000 neurons with an average degree of 100, which is the typical value estimated in mature neuronal cultures (Cohen et al., 2010).

Activity Analysis

For each simulation we computed the average firing rate $\nu = \frac{N_s}{T}$, where N_s is the total number of spike and T is the simulation time. This gives us a characteristic timescale t_ν , which would be the average interspike if the spikes were distributed uniformly. Considering d as the transmission delay of action potentials, bursts are identified as uninterrupted sequences of spikes separated by less than $\min(t_\nu/2, 3d)$; they must also involve at least 20% of the neurons. This analysis was performed using tools from the NNGT library and extra functions available on our GitHub repository.

$$\begin{cases} \dot{V} = -(V - E_L) + e^V - w + I_e + \underbrace{\sum_j ksI_0 \cdot (t - t_j - d)\Theta(t - t_j - d)e^{-\frac{t-t_j-d}{\tau_s}}}_{I_{syn}(t)} \\ \tau_w \dot{w} = a(V - E_L) - w \end{cases} \quad (6)$$

Equivalent Analytical Model

We derived an equivalent model that describes the system dynamics and predicts the range over which the characteristic frequencies can vary without the need to simulate the network dynamics. The model focuses on the fully synchronized dynamics, for which all neurons behave almost identically. The rationale of the model is most apparent if we first consider the case of a fixed in-degree network. As illustrated on **Figure 1**, in this case, once the population is synchronized, all neurons receive the same input, that is the contribution of k simultaneous spikes given by the sum of k PSCs. Here, one neuron behaves exactly as any other neuron, thus, $\forall i, j, t \quad V_i(t) = V_j(t) = V(t)$.

This means that the network of N neurons receiving k inputs of strength s is equivalent to N isolated neurons, each one forming a close loop with one autapse—that is, a self-loop—of strength $k \times s$. This simplification is inexact if all neurons do not have the same number of incoming connections, however, as shown in the Results section, this approximation holds very well for homogeneous Gaussian networks and, through a slight modification of the synaptic dynamics, even the behavior of more heterogeneous Gaussian or scale-free networks can be estimated.

Based on this observation, exact for fixed in-degree networks, we propose a model of bursting dynamics for any synchronized

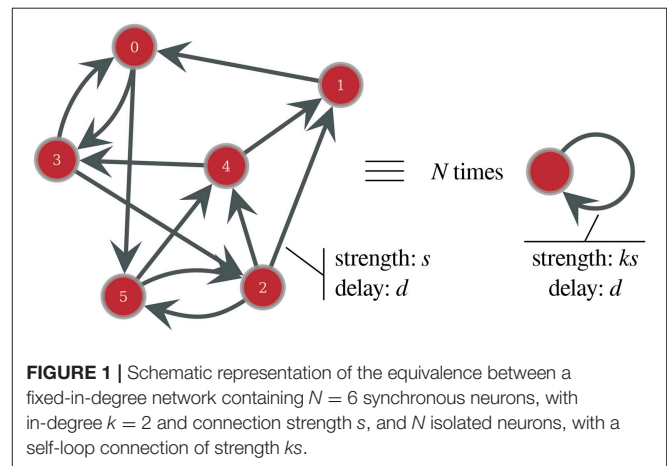


FIGURE 1 | Schematic representation of the equivalence between a fixed-in-degree network containing $N = 6$ synchronous neurons, with in-degree $k = 2$ and connection strength s , and N isolated neurons, with a self-loop connection of strength ks .

network, where we describe the whole population through the behavior of an equivalent neuron, representative of the “average” dynamics. This neuron is subjected to the “average” input received by neurons in the network, and, under this simplified description, Equation (5) is now the same for every neuron in the network, since they are all approximated by this equivalent neuron. As they all receive the same number of spikes (n_s) emitted at the same times $\{t_j, j \in [1, \dots, n_s]\}$, and from the same number k of neighbors, we obtain:

This single dynamical system is then solved through several approximations depending on the network state. A typical approximation in the burst, on the interval $[t_i, t_i + d]$ between the emission of a spike and its arrival, consists in linearizing the exponential term when $V < V_{th}$. On this interval, $I_{syn} = 0$ and since $d \ll \tau_w$, w can be considered as constant. This leads to an approximate solution for $V(t)$ that we will call $V_l(t)$, with $V_l(t_i) = V_r$ (see also Equations S2, S3 in Supplementary Material):

$$V_l(t) = V_r e^{-t} + (E_L + I_e - w)(1 - e^{-t}) \quad \text{for } t_i \leq t < t_i + d. \quad (7)$$

For $V \in [V_{th}, V_{peak}]$, we cannot solve the equation, but know from simulations that this simply leads the neuron to spike with a typical timescale of $\tau_m = 1$.

From these analytic formula, we can then constrain the final solution through a self-consistent equation. The solution of the self-consistent equation will therefore assure that the spikes of one neuron during a burst sustain the burst itself and drive the subsequent ones (self-loop in the equivalent representation of **Figure 1**), thus shaping a permanent and self-sustained bursting activity, as observed experimentally. Such a solution gives a complete description of the neuron’s dynamical properties in time and allows us to obtain all the characteristics of the bursting dynamics.

This equivalent approach is applied here to three different synaptic models (instantaneous, continuous, and alpha-shaped synapses) leading to three transcendental self-consistent equations; details of mathematical developments can be found in the Supplementary Material. Python tools to solve the self-consistent equations and compute the characteristics of the bursting behavior are available on our GitHub repository; they are based on the `scipy` implementation of Brent's root-finding method.

Exploration of Parameter Space

Thanks to the fast computation of the equivalent model, we were able to compute the dynamical properties for a large number of parameter sets. These results were normalized and analyzed through a Principal Component Analysis algorithm, using the `scikit.learn` package, in order to obtain the correlation matrix linking the collective dynamical properties to the precise values of the neuronal parameters.

For each parameter set, we first ensure that there is no stable fixed-point in phase-space and that the model predicts a solution, i.e., the existence of bursts with mathematically coherent properties. Secondly, we assess the biological relevance of the solution by (1) ruling out dynamics for which the voltage decreases to values lower than -120 mV during the giant hyperpolarization following a burst; (2) restricting the maximum value of the slow current w to $1,000$ pA; (3) preventing cellular bursting for individual neurons by asserting $V_r < V_{th}$ —this restricts the neurons to single-spike intrinsic behaviors (Naud et al., 2008).

These constraints limit the number of “valid” parameter sets and make the parameters inter-dependent; this leads to a non-trivial parameter/parameter correlation matrix (Figure S1).

RESULTS

As mentioned in the introduction and discussed in the Supplementary Material, synchronization is highly resilient and we focus here solely on the fully synchronized bursting network. We start from individual neurons which are spiking periodically, a behavior that seems to originate from persistent sodium currents like $I_{Na,p}$ or I_h in neuronal cultures (Penn et al., 2016); it is modeled here by a constant input current I_e . When these neurons are coupled, however, their periodic dynamics is drastically modified as they adopt a collective bursting behavior (Borges et al., 2017).

We describe the attractor characterizing the dynamics of the synchronous bursting state. Our key result details the properties of this attractor and shows how they are linked to both the biological parameters of the neurons and the network topology.

The behavior shows features of a relaxation oscillator (see **Figure 4A**): the current w slowly decreases during the quiescent phase, then rapidly increases during the bursting phase until it reaches a threshold value w^* , which determines the burst termination and the start of a new cycle.

The main characteristic which determines the dynamics is the maximum value of the adaptation current, w^* reached at the end of a burst. It depends on the neuronal and network

parameters, and qualitatively obeys the following equation (details in subsection 5.3 of the Supplementary Material):

$$w^* \approx E_L + I_e + \frac{V_r e^{-d} + \bar{k}Q_s}{1 - e^{-d}} + C \quad (8)$$

where C is a constant. Since the firing rate during the burst is mostly linked to w^* , this equation directly shows that higher coupling ($\bar{k}Q_s$), higher excitability (E_L), or higher reset voltage (V_r) will increase the bursting intensity. The effect of the transmission delay d is slightly more complex but roughly decreases bursting intensity when increased.

Taking into account finer effects and spike-driven adaptation then leads to more complete equations delivering additional results about the influence of the remaining parameters. These are considered in more details in the Discussion section.

In the following subsections, we describe and explain the bursting dynamics, then discuss the more detailed, self-consistent versions of Equation (8) (complete derivation of these equations can be found in the Supplementary Material). Finally, we describe how our model accounts for the structural heterogeneity that is present in neuronal cultures.

The Attractor, Inner Structure of a Burst

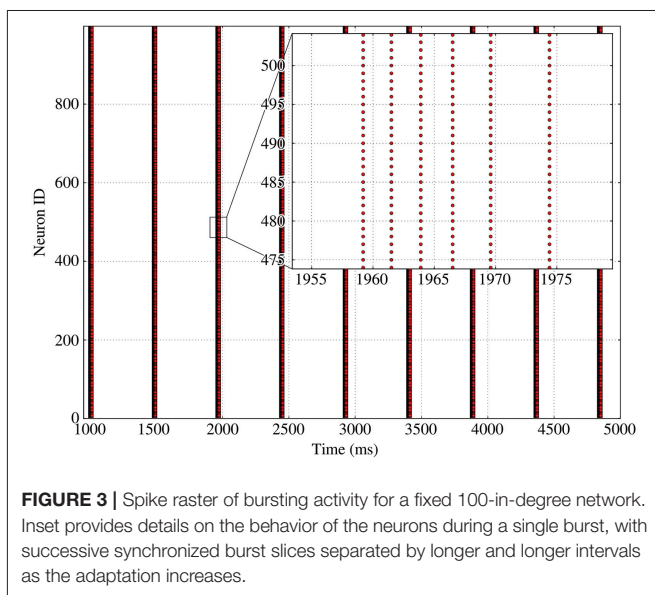
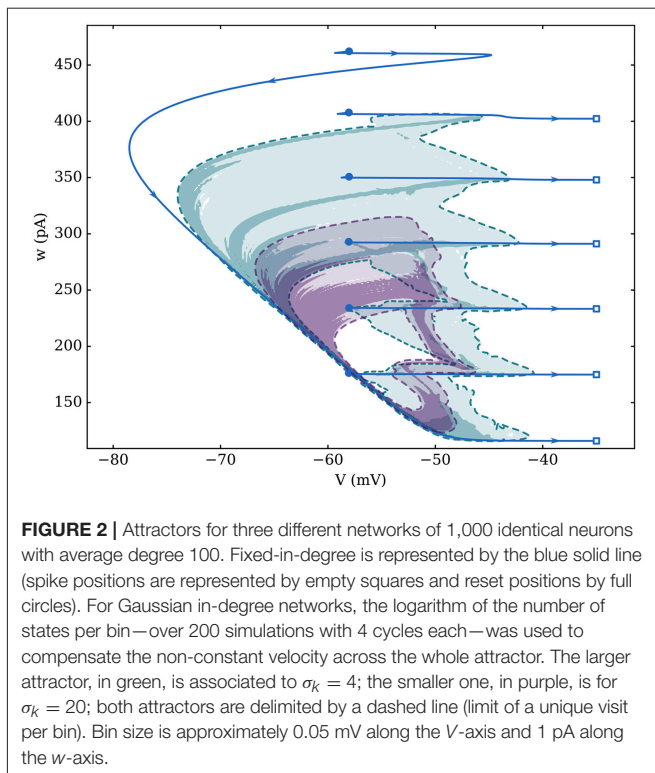
The synchronous attractor is composed of intermittent bursts of activity, as shown in **Figure 2** in the (V, w) phase space. During a cycle, the neuron state variables (V, w) do not follow the attractor at constant velocity: the neuron spends much longer on the recovery path (low V) compared to the bursting period (high V)—see **Figure 4** to see this trajectory in time.

This attractor is modified by the presence of heterogeneity in the network's topology—quantified by σ_k for Gaussian in-degree networks—which impacts both its duration and regularity. Indeed, heterogeneity noticeably smooths the average behavior and reduces the number of spikes in a burst which goes down from 6 spikes per burst for the fixed in-degree graph, to 3–5 if $\sigma_k = 4$, and is roughly reduced to 2 when $\sigma_k = 20$. For the fully synchronized fixed in-degree network, all neurons are responding to the exact same input—they receive spikes from the same number of neighbors—hence they are all equivalent to a single average neuron.

As can be seen on **Figure 3** for a fixed in-degree network, synchronized bursting of the population consists of a succession of active periods, called *bursts*¹, separated by long inactive intervals, which we call recovery periods. As can be seen on the inset, the burst displays a strongly ordered inner structure composed of successive *synchronized burst slices*, which are consistent sets of spikes stemming from a common input.

This inner structure, based on spike events, helps us define several quantities that characterize the dynamics such as the

¹Let us insist once again that the term *burst* always refers here to the concerted activity of a large fraction of the neuronal population (i.e., a *network burst*) and should not be confused with single neuron bursting behavior—though they share common characteristics—since they have different origins and population bursts occur on much longer timescales.



burst and inter-burst durations. However, information about the spike times alone is not sufficient to provide insights regarding the phenomena involved in the burst initiation or termination. Therefore, we will use the time evolution of the neuron's state variables to perform a phase-plane analysis and investigate possible mechanisms for both the bursting and recovery periods.

Neuronal Trajectory, Assessment of the Theoretical Model

From the simulation, we can record the evolution of V and w during the whole dynamics to reconstruct the trajectory of the neuronal state, both in time and in phase-space. **Figure 4A** represents the time evolution of the equivalent neuron (see **Figure 1**) during a bursting dynamics on a regular fixed in-degree network and the comparison with the trajectory predicted by the “alpha” equivalent model (see section 6 of the Supplementary Material, “A more detailed model: alpha-shaped synapses”). The close agreement between these trajectories shows that the theoretical model has a good predictive power. Indeed, the most visible discrepancy between the equivalent model and the simulations concerns the precise spike times, as shown in the inset of **Figure 4A**; however, though the difference can be significant on the intraburst timescale, it is in fact limited to a few milliseconds, which is negligible compared to the duration of a cycle.

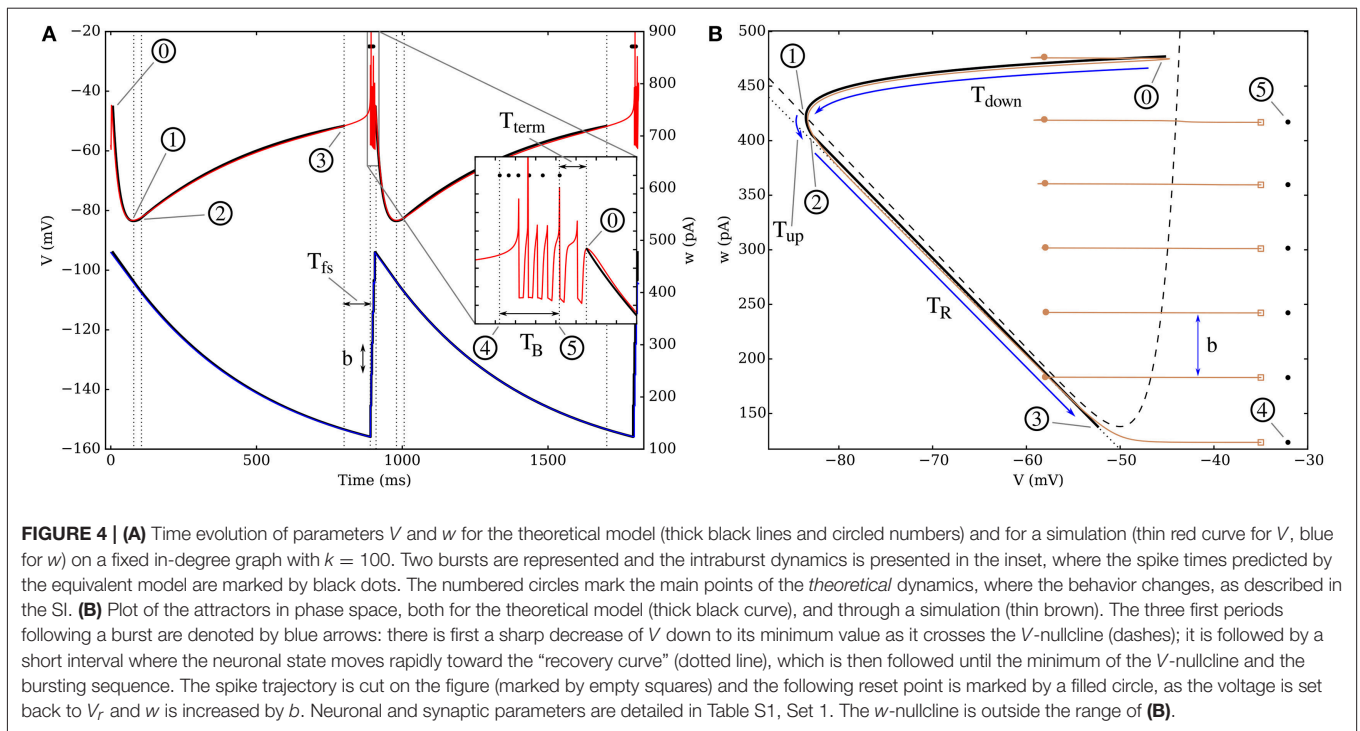
The dynamics can be understood most easily when looking at w since its behavior can be seen as relaxation oscillations: after a burst (0), the adaptation variable undergoes a quasi-exponential decrease until it reaches its minimum value w_{min} —passing through points (1) to (4). At this point, the burst starts and w increases rapidly toward a peak value w^* —point (5) on **Figure 4**, which characterizes the trajectory, and will be derived below. Once this maximum value is reached, the neuron stops spiking, the increase of w stops, then the cycle starts again (see Supplementary animation online).

The evolution of V can then be seen as an interplay between the influence of w , I_e , and the synaptic currents in the active period:

- During the burst, each new spike induces a strong depolarization of the membrane, thus leading to another spike—point (4) to (5) on the figure.
- Once w reaches its peak value w^* , its influence becomes predominant and prevents the neuron from firing; once the effect of the last spike vanishes, it drives a fast hyperpolarization of the neuron down to point (1).
- After V has reached a quasi-equilibrium value along its nullcline, it instantaneously adapts to the slow decay of w and increases progressively until the trajectory reaches the lowest point of the V -nullcline—point (3). This recovery from the strong hyperpolarization is greatly influenced by I_e .
- At this point, the potential starts increasing more rapidly as the first spike is initiated until the bursting starts again with (4), where the first spike predicted by the equivalent model occurs.

Understanding the Initiation and Termination of a Burst

One of the main interests of this equivalent model is that it provides an intuitive understanding of the mathematical conditions describing the initiation and the termination of bursts. As shown on **Figures 4B, 5**, the whole existence of the short active period can be understood from the position of the neuronal state in phase space compared to the V -nullcline (curve $\dot{V} = 0$), which can be seen as an effective threshold. Indeed, the initiation



of the burst simply occurs when w becomes low enough so that the trajectory can “pass under” the V -nullcline; this can be understood easily since the excitability of the neuron increases when w decreases. The lowest value w_{min} represent the situation where the excitability of the neuron has become so high that it spontaneously emits a spike.

A key result is then the derivation of a condition for burst termination. We show that the end of the spiking sequence that constitutes a burst is ensured by the intrinsic dynamical properties of single neurons—through adaptation mechanisms—and does not require inhibition nor plastic synapses.

To understand the succession of spikes during the burst and why this spiking process comes to an end, we must introduce a description of the dynamic coupling between the neurons. We first explicit this coupling for two limit cases: firstly instantaneous couplings in perfectly regular fixed in-degree networks, using synapses modeled by Dirac delta functions (called Dirac synapses in the following); secondly, mimicking the effect of highly disordered networks, where synapses release a constant current over the entire burst duration. Thirdly, we consider a more biologically relevant coupling using alpha-shaped synapses, detailed in section 6 of the Supplementary Material, which lies between these two previous limits.

In general, the synaptic coupling I_s between the neurons is time-dependent, which makes the resolution of the system’s dynamics (Equation 2) highly complex. As a result the V -nullcline ($\dot{V} = 0$) is not generally fixed over a whole cycle. This complicates the threshold condition on w^* in the case of the “alpha” synapses. Therefore, the Dirac and continuous synaptic models are more convenient since they enable us to get an insight on the bursting mechanisms through a static representation of the phase diagram during a burst.

Regular Networks and Dirac Synapses

The rationale for the condition of burst termination is most easily understandable in the case of regular networks assuming a coupling in the form of Dirac synapses. Indeed, the arrival of a spike then simply results in a step increment of the post-synaptic neuron’s membrane potential:

$$V(t_{sp}^+) = V(t_{sp}^-) + \bar{k}Q_s \tag{9}$$

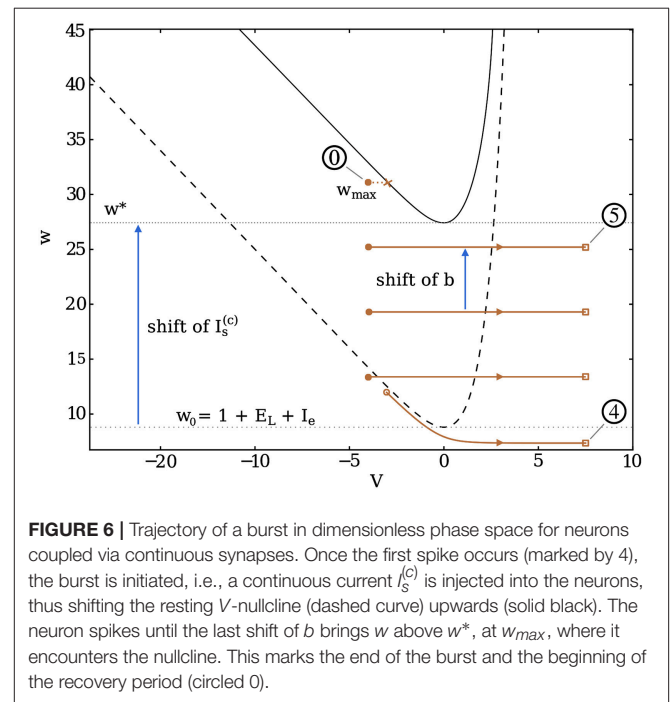
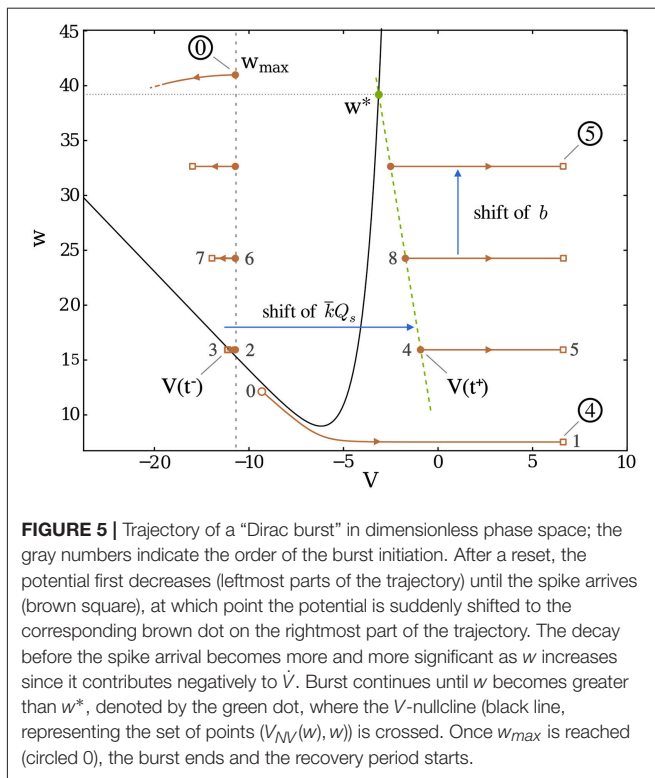
where t_{sp} is the time at which the spike is delivered to the post-synaptic neuron; t_{sp}^- , t_{sp}^+ are respectively the instants immediately before and after spike delivery. Q_s is the total charge delivered by the spike and reflects the coupling strength in the network.

The behavior of the neuron can easily be understood by looking at the situation in phase space on **Figure 5**. Due to the instantaneous coupling through the Dirac function, there is no finite period of time where the equation for V receives a non-zero input. Consequently, in this limit the V -nullcline remains fixed at all times. Therefore, the condition for the occurrence of a new spike during the burst depends only on the position of $V(t_{sp}^+)$ compared with the value of the V -nullcline at the same w : $V_{NV}(w)$. During an interspike of duration $T_I(w)$, w can be considered as constant since $\tau_m, T_I(w) \ll \tau_w$ (quasi-static approximation). Hence, either $V(t_{sp}^+) > V_{NV}(w)$ and a new spike occurs, or $V(t_{sp}^+) \leq V_{NV}(w)$ and the burst terminates.

Developing this condition mathematically leads to the following self-consistent equation:

$$w^* = E_L + I_e - V_r + \left[\mathcal{W}_{-1} \left(-e^{E_L + I_e - w^*} \right) + \bar{k}Q_s \right] e^d \tag{10}$$

where \mathcal{W}_{-1} is the lower branch of the Lambert W function.



Heterogeneous Networks and Continuous Synapses

For very heterogeneous networks, the broad in-degree distribution leads the neurons to fire at seemingly random times during the bursting period. In the limit where the time distribution of the spikes inside a burst becomes completely uniform, we can approximate it through a window-like synaptic current which is zero during the interburst, then jumps to a finite constant value during the burst.

To obtain an effect equivalent to the spikes described in the previous subsection, devoted the Dirac model, the total charge transmitted during the burst should be the same if an equal number of spikes is emitted. This condition reads, for an average in-degree \bar{k} , and a mean synaptic current $I_s^{(c)}$ during the burst,

$$I_s^{(c)} T_B = n_s \bar{k} Q_s, \tag{11}$$

where n_s is the number of spikes inside the burst. As described previously, the burst termination occurs when the trajectory crosses the V -nullcline. **Figure 6** shows this condition in this heterogeneous limit, i.e., as the input received by the neurons becomes continuous during the burst.

Because of the quasi-static hypothesis on w during an interspike, burst termination arises when w goes above the lowest point of the V -nullcline, which occurs for $w^* = 1 + E_L + I_s^{(c)} + I_e$. This is obtained by setting $V = 0$ in $w_{NV}(V)$. After a few lines of calculation detailed in the Supplementary Material (Equations S8–S10), we obtain the self-consistent equation:

$$w^* = w_{min} + b [\bar{t}_s(w^*) - d] + \bar{k} Q_s. \tag{12}$$

where $\bar{t}_s(w^*)$ is the average interspike interval (ISI) in the burst. As in the previous equations (Equations 8, 10), the critical value of the adaptation current w_j at which the burst terminates (1) increases when the coupling strength ($\bar{k}Q_s$) increases (2) decreases when the transmission delay d increases. Furthermore, this self-consistent equation also shows the effect of the spike-driven adaptation b which increases the maximum value of the adaptation current that can be reached.

Summary of the Theoretical Description

Once w^* has been computed using one of the theoretical models, we can derive all the dynamical properties, starting with:

$$w_{max} = \begin{cases} \left\lceil \frac{w^* - w_{min}}{b} \right\rceil b & \text{for fixed in-degree networks} \\ w^* & \text{with heterogeneity} \end{cases} \tag{13}$$

where $\lceil \cdot \rceil$ denotes the ceiling function. Though the self-consistent equations derived above are less easy to interpret compared to the approximated solution (Equation 8), they allow precise quantitative predictions of the network's dynamics without too much computational cost.

Note that the neurons follow a well-defined and unique attractor, with w changing by discrete steps, only in the case of a fixed in-degree network, where they are all equivalent and synchronous, hence the dual form of Equation (13). In the presence of heterogeneity, the attractor has fuzzy boundaries, as shown by numerical simulations on **Figure 2**. In this case, the average adaptation over all neurons has a smooth dynamics and w_{max} is closer to the statistical value at which the neurons stop bursting: w^* .

The complete dynamics of the model can be completely captured by the relaxation behavior of w , which displays

two phases: one resting period where the adaptation variable decreases until it reaches its lowest value, and an active period where w increases rapidly up to its peak value. The duration of the resting period (interburst interval, or IBI) can be approximated as the sum of the following terms:

T_{down} characterizes the time necessary for the neuron to undergo its strong hyperpolarization and reach its lowest membrane potential—from (0) to (1) on **Figure 4**,

T_R is the duration of the recovery—from (2) to (3),

T_{fs} is the time necessary for the initiation of the first spike which is roughly equivalent to the membrane time constant τ_m —from (3) to (4).

This allows us to obtain the characteristic values of the dynamics (see section 8 of the Supplementary Material, “Resting period”, for detailed calculations):

$$n_s = \left\lceil \frac{w^* - w_{min}}{b} \right\rceil \text{ (average number of spikes in a burst),}$$

$$T_B = \sum_{j=1}^{n_s-1} t_s(w_{min} + jb), \text{ where } t_s(w) \text{ is the interspike interval (ISI) for a given value of } w,$$

$$T_{down} = \ln \left(\frac{\lambda}{\lambda - V_{max} + E_L + I_e - w_{max}} \right),$$

$$T_R = \frac{\tau_w - a}{1 + a} \ln \left(\frac{w^{(2)} - \frac{a}{1+a} I_e}{w_{min} - \frac{a}{1+a} I_e} \right), \text{ where } w^{(2)} \text{ is the value of } w \text{ at point (2),}$$

$$IBI \approx T_{down} + T_R + 1.$$

Because these results are analytic, thus immediate to compute, this has the significant advantage over simulations that it allows us to quickly predict the properties of the collective dynamics for a large number of parameter sets, i.e., of individual neuron’s behaviors.

Evolution of the Properties with Neuronal and Synaptic Parameters

In order to assess the separate influence of the different neuronal parameters on the bursting properties, we used the model to test in a systematic way the influence of the separate variables. As can be seen on **Figure 7**, this allows to compare the relative influence of any desired set of parameters in a fast and systematic way. Thus, it is a valuable tool to make preliminary explorations in order to prepare for subsequent experimental tests.

This matrix allows us to confirm obvious trends, such as the negative influence of the driving current I_e on the IBI , as it tends to quicken the depolarization of the neurons. Likewise, τ_w is almost linearly related to the IBI since it dictates the decay time for w . However, this systematic study also revealed less predictable correlations. Indeed, one of the most interesting features is the quasi-absence of influence of the subthreshold adaptation variable a compared to the spike-driven adaptation (characterized by b and V_r) on the most visible features of the activity, namely the IBI and burst duration.

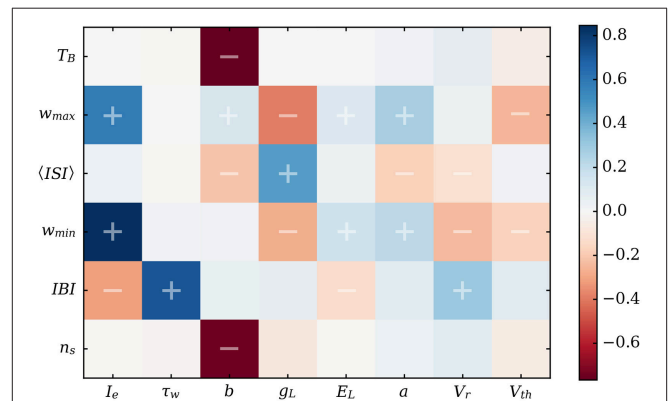


FIGURE 7 | Correlation matrix for the main characteristics of the bursting dynamics vs. neuronal parameters. $\langle ISI \rangle$ is the mean value of the interspike interval over one burst. Correlations were performed over 2 million randomly-drawn neuronal parameter sets using the predictions of the equivalent model. The experimentally observable features are the IBI , T_B , n_s , and $\langle ISI \rangle$.

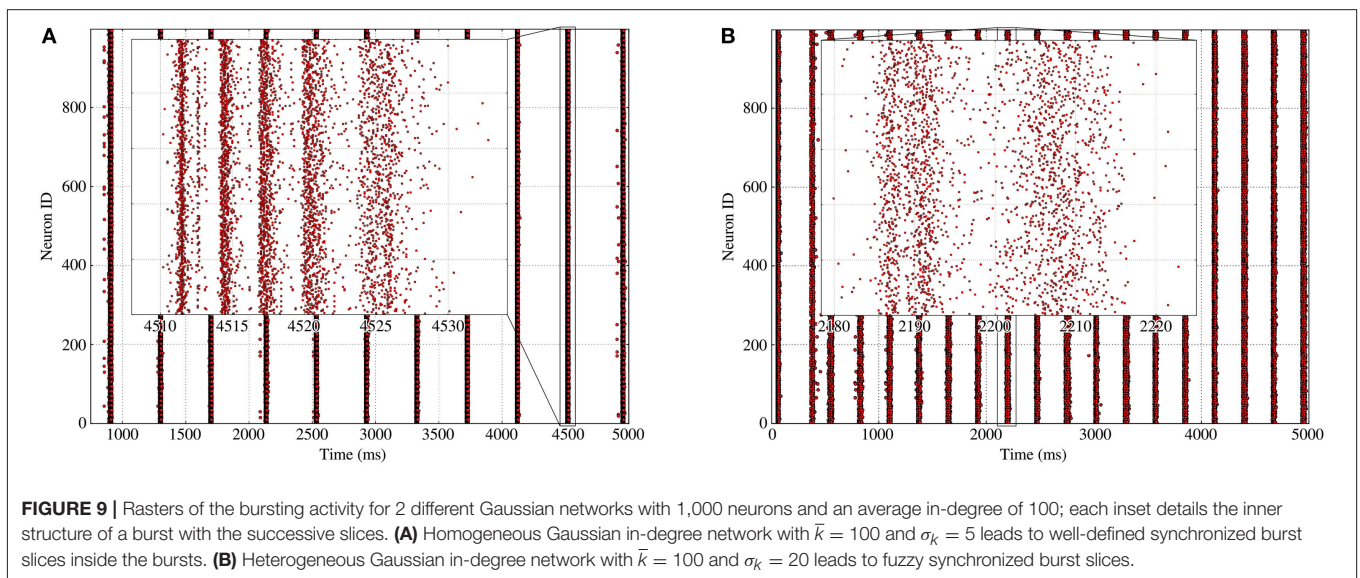
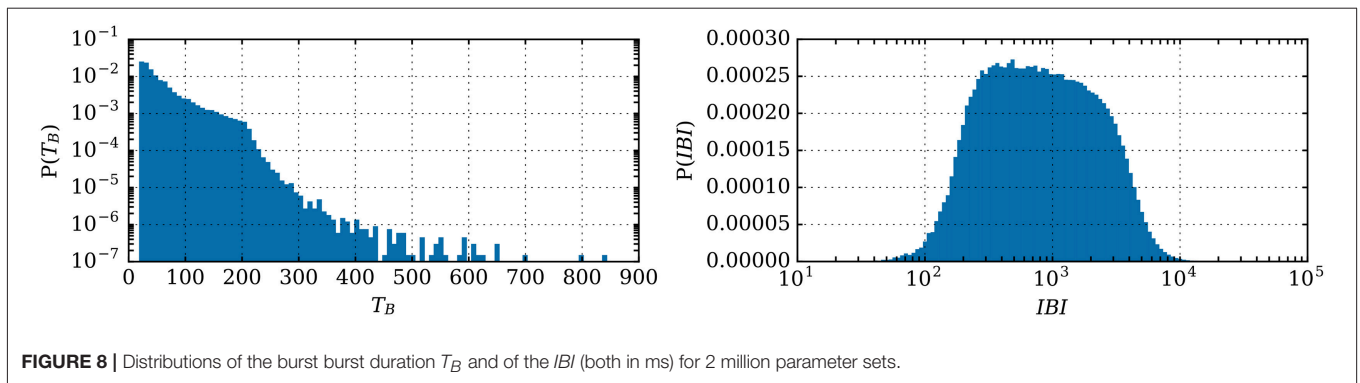
Correlations for $\langle ISI \rangle$ should be treated with care as this value is the average of the interspike interval over a burst. An additional spike (increment in n_s) automatically increases $\langle ISI \rangle$ since the new interspike interval will be larger than the previous ones. This is due to the monotonic growth of ISI with w as the burst progresses. Thus, if V_r indeed reduces the interspike duration on the whole, the negative correlation between $\langle ISI \rangle$ and b mainly comes from the decrease of n_s as b increases.

Due to the sheer amount of calculation this would require, the theoretical values returned by the equivalent model during this large exploration of parameter-space cannot be verified by simulations in a systematic way. However, the distributions of the bursting characteristics (number of spikes, interburst, and burst duration) are in biologically relevant ranges—see **Figure 8**. This shows that adaptation alone can lead to network bursts with periods varying from a few tenths of milliseconds to several seconds.

Predictive Ability of the Burst Model for Heterogeneous Networks

Our description of periodic bursts predicts the main features of the synchronized bursting rhythmic activity such as its period and firing rate, which are significantly influenced by the presence of heterogeneity in the network’s structure, as was already visible in **Figure 2**. Indeed, as the heterogeneity—namely σ_k —increases, the sharpness of the synchronized burst slices decreases until the spikes contained in the burst become more uniformly distributed; this is clearly visible on **Figure 9**, which shows the comparison of a burst for two Gaussian in-degree networks with different standard deviations.

Our model is able to take this heterogeneity into account through three synaptic descriptions (Dirac, alpha-shaped, or “continuous”): this allows us to predict the interval in which the bursting properties of most networks should be contained. As shown on **Figure 10**, they fall in between the Dirac and



“continuous-synapses” models. This description successfully accounts for dynamics of networks with low heterogeneity. For high levels of heterogeneity and low synaptic strengths, the model tends to overestimate the synchrony, although prediction of the bursting period remains correct.

DISCUSSION

In all the simulations we performed, we observed that oscillating adaptive spiking neurons synchronize, then start emitting bursts of spikes as the coupling increases.

Our model provides a predictive framework which allows us to determine how this bursting behavior is affected by changes in the individual properties of the neurons.

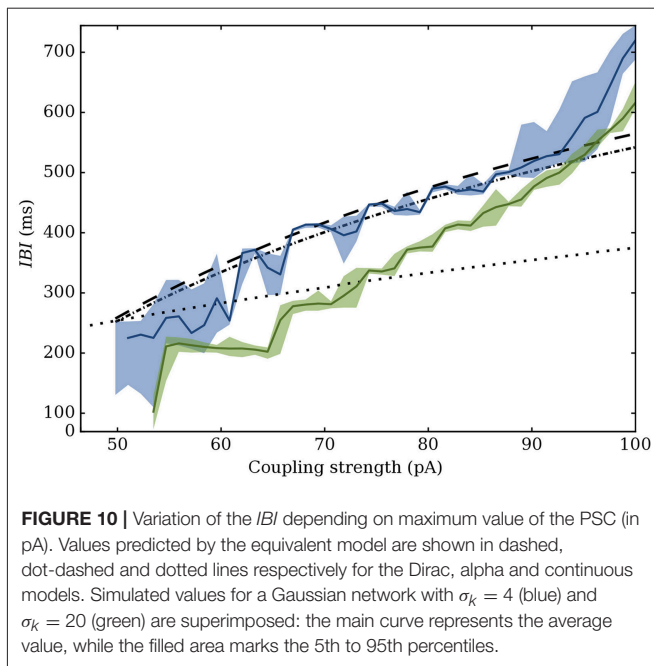
In the following subsections, we first discuss the validity range of the analytic model. Then, through a thorough mapping of the aEIF parameters to ion channels and biological mechanisms, we make experimentally-testable predictions about the possible influence the main adaptation channels on the bursting behavior. Namely, we suggest how adaptation-channel blockers may affect the dynamics when applied on a bursting neuronal culture.

Validity Range of the Equivalent Model

In order to get meaningful results within the framework of the present model, one must take care to use sets of parameters that lead to adaptive spiking neurons.

More importantly, the conceptual boundaries of the model are reached in the limit of either a very weakly or very strongly coupled neuronal network. For strong coupling the discrepancy between the equivalent model and the simulations mostly occurs because PSCs becomes so intense that a single input can generate several spikes. This can occur *in silico* but has little biological relevance for adaptive spiking neurons. The weak coupling limit, however, is more revealing since a progressive transition from an asynchronous state to a bursting phase occurs. This transition first involves oscillating firing rates, then synchronous slices containing between one and two spikes, before bursts containing multiple spikes appear. Our equivalent model, designed to describe a fully synchronous bursting dynamics, cannot faithfully capture this smooth transition.

Regarding the network structure, more heterogeneous (e.g., scale-free) networks may also be described by the “continuous-synapse” model on some range of the coupling strength



as the qualitative bursting behavior is still present on such networks.

The Influence of Adaptation and Its Biological Origin

Despite its simplicity, the aEIF model takes into account most of the adaptation phenomena involved in biological neurons. Thus, voltage-gated subthreshold adaptation currents, like the muscarinic potassium current I_M (Womble and Moises, 1992) are quantified by the constant a in Equation (2). On the other hand, spike-triggered adaptation, which mostly comes from calcium-gated potassium channels leading to after-hyperpolarization (AHP) phenomena (Sah and Louise Faber, 2002), are quantified by the reset conditions. These calcium-activated currents can be separated into three main types (Sah, 1996; Sah and Louise Faber, 2002; Vogalis et al., 2003) according to their timescales. Over a few milliseconds (1–10 ms) the fast hyperpolarization current $fAHP$ contributes to action potential repolarization, and is thus taken into account by the model through the value of V_r in Equation (1). On an intermediate (“medium”) timescale, the current $mAHP$ has a fast rise-time (less than 10 ms), followed by a decay over 50 to several hundred milliseconds (Storm, 1989); it is modeled by the b step of w after a spike, in Equation (1). Finally, the slow hyperpolarization (Shah and Haylett, 2000; Andrade et al., 2012) current $sAHP$ has a slow rise of 100 ms or more, and an even slower decay over several seconds. It is mostly revealed after a train of action potentials and peaks between 400 and 700 ms. Though this current is not explicitly taken into account by the aEIF model, in the case of bursts, its qualitative effect can be obtained approximately by an increase of τ_w , which lengthens the effect of the potassium current after a burst. One of the limits of the

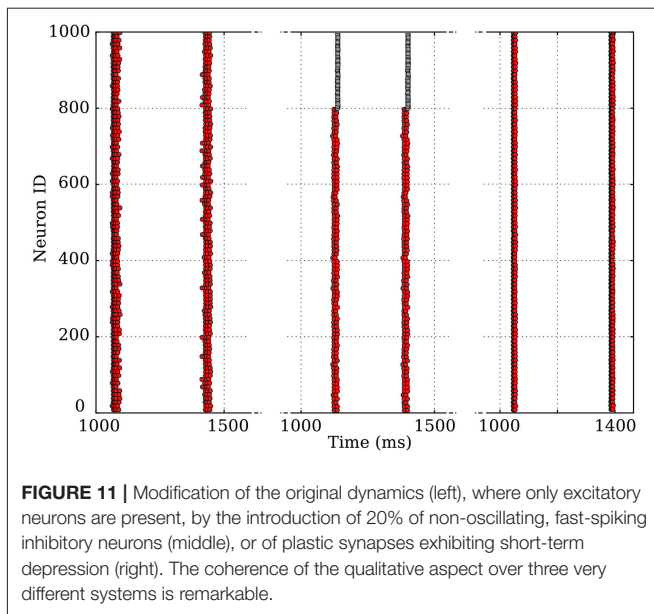
model is its unique timescale for all of the adaptation-related features.

From the exploration of parameter-space, we obtain the correlation matrix of **Figure 7**, which shows a significant influence of spike-triggered adaptation on the dynamics compared to subthreshold adaptation. A previous study (Augustin et al., 2013) also hinted at the importance of a non-zero b value to obtain low-frequency oscillations. Using the equivalent model, this can be explained easily by the quasi-static hypothesis and the shape of Equation (12). Indeed, the second term of the right-hand side involves the average ISI—which is an increasing function of w^* —and the spike-driven increment for the adaptation, b . Thus, the higher the effect of the spike-driven adaptation, the higher w^* , which leads to longer interbursts. On the other hand, the quasi-static hypothesis states that the evolution of w is slow compared to that of V , meaning that the subthreshold variations given by a are limited by their slow evolution on a timescale of τ_w .

A significant advantage of this simple description is that the mechanisms proposed by our equivalent model, in light of the correlation matrix on **Figure 7**, allow us to make qualitative predictions that could be tested to validate it experimentally. Thus, we predict that blocking the voltage-gated adaptation (Stiefel et al., 2008) should have only limited influence on the dynamics through a slight increase in the number of spikes during a burst. On the contrary, blocking one of the calcium-gated channels should lead to drastic changes in the collective behavior:

- Blocking the $fAHP$ channels should be equivalent to increasing V_r , hence increasing the number of spikes in a burst, leading to higher w_{max} , therefore longer *IBI*.
- Blocking the $mAHP$ channels through apamin (Sah and Louise Faber, 2002) would be equivalent to lowering the value of b , which should strongly impact the number of spikes inside a burst, therefore its duration. Yet, this should not change w_{max} significantly, so it should not strongly impact the *IBI* if the $sAHP$ is significant enough. However, in the case of complete blocking, if the $sAHP$ is not strong enough to compensate, this should lead to the complete disappearance of the bursting behavior.
- Specific blocking of $sAHP$ channels via noradrenaline (Sah and Louise Faber, 2002) should lead to a small increase of the number of spikes during a burst, but would mostly be equivalent to lowering τ_w . In situation where adaptation has the strongest influence over the bursting period, this would lead to a significant decrease of the *IBI*. This is however unlikely to happen in neuronal cultures, as will be explained below.

These experiments would enable to test the adaptation hypothesis and assess the relative strength of the different processes we described. In fact, some previous studies by Empson and Jefferys (2001) and de Sevilla et al. (2006) have shown results that seem to corroborate the previous predictions, at least regarding the effect of apamin on bursting in slices. However, the first study records only from few individual neurons, and the second uses 4-aminopyridine and Mg^{2+} -free medium to



trigger the epileptiform activity. To assess the general validity of the proposed mechanisms, one would thus need additional measurements using cultures in physiological conditions, and where each ion-channel would be tested independently while recording larger fractions of the network, either through calcium imaging or MEAs.

Moreover, other features, such as slow modulation of extracellular potassium concentration due to neuronal activity (Bazhenov et al., 2008) have been described in the context of rhythmic activities; these experiments would also help determine whether such phenomena are required as driving forces or only contribute to strengthening existing bursting activities. In our simulations, network bursting is very robust against the following modifications of the system: addition of inhibitory neurons in the network or inclusion of short-time depression in the synaptic dynamics, as shown on **Figure 11**. It is thus likely that the underlying mechanism we detailed for excitatory synapses can be generalized to these cases. Indeed, the mechanism remains unchanged by plasticity, while adding inhibitory neurons in the population essentially translates into an effective decrease of the excitatory coupling; the latter has been pointed out for percolation in networks of integrate-and-fire neurons.

Eventually, previous studies (Cohen and Segal, 2011) have hinted at the importance of synaptic fatigue in the burst termination: they showed that the duration of an evoked burst was strongly dependent on the elapsed time since the previous burst, due to the time needed to repopulate the pools of neurotransmitters. What we showed here is also compatible with these results, since they can easily be understood in the framework of our model: a smaller recovery time leads to a higher initial value of the adaptation current, thus shortening the burst duration because the maximum value of w is reached sooner. The effects of synaptic plasticity and adaptation should thus be similar; however, given the timescales reported in the literature, termination could be mostly mediated by adaptation,

while the *IBI* might depend more strongly on synaptic recovery time. In such a case, blocking sAHP as proposed above should not dramatically change the *IBI* of neuronal cultures.

CONCLUSION

This study explains the dynamical processes determining synchronous network bursting of a population of oscillating neurons coupled through excitatory synapses. In particular we explain why adaptation is a sufficient condition for collective bursting. We reproduce a large range of biological rhythms with burst frequencies spanning almost 3 orders of magnitude, from a few hundred milliseconds to tens of seconds, in agreement with experimental observations.

Thanks to a phase-space analysis, we are able to propose a mechanism for the initiation and termination of the bursting period related to spike-driven adaptation, which we link to the underlying biological phenomena. The derivation of analytic equivalent models describing the complete bursting dynamics allows us to predict the evolution of the characteristics of the global behavior from the properties of the individual units—neurons and synapses. This enables us to propose a set of experiments which should clarify the role of adaptation currents in network bursting, as well as their relative importance compared to other biological processes such as exhaustion of vesicle pools.

In our description, each new spike in the burst is caused by the previous one, which means that the delay between the emission of a spike and its reception by the post-synaptic neuron has a significant influence on the dynamics. Indeed, we understand intuitively that the longer the delay, the lower the excitability of the neurons when the PSC arrives, since the membrane potential can decay to lower values. This fact, added to the effect of heterogeneity—which tends to reduce the interburst interval—hints at the existence of a limit to the spatial extension which can sustain coherent bursting. Exploring the effect of heterogeneity and spatial embedding (through propagation delays) therefore constitutes a natural continuation of this work. This is certainly necessary to address experimental observations in large cultures, such as the tendency of the activity to initiate in specific regions before it propagates to the rest of the network (Orlandi et al., 2013).

AUTHOR CONTRIBUTIONS

Analytical study was conducted by MB and TF. TF also performed the numerical simulations and redaction of first draft. Additional simulations and analytical work were performed, respectively, by PM and SM. Final restructuring and adjustments were performed together by SB, TF, SM, and PM.

FUNDING

This work was granted access to HPC resources from the IDRIS (Orsay) under the allocation 2016057701 made by GENCI (Grand équipement national de calcul intensif).

ACKNOWLEDGMENTS

We would like to thank Elisha Moses, Yaron Penn, and Menahem Segal for their help and the invaluable discussions we had, as well as for sharing their data with us; Hans Ekkehard Plesser for his help and thorough reviews during the implementation and improvements of the numerical models in NEST; Sylvie Thérond for helping with the installation of NEST on the Turing supercomputer.

REFERENCES

- Andrade, R., Foehring, R. C., and Tzingounis, A. V. (2012). The calcium-activated slow AHP: cutting through the Gordian knot. *Front. Cell. Neurosci.* 6:47. doi: 10.3389/fncel.2012.00047
- Augustin, M., Ladenbauer, J., and Obermayer, K. (2013). How adaptation shapes spike rate oscillations in recurrent neuronal networks. *Front. Comput. Neurosci.* 7:9. doi: 10.3389/fncom.2013.00009
- Bazhenov, M., Timofeev, I., Fröhlich, F., and Sejnowski, T. J. (2008). Cellular and network mechanisms of electrographic seizures. *Drug Discov. Today Dis. Models* 5, 45–57. doi: 10.1016/j.ddmod.2008.07.005
- Blankenship, A. G., and Feller, M. B. (2009). Mechanisms underlying spontaneous patterned activity in developing neural circuits. *Nat. Rev. Neurosci.* 11, 18–29. doi: 10.1038/nrn2759
- Borges, F., Protachevich, P., Lameu, E., Bonetti, R., Iarosz, K., Caldas, I., et al. (2017). Synchronised firing patterns in a random network of adaptive exponential integrate-and-fire neuron model. *Neural Netw.* 90, 1–7. doi: 10.1016/j.neunet.2017.03.005
- Bottani, S. (1995). Pulse-coupled relaxation oscillators: from biological synchronization to self-organized criticality. *Phys. Rev. Lett.* 74, 4189–4192. doi: 10.1103/PhysRevLett.74.4189
- Brette, R., and Gerstner, W. (2005). Adaptive exponential integrate-and-fire model as an effective description of neuronal activity. *J. Neurophysiol.* 94, 3637–3642. doi: 10.1152/jn.00686.2005
- Cohen, D., and Segal, M. (2011). Network bursts in hippocampal microcultures are terminated by exhaustion of vesicle pools. *J. Neurophysiol.* 106, 2314–2321. doi: 10.1152/jn.00969.2010
- Cohen, O., Keselman, A., Moses, E., Soriano, J., and Tlusty, T. (2010). Quorum percolation in living neural networks. *EPL (Europhys. Lett.)* 89, 1–6. doi: 10.1209/0295-5075/89/18008
- Connors, B. W., and Gutnick, M. J. (1990). Intrinsic firing patterns of diverse neocortical neurons. *Trends Neurosci.* 13, 99–104. doi: 10.1016/0166-2236(90)90185-D
- de Sevilla, D. F., Garduno, J., Galvan, E., and Buno, W. (2006). Calcium-activated afterhyperpolarizations regulate synchronization and timing of epileptiform bursts in hippocampal CA3 pyramidal neurons. *J. Neurophysiol.* 96, 3028–3041. doi: 10.1152/jn.00434.2006
- Derchansky, M., Jahromi, S. S., Mamani, M., Shin, D. S., Sik, A., and Carlen, P. L. (2008). Transition to seizures in the isolated immature mouse hippocampus: a switch from dominant phasic inhibition to dominant phasic excitation. *J. Physiol.* 586, 477–494. doi: 10.1113/jphysiol.2007.143065
- Empson, R. M., and Jefferys, J. G. (2001). Ca²⁺ entry through L-type Ca²⁺ channels helps terminate epileptiform activity by activation of a Ca²⁺ dependent afterhyperpolarisation in hippocampal CA3. *Neuroscience* 102, 297–306. doi: 10.1016/S0306-4522(00)00494-2
- Ferguson, K. A., Njap, F., Nicola, W., Skinner, F. K., and Campbell, S. A. (2015). Examining the limits of cellular adaptation bursting mechanisms in biologically-based excitatory networks of the hippocampus. *J. Comput. Neurosci.* 39, 289–309. doi: 10.1007/s10827-015-0577-1
- Golomb, D., Donner, K., Shacham, L., Shlosberg, D., Amitai, Y., Hansel, D., et al. (2006). Contribution of persistent Na⁺ current and M-type K⁺ current to

SUPPLEMENTARY MATERIAL

The Supplementary Material for this article can be found online at: <https://www.frontiersin.org/articles/10.3389/fnins.2018.00041/full#supplementary-material>

All codes used in this article are available on our GitHub repositories (<https://github.com/SENeC-Initiative/PyNeurActiv> and https://github.com/SENeC-Initiative/figures_examples). Note that some of the code might require additional libraries such as NNGT or NEST to run.

- somatic bursting in CA1 pyramidal cells: combined experimental and modeling study. *J. Neurophysiol.* 96, 1912–1926. doi: 10.1152/jn.00205.2006
- Gritsun, T. A., Le Feber, J., Stegenga, J., and Rutten, W. L. C. (2010). Network bursts in cortical cultures are best simulated using pacemaker neurons and adaptive synapses. *Biol. Cybern.* 102, 293–310. doi: 10.1007/s00422-010-0366-x
- Izhikevich, E. M. (2007). *Dynamical Systems in Neuroscience*. Cambridge, MA; London, UK: The MIT Press.
- Kunkel, S., Morrison, A., Weidel, P., Eppler, J. M., Sinha, A., Schenck, W., et al. (2017). NEST 2.12.0. doi: 10.5281/zenodo.259534
- Lüthi, A., and McCormick, D. A. (1998). H-current: properties of a neuronal and network pacemaker. *Neuron* 21, 9–12. doi: 10.1016/S0896-6273(00)80509-7
- Masquelier, T., and Deco, G. (2013). Network bursting dynamics in excitatory cortical neuron cultures results from the combination of different adaptive mechanism. *PLoS ONE* 8:e75824. doi: 10.1371/journal.pone.0075824
- Meister, M., Wong, R. O., Baylor, D. A., and Shatz, C. J. (1991). Synchronous bursts of action potentials in ganglion cells of the developing mammalian retina. *Science* 252, 939–943. doi: 10.1126/science.2035024
- Naud, R., Marcille, N., Clopath, C., and Gerstner, W. (2008). Firing patterns in the adaptive exponential integrate-and-fire model. *Biol. Cybern.* 99, 335–347. doi: 10.1007/s00422-008-0264-7
- Orlandi, J. G., Soriano, J., Alvarez-Lacalle, E., Teller, S., and Casademunt, J. (2013). Noise focusing and the emergence of coherent activity in neuronal cultures. *Nat. Phys.* 9, 582–590. doi: 10.1038/nphys2686
- Penn, Y., Segal, M., and Moses, E. (2016). Network synchronization in hippocampal neurons. *Proc. Natl. Acad. Sci. U.S.A.* 113, 3341–3346. doi: 10.1073/pnas.1515105113
- Ramirez, J. M., Tryba, A. K., and Peña, F. (2004). Pacemaker neurons and neuronal networks: an integrative view. *Curr. Opin. Neurobiol.* 14, 665–674. doi: 10.1016/j.conb.2004.10.011
- Roth, A., and van Rossum, M. C. W. (2009). Modeling synapses. *Comput. Model. Methods Neurosci.* 6, 139–160. doi: 10.7551/mitpress/9780262013277.003.0007
- Rybak, I. A., Molkov, Y. I., Jasinski, P. E., Shevtsova, N. A., and Smith, J. C. (2014). Rhythmic bursting in the pre-Bötzing complex: mechanisms and models. *Progr. Brain Res.* 209, 1–23. doi: 10.1016/B978-0-444-63274-6.00001-1
- Sah, P. (1996). Ca²⁺-activated K⁺ currents in neurones: types, physiological roles and modulation. *Trends Neurosci.* 19, 150–154. doi: 10.1016/S0166-2236(96)80026-9
- Sah, P., and Louise Faber, E. S. (2002). Channels underlying neuronal calcium-activated potassium currents. *Progr. Neurobiol.* 66, 345–353. doi: 10.1016/S0301-0082(02)00004-7
- Shah, M., and Haylett, D. G. (2000). Ca²⁺ channels involved in the generation of the slow afterhyperpolarization in cultured rat hippocampal pyramidal neurons. *J. Neurophysiol.* 83, 2554–2561. doi: 10.1152/jn.2000.83.5.2554
- Sipilä, S. T., Huttu, K., Voipio, J., and Kaila, K. (2006). Intrinsic bursting of immature CA3 pyramidal neurons and consequent giant depolarizing potentials are driven by a persistent Na⁺ current and terminated by a slow Ca²⁺-activated K⁺ current. *Eur. J. Neurosci.* 23, 2330–2338. doi: 10.1111/j.1460-9568.2006.04757.x
- Somers, D., and Kopell, N. (1993). Rapid synchronization through fast threshold modulation. *Biol. Cybern.* 68, 393–407. doi: 10.1007/BF00198772
- Stegenga, J., Le Feber, J., Marani, E., and Rutten, W. L. C. (2008). Analysis of cultured neuronal networks using intraburst firing characteristics.

- IEEE Trans. Biomed. Eng.* 55, 1382–1390. doi: 10.1109/TBME.2007.913987
- Stiefel, K. M., Gutkin, B. S., and Sejnowski, T. J. (2008). Cholinergic neuromodulation changes phase response curve shape and type in cortical pyramidal neurons. *PLoS ONE* 3:e3947. doi: 10.1371/journal.pone.0003947
- Storm, J. F. (1989). An after-hyperpolarization of medium duration in rat hippocampal pyramidal cells. *J. Physiol.* 409, 171–190. doi: 10.1113/jphysiol.1989.sp017491
- Suresh, J., Radojicic, M., Pesce, L. L., Bhansali, A., Wang, J., Tryba, A. K., et al. (2016). Network burst activity in hippocampal neuronal cultures: the role of synaptic and intrinsic currents. *J. Neurophysiol.* 115, 3073–3089. doi: 10.1152/jn.00995.2015
- Touboul, J. (2009). Importance of the cutoff value in the quadratic adaptive integrate-and-fire model. *Neural comput.* 21, 2114–2122. doi: 10.1162/neco.2009.09-08-853
- Touboul, J., and Brette, R. (2008). Dynamics and bifurcations of the adaptive exponential integrate-and-fire model. *Biol. Cybern.* 99, 319–334. doi: 10.1007/s00422-008-0267-4
- Van Vreeswijk, C., and Hansel, D. (2001). Patterns of synchrony in neural networks with spike adaptation. *Neural Comput.* 13, 959–992. doi: 10.1162/08997660151134280
- Vogalis, F., Storm, J. F., and Lancaster, B. (2003). SK channels and the varieties of slow after-hyperpolarizations in neurons. *Eur. J. Neurosci.* 18, 3155–3166. doi: 10.1111/j.1460-9568.2003.03040.x
- Wagenaar, D. A., Nadasdy, Z., and Potter, S. M. (2006). Persistent dynamic attractors in activity patterns of cultured neuronal networks. *Phys. Rev. E Stat. Nonlinear Soft Matter Phys.* 73:051907. doi: 10.1103/PhysRevE.73.051907
- Womble, M. D., and Moises, H. C. (1992). Muscarinic inhibition of M-current and a potassium leak conductance in neurones of the rat basolateral amygdala. *J. Physiol.* 457, 93–114. doi: 10.1113/jphysiol.1992.sp019366

Conflict of Interest Statement: The authors declare that the research was conducted in the absence of any commercial or financial relationships that could be construed as a potential conflict of interest.

Copyright © 2018 Fardet, Ballandras, Bottani, Mérens and Monceau. This is an open-access article distributed under the terms of the Creative Commons Attribution License (CC BY). The use, distribution or reproduction in other forums is permitted, provided the original author(s) and the copyright owner are credited and that the original publication in this journal is cited, in accordance with accepted academic practice. No use, distribution or reproduction is permitted which does not comply with these terms.

Bibliography

Books

- Amini, S. and White, M. K.**, eds. (2013). *Neuronal Cell Culture: Methods and Protocols (Methods in Molecular Biology)*. Humana Press. ISBN: 1627036393 (cit. on pp. 4, 6).
- Barabási, A.-L.** (2016). *Network Science*. Cambridge University Press. ISBN: 1107076269 (cit. on p. 75).
- Benchenane, K.** (2006). *Neural Synchrony and Memory In and Out of Sleep*. Second Edition. Vol. 4. Elsevier, pp. 563–583. ISBN: 9780128093245. DOI: 10.1016/B978-0-12-809324-5.21117-6 (cit. on p. 132).
- Costa, L. G., Giordano, G., and Guizzetti, M.**, eds. (2011). *In Vitro Neurotoxicology*. Humana Press. ISBN: 9781617791697 (cit. on p. 6).
- Dichter, M.** (2009). “MODELS | The use of Cell Culture Models to Study Mechanisms Related to Epilepsy and Antiepileptic Drugs”. In: *Encyclopedia of Basic Epilepsy Research*. Elsevier, pp. 808–814. DOI: 10.1016/B978-012373961-2.00322-2 (cit. on p. 6).
- Gross, G. W., Rhoades, B. K., and Kowalski, J. M.** (1993). “Dynamics of burst patterns generated by monolayer networks in culture”. In: *Neurobionics : an interdisciplinary approach to substitute impaired functions of the human nervous system*. Ed. by **Bothe, H.-W., Samii, M., and Eckmiller, R.** North-Holland. ISBN: 978-0-444-89958-3 (cit. on p. 27).
- Izhikevich, E. M.** (2007). *Dynamical systems in neuroscience: the geometry of excitability and bursting*. Ed. by **Izhikevich, E. M.** Cambridge, Mass. London: MIT Press. ISBN: 9780262514200 (cit. on p. 16).
- Leonetti, M.** (2001). *Branching in Nature*. Ed. by **Fleury, V., Gouyet, J.-F., and Léonetti, M.** Berlin, Heidelberg: Springer Berlin Heidelberg. ISBN: 978-3-540-41888-7. DOI: 10.1007/978-3-662-06162-6 (cit. on p. 108).
- Neumann, J. von** (1956). “Probabilistic logics and the synthesis of reliable organisms from unreliable components.” In: *Automata studies*. Ed. by **Shannon, J. C. and McCarthy, J.** Princeton, NJ: Princeton University Press, pp. 43–98 (cit. on p. 7).
- Ooyen, A. van** (2003). *Modeling neural development*. Ed. by **Ooyen, A. van.** MIT Press, p. 339. ISBN: 0262220660 (cit. on pp. 108, 109).
- Renault, R.** (2015). “Emergent design of neuronal devices”. PhD thesis. Université Paris Diderot (cit. on pp. 6, 106, 107).
- Russell, S. J. and Norvig, P.** (1995). *Artificial Intelligence: A Modern Approach*. Vol. 9. 2, pp. 215–218. ISBN: 9780131038059. DOI: 10.1016/0925-2312(95)90020-9. arXiv: 9809069v1 [arXiv:gr-qc] (cit. on p. 2).

- Schwartz, E. L.** (1993). *Computational Neuroscience*. Bradford Books. MIT Press. ISBN: 9780262691642 (cit. on p. 7).
- Strogatz, S.** (2007). *Nonlinear Dynamics and Chaos*. Ed. by **Strogatz, S.** Studies in Nonlinearity. Sarat Book House. ISBN: 9780813349114 (cit. on p. 28).
- Stuart, G., Spruston, N., and Häusser, M.**, eds. (1999). *Dendrites*. Oxford New York: Oxford University Press. ISBN: 0198504888 (cit. on p. 117).
- Trappenberg, T.** (2010). *Fundamentals of Computational Neuroscience*. Fundamentals of Computational Neuroscience. OUP Oxford. ISBN: 9780199568413 (cit. on p. 7).

Articles

- Aimovi, J. et al.** (2011). “Modeling of Neuronal Growth In Vitro: Comparison of Simulation Tools NETMORPH and CX3D.” In: *EURASIP journal on bioinformatics & systems biology* 2011, p. 616382. ISSN: 16874153. DOI: 10.1155/2011/616382 (cit. on p. 94).
- Afshar, G. et al.** (2015). “Enhancing burst activation and propagation in cultured neuronal networks by photo-stimulation”. In: *bioRxiv*. DOI: 10.1101/027177. eprint: <https://www.biorxiv.org/content/early/2015/09/18/027177.full.pdf> (cit. on p. 71).
- Arbib, M. A.** (2018). “From cybernetics to brain theory, and more: A memoir”. In: *Cognitive Systems Research* 50, pp. 83–145. ISSN: 13890417. DOI: 10.1016/j.cogsys.2018.04.001 (cit. on p. 7).
- Athamneh, A. I. M. and Suter, D. M.** (Sept. 2015). “Quantifying mechanical force in axonal growth and guidance”. In: *Frontiers in Cellular Neuroscience* 9.SEPTEMBER 2015, p. 359. ISSN: 1662-5102. DOI: 10.3389/fncel.2015.00359 (cit. on p. 104).
- Augustin, M., Ladenbauer, J., and Obermayer, K.** (2013). “How adaptation shapes spike rate oscillations in recurrent neuronal networks”. In: *Frontiers in Computational Neuroscience* 7.February, pp. 1–11. ISSN: 1662-5188. DOI: 10.3389/fncom.2013.00009 (cit. on p. 41).
- Baj, G. et al.** (2014). “Developmental and maintenance defects in Rett syndrome neurons identified by a new mouse staging system in vitro”. In: *Frontiers in Cellular Neuroscience* 8.February, pp. 1–15. ISSN: 1662-5102. DOI: 10.3389/fncel.2014.00018 (cit. on p. 12).
- Bakkum, D. J. et al.** (2007). “MEART: The semi-living artist”. In: *Frontiers in Neurorobotics* 1.November, p. 5. ISSN: 1662-5218. DOI: 10.3389/neuro.12.005.2007 (cit. on p. 4).
- Baltz, T., Herzog, A., and Voigt, T.** (Sept. 2011). “Slow oscillating population activity in developing cortical networks: models and experimental results”. In: *Journal of Neurophysiology* 106.3, pp. 1500–1514. ISSN: 0022-3077. DOI: 10.1152/jn.00889.2010 (cit. on pp. 38, 75).
- Barral, J. and Reyes, A. D.** (Dec. 2016). “Synaptic scaling rule preserves excitatory/inhibitory balance and salient neuronal network dynamics”. In: *Nature Neuroscience* 19.12, pp. 1690–1696. ISSN: 1097-6256. DOI: 10.1038/nn.4415 (cit. on pp. 87, 124, 163).

- Beaudoin, G. M. J. et al.** (Aug. 2012). “Culturing pyramidal neurons from the early postnatal mouse hippocampus and cortex”. In: *Nature Protocols* 7.9, pp. 1741–1754. ISSN: 1754-2189. DOI: 10.1038/nprot.2012.099 (cit. on pp. 3, 4).
- Bekkers, J. M.** (Dec. 2003). “Convolution of mini distributions for fitting evoked synaptic amplitude histograms”. In: *Journal of Neuroscience Methods* 130.2, pp. 105–114. ISSN: 01650270. DOI: 10.1016/j.jneumeth.2003.09.018 (cit. on p. 72).
- Ben-Menachem, E. et al.** (2015). “Surgically implanted and non-invasive vagus nerve stimulation: A review of efficacy, safety and tolerability”. In: *European Journal of Neurology* 22.9, pp. 1260–1268. ISSN: 14681331. DOI: 10.1111/ene.12629 (cit. on p. 7).
- Betz, T. et al.** (2011). “Growth cones as soft and weak force generators.” In: *Proceedings of the National Academy of Sciences of the United States of America* 108.33, pp. 13420–13425. ISSN: 0027-8424. DOI: 10.1073/pnas.1106145108 (cit. on p. 105).
- Bonifazi, P. et al.** (Dec. 2009). “GABAergic Hub Neurons Orchestrate Synchrony in Developing Hippocampal Networks”. In: *Science* 326.5958, pp. 1419–1424. ISSN: 0036-8075. DOI: 10.1126/science.1175509 (cit. on p. 75).
- Bornschrögl, T. et al.** (2013). “Filopodial retraction force is generated by cortical actin dynamics and controlled by reversible tethering at the tip.” In: *Proceedings of the National Academy of Sciences of the United States of America* 110.47, pp. 18928–33. ISSN: 1091-6490. DOI: 10.1073/pnas.1316572110 (cit. on p. 104).
- Bottani, S.** (May 1995). “Pulse-Coupled Relaxation Oscillators: From Biological Synchronization to Self-Organized Criticality”. In: *Physical Review Letters* 74.21, pp. 4189–4192. ISSN: 0031-9007. DOI: 10.1103/PhysRevLett.74.4189. arXiv: 9503079v1 [arXiv:cond-mat] (cit. on p. 151).
- Breskin, I. et al.** (Oct. 2006). “Percolation in Living Neural Networks”. In: *Physical Review Letters* 97.18, p. 188102. ISSN: 0031-9007. DOI: 10.1103/PhysRevLett.97.188102 (cit. on p. 58).
- Brette, R.** (2012). “Computing with neural synchrony”. In: *PLoS Computational Biology* 8.6. ISSN: 1553734X. DOI: 10.1371/journal.pcbi.1002561 (cit. on p. 132).
- Brette, R. and Gerstner, W.** (Nov. 2005). “Adaptive exponential integrate-and-fire model as an effective description of neuronal activity”. In: *J. Neurophysiol.* 94.5, pp. 3637–3642. ISSN: 0022-3077. DOI: 10.1152/jn.00686.2005 (cit. on p. 17).
- Brette, R., Rudolph, M., et al.** (2007). “Simulation of networks of spiking neurons: A review of tools and strategies”. In: *Journal of Computational Neuroscience* 23.3, pp. 349–398. ISSN: 1573-6873. DOI: 10.1007/s10827-007-0038-6. arXiv: 0611089 [q-bio] (cit. on p. 159).
- Brown, A.** (2003). “Axonal transport of membranous and nonmembranous cargoes: A unified perspective”. In: *Journal of Cell Biology* 160.6, pp. 817–821. ISSN: 00219525. DOI: 10.1083/jcb.200212017 (cit. on p. 101).
- Brown, K. M., Gillette, T. A., and Ascoli, G. A.** (2008). “Quantifying neuronal size: Summing up trees and splitting the branch difference”. In: *Seminars in Cell and Developmental Biology* 19.6, pp. 485–493. ISSN: 10849521. DOI: 10.1016/j.semcd.2008.08.005. arXiv: NIHMS150003 (cit. on pp. 117, 178).

- Brunel, N.** (2000). “Dynamics of sparsely connected networks of excitatory and inhibitory spiking neurons”. In: *Journal of computational neuroscience* 208, pp. 183–208. ISSN: 1573-6873. DOI: 10.1023/A:1008925309027 (cit. on p. 54).
- Brunel, N. and Hakim, V.** (2008). “Sparsely synchronized neuronal oscillations”. In: *Chaos* 18.1, pp. 1–12. ISSN: 10541500. DOI: 10.1063/1.2779858 (cit. on p. 54).
- Brunel, N. and Van Rossum, M. C.** (2007). “Lapicque’s 1907 paper: From frogs to integrate-and-fire”. In: *Biological Cybernetics* 97.5-6, pp. 337–339. ISSN: 03401200. DOI: 10.1007/s00422-007-0190-0 (cit. on pp. 16, 17).
- Cammarata, G. M., Bearce, E. A., and Lowery, L. A.** (2016). “Cytoskeletal social networking in the growth cone: How +TIPs mediate microtubule-actin cross-linking to drive axon outgrowth and guidance”. In: *Cytoskeleton* 73.9, pp. 461–476. ISSN: 19493592. DOI: 10.1002/cm.21272 (cit. on p. 104).
- Chever, O. et al.** (2016). “Astroglial networks promote neuronal coordination”. In: *Science Signaling* 9.410. ISSN: 19379145. DOI: 10.1126/scisignal.aad3066 (cit. on p. 38).
- Chklovskii, D. B. and Stepanyants, A.** (2003). “Power-law for axon diameters at branch point”. In: *BMC Neuroscience* 4.1, p. 18. ISSN: 14712202. DOI: 10.1186/1471-2202-4-18. arXiv: 0302039 [physics] (cit. on p. 109).
- Cohen, D. and Segal, M.** (2011). “Network bursts in hippocampal microcultures are terminated by exhaustion of vesicle pools”. In: *Journal of Neurophysiology* 106.August 2011, pp. 2314–2321. ISSN: 0022-3077. DOI: 10.1152/jn.00969.2010 (cit. on pp. 40, 73–75).
- Cohen, O. et al.** (Jan. 2010). “Quorum percolation in living neural networks”. In: *EPL (Europhysics Letters)* 89.1, p. 18008. ISSN: 0295-5075. DOI: 10.1209/0295-5075/89/18008 (cit. on p. 58).
- Coles, C. H. and Bradke, F.** (Aug. 2015). “Coordinating Neuronal ActinMicrotubule Dynamics”. In: *Current Biology* 25.15, R677–R691. ISSN: 09609822. DOI: 10.1016/j.cub.2015.06.020 (cit. on pp. 12, 13, 104).
- Compte, A. et al.** (May 2003). “Cellular and Network Mechanisms of Slow Oscillatory Activity (<1 Hz) and Wave Propagations in a Cortical Network Model”. In: *Journal of Neurophysiology* 89.5, pp. 2707–2725. ISSN: 0022-3077. DOI: 10.1152/jn.00845.2002 (cit. on p. 41).
- Conde, C. and Cáceres, A.** (2009). “Microtubule assembly, organization and dynamics in axons and dendrites.” In: *Nature reviews. Neuroscience* 10.5, pp. 319–332. ISSN: 1471-003X. DOI: 10.1038/nrn2631. arXiv: NIHMS150003 (cit. on p. 12).
- Courchesne, E. and Pierce, K.** (2005). “Why the frontal cortex in autism might be talking only to itself: Local over-connectivity but long-distance disconnection”. In: *Current Opinion in Neurobiology* 15.2, pp. 225–230. ISSN: 09594388. DOI: 10.1016/j.conb.2005.03.001 (cit. on p. 92).
- Craig, E. M. et al.** (2012). “Membrane tension, myosin force, and actin turnover maintain actin treadmill in the nerve growth cone”. In: *Biophysical Journal* 102.7, pp. 1503–1513. ISSN: 00063495. DOI: 10.1016/j.bpj.2012.03.003 (cit. on p. 104).
- Curtis, T. M. and Scholfield, C. N.** (2001). “Nifedipine blocks Ca²⁺ store refilling through a pathway not involving L-type Ca²⁺ channels in rabbit arteriolar smooth muscle”. In: *Journal of Physiology* 532.3, pp. 609–623. ISSN: 00223751. DOI: 10.1111/j.1469-7793.2001.0609e.x (cit. on p. 39).

- Darville, H. et al.** (2016). “Human Pluripotent Stem Cell-derived Cortical Neurons for High Throughput Medication Screening in Autism: A Proof of Concept Study in SHANK3 Haploinsufficiency Syndrome”. In: *EBioMedicine* 9, pp. 293–305. ISSN: 23523964. DOI: 10.1016/j.ebiom.2016.05.032 (cit. on p. 4).
- Deer, T. R. et al.** (2014). “Effectiveness of Cervical Spinal Cord Stimulation for the Management of Chronic Pain”. In: *Neuromodulation: Technology at the Neural Interface* 17.3, pp. 265–271. ISSN: 10947159. DOI: 10.1111/ner.12119 (cit. on p. 7).
- DeMarse, T. B. et al.** (Apr. 2016). “Feed-Forward Propagation of Temporal and Rate Information between Cortical Populations during Coherent Activation in Engineered In Vitro Networks”. In: *Frontiers in Neural Circuits* 10.April. ISSN: 1662-5110. DOI: 10.3389/fncir.2016.00032 (cit. on p. 135).
- DeRosa, B. A. et al.** (2015). “HVGAT-mCherry: A novel molecular tool for analysis of GABAergic neurons derived from human pluripotent stem cells”. In: *Molecular and Cellular Neuroscience* 68, pp. 244–257. ISSN: 10959327. DOI: 10.1016/j.mcn.2015.08.007. arXiv: 15334406 (cit. on p. 5).
- Destexhe, A.** (2009). “Self-sustained asynchronous irregular states and Up-Down states in thalamic, cortical and thalamocortical networks of nonlinear integrate-and-fire neurons”. In: *Journal of Computational Neuroscience* 27.3, pp. 493–506. ISSN: 09295313. DOI: 10.1007/s10827-009-0164-4. arXiv: 0809.0654 (cit. on pp. 36, 54).
- Eckmann, J. P. et al.** (2008). “Leader neurons in population bursts of 2D living neural networks”. In: *New Journal of Physics* 10. ISSN: 13672630. DOI: 10.1088/1367-2630/10/1/015011 (cit. on pp. 70, 71).
- Eckmann, J.-P. et al.** (Sept. 2010). “Leaders of neuronal cultures in a quorum percolation model”. In: *Frontiers in Computational Neuroscience* 4.September, pp. 1–12. ISSN: 16625188. DOI: 10.3389/fncom.2010.00132. eprint: 1009.5355 (cit. on p. 59).
- Egorov, A. V. and Draguhn, A.** (2013). “Development of coherent neuronal activity patterns in mammalian cortical networks: Common principles and local heterogeneity”. In: *Mechanisms of Development* 130.6-8, pp. 412–423. ISSN: 09254773. DOI: 10.1016/j.mod.2012.09.006 (cit. on p. 27).
- Empson, R. M. and Jefferys, J. G.** (2001). “Ca(2+) entry through L-type Ca(2+) channels helps terminate epileptiform activity by activation of a Ca(2+) dependent afterhyperpolarisation in hippocampal CA3.” In: *Neuroscience* 102.2, pp. 297–306. ISSN: 0306-4522. DOI: 10.1016/S0306-4522(00)00494-2 (cit. on pp. 39, 49).
- Ermentrout, B.** (July 1996). “Type I Membranes, Phase Resetting Curves, and Synchrony”. In: *Neural Computation* 8.5, pp. 979–1001. ISSN: 0899-7667. DOI: 10.1162/neco.1996.8.5.979 (cit. on p. 20).
- Ester, M. et al.** (1996). “A density-based algorithm for discovering clusters in large spatial databases with noise”. In: AAAI Press, pp. 226–231 (cit. on p. 78).
- Estrada, E. and Rodriguez-Velazquez, J. a.** (2005). “Subgraph Centrality in Complex Networks”. In: *Physical Review E* 71.5, p. 29. ISSN: 1539-3755. DOI: 10.1103/PhysRevE.71.056103. arXiv: 0504730 [cond-mat] (cit. on p. 168).
- Fardet, T., Bottani, S., et al.** (2018). “Effects of inhibitory neurons on the quorum percolation model and dynamical extension with the BretteGerstner model”. In:

- Physica A: Statistical Mechanics and its Applications* 499. ISSN: 03784371. DOI: 10.1016/j.physa.2018.02.002 (cit. on pp. 59, 133, 179).
- Fardet, T., Ballandras, M., et al.** (2018). “Understanding the generation of network bursts by adaptive oscillatory neurons”. In: *Frontiers in Neuroscience* 12.FEB. ISSN: 1662453X. DOI: 10.3389/fnins.2018.00041 (cit. on pp. 41, 45, 46, 151, 179).
- Feinerman, O., Rotem, A., and Moses, E.** (2008). “Reliable neuronal logic devices from patterned hippocampal cultures”. In: *Nature Physics* 4.12, pp. 967–973. ISSN: 1745-2473. DOI: 10.1038/nphys1099 (cit. on pp. 133, 134).
- Ferguson, K. A. et al.** (2015). “Examining the limits of cellular adaptation bursting mechanisms in biologically-based excitatory networks of the hippocampus”. In: *Journal of Computational Neuroscience* 39.3, pp. 289–309. ISSN: 15736873. DOI: 10.1007/s10827-015-0577-1 (cit. on pp. 41, 74).
- Flynn, K. C. et al.** (2009). “Growth cone-like waves transport actin and promote axonogenesis and neurite branching”. In: *Developmental Neurobiology* 69.12, pp. 761–779. ISSN: 19328451. DOI: 10.1002/dneu.20734 (cit. on p. 109).
- Fourcaud-Trocme, N. et al.** (2003). “How spike generation mechanisms determine the neuronal response to fluctuating inputs”. In: *J. Neurosci.* 23.37, pp. 11628–11640. ISSN: 1529-2401. DOI: 10.1523/JNEUROSCI.2337-03.2003 (cit. on p. 17).
- Galarreta, M. and Hestrin, S.** (2001). “Electrical synapses between GABA-releasing interneurons.” In: *Nature reviews. Neuroscience* 2.6, pp. 425–433. ISSN: 14710048. DOI: 10.1038/35077566 (cit. on p. 25).
- Gallo, G.** (2011). “The cytoskeletal and signaling mechanisms of axon collateral branching”. In: *Developmental Neurobiology* 71.3, pp. 201–220. ISSN: 19328451. DOI: 10.1002/dneu.20852 (cit. on pp. 108, 112).
- Gibson, D. A. and Ma, L.** (2011). “Developmental regulation of axon branching in the vertebrate nervous system”. In: *Development* 138.2, pp. 183–195. ISSN: 0950-1991. DOI: 10.1242/dev.046441 (cit. on p. 113).
- Gleeson, P. et al.** (Dec. 2017). “A commitment to open source in neuroscience”. In: *Neuron* 96, pp. 964–965. DOI: 10.1016/j.neuron.2017.10.013 (cit. on p. 8).
- Goldin, A. L.** (2003). “Mechanisms of sodium channel inactivation”. In: *Current Opinion in Neurobiology* 13.3, pp. 284–290. ISSN: 09594388. DOI: 10.1016/S0959-4388(03)00065-5 (cit. on p. 38).
- Grabham, P. W.** (2003). “Microtubule and Rac 1-dependent F-actin in growth cones”. In: *Journal of Cell Science* 116.18, pp. 3739–3748. ISSN: 0021-9533. DOI: 10.1242/jcs.00686 (cit. on p. 105).
- Gritsun, T. A., Le Feber, J., et al.** (2010). “Network bursts in cortical cultures are best simulated using pacemaker neurons and adaptive synapses”. In: *Biological Cybernetics* 102.4, pp. 293–310. ISSN: 03401200. DOI: 10.1007/s00422-010-0366-x (cit. on pp. 38, 59, 62, 73, 75, 139).
- Gritsun, T. A., Feber, J. le, and Rutten, W. L. C.** (Jan. 2012). “Growth dynamics explain the development of spatiotemporal burst activity of young cultured neuronal networks in detail.” In: *PloS one* 7.9. Ed. by **Wennekers, T.**, e43352. ISSN: 1932-6203. DOI: 10.1371/journal.pone.0043352 (cit. on p. 132).
- Gritsun, T. et al.** (Apr. 2009). “Network bursts in cortical neuronal cultures ‘Noise-versus pacemaker’- driven neural network simulations”. In: *2009 4th International IEEE/EMBS Conference on Neural Engineering*. August 2009. IEEE, pp. 626–628. ISBN: 978-1-4244-2072-8. DOI: 10.1109/NER.2009.5109374 (cit. on p. 59).

- Grueber, W. B. and Sagasti, A.** (Sept. 2010). “Self-avoidance and Tiling: Mechanisms of Dendrite and Axon Spacing”. In: *Cold Spring Harbor Perspectives in Biology* 2.9, a001750–a001750. ISSN: 1943-0264. DOI: 10.1101/cshperspect.a001750 (cit. on p. 106).
- Gulledge, A. T. et al.** (2013). “A Sodium-Pump-Mediated Afterhyperpolarization in Pyramidal Neurons”. In: *Journal of Neuroscience* 33.32, pp. 13025–13041. ISSN: 0270-6474. DOI: 10.1523/JNEUROSCI.0220-13.2013 (cit. on p. 39).
- Harrison, R.** (1907). “Observations on the living developing nerve fiber”. In: *The Anatomical Record* 1, pp. 116–128 (cit. on p. 3).
- Hasler, J. and Marr, B.** (2013). “Finding a roadmap to achieve large neuromorphic hardware systems”. In: *Frontiers in Neuroscience* 7.7 SEP, pp. 1–29. ISSN: 1662453X. DOI: 10.3389/fnins.2013.00118 (cit. on p. 3).
- Hely, T. A., Graham, B. P., and Ooyen, A. van** (June 2001). “A Computational Model of Dendrite Elongation and Branching Based on MAP2 Phosphorylation”. In: *Journal of Theoretical Biology* 210.3, pp. 375–384. ISSN: 00225193. DOI: 10.1006/jtbi.2001.2314 (cit. on p. 99).
- Hernandez-Hernandez, G. et al.** (Mar. 2017). “Nonlinear signaling on biological networks: The role of stochasticity and spectral clustering”. In: *Physical Review E* 95.3, p. 032313. ISSN: 2470-0045. DOI: 10.1103/PhysRevE.95.032313 (cit. on p. 71).
- Hirasawa, M. and Pittman, Q. J.** (2003). “Nifedipine facilitates neurotransmitter release independently of calcium channels”. In: *Proceedings of the National Academy of Sciences* 100.10, pp. 6139–6144. ISSN: 0027-8424. DOI: 10.1073/pnas.0936131100 (cit. on p. 39).
- Hjorth, J. J. J. et al.** (2014). “Competitive dynamics during resource-driven neurite outgrowth”. In: *PLoS ONE* 9.2. ISSN: 19326203. DOI: 10.1371/journal.pone.0086741 (cit. on p. 99).
- Hodgkin, A. L. and Huxley, A. F.** (Apr. 1952). “Currents carried by sodium and potassium ions through the membrane of the giant axon of *Loligo*”. In: *The Journal of Physiology* 116.4, pp. 449–472. ISSN: 00223751. DOI: 10.1113/jphysiol.1952.sp004717 (cit. on p. 17).
- Horvát, S. et al.** (2016). “Spatial Embedding and Wiring Cost Constrain the Functional Layout of the Cortical Network of Rodents and Primates”. In: *PLoS Biology* 14.7, pp. 1–30. ISSN: 15457885. DOI: 10.1371/journal.pbio.1002512 (cit. on p. 87).
- Humpel, C.** (2015). “Neuroscience forefront review organotypic brain slice cultures: A review”. In: *Neuroscience* 305, pp. 86–98. ISSN: 18737544. DOI: 10.1016/j.neuroscience.2015.07.086 (cit. on p. 4).
- Ievins, A. and Moritz, C. T.** (2017). “Therapeutic Stimulation for Restoration of Function After Spinal Cord Injury”. In: *Physiology* 32.5, pp. 391–398. ISSN: 1548-9213. DOI: 10.1152/physiol.00010.2017 (cit. on p. 7).
- Ikonomovic, M. et al.** (2007). “Superior frontal cortex cholinergic axon density in mild cognitive impairment and early Alzheimer disease”. In: *Archives of neurology* 64.9, pp. 1312–1317. DOI: 10.1001/archneur.64.9.1312 (cit. on p. 120).
- Izhikevich, E. M.** (Nov. 2003). “Simple model of spiking neurons”. In: *IEEE Transactions on Neural Networks* 14.6, pp. 1569–1572. ISSN: 1045-9227. DOI: 10.1109/TNN.2003.820440 (cit. on p. 16, 17).

- Jan, Y. N. and Jan, L. Y.** (2010). “Branching out: Mechanisms of dendritic arborization”. In: *Nature Reviews Neuroscience* 11.5, pp. 316–328. ISSN: 1471003X. DOI: 10.1038/nrn2836. arXiv: NIHMS150003 (cit. on p. 108).
- Janeiro, R. D. et al.** (1999). “Gap-junctional coupling between neurons and astrocytes in”. In: *Proceedings of the National Academy of Sciences of the United States of America* 96.June, pp. 7541–7546 (cit. on p. 25).
- Jarvis, S. J., Rotter, S., and Egert, U.** (2011). “Burst initiation and propagation in cortical cultures requires an inhomogeneous connectivity distribution and synaptic rescaling”. In: *BMC Neuroscience* 12.Suppl 1, P85. ISSN: 1471-2202. DOI: 10.1186/1471-2202-12-S1-P85 (cit. on p. 70).
- Kaesler, P. S. and Regehr, W. G.** (2014). “Molecular Mechanisms for Synchronous, Asynchronous, and Spontaneous Neurotransmitter Release”. In: *Annual Review of Physiology* 76.1, pp. 333–363. ISSN: 0066-4278. DOI: 10.1146/annurev-physiol-021113-170338 (cit. on pp. 23, 39).
- Kahn, O. I. and Baas, P. W.** (2016). “Microtubules and Growth Cones: Motors Drive the Turn”. In: *Trends in Neurosciences* 39.7, pp. 433–440. ISSN: 1878108X. DOI: 10.1016/j.tins.2016.04.009 (cit. on pp. 98, 106).
- Kamioka, H. et al.** (Mar. 1996). “Spontaneous periodic synchronized bursting during formation of mature patterns of connections in cortical cultures”. In: *Neuroscience Letters* 206.2-3, pp. 109–112. ISSN: 03043940. DOI: 10.1016/S0304-3940(96)12448-4 (cit. on p. 27).
- Kavalali, E. T.** (2014). “The mechanisms and functions of spontaneous neurotransmitter release”. In: *Nature Reviews Neuroscience* 16.1, pp. 5–16. ISSN: 1471-003X. DOI: 10.1038/nrn3875 (cit. on pp. 37, 72).
- Kirkegaard, J. B. and Goldstein, R. E.** (2018). “The role of tumbling frequency and persistence in optimal run-and-tumble chemotaxis”. In: *IMA Journal of Applied Mathematics (Institute of Mathematics and Its Applications)* 83.4, pp. 700–719. ISSN: 14643634. DOI: 10.1093/imamat/hxy013. arXiv: 1709.04375 (cit. on p. 169).
- Koene, R. a. et al.** (Sept. 2009). “NETMORPH: a framework for the stochastic generation of large scale neuronal networks with realistic neuron morphologies.” In: *Neuroinformatics* 7.3, pp. 195–210. DOI: 10.1007/s12021-009-9052-3 (cit. on pp. 91, 92).
- Koppert, M. M. et al.** (2011). “Plasticity-modulated seizure dynamics for seizure termination in realistic neuronal models”. In: *Journal of Neural Engineering* 8.4. ISSN: 17412560. DOI: 10.1088/1741-2560/8/4/046027 (cit. on p. 73).
- Kulkarni, V. A. and Firestein, B. L.** (May 2012). “The dendritic tree and brain disorders”. In: *Molecular and Cellular Neuroscience* 50.1, pp. 10–20. ISSN: 10447431. DOI: 10.1016/j.mcn.2012.03.005 (cit. on p. 92).
- Ladenbauer, J. et al.** (2012). “Impact of Adaptation Currents on Synchronization of Coupled Exponential Integrate-and-Fire Neurons.” In: *PLOS Comput. Biol.* 8.4, e1002478. ISSN: 1553-7358. DOI: 10.1371/journal.pcbi.1002478. arXiv: arXiv:1310.2430v1 (cit. on p. 54).
- Lewis, T. L., Courchet, J., and Polleux, F.** (2013). “Cell biology in neuroscience: Cellular and molecular mechanisms underlying axon formation, growth, and branching.” In: *The Journal of cell biology* 202.6, pp. 837–48. ISSN: 1540-8140. DOI: 10.1083/jcb.201305098 (cit. on p. 108).

- Leyva, I. et al.** (2011). “Synchronization waves in geometric networks”. In: *Physical Review E* 84.6, p. 065101. ISSN: 1539-3755. DOI: 10.1103/PhysRevE.84.065101 (cit. on p. 92).
- Lima, P. A. and Marrion, N. V.** (2007). “Mechanisms underlying activation of the slow AHP in rat hippocampal neurons”. In: *Brain Research* 1150.1, pp. 74–82. ISSN: 00068993. DOI: 10.1016/j.brainres.2007.02.067 (cit. on pp. 39, 49).
- Loebel, A. and Tsodyks, M.** (2002). “Computation by ensemble synchronization in recurrent networks with synaptic depression”. In: *Journal of Computational Neuroscience* 13.2, pp. 111–124. ISSN: 0929-5313. DOI: 10.1023/A:1020110223441 (cit. on pp. 53, 161).
- Lonardoni, D. et al.** (July 2017). “Recurrently connected and localized neuronal communities initiate coordinated spontaneous activity in neuronal networks”. In: *PLOS Computational Biology* 13.7. Ed. by **Battaglia, F. P.**, e1005672. ISSN: 1553-7358. DOI: 10.1371/journal.pcbi.1005672 (cit. on pp. 70, 75, 81).
- Lowery, L. A. and Vactor, D. V.** (2009). “The trip of the tip: understanding the growth cone machinery”. In: *Nature Reviews Molecular Cell Biology* 10.5, pp. 332–343. ISSN: 1471-0072. DOI: 10.1038/nrm2679 (cit. on p. 96).
- Loy, K. et al.** (2014). “Common strength and localization of spontaneous and evoked synaptic vesicle release sites”. In: *Molecular Brain* 7.1, pp. 1–6. ISSN: Molecular Brain. DOI: 10.1186/1756-6606-7-23 (cit. on p. 37).
- Lukojević, M. and Jaeger, H.** (2009). “Reservoir computing approaches to recurrent neural network training”. In: *Computer Science Review* 3, pp. 127–149. ISSN: 15740137. DOI: 10.1016/j.cosrev.2009.03.005 (cit. on p. 3).
- Lv, Z. S. et al.** (2017). “Exponential distance distribution of connected neurons in simulations of two-dimensional in vitro neural network development”. In: *Frontiers of Physics* 12.3. ISSN: 20950470. DOI: 10.1007/s11467-017-0602-0. arXiv: 1702.03418 (cit. on p. 87).
- Magee, J. C. and Cook, E. P.** (Sept. 2000). “Somatic EPSP amplitude is independent of synapse location in hippocampal pyramidal neurons”. In: *Nature Neuroscience* 3.9, pp. 895–903. ISSN: 1097-6256. DOI: 10.1038/78800 (cit. on p. 163).
- Manninen, T. et al.** (2018). “Challenges in Reproducibility, Replicability, and Comparability of Computational Models and Tools for Neuronal and Glial Networks, Cells, and Subcellular Structures”. In: *Frontiers in Neuroinformatics* 12.May, p. 20. ISSN: 1662-5196. DOI: 10.3389/fninf.2018.00020 (cit. on p. 8).
- Marblestone, A., Wayne, G., and Kording, K.** (2016). “Towards an integration of deep learning and neuroscience”. In: 10.September, pp. 1–41. ISSN: 1662-5188. DOI: 10.3389/fncom.2016.00094. arXiv: 1606.03813 (cit. on p. 2).
- Markram, H., Gerstner, W., and Sjöström, P. J.** (2012). “Spike-Timing-Dependent Plasticity: A Comprehensive Overview”. In: *Frontiers in Synaptic Neuroscience* 4.July, pp. 2010–2012. ISSN: 1663-3563. DOI: 10.3389/fnsyn.2012.00002 (cit. on p. 26).
- Masquelier, T. and Deco, G.** (2013). “Network Bursting Dynamics in Excitatory Cortical Neuron Cultures Results from the Combination of Different Adaptive Mechanism”. In: *PLoS ONE* 8.10, pp. 1–11. DOI: 10.1371/journal.pone.0075824 (cit. on p. 27).
- Mathis, D. M., Furman, J. L., and Norris, C. M.** (Mar. 2011). “Preparation of Acute Hippocampal Slices from Rats and Transgenic Mice for the Study of Synaptic

- Alterations during Aging and Amyloid Pathology”. In: *Journal of Visualized Experiments* 49. ISSN: 1940-087X. DOI: 10.3791/2330 (cit. on p. 4).
- McCulloch, W. S. and Pitts, W.** (Dec. 1943). “A logical calculus of the ideas immanent in nervous activity”. In: *The bulletin of mathematical biophysics* 5.4, pp. 115–133. ISSN: 1522-9602. DOI: 10.1007/BF02478259 (cit. on p. 7).
- Mekhail, N. A. et al.** (2011). “Retrospective Review of 707 Cases of Spinal Cord Stimulation: Indications and Complications”. In: *Pain Practice* 11.2, pp. 148–153. ISSN: 15332500. DOI: 10.1111/j.1533-2500.2010.00407.x (cit. on p. 7).
- Memelli, H., Torben-Nielsen, B., and Kozloski, J.** (Jan. 2013). “Self-referential forces are sufficient to explain different dendritic morphologies.” In: *Frontiers in neuroinformatics* 7, p. 1. ISSN: 16625196. DOI: 10.3389/fninf.2013.00001 (cit. on pp. 98, 102).
- Métens, S. et al.** (Mar. 2016). “Finite-size effects and dynamics of giant transition of a continuum quorum percolation model on random networks”. In: *Physical Review E* 93.3, p. 032112. ISSN: 2470-0045. DOI: 10.1103/PhysRevE.93.032112 (cit. on p. 59).
- Monceau, P., Renault, R., Métens, S., Bottani, S., and Fardet, T.** (2017). “Phase transition approach to bursting in neuronal cultures: Quorum percolation models”. In: *Journal of Physics: Conference Series*. Vol. 905. 1. DOI: 10.1088/1742-6596/905/1/012008 (cit. on pp. 58, 179).
- Monceau, P., Renault, R., Métens, S., and Bottani, S.** (July 2016). “Effect of threshold disorder on the quorum percolation model”. In: *Physical Review E* 94.1, p. 012316. ISSN: 2470-0045. DOI: 10.1103/PhysRevE.94.012316 (cit. on p. 59).
- Naud, R. et al.** (2008). “Firing patterns in the adaptive exponential integrate-and-fire model”. In: *Biological Cybernetics* 99.4-5, pp. 335–347. ISSN: 03401200. DOI: 10.1007/s00422-008-0264-7 (cit. on pp. 17, 145, 147).
- Neher, E. and Sakaba, T.** (2008). “Multiple Roles of Calcium Ions in the Regulation of Neurotransmitter Release”. In: *Neuron* 59.6, pp. 861–872. ISSN: 08966273. DOI: 10.1016/j.neuron.2008.08.019 (cit. on pp. 39, 54).
- Nordlie, E., Gewaltig, M.-O., and Plesser, H. E.** (Aug. 2009). “Towards Reproducible Descriptions of Neuronal Network Models”. In: *PLoS Computational Biology* 5.8, e1000456. DOI: 10.1371/journal.pcbi.1000456 (cit. on p. 8).
- Ocker, G. K., Litwin-Kumar, A., and Doiron, B.** (2015). “Self-Organization of Microcircuits in Networks of Spiking Neurons with Plastic Synapses”. In: *PLoS Computational Biology* 11.8, e1004458. ISSN: 1553-7358. DOI: 10.1371/journal.pcbi.1004458 (cit. on p. 132).
- Okujeni, S., Kandler, S., and Egert, U.** (2017). “Mesoscale architecture shapes initiation and richness of spontaneous network activity”. In: *The Journal of Neuroscience* 37.14, pp. 2552–16. ISSN: 0270-6474. DOI: 10.1523/JNEUROSCI.2552-16.2017 (cit. on p. 27).
- Opitz, T.** (2002). “Spontaneous Development of Synchronous Oscillatory Activity During Maturation of Cortical Networks In Vitro”. In: *Journal of Neurophysiology* 88.5, pp. 2196–2206. ISSN: 0022-3077. DOI: 10.1152/jn.00316.2002 (cit. on p. 27).
- Orlandi, J. G. et al.** (Sept. 2013). “Noise focusing and the emergence of coherent activity in neuronal cultures”. In: *Nature Physics* 9.9, pp. 582–590. ISSN: 1745-2473. DOI: 10.1038/nphys2686 (cit. on pp. 5, 27, 70, 71, 75).

- Oan, R., Su, E., and Shinbrot, T.** (Oct. 2011). “The Interplay between Branching and Pruning on Neuronal Target Search during Developmental Growth: Functional Role and Implications”. In: *PLoS ONE* 6.10. Ed. by **Zheng, J. C.**, e25135. ISSN: 1932-6203. DOI: 10.1371/journal.pone.0025135 (cit. on p. 114).
- Pasquale, V. et al.** (2008). “Self-organization and neuronal avalanches in networks of dissociated cortical neurons”. In: *Neuroscience* 153.4, pp. 1354–1369. ISSN: 03064522. DOI: 10.1016/j.neuroscience.2008.03.050 (cit. on pp. 27, 132).
- Pelt, J. van, Ooyen, A. van, and Uylings, H. B. M.** (2001). “The need for integrating neuronal morphology databases and computational environments in exploring neuronal structure and function”. In: *Anatomy and Embryology* 204.4, pp. 255–265. ISSN: 03402061. DOI: 10.1007/s004290100197 (cit. on p. 110).
- Pelt, J. van and Uylings, H. B. M.** (2002). “Branching rates and growth functions in the outgrowth of dendritic branching patterns.” In: *Network* 13.3, pp. 261–281. ISSN: 0954-898X. DOI: 10.1088/0954-898X/13/3/302 (cit. on pp. 108, 110).
- Penn, Y., Segal, M., and Moses, E.** (2016). “Network synchronization in hippocampal neurons.” In: *Proceedings of the National Academy of Sciences of the United States of America* 113.12, pp. 3341–3346. ISSN: 00278424. DOI: 10.1073/pnas.1515105113 (cit. on pp. 25, 38, 41, 54, 55, 61).
- Pernice, V. et al.** (2013). “The relevance of network micro-structure for neural dynamics.” In: *Frontiers in computational neuroscience* 7.June, p. 72. ISSN: 1662-5188. DOI: 10.3389/fncom.2013.00072 (cit. on p. 92).
- Peter, S. J. and Mofrad, M. R. K.** (2017). “Computational Modeling of Axonal Microtubule Bundles under Tension”. In: *Biophysj* 102.4, pp. 749–757. ISSN: 0006-3495. DOI: 10.1016/j.bpj.2011.11.4024 (cit. on p. 98).
- Potter, S. M. and DeMarse, T. B.** (2001). “A new approach to neural cell culture for long-term studies”. In: *Journal of Neuroscience Methods* 110.1, pp. 17–24. ISSN: 01650270. DOI: 10.1016/S0165-0270(01)00412-5 (cit. on p. 3).
- ReiSS, P. and Koert, U.** (Aug. 2006). “Voltage-Gated Ion Channels as Drug Targets. Methods and Principles in Medicinal Chemistry, Vol. 29. Edited by David J. Triggle, Murali Gopalakrishnan, David Rampe and Wei Zheng.” In: *Angewandte Chemie International Edition* 45.33, pp. 5414–5414. DOI: 10.1002/anie.200685419 (cit. on p. 49).
- Renault, R.** (2015). “Emergent design of neuronal devices”. PhD thesis. Université Paris Diderot (cit. on pp. 6, 106, 107).
- Renault, R., Durand, J.-B., et al.** (2016). “Asymmetric axonal edge guidance: a new paradigm for building oriented neuronal networks”. In: *Lab on a Chip* 16.12, pp. 2188–2191. ISSN: 1473-0197. DOI: 10.1039/C6LC00479B (cit. on pp. 133, 134).
- Renault, R., Monceau, P., and Bottani, S.** (Dec. 2013). “Memory decay and loss of criticality in quorum percolation”. In: *Physical Review E* 88.6, p. 062134. ISSN: 1539-3755. DOI: 10.1103/PhysRevE.88.062134 (cit. on pp. 59, 133).
- Renault, R., Monceau, P., Bottani, S., and Métens, S.** (2014). “Effective non-universality of the quorum percolation model on directed graphs with Gaussian in-degree”. In: *Physica A: Statistical Mechanics and its Applications* 414.m, pp. 352–359. ISSN: 03784371. DOI: 10.1016/j.physa.2014.07.028 (cit. on p. 133).
- Renault, R., Sukenik, N., et al.** (2015). “Combining Microfluidics, Optogenetics and Calcium Imaging to Study Neuronal Communication In Vitro”. In: *Plos One*

- 10.4, pp. 1–15. ISSN: 1932-6203. DOI: 10.1371/journal.pone.0120680 (cit. on pp. 133, 134, 165).
- Rico, B. et al.** (2004). “Control of axonal branching and synapse formation by focal adhesion kinase.” In: *Nature neuroscience* 7.10, pp. 1059–69. ISSN: 1097-6256. DOI: 10.1038/nn1317 (cit. on p. 104).
- Sah, P. and Louise Faber, E. S.** (2002). “Channels underlying neuronal calcium-activated potassium currents”. In: *Progress in Neurobiology* 66.5, pp. 345–353. ISSN: 03010082. DOI: 10.1016/S0301-0082(02)00004-7 (cit. on pp. 38, 49).
- Sakakibara, A. et al.** (2013). “Microtubule dynamics in neuronal morphogenesis”. In: *Open Biology* 3.7, pp. 130061–130061. ISSN: 2046-2441. DOI: 10.1098/rsob.130061 (cit. on p. 12).
- Sang, Q. and Tan, S. S.** (2003). “Contact-associated neurite outgrowth and branching of immature cortical interneurons”. In: *Cerebral Cortex* 13.6, pp. 677–683. ISSN: 10473211. DOI: 10.1093/cercor/13.6.677 (cit. on p. 105).
- Sayer, R. J., Friedlander, M. J., and Redman, S. J.** (1990). “The time course and amplitude of EPSPs evoked at synapses between pairs of CA3/CA1 neurons in the hippocampal slice.” In: *The Journal of neuroscience : the official journal of the Society for Neuroscience* 10.3, pp. 826–836. ISSN: 0270-6474 (cit. on p. 87).
- Schlachetzki, J. C. M., Saliba, S. W., and Oliveira, A. C. P. de** (2013). “Studying neurodegenerative diseases in culture models”. In: *Revista Brasileira de Psiquiatria* 35.SUPPL.2, pp. 92–100. ISSN: 15164446. DOI: 10.1590/1516-4446-2013-1159 (cit. on p. 6).
- Schonfeld-Dado, E. and Segal, M.** (2011). “Activity deprivation induces neuronal cell death: Mediation by tissue-type plasminogen activator”. In: *PLoS ONE* 6.10, pp. 1–5. ISSN: 19326203. DOI: 10.1371/journal.pone.0025919 (cit. on p. 132).
- Searle, J. R.** (1980). “Minds, brains, and programs”. In: *Behavioral and Brain Sciences* 3.03, p. 417. ISSN: 0140-525X. DOI: 10.1017/S0140525X00005756 (cit. on p. 2).
- Sevilla, D. F. de et al.** (Aug. 2006). “Calcium-Activated Afterhyperpolarizations Regulate Synchronization and Timing of Epileptiform Bursts in Hippocampal CA3 Pyramidal Neurons”. In: *Journal of Neurophysiology* 96.6, pp. 3028–3041. ISSN: 0022-3077. DOI: 10.1152/jn.00434.2006 (cit. on p. 39).
- Shao, L. R. et al.** (1999). “The role of BK-type Ca²⁺-dependent K⁺ channels in spike broadening during repetitive firing in rat hippocampal pyramidal cells”. In: *Journal of Physiology* 521.1, pp. 135–146. ISSN: 00223751. DOI: 10.1111/j.1469-7793.1999.00135.x (cit. on p. 49).
- Shefi, O., Golebowicz, S., et al.** (2005). “A two-phase growth strategy in cultured neuronal networks as reflected by the distribution of neurite branching angles”. In: *Journal of Neurobiology* 62.3, pp. 361–368. ISSN: 00223034. DOI: 10.1002/neu.20108 (cit. on p. 112).
- Shefi, O., Harel, A., et al.** (June 2004). “Biophysical constraints on neuronal branching”. In: *Neurocomputing* 58-60, pp. 487–495. ISSN: 09252312. DOI: 10.1016/j.neucom.2004.01.085 (cit. on p. 109).
- Sholl, D. A.** (Oct. 1953). “Dendritic organization in the neurons of the visual and motor cortices of the cat.” In: *Journal of anatomy* 87.4, pp. 387–406. ISSN: 0021-8782 (cit. on p. 178).
- Sibarov, D. A. and Antonov, S. M.** (May 2015). “Characteristics of Postsynaptic Currents in Primary Cultures of Rat Cerebral Cortical Neurons”. In: *Neuroscience*

- and *Behavioral Physiology* 45.4, pp. 431–439. ISSN: 0097-0549. DOI: 10.1007/s11055-015-0093-9 (cit. on p. 37, 72).
- Sipilä, S. T. et al.** (2006). “Intrinsic bursting of immature CA3 pyramidal neurons and consequent giant depolarizing potentials are driven by a persistent Na⁺ current and terminated by a slow Ca²⁺-activated K⁺ current”. In: *European Journal of Neuroscience* 23, pp. 2330–2338. ISSN: 0953816X. DOI: 10.1111/j.1460-9568.2006.04757.x (cit. on p. 19).
- Somers, D. and Kopell, N.** (1993). “Rapid synchronization through fast threshold modulation”. In: *Biological Cybernetics* 68.5, pp. 393–407. ISSN: 03401200. DOI: 10.1007/BF00198772 (cit. on p. 151).
- Song, S. et al.** (Mar. 2005). “Highly nonrandom features of synaptic connectivity in local cortical circuits.” In: *PLoS biology* 3.3, e68. ISSN: 1545-7885. DOI: 10.1371/journal.pbio.0030068 (cit. on p. 87).
- Soriano, J., Breskin, I., et al.** (2007). “Percolation approach to study connectivity in living neural networks”. In: *AIP Conference Proceedings* 887, pp. 96–106. ISSN: 0094243X. DOI: 10.1063/1.2709591. arXiv: 1007.5016 (cit. on p. 133).
- Soriano, J., Rodríguez Martínez, M., et al.** (2008). “Development of input connections in neural cultures.” In: *Proceedings of the National Academy of Sciences of the United States of America* 105.37, pp. 13758–13763. ISSN: 00278424. DOI: 10.1073/pnas.0707492105. arXiv: 1008.0062 (cit. on pp. 58, 124).
- Strogatz, S. H.** (2000). “From Kuramoto to Crawford: exploring the onset of synchronization in populations of coupled oscillators”. In: *Physica D: Nonlinear Phenomena* 143.1-4, pp. 1–20. ISSN: 01672789. DOI: 10.1016/S0167-2789(00)00094-4 (cit. on p. 28).
- Su, H. et al.** (2001). “Extracellular calcium modulates persistent sodium current-dependent burst-firing in hippocampal pyramidal neurons.” In: *The Journal of neuroscience : the official journal of the Society for Neuroscience* 21.12, pp. 4173–4182. ISSN: 1529-2401 (cit. on p. 55).
- Suresh, J. et al.** (2016). “Network burst activity in hippocampal neuronal cultures: the role of synaptic and intrinsic currents”. In: *Journal of Neurophysiology* 115.6, pp. 3073–3089. ISSN: 0022-3077. DOI: 10.1152/jn.00995.2015 (cit. on p. 25).
- Takeda, S. et al.** (2015). “Neuronal uptake and propagation of a rare phosphorylated high-molecular-weight tau derived from Alzheimer’s disease brain”. In: *Nature Communications* 6. ISSN: 20411723. DOI: 10.1038/ncomms9490. arXiv: arXiv:1011.1669v3 (cit. on pp. 7, 92).
- Taylor, A. M. et al.** (Mar. 2003). “Microfluidic Multicompartment Device for Neuroscience Research”. In: *Langmuir* 19.5, pp. 1551–1556. ISSN: 0743-7463. DOI: 10.1021/la026417v (cit. on p. 133).
- Tazerart, S., Vinay, L., and Brocard, F.** (2008). “The persistent sodium current generates pacemaker activities in the central pattern generator for locomotion and regulates the locomotor rhythm.” In: *The Journal of neuroscience : the official journal of the Society for Neuroscience* 28.34, pp. 8577–8589. ISSN: 0270-6474. DOI: 10.1523/JNEUROSCI.1437-08.2008 (cit. on p. 19).
- Tetzlaff, C. et al.** (Dec. 2010). “Self-Organized Criticality in Developing Neuronal Networks”. In: *PLoS Computational Biology* 6.12. Ed. by **Friston, K. J.**, e1001013. ISSN: 1553-7358. DOI: 10.1371/journal.pcbi.1001013 (cit. on p. 132).
- Tibau, E. et al.** (2013). “Interplay activity-connectivity: Dynamics in patterned neuronal cultures”. In: *Physics, Computation, and the Mind - Advances and*

- Challenges at Interfaces*. Vol. 1510. AIP Conference Proceedings, pp. 54–63. ISBN: 9780735411289. DOI: 10.1063/1.4776501 (cit. on pp. 92, 136).
- Tiwari, M. N. et al.** (2018). “Differential contributions of Ca²⁺-activated K⁺ channels and Na⁺/K⁺-ATPases to the generation of the slow afterhyperpolarization in CA1 pyramidal cells”. In: *Hippocampus* 28.5, pp. 338–357. ISSN: 10981063. DOI: 10.1002/hipo.22836 (cit. on p. 39).
- Tong, Z. et al.** (2015). “A microfluidic neuronal platform for neuron axotomy and controlled regenerative studies”. In: *RSC Advances* 5.90, pp. 73457–73466. ISSN: 20462069. DOI: 10.1039/c5ra11522a (cit. on p. 7).
- Torben-Nielsen, B. and De Schutter, E.** (2014). “Context-aware modeling of neuronal morphologies.” In: *Frontiers in neuroanatomy* 8.September, p. 92. DOI: 10.3389/fnana.2014.00092 (cit. on pp. 91, 92, 98, 170).
- Touboul, J. and Brette, R.** (2008). “Dynamics and bifurcations of the adaptive exponential integrate-and-fire model”. In: *Biological Cybernetics* 99.4-5, pp. 319–334. ISSN: 03401200. DOI: 10.1007/s00422-008-0267-4 (cit. on p. 17).
- Toyoizumi, T. et al.** (2014). “Modeling the Dynamic Interaction of Hebbian and Homeostatic Plasticity”. In: *Neuron* 84.2, pp. 497–510. ISSN: 10974199. DOI: 10.1016/j.neuron.2014.09.036 (cit. on p. 26).
- Turrigiano, G. G. and Nelson, S. B.** (Feb. 2004). “Homeostatic plasticity in the developing nervous system”. In: *Nature Reviews Neuroscience* 5.2, pp. 97–107. ISSN: 1471-003X. DOI: 10.1038/nrn1327 (cit. on p. 26).
- Van Ooyen, A.** (2011). “Using theoretical models to analyse neural development”. In: *Nature Reviews Neuroscience* 12.6, pp. 311–326. ISSN: 1471003X. DOI: 10.1038/nrn3031 (cit. on p. 96).
- Van Pelt, J., Corner, M. A., et al.** (1993). “The self-organizing brain: from growth cones to functional networks”. In: *18th International Summer School of brain research*, p. 446. ISBN: 0444818197 (cit. on p. 132).
- Van Pelt, J., Dityatev, A. E., and Uylings, H. B. M.** (1997). “Natural variability in the number of dendritic segments: Model-based inferences about branching during neurite outgrowth”. In: *Journal of Comparative Neurology* 387.3, pp. 325–340. ISSN: 00219967. DOI: 10.1002/(SICI)1096-9861(19971027)387:3<325::AID-CNE1>3.0.CO;2-2 (cit. on p. 109).
- Van Pelt, J., Uylings, H. B., et al.** (1992). “Tree asymmetry-A sensitive and practical measure for binary topological trees”. In: *Bulletin of Mathematical Biology* 54.5, pp. 759–784. ISSN: 15229602. DOI: 10.1007/BF02459929 (cit. on pp. 108, 178).
- Van Vreeswijk, C. and Hansel, D.** (2001). “Patterns of synchrony in neural networks with spike adaptation”. In: *Neural Computation* 13.5, pp. 959–992. ISSN: 0899-7667. DOI: 10.1162/089976601511134280 (cit. on pp. 41, 151).
- Wagenaar, D. a., Pine, J., and Potter, S. M.** (2006). “An extremely rich repertoire of bursting patterns during the development of cortical cultures.” In: *BMC neuroscience* 7, p. 11. ISSN: 1471-2202. DOI: 10.1186/1471-2202-7-11 (cit. on p. 27).
- Wang, D.** (1999). “Relaxation Oscillators and Networks”. In: *Wiley Encyclopedia of Electrical and Electronics Engineering* 18.2, pp. 396–405. DOI: 10.1002/047134608X.W2282 (cit. on p. 28).
- Wang, L. and Marquardt, T.** (2013). “What axons tell each other: Axon-axon signaling in nerve and circuit assembly”. In: *Current Opinion in Neurobiology*

- 23.6, pp. 974–982. ISSN: 09594388. DOI: 10.1016/j.conb.2013.08.004 (cit. on p. 106).
- Wessells, N. K. and Nuttall, R. P.** (Aug. 1978). “Normal branching, induced branching, and steering of cultured parasympathetic motor neurons”. In: *Experimental Cell Research* 115.1, pp. 111–122. ISSN: 00144827. DOI: 10.1016/0014-4827(78)90408-1 (cit. on p. 108).
- Williams, C. L. and Smith, S. M.** (2018). “Calcium dependence of spontaneous neurotransmitter release”. In: *Journal of Neuroscience Research* 96.3, pp. 335–347. ISSN: 10974547. DOI: 10.1002/jnr.24116 (cit. on p. 54).
- Withers, G. S. et al.** (Sept. 2006). “Effects of substrate geometry on growth cone behavior and axon branching”. In: *Journal of Neurobiology* 66.11, pp. 1183–1194. ISSN: 0022-3034. DOI: 10.1002/neu.20298 (cit. on p. 109).
- Xu, K. et al.** (2015). “Show, Attend and Tell: Neural Image Caption Generation with Visual Attention”. In: *CoRR* abs/1502.03044. arXiv: 1502.03044 (cit. on p. 2).
- Yaghoubi, M. et al.** (2018). “Neuronal avalanche dynamics indicates different universality classes in neuronal cultures”. In: *Scientific Reports* 8.1, pp. 1–11. ISSN: 20452322. DOI: 10.1038/s41598-018-21730-1 (cit. on pp. 27, 28).
- Yu, L. M. Y., Leipzig, N. D., and Shoichet, M. S.** (2008). “Promoting neuron adhesion and growth”. In: *Materials Today* 11.5, pp. 36–43. ISSN: 13697021. DOI: 10.1016/S1369-7021(08)70088-9. arXiv: 13697021 (cit. on p. 105).
- Zbinden, C.** (2011). “Leader neurons in leaky integrate and fire neural network simulations”. In: *Journal of Computational Neuroscience* 31, pp. 285–304. ISSN: 09295313. DOI: 10.1007/s10827-010-0308-6. arXiv: 1004.2787 (cit. on pp. 71, 75).
- Zhang, Z. W., Kang, J. I., and Vaucher, E.** (2011). “Axonal varicosity density as an index of local neuronal interactions”. In: *PLoS ONE* 6.7. ISSN: 19326203. DOI: 10.1371/journal.pone.0022543 (cit. on p. 120).
- Zubler, F. and Douglas, R.** (2009). “A framework for modeling the growth and development of neurons and networks.” In: *Frontiers in computational neuroscience* 3.November, p. 25. DOI: 10.3389/neuro.10.025.2009 (cit. on pp. 91, 92).

Online

- Fields, D. R.** (2017). URL: <https://www.quantamagazine.org/why-the-first-drawings-of-neurons-were-defaced-20170928/> (cit. on p. 10).
- Garay, P. M. et al.** (2013). *CellPlayer 96-Well Kinetic NeuroTrack Assay*. URL: https://www.essenbioscience.com/media/uploads/files/8000-0211-A00%7B%5C_%7D-%7B%5C_%7DCellPlayer%7B%5C_%7D96-well%7B%5C_%7DNeuroTrack%7B%5C_%7DAssay%7B%5C_%7DApplication%7B%5C_%7DNote.pdf (cit. on p. 122).
- Gewaltig, M.-O. and Diesmann, M.** (2007). *NEST (NEural Simulation Tool)*. URL: http://www.scholarpedia.org/article/NEST_%28NEural_Simulation_Tool%29 (cit. on p. 94).
- Olah, C. and Carter, S.** (2016). *Attention and Augmented Recurrent Neural Networks*. URL: <http://distill.pub/2016/augmented-rnns> (cit. on p. 2).

- Peyser, A. et al.** (Oct. 2017). *NEST 2.14.0*. URL: <https://doi.org/10.5281/zenodo.882971> (cit. on p. 91).
- Shenoy, K. and Chestek, C.** (2012). *Neural Prosthetics*. revision #124016 (cit. on p. 7).
- Wilson, C.** (2008). *Up and down states*. revision #91903. URL: http://www.scholarpedia.org/article/Up_and_down_states (cit. on p. 36).

